BOND PERFORMANCE BETWEEN CORRODED STEEL AND RECYCLED AGGREGATE CONCRETE INCORPORATING NANO SILICA

M. M. ALHAWAT

PHD

UNIVERSITY OF BRADFORD

2020

BOND PEFORMANCE BETWEEN CORRODED STEEL AND RECYCLED AGGREGATE CONCRETE INCORPORATING NANO SILICA

M. M. ALHAWAT

Submitted for the Degree of
Doctor of Philosophy

Faculty of Engineering and Informatics

University of Bradford

2020

ABSTRACT

Musab Masoud Alhawat

Bond Performance between Corroded Steel and Recycled Aggregate Concrete Incorporating Nano Silica

Keywords: Bond strength; Pull-out test; Mass loss method; Reinforcement corrosion; Nano silica; Recycled aggregate; Specific surface area; Impact-echo method; Artificial Neural Network.

The current research project mainly aims to investigate the corrosion resistance and bond performance of steel reinforced recycled aggregate concrete incorporating nano-silica under both normal and corrosive environmental conditions. The experimental part includes testing of 180 pull-out specimens prepared from 12 different mixtures. The main parameters studied were the amount of recycled aggregate (RCA) (i.e. 0%, 25%, 50% and 100%), nano silica (1.5% and 3%), steel embedment length as well as steel bar diameter (12 and 20mm). Different levels of corrosion were electrochemically induced by applying impressed voltage technique for 2, 5, 10 and 15 days. The experimental observations mainly focused on the corrosion level in addition to the ultimate bond, failure modes and slips occurred.

Experimental results showed that the bond performance between un-corroded steel and recycled aggregate concrete slightly reduced, while a significant degradation was observed after being exposed to corrosive conditions, in comparison to normal concrete. On the other hand, the use of nano silica (NS) showed a reasonable bond enhancement with both normal and RCA concretes under normal conditions. However, much better influence in terms of bond and corrosion resistance was observed under advancing levels of corrosion exposure, reflecting the improvement in corrosion resistance. Therefore, NS was superbly effective in recovering the poor performance in bond for RCA concretes. More efficiency was reported with RCA concretes compared to the conventional concrete. The bond resistance slightly with a small amount of corrosion (almost 2% weight loss), then a significant bond degradation occurs with further corrosion.

The influence of specific surface area and amount of nano silica on the performance of concrete with different water/binder (w/b) ratios has been also studied, using 63 different mixtures produced with three different types of colloidal NS having various surface areas and particle sizes. The results showed that the performance of concrete is heavily influenced by changing the surface area of nano silica. Amongst the three used types of nano silica, NS with SSA of 250 m^2/g achieved the

highest enhancement rate in terms of compressive strength, water absorption and microstructure analysis, followed by NS with SSA of 500 m2/g, whilst NS with SSA of 51.4 m^2/g was less advantageous for all mixtures. The optimum nano silica ratio in concrete is affected by its particle size as well as water to binder ratio.

The feasibility of the impact-echo method for identifying the corrosion was evaluated and compared to the corrosion obtained by mass loss method. The results showed that the impact-echo testing can be effectively used to qualitatively detect the damage caused by corrosion in reinforced concrete structures. A significant difference in the dominant frequencies response was observed after exposure to the high and moderate levels of corrosion, whilst no clear trend was observed at the initial stage of corrosion.

Artificial neural network models were also developed to predict bond strength for corroded/un-corroded steel bars in concrete using the main influencing parameters (i.e., concrete strength, concrete cover, bar diameter, embedment length and corrosion rate). The developed models were able to predict the bond strength with a high level of accuracy, which was confirmed by conducting a parametric study.

PAPERS PRODUCED FROM THIS THESIS

1. Alhawat, M. and Ashour, A., 2019, June. Bond strength between corroded steel reinforcement and recycled aggregate concrete. In Structures (Vol. 19, pp. 369-385). Elsevier.

2. Alhawat, M., Ashour, A. and El-Khoja, A., 2019. Properties of concrete incorporating different nano silica particles. Materials Research Innovations, pp.1-12.

3. Alhawat, M., Ashour, A. and El-Khoja, A., 2019, August. Influence of using different surface areas of nano silica on concrete properties. In AIP Conference Proceedings (Vol. 2146, No. 1, p. 020007). AIP Publishing.

4. Alhawat, M. and Ashour, A., 2020. Bond strength between corroded steel and recycled aggregate concrete incorporating nano silica. Construction and Building Materials (Vol. 237, pp.117441). Elsevier.

5. Alhawat, M., Khan, A and Ashour, A., 2020. Evaluation of steel corrosion in concrete structures using impact-echo method. Advanced Materials Research.

6. Alhawat, M., Ashour, A., Khan, A and Rahmanian, N., “Evaluation of bond performance of reinforced concrete under corrosive environments”. 2nd best paper in 1st annual Innovative Engineering Research Conference, AIERC17, held at University of Bradford 17 July 2017.

7. Alhawat, M., Ashour, A., Khan, A, and Rahmanian, N., ‘Effect of nano silica on the properties of recycled aggregate concrete’. 3rd annual Innovative Engineering Research Conference, AIERC19, held at University of Bradford 17 October 2019.

DECLERATION

I declare that this thesis is the result of my own work except where references have been made to the work related to others. This thesis has not been submitted anywhere for the application of another degree, diploma, or other qualification.

Musab M Alhawat

ACKNOWLEDGMENTS

It is a pleasure to thank those who made this thesis possible. First and foremost, I would like to thank **Allah**; our Lord, the All-Knowing, the Almighty, the most Merciful and the most Compassionate.

I would like to express my sincere appreciation and special thanks to my supervisors **Prof. Ashraf Ashour** for his excellent supervision, constant encouragement and approachability throughout the period of this work.

Special thanks go to the **Laboratory staff** who were always ready to help in times of needs. I would like to particularly thank **Stephen Robinson** for his expert advice and help during the experimental investigation.

I am forever deeply grateful to **my parents** and **my wife** for their moral support, help and understanding during the whole period of this work. I take the chance also to thank and express my gratitude to **friends** for their all **my** encouragement, advice and understanding.

The author wish to thank **MONE BROS** Company in Leeds (UK) for providing recycled aggregates used in this study. The authors also gratefully acknowledge **BASF** and **Akzonobe**l Companies for providing nano silica NS, and Hanson **Ltd**, UK, for suppling cement require in this study.

I do appreciate the grant and financial support provided by the Higher Education Institute in the **Libyan Government** needed to finish this research.

Finally, I would like to thank everybody who was involved in this work as well as expressing my apology to those I did not mention in this acknowledgment.

Table of Contents

List of Figures

List of Tables

Notations

The following symbols are used in the present thesis:

Ø = Bar diameter (mm)

l_d = Embedment length (mm)

f_c' = Cylinder compressive strength of concrete (MPa)

f_{cu} = Cube compressive strength of concrete (MPa)

f_{ct} = Tensile strength of concrete (MPa).

τ_{max} = Maximum bond stress (MPa)

S = Slip at the peak bond stress (mm)

β = shape factor correction

t = time

I = Initial current applied

M = Atomic weight for reinforcing steel

Z = valence charge of iron

C_F = Faraday' constant, which represents the amount of electrical charge in one mole of electrons

E = Young's modulus of elasticity

C = Wave velocity

f = Frequency

$Ca(OH)_2$ = Portlandite

R = Reflection coefficient

Z_i = Acoustic impedance of the structural element

Z_t = Acoustic impedance of the internal interface or boundary

C_2S = Alite

C_3S = Belite

η = Corrosion level of reinforcing steel bars

G_1 and G_2 = the weights of steel bar before and after corrosion

g_0 = Weight per unit length

P = Applied load

NaCl = Sodium chloride

$Fe(OH)_2$ = Ferrous hydroxide

w_i = Weight of input

x_i = Input

y_i = Output signal of neuron

S_i = Net input signal of neurons

b = Bias

n = Number of neurons in a layer

I_n and I = Normalised and un-normalised values of the training set

I_{min} and I_{max} = Minimum and maximum values of the data set

R = Regression value

Fe_3O_4 =Magnetite γ–

FeOOH =Lepidocrocite

α–FeOOH =Goethite α–

Fe2O3 = Hematite

Fe $(OH)_2$ = Ferrous hydroxide

Abbreviations

The following abbreviations are used in the present thesis:

RCA= Recycled Coarse Aggregate

NCA= Natural Coarse Aggregate

NS = Nano Silica

SSA = Specific Surface Area

Rr = Relative rib area

SEM = scanning electron microscopy

SP = superplasticizers

XRD = X-ray diffraction analysis

SSD = saturated surface dry condition

C-S-H = calcium-silicate-hydrate

ITZ = Interfacial Transition Zone

IE = Impact Echo

NDT = Non-Destructive Testing

AE = acoustic emission

UPV = ultrasonic pulse velocity

ANNs = Artificial Neural Networks

ACI = American Concrete Institute

BS = British Standards

CEB = Comite Euro-international du Beton

FIB = Federation International du Beton

JSCE = Japanese Society of Civil Engineers

SD = Standard Deviation

COV = Coefficient of Variation

MAPE = Mean Absolute Percentage Error

SDD = Saturated Surface Dry Condition

NACE = National Association of Corrosion Engineers

LVDT = linear variable differential transducers =

GPM = Galvanostatic pulse method

FBG = Fiber Bragg grating

IRT = Infrared Thermography Method

EN = Electrochemical noise

Chapter one
Introduction

1.1 General background

The durability and sustainability of concrete buildings are very challenging issues in construction industry. The use of recycled coarse aggregate (RCA) produced from construction and demolition waste has received increasing interest owing to its potential environmental and economic benefits. The employment of recycled coarse aggregate in concrete can significantly contribute to minimizing the consumption of natural resource as well as landfill places (Pour & Alam, 2016). It is estimated that about 850 million tons of demolished concrete are being generated yearly just in European countries (Ferrari et al., 2014). Nevertheless, the use of RCA in concrete is still limited due to the inferiority in some of its properties, compared to normal aggregate. RCA is mainly composed of natural aggregate and adhered mortar, causing more porous to concrete, and creating a weak interfacial zone in concrete, and hence increasing their water absorption capacity compared to normal aggregate (Kim et al., 2014; De Brito & Saikia, 2012). This can lead to difficulties in controlling the fresh properties of concrete and consequently affecting the mechanical properties of hardened concrete, however, the main challenges are still how to effectively improve properties related to durability (Behera et al., 2014). Therefore, the improvement of RCA properties has been one of the significant issues that attract researchers for extending the application of RCA in construction industry.

The service life of RC structures can be seriously influenced by corrosion phenomenon. Corrosion can lead to cracking, spalling, reducing the cross-sectional area of steel, losing bond strength between steel bars and concrete, and eventually losing the serviceability of the structure. Economically, the annual costs for repairing and maintaining RC structures due to corrosion exceed billions of dollars around the world. According to a study executed by the National Association of Corrosion Engineers in the USA (NACE) in 2017, the annual global cost of corrosion is approximately $2.5 trillion, representing about 3.4% of the global Gross Domestic Product.

Bond strength of reinforced concrete is one of the fundamental properties which needs to be significantly evaluated to ensure the performance of steel reinforcing in structures, especially in severe environments. Bond strength is responsible for transferring the force between steel and concrete, and it is heavily affected by different parameters such as concrete strength, embedment length, and bar diameter. Corrosion in steel reinforcement has been recently considered as another significant factor influencing the bond between steel and surrounding concrete. Bond strength might also be affected by the type and amount of aggregate used either; normal or recycled aggregate. Recent experimental investigations showed a slight decrease or comparable bond for RCA concrete, compared to conventional concrete (Kim et al., 2014; Yang et al., 2015). However, very limited research has been found in the literature regarding the bond behaviour of RCA concretes under exposure to corrosive environments.

In the literature, several techniques and approaches have been adopted for improving the performance of RCA in concrete. However, these techniques can be fundamentally classified in two routes, namely removing the weak surface of RCA, resulting from the

existence of old cement mortar or strengthen and modifying the quality of adhered mortar. Removing the old mortar requires one of the following treatments, namely mechanical grinding, pre-soaking in acidic solutions or ultrasonic cleaning (Katz, 2004). On the other hand, improving the quality of adhered mortar can be achieved by coating the surface of RCA with different materials such as polymer emulsion, lime powder filler and pozzolanic materials such as silica fume and fly ash (Speath & Tegguer, 2013; Wang et al., 2013).

Recently, nano silica has been successfully employed in concrete for improving concrete properties, owing to its beneficial contributions in filling nano and micro-voids available in the concrete matrix, enhancing the pozzolanic reaction and acting as a nuclear for producing additional calcium-silicate-hydrate gels (Senff et al., 2009). All these features are directly correlated to the ultra-small size and high specific surface area of its particles. Therefore, nano silica is seemingly a promising solution to enhance and compensate for the inferior performance of RCA in concrete (Shaikh et al., 2014; Li et al., 2017). Some aspects of this modified concrete have been successfully tested (i.e. mechanical and microstructural properties), whilst there are still important aspects need to be comprehensively investigated.

1. 2 Research significance

Even though the use of RCA in the construction industry has received considerable attention, its uses is still limited due to the deficiency in its properties, especially those related to durability. Several approaches have been investigated for improving the performance of RCA concrete, however, more effective techniques are still needed. Recently, nano silica has been successfully applied in concrete field for improving concrete properties. Therefore, nano silica is seemingly a very

effective solution to enhance the performance of RCA concrete and compensate the potential deficiency. In this context, very limited information related to the application of nano silica in RCA concrete has been published in the literature. The results obtained from the available research revealed the superior mechanical properties and microstructural enhancements of this modified concrete, however, investigations on some significant properties such as corrosion resistance and the bond strength have not been investigated yet. Thus, the modified concrete has a huge potential to address different economic and environmental issues (i.e. reducing the cost of aggregate and reducing CO_2 emissions associated with aggregate transportation, especially when local aggregates are recycled). It is estimated that about 60% of natural limestone resources can be saved in addition to reducing about 15-20% of CO_2 emissions (Guo et al., 2018). Moreover, the present investigation provides valuable information regarding the influence of nano silica particles' characteristics (i.e. specific surface area and particle size) on the performance of concrete with different water/binder (w/b) ratios. This research also focused on the feasibility of detecting corrosion by using the impact-echo method, since limited information available in this topic.

1.3 Research aims and objectives

The main aim of the current study is to investigate the corrosion resistance and bond performance of recycled aggregate concrete incorporating nano-silica under both normal and corrosive environmental conditions. The main objectives of this study are summarised below:

- To investigate the corrosion resistance and bond performance of reinforcement embedded in recycled aggregate concrete under different corrosive environmental conditions.
- To evaluate the influence of nano silica amount and characteristics (i.e. specific surface area and particle size) on the performance of concrete with different water/binder (w/b) ratios.
- To study the influence of nano silica on the corrosion resistance and bond performance of both normal and recycled reinforced concrete under different levels of corrosive environmental conditions.
- To study the influence of corrosion level induced in different mixtures on the behaviour of bond including bond-slip relationship, failure mode and bond strength.
- To investigate the feasibility of the impact-echo method for identifying corrosion level of steel reinforcement in concrete structures.
- To develop an artificial neural network model using MATLAB for predicting the bond strength of corroded/uncorroded bars in concrete and conduct a series of parametric studies.

1.4 Research methodology

To achieve the aims and objectives that mentioned above, the following approaches have been conducted:

- Sixty pull-out specimens containing different percentages of RCA (i.e. 0%,25%, 50% and 100%) and steel bars of two diameters (12 and 20 mm) and different embedment lengths were tested to investigates the bond performance of RCA reinforced concrete under normal and corrosive environmental conditions. In order to establish various levels of corrosion, specimens were exposed to electrochemical corrosion for 2, 5, 10 and 15 days.

- Sixty three mixtures were produced using NS having different surface areas (52, 250 and 500 m^2/g) and w/b ratios (0.4, 0.5 and 0.6) to evaluate the influence of specific surface area and w/b ratios on the performance of concrete, in addition to determining the optimum ratio of NS. The microstructural properties of concrete mixtures are analysed using a scanning electron microscope (SEM) and X-ray diffraction (XRD).
- A hundred and twenty pull-out cubes having small contents of NS (1.5% and 3%) were performed and tested and compared with the previous specimens to investigate the influence of NS on the corrosion and bond resistance of RCA reinforced concretes under different corrosive conditions.
- Two different groups of database have been collected from the literature review to be used for developing an artificial neural network model to predict the bond strength of corroded/uncorroded bars embedded in concrete.

Figure 1.1 presents the general methodology of the current research program.

1.5 Outline of the thesis

In addition to the introduction chapter, this thesis contains seven more chapters. Research significance, the aims and objectives and research methodology have been obviously set out in this chapter.

Chapter two involves reviewing the current literature relevant to the present work, including a summary of the important aspects related to corrosion (corrosion mechanisms, influencing factors and corrosion measurements). The bond behaviour of reinforced concrete is also comprehensively reviewed, including bond mechanism and failure, the main affecting parameters bonds strength, bond tests, and bond stress–slip relationship.

The use of recycled aggregate (RCA) in concrete is also reviewed in this chapter, followed by the key points related to using nano silica (NS) in concrete. The literature review also discusses the main findings available regarding the incorporation of nano silica in RCA concrete. The last section in chapter presents the main findings on concrete containing RCA and NS. Information presented in this chapter enables to explain the gaps in the previous works.

Chapter three discuss the experimental findings regarding two distinct phenomena, namely the influence of RCA content on the corrosion resistance of reinforcement embedded in concrete, and the bond performance between RCA concrete and reinforcing steel bars, either corroded or un-corroded. This chapter also describes the main properties of materials used, specimen's details, the setup procedures for accelerating corrosion and testing the bond.

In chapter four, the influence of nano silica characteristics, nano silica dosages and water/binder (w/b) ratios on the performance of concrete was evaluated using colloidal nano silica having different surface areas and particle sizes. The optimal ratio for each nano silica type is also discussed, whilst the type shows the highest enhancement ratio would be selected for using in chapter five.

Chapter five presents the experimental results and discussions related to the influence of the selected nano silica on the corrosion resistance of RCA concretes and

the bond performance of RCA reinforced concretes incorporating nano silica under both normal and corrosive environmental conditions. Investigations on the stress-slip relationship, failure mode and bond strength are analysed, with consideration the influence of other parameters, namely RCA content, embedment length, bar diameter and corrosion acceleration time.

In chapter six, the corrosion produced in chapter three and five was detected using the impact-echo method to investigate the feasibility of this method for detecting steel corrosion damage in reinforced concrete structures, and the results were compared with those obtained by mass-loss method.

Chapter seven displays the neural network models developed using MATLAB to predict the bond strength of corroded/un-corroded embedded in concrete. A parametric study was also conducted in this chapter to examine the generalization ability of the developed models.

Finally, chapter eight represents the main conclusions of this research and as well as provides some suggestions and recommendations for future research.

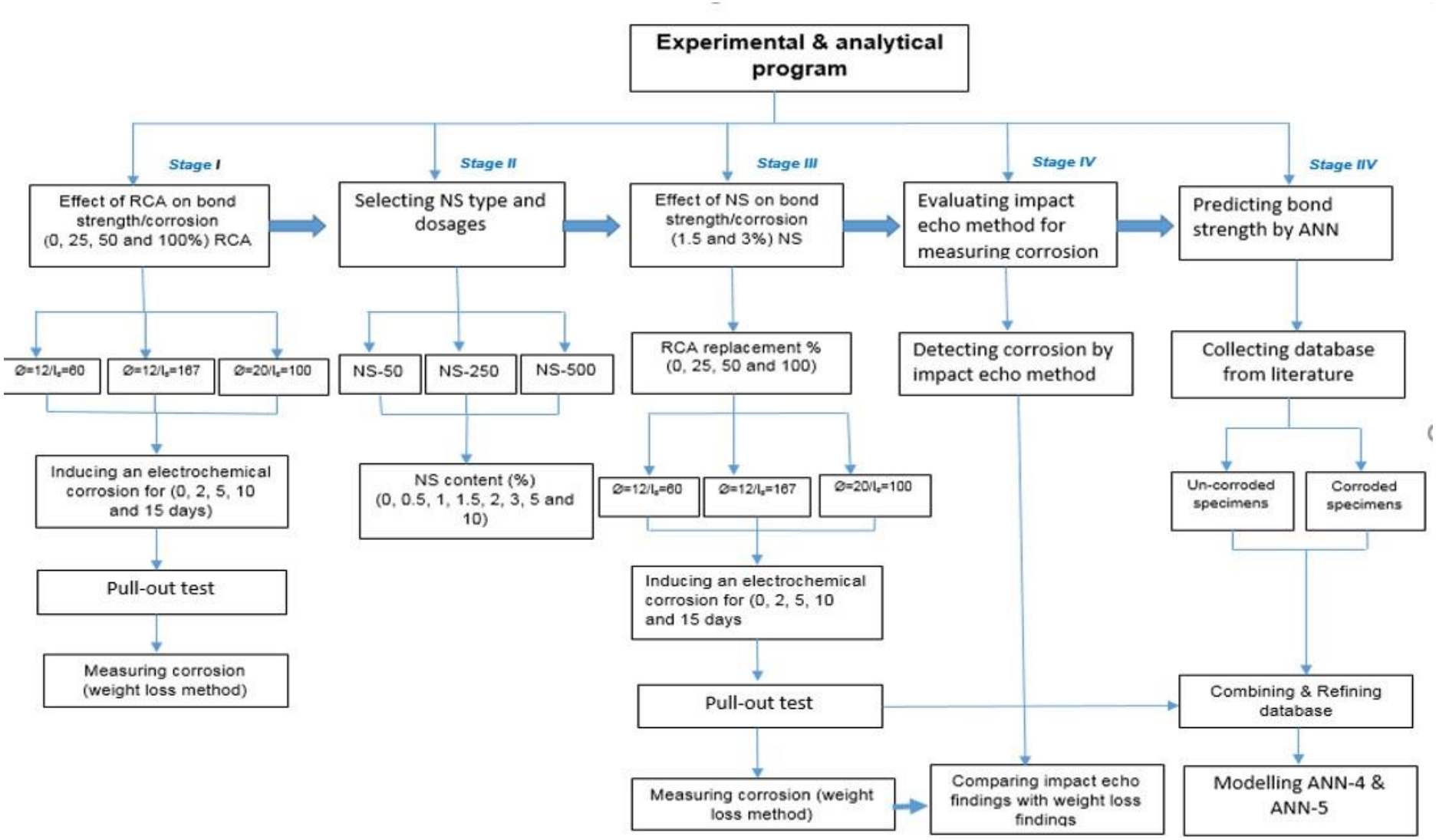

Figure 1.1 General overview of the experimental and analytical program.

Chapter two

Literature review

2.1 Introduction

This chapter introduces a comprehensive review and summary of the most valuable information related to the current research, which is mainly divided into seven main sections. It begins with a summary of corrosion mechanism, the main parameters affecting the corrosion resistance of reinforced concrete, the main methods of reinforcement corrosion measurements and the techniques used for preventing corrosion in reinforced concrete. The second part explains the fundamental of bond mechanism and the influence of corrosion on bond strength and other main influencing parameters as well as the methods of measuring bond. The relevant instigations of using recycled aggregate as a replacement to normal aggregate in concrete will be described in the third part. The fourth part of this chapter describes the characteristics of nano silica (NS) and its effect on concrete when it is used as a cement replacement. The fifth part discusses the available studies related to the effect of nano silica on the properties of RCA concrete. The sixth section demonstrates the use of Artificial Neural Network (ANN) in predicting the properties of reinforced concrete, while the conclusion of this chapter will be found in the last section.

2.2 Principles of corrosion of reinforced concrete

The durability of concrete can be highly deteriorated by the occurrence of several phenomena such as alkali-aggregate reaction, sulfate attack and freeze-thaw etc.

Whilst such phenomena mainly cause degradation to concrete, corrosion is recognized as the main cause of degradation in reinforced concrete. Three main consequences can be potentially resulted from corrosion phenomenon, namely the cross-section reduction of the steel bar, the creation of a weak layer at the interface of steel-concrete, and volumetric expansion of corrosion products. These consequences might lead to generating internal tensile stresses, causing a loss in bonding, followed by cracking, spalling, which in turn significantly affect the load-carrying capacity, and thus, the service life of reinforced concrete structure would be shortened. The consequences of these effects are presented in Figure 2.1, and the main aspects related to corrosion phenomenon are explained in the following sections.

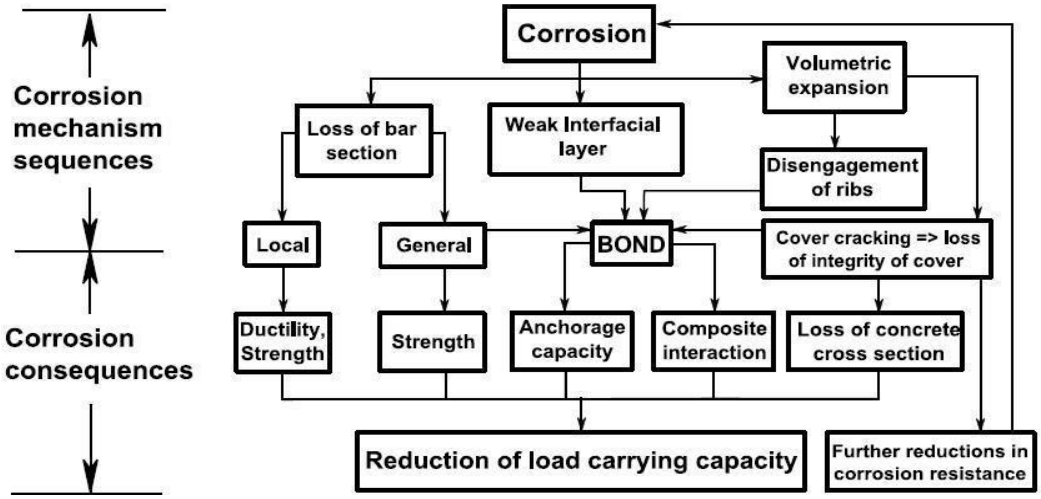

Figure 2.1 Effects of reinforcement corrosion on concrete performance (Vidal et al., 2004).

2.2.1 Mechanism of corrosion in reinforced concrete

Reinforcement corrosion in concrete is an electrochemical process including two main reactions, namely oxidation, and reduction reactions. Corrosion process cannot happen without completing the electrochemical cell which consists of an electrolyte (moisture in concrete), anode, cathode and electrical connection between anodes and cathodes to permit the electrons to move through the cell (the body of reinforcement).

Anodes and cathodes can be found on the same steel bar which is called as micro-cell corrosion or it can be located on different bars and connected electrically through tying by metals, which is known as marco-cell corrosion. A schematic of corrosion process is shown in Figure 2.2. The process of corrosion happens by two opposite reactions: anodic and cathodic reactions. Oxidation (anodic) reactions occur at the anode where the electrons are lost through the chemical reactions and move into cathode site as ferrous ions [Eq. (2.1)].

$$Fe \rightarrow Fe2^{+} + 2e^{-} \quad (2.1)$$

At cathode site, the electrons are gained from dissolved steel atoms due to the oxidation at the anode react with oxygen and water available inside concrete pores, forming hydroxyl ions as shown in Eq. (2.2)

$$2e^{-} + H_2O + 1/2O2 \rightarrow 2OH \quad (2.2)$$

Hydroxyl ions react further with iron ions to produce ferrous hydroxide which is known as rust [Eq. (2.3)].

$$Fe2^{+} + 2OH^{-} \rightarrow Fe(OH)_2 \quad \text{(ferrous hydroxide)} \quad (2.3)$$

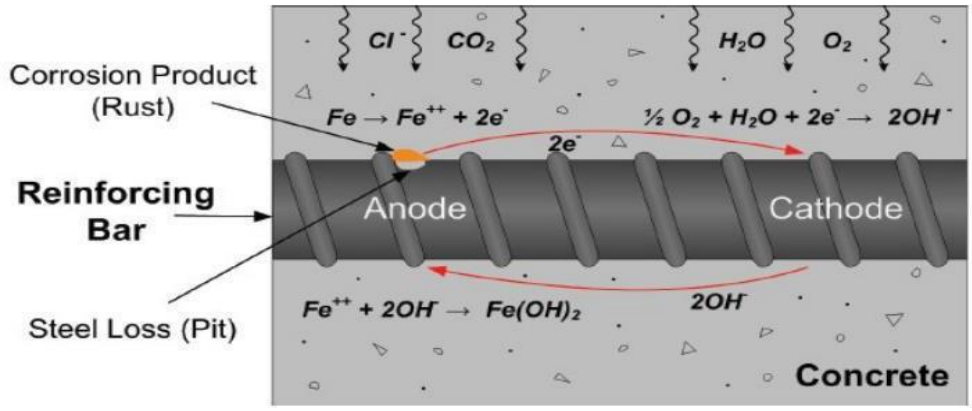

Figure 2.2 Schematic illustration of the corrosion of reinforcement in concrete (Ahmad et al., 2003).

With the availability of water and oxygen, reinforcing steel continues its oxidation from $Fe(OH)_2$ and form further rust [Equations. (2.4), (2.5)].

$$4Fe(OH)_2 + H_2O + O2 \rightarrow 4Fe(OH)3 \quad \text{(Ferric hydroxide)} \quad (2.4)$$

$$2Fe(OH)_2 \rightarrow Fe_2O3.H_2O + H_2O \quad \text{(Hydrated ferric oxide)} \quad (2.5)$$

Gamma ferric oxyhydroxide more impermeable compound that can be produced from the oxidation of ferrous hydroxide in the high level of pH [Eq. (2.6)].

$$2Fe(OH)_2 + 1/2O2 \rightarrow 2\gamma + FeOOH + H_2O \quad (2.6)$$

With the high alkalinity of concrete, those products form a very thin passive film on the steel surface to protect steel bars from corrosion as long as chloride and carbon ions are absent (Montemor et al., 2003). Many studies have been carried out on the nature of this stable layer. For instance, Hansson (1984) found that Fe2O3 and Fe3O4 are the main reasons of passivation of this layer, whilst Mehta & Monteiro (1993) suggested that gamma ferric oxyhydroxide is the main responsible for the stability of this film. Other researchers found that Ca(OH)2 steel layer passivity (Page & Treadaway, 1982). The main corrosion products (rustiness) are demonstrated in Figure 2.3, and their volume might occupy up to six times of original steel volume. This expansion could lead to tensile stress in concrete followed by cracking, spalling and reducing bond strengths between steel and concrete, which may cause the failure of reinforced concrete structures (Andrade & Alonso, 2001). The passivation of the reinforcement steel layer can be broken down by two different mechanisms: carbonation and chloride ingress, or it can be destroyed by the combination of both.

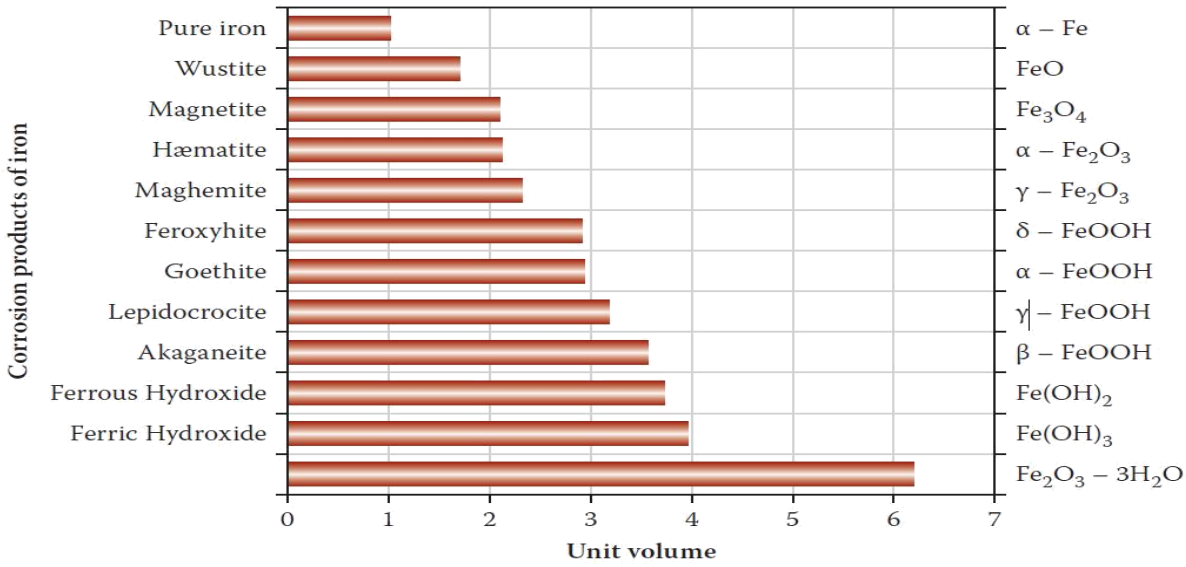

Figure 2.3 Corrosion products of iron (Jaffer & Hansson, 2009).

2.2.1.1 Carbonation induced corrosion

Carbonation is a process that can occur in reinforced concrete when carbon dioxide diffuses through concrete and dissolves through pore solution, producing carbonic acid [Eq. (2.7)], which, in turn, acts to neutralise the alkalis in concrete, and then it may react with calcium hydroxide forming calcium carbonate and water [Eq. (2.8)].

$$CO2 + HO2 \rightarrow H2CO3 \quad (2.7)$$

$$Ca(OH)3 + H2CO3 \rightarrow CaCO3 + 2HO2 \quad (2.8)$$

Once calcium carbonate is formed, the pH of concrete pore solution decreases to less than 9.0 (which typically ranges between 12 and 13.6), and as a result, a stable layer on the steel surface is de-passivated and the corrosion process is initiated (Ann et al., 2007). Several studies focused on the limitations of pH that affect the passive layer. Mehta & Monteiro (1993) reported that as long as the pH of pore solution concrete above 11.5 and chloride ions are absent, the passive film is stable. Another study by Berkely & Pathmanaban (1990) recorded that pH value 9.5 is the critical limit that initiates corrosion process.

2.2.1.2 Chloride induced corrosion

The riskiness of corrosion due to chloride ions is more common and dangerous than that resulting from the carbonation. Chloride can be introduced to concrete in different ways, it can be found in concrete constituents such as contaminated aggregates, polluted water, or from external sources such as seawater spray and de-icing salts. According to Winston (2000), complex ions (FeCl3) are formed when Cl ions oxidise steel and draw unstable ions into pore solution. Afterwards, they react with hydroxyl ions forming ferric hydroxide (Fe(OH)2) which releases Cl ions again to consume hydroxyl ions as shown in Eq.(2.9) & (2.10).

$$2Fe + 6Cl^- \rightarrow 2FeCl3^- + 4e^- \quad (2.9)$$

$$FeCl3^- + 2OH^- \rightarrow Fe(OH)2 + 3Cl^- \quad (2.10)$$

Simultaneously, electrons move into the cathode areas of steel surface, whilst chloride ions are accumulated causing a reduction in the value of pH and initiating corrosion process.

Alternative ways for chloride ions to form other products are seen in following reactions:

$$Fe^{2+} + 6Cl^- \rightarrow FeCl_6 + 4e^- \quad (2.11)$$

or

$$Fe^{3+} + 6Cl^- \rightarrow FeCl_6 + 3e^- \quad (2.12)$$

The reaction in Eq (2.12) leads to removing ferrous ions (Fe^{3+}) from cathode site and deposing them away from steel as demonstrated in Eq. (2.13).

$$FeCl6 + 3e^- + 2OH^- \rightarrow Fe(OH)2\ 6Cl^- \quad (2.13)$$

Through the latter reaction, rust can be produced, and further reactions may happen when chloride ions are liberated to react with ferrous ions (Winston, 2000). In the presence of water and oxygen, the risk of corrosion is escalated by increasing the chloride content in concrete, especially at steel surface exceeding a certain amount which is known as a chloride threshold value (Ann & Song, 2007). Owing to the high number of parameters that may influence chloride threshold value such as pH, w/c ratio and capillary structure, there is a difficulty to universal value applicable to all structures, but it generally can be stated between 0.15% and 0.6% by weight of cement for all reinforced concrete applications (Lounis et al., 2004)

The development of corrosion in reinforced concrete is typically divided into two main separate phases: initiation and propagation phase. However, The JSCE standard specifications for concrete structures (JSCE, 2007) classified the service life of structures exposed to corrosion into four stages, namely initial stage, propagation stage, acceleration stage and deterioration stage as demonstrated in Figure 2.4. During the first period, a sufficient amount of chloride ions reach steel surface, causing a de-passivation of stable film located on the steel surface, and initiating the process of corrosion. This phase is governed by several factors (e.g. concrete cover thickness, exposure conditions and reinforced steel properties). The propagation stage is described as the period time from the onset of corrosion to the appearance of cracks. In this stage, corrosion products create tensile stresses on the surrounding concrete owing to the increase of the volume of corrosion products, which ultimately causing concrete cracking. In the third phase, cracks enhance the transportation process of water and chloride in concrete, simultaneously, cracks become wider and interconnected, and leading to higher corrosion than found in the propagation phase. The appearance of cover spalling is considered as an indicator of the deterioration

phase. In this stage, the collapse of structures could happen at any time (Akiyama et al. 2014).

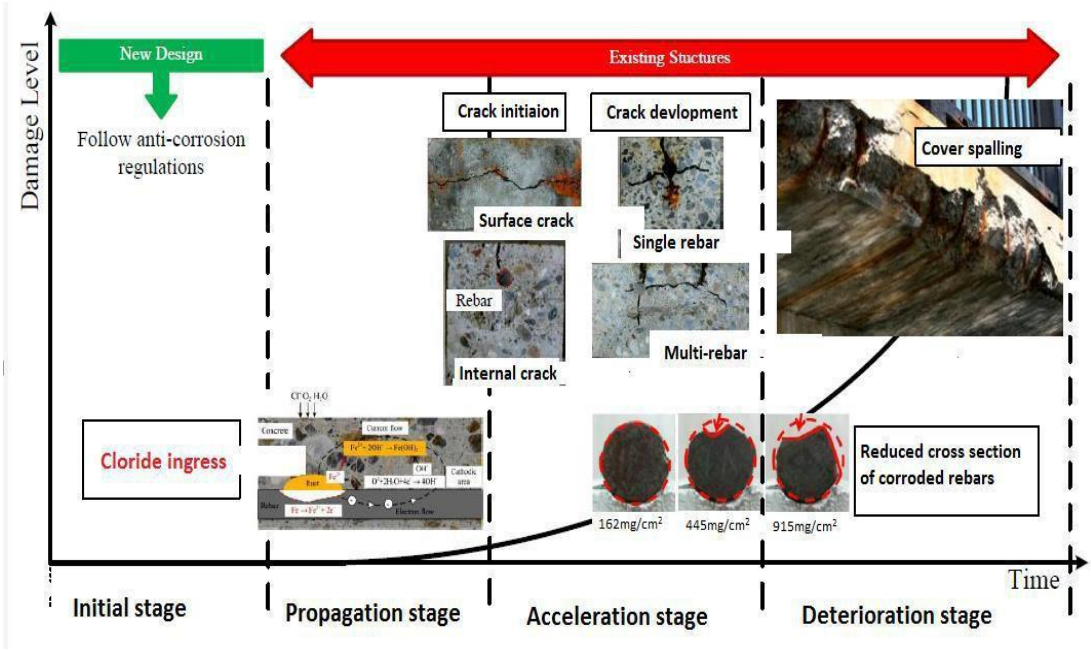

Figure 2.4 Service life of structures subjected to corrosion process (JSCE, 2007).

2.2.2 Factors affecting the corrosion of reinforced concrete

Corrosion in reinforced concrete is a complicated process, and it is governed by a large number of internal and external factors. Internal factors are those tied to the structure such as steel structure, surface condition, concrete cover and components, and the presence of cracks. The external factors are those associated with the exposure conditions such as temperature and moisture. The influence of some of those factors is briefly summarised in Table 2.1.

Table 2.1 Parameters affecting corrosion process.

Parameter	Effect	References
Concrete components	The ability of cement to bind chloride ions in the matrix is dependent on the content of C_3A in cement. The higher C_3A, the better binding capacity. Using lower w/c and supplementary materials can directly minimise the pores in concrete to be less interconnected, and hence reducing the possibility of corrosion. Admixtures can effectively enhance concrete durability in different ways; increasing chloride binding, reducing permeability and promoting threshold chloride value.	Webster, (2000)
Concrete cover	The larger concrete cover, the longer time for chloride ions to reach reinforcements.	Gonzalez et al., (1992)
Relative humidity	Moisture is initially needed for cathodic reactions and for the rust to be formed at the anode. It was reported that corrosion cannot occur if humidity is less than 35%, and even at high humid environments due to the lack of oxygen. It is stated that the diffusion rate of oxygen in concrete reduces as relative humidity (RH) increases. The rate of corrosion mostly reaches the peak at moderate humidity	Geng et al., (2009); Bai et al., (2011); (López & González, 1993).
Temperature	Resistivity is controlled by the internal relative humidity, and the Anodic and cathodic reactions would be faster at higher temperatures with increasing the temperature, accelerating the accumulation of corrosion products on the steel surface. It is found that the increase of temperature by just 10ºC can lead to doubling the corrosion rate when other conditions are the same. However, resistivity probably rises with increasing temperature, which might partially cancel the increase of reinforcement potential.	Schiessl & Raupach (1994)
Cracking	Cracks allow chlorides to be easily reached at reinforcement. Corrosion can be affected by cracks in different ways such as crack width, crack geometry and crack depth. The width of crack may accelerate the corrosion process during the initiation phase, while there is still controversy about the influence of cracks on corrosion propagation. It is found that the depth of cracks is more important than the width especially with longer duration of exposure. The maximum allowable crack width is associated to the exposure condition and it differs from code to code. For example, under harsh environments, BS 8110 (1997) and ACI 318 (1994) prescribed the maximum allowable surface crack width 0.30 and 0.15 mm, respectively.	Otieno, (2010); Vidal et al, 2004); Audenaert et al (2009)

2.2.3 Corrosion acceleration

Corrosion of reinforced concrete is a very slow process under natural conditions and it might take tens of years to occur, which cannot be afforded in laboratory tests, and therefore researchers find the necessity to accelerate corrosion process to obtain the

required damage in a short time. Unfortunately, standard procedures to shorten laboratory corrosion tests in RC specimens are not available, however, three techniques have been applied in research laboratories, namely wet/drying technique, artificial climate environment technique, and impressed current/voltage.

Impressed current is the most common technique for producing corrosion artificially, since the level of corrosion and the needed testing time for accelrating corrosion can be controlled by modifying either the applied current or voltage. Current density in natural corrosion typically ranges between 0.1and 10 mA/cm^2, and it might reach 100 mA/cm^2, where cracked concretes submerged in seawater (Andrade & Alonso, 2001). In the impressed current /voltage technique, great varying levels of current density have been stated in the literature, ranging between 45 and 10400 mA/cm^2, however, between current density between 200 and 3000 mA/cm^2 is typically used to speed up the laboratory test. The effect of such differences on the performance of RC members is still not fully understood. Chlorides are mostly used to speed up laboratory tests by providing electrical contact between the cathode and the anode with a level of concentration ranges between 3-5% to simulate the concentration of salt in seawater (almost 3.5%). Chlorides can be either mixed with concrete components as by weight of cement before casting (Mangat & Elgarf, 1999; El-Maaddawy & Soudki 2003), or it can be immersed in tanks containing a NaCl solution (Cabrera 1996; Cairns et al 2008), however, the former procedure is not highly recommended since the de-passivation of reinforcement would immediately occur and time for passivating does not exist (Poursaee & Hansson, 2009).

Whilst the reinforcement embedded in concrete is used as an anode, metals have good electrical conductivity (e.g. Copper, stainless steel and titanium) have been used as a cathode. The anode may be embedded in concrete, and therefore hydroxyl ions

are produced inside concrete, and move to the anodic sites (El Maaddawy et al 2005b; El Maaddawy & Soudki 2003; Badawi & Soudki 2005), or it can be externally placed on the surface of specimen (Malumbela et al 2009; Ballim et al 2001). It should be noted that the rust produced by this technique is not fully simulative to that occurs in nature due to the difference in the electrochemistry behind the mechanism, in addition to the possibility of inducing more uniform corrosion along the surface of steel bar than that achieved under a natural environment (Ahmad, 2009). A summary of some of the previous techniques used for inducing corrosion is presented in Table 2.2.

Table 2.2 Summery of some previous accelerated corrosion procedures.

Current (mA)/ (Voltage (V))	**Current density ($\mu A/cm^2$)**	**Cathode type**	**Corrosion environments**	**Reference**
0-2000	1214	External stainless steel plates.	Immersing in 5% NaCl solution.	Fang et al (2004)
-	45	Internal stainless steel bars.	Concrete mixed with 2% NaCl and specimens subjected to 2½-day wet and 1day dry cycles in 3% NaCl solution	Bonacci et al. (1998)
Varied	76 - 674	External stainless steel plates.	Concrete mixed with 2% NaCl and specimens immersed in 5% NaCl solution.	Cabrera (1996)
(15 - 60 V)	Varied	Internal stainless steel bars.	Concrete mixed with 3% NaCl.	El Maaddawy et al (2006)
1500	2000- 3000	External stainless steel plates.	Concrete mixed with 2% NaCl and Specimens immersed in 5% NaCl.	Azad et al (2007)
400	10400	External stainless steel plates.	Immersing in 3% NaCl solution.	Almusallam et al., (1996)
(6V)	600	External steel meshes.	Immersing in 3% NaCl solution.	Phillips (1991)
1000	2000	External copper plates.	Immersing in 3% NaCl solution.	Lee et al., (1996)
Varied	2000	External stainless steel plates.	Immersing in 3.3% NaCl solution.	Al- Suiaimain et al (1990)
(13V)	1087	External steel meshes	Immersing in 5% NaCl solution.	Kearsley & Joyce, (2014)

2.2.4 Measurements of reinforcement corrosion

Corrosion rate can give details on the level of corrosion in reinforced concrete as it can give an early warning about the damage inside concrete structures, and hence the method of treatment could be efficiently determined. The rate of corrosion can be measured by various techniques such as weight loss method or non-destructive methods including electrochemical methods, elastic wave methods, electromagnetic method, infrared thermography and optical sensing method. While the last three methods are still new in corrosion field, the electrochemical method is the most adopted in measuring corrosion in reinforced concrete, particularly half-cell potential and linear polarization resistance (LRP) technique. Half-cell potential is supposed as the easiest way of measuring corrosion among electrochemical methods, this method cannot measure the corrosion accurately compared to LRP, it can just indicate the existence and the level of corrosion. However, corrosion can also be measured electrochemically by other techniques including galvanostatic pulse technique, resistivity method, electrochemical noise, and potentiodynamic polarization curve. Weight loss method is still the most common practical technique in measuring the corrosion in concrete. This probably owing to the simplicity of this method, in addition to its efficiency in determining the actual corrosion rate in reinforcement. However, the amount of corrosion cannot be measured at different periods of concrete age, it just can be determined at the end of the test period (Zaki et al., 2015).

Measuring corrosion rate by elastic wave methods can be achieved by one of three techniques including impact echo (IE), acoustic emission (AE) and ultrasonic pulse velocity (UPV). IE method has been used to detect the development of micro-cracks, however, in recent years this method is being developed to detect the occurrence and position of corrosion in reinforced concrete. Samarkova et al., (2014) reported that the

dominant frequency in the response signal is the main key to revealing information for detecting corrosion and internal defects in concrete, making it a simple and fast technique, however, only a limited number of research can be found regarding this method. The UPV method measures the speed of sound through concrete by propagating ultrasonic waves, even with large thicknesses, however, the evaluation of UPV results needs an expert to analyse the results. Moreover, more investigations are required to be developed since measuring mechanical properties is the main application for this technique. Acoustic emission is a cost-effective technique that can detect corrosion in the early stages by generating elastic waves, especially with active defects, while passive defects cannot be easily recognised (Zaki et al., 2015). A brief summary of the principle of these methods is presented in Table 2. 3.

Table 2.3 NDT methods for evaluating corrosion in RC structures.

NDT Methods	Principles	Corrosion index	Reference
1. Electrochemical Method			
Half-Cell monitoring	The value of electrical potential is measured between the reference electrode and steel reinforcement.	Potential level (mV or V)	Assouli et al., (2008)
Resistivity method	Resistivity is measured when the current pass between cathode and anode areas of the concrete.	Resistivity (Ω·cm)	Polder et al., (2000)
Polarization resistance	The variations in potential during corrosion reactions are recorded by an electrode plate placed on the surface of concrete.	Corrosion current (Icorr(A/cm^2))	Sadowski (2010)
Galvanostatic pulse method (GPM)	The anodic current pulse is galvanostatically applied from a counter electrode placed on the surface of concrete.	Potential resistance (Rct (kΩ·cm^2))	Elsener et al., (1994)
Electrochemical noise (EN)	EN characterizes the fluctuations of potential and current produced by corrosion reactions.	Noise resistance (Rn (kΩ·cm^2))	Mansfeld et al., (2001)
2. Elastic Wave Method			
Ultrasonic pulse velocity (UPV)	Mechanical energy (stress waves) are propagated through concrete, and transformed into electrical energy using a transducer.	Pulse velocity (V)	Li et al., (2014); Aggelis et al., (2010)
Acoustic emission (AE)	Elastic waves are created when rapid energy from a localised source is released within RC structures.	AE parameters	Mangual, et al, (2013); Yu et al., (2014)
Impact echo (IE)	Stress waves are propagated through impact load and vibrations within RC structures.	Wave velocity (Vp)	Samarkova et al., (2014)
3. Electromagnetic Method			
Ground penetrating radar (GPR)	Transmission of electromagnetic wave velocity (EM) into RC structures is still under investigation.	EM wave velocity (V)	Hong et al., (2012)
4. Optical Sensing Method			
Fiber Bragg grating (FBG)	The shift in the wavelength of fiber Bragg grating (FBG) measures the development in fiber strains with the increase of cross-section of corroded steel in RC structures.	Bragg wavelength (λB)	Geng et al., (2009); Gao et al., (2011)
5. Infrared Thermography Method			
Infrared thermography (IRT)	Infrared thermography radiation released by the material of concrete is transformed into an electrical signal, and used to produce maps of the surface temperature.	Radiation power (E)	Baek et al., (2012); Kwon, et al., (2011)

2.2.5 Strategies for improving the corrosion resistance of reinforced concrete

Corrosion is a costly issue from both ways: repairing or delaying the productivity of the structure as well as it can affect structure safety (Jung et al. 2003). According to a recent study executed by the National Association of Corrosion Engineers in the

USA (NACE) in 2017, the annual global cost of corrosion is approximately $2.5 trillion, representing about 3.4% of the global Gross Domestic Product (GDP). Hence, various approaches have been adopted to enhance corrosion resistance by delaying the onset of corrosion and prolonging the service life of these structures. Many effective methods are being used to increase the durability of reinforced concrete against corrosion. The use of mineral admixtures in concrete as a replacement to cement is one of the successful solutions (e.g. fly ash, GGBS, silica fume and metakaolin) (Song et al., 2010; Thomas et al., 2008). This is owing to the low cost of these materials and ease of use, whilst the main role of these admixtures in terms of durability is reducing the permeability of concrete.

Corrosion in reinforced concrete can be delayed by coating the steel bars by some materials that can prevent the chloride ions or carbon dioxide from reaching steel bars. These materials can be dipped, painted or sprayed on the steel. Epoxy coating, enamel coating and hot-dip galvanizing are the most famous ways of this method. These coatings are working as barriers preventing the aggressive agents reaching steel surface. In terms of corrosion resistance, the use of epoxy-coating achieves better performance than the others, however, the bond performance between epoxy-coating bar and concrete is considered less than that found with conventional steel. On the other hand, the zinc coating can work as a sacrificial and barrier to steel bars, but the main issue associated with using it is the ability of zinc metal to corrode over time (Revie et al., 2011).

Corrosion resistance can also be enhanced by adding corrosion inhibitors to concrete mixtures (e.g. calcium nitrate and zinc oxide). The effectiveness of inhibitors mechanism in concrete involves extending the initiation time of corrosion by raising

the chloride threshold value, and a formulation of coating which can passivate a layer on steel surface for a long time (Tang et al., 2015). Instead of conventional steel, stainless steel is utilized for protecting the structures from corrosion. It was found that the chloride threshold content of stainless steel ranging between three to five times higher than conventional steel. The main obstacle faces this method is the high cost of stainless steel compared to other methods, however, many attempts are still being done to reduce the cost of this material. Fibrous composites are usually produced from carbon and stable glass to be used as reinforcement, while polymers are used as a matrix. These materials can effectively reduce corrosion, however, those composites are very expensive and highly sensitive to temperature (Tang et al., 2015). Cathodic protection is a widespread technique applied for the structures located in severe weather or marine environments to prevent them from corrosion. This approach is classified into two kinds: sacrificial anodes system and impressed current system. The mechanism of the former can be simplified by connection the steel bars to another metal that easily to corrode such as zinc or magnesium to act as an anode, allowing those sacrificial metal to be corroded instead of steel reinforcement. The latter protection system is composed of anodes connected to a DC power source, and it is mainly used for large structures or where electrolyte resistivity is high, however, the installation of this method is relatively expensive compared with others (Cheung & Cao, 2013). In recent years, nanomaterials are getting a widespread interest when they utilized in concrete as a replacement material to cement to enhance the durability and mechanical properties of concrete. Amongst those materials, nano silica is considered the most common one that significantly improved the performance of reinforced concrete against corrosion.

2.3 Fundamentals of bond strength

Adequate bonding between concrete and reinforcing steel is essential for achieving a satisfactory performance of reinforced concrete structures. Bond at the interface of steel-concrete can be simply defined as the shear stress distributed over the surface of the embedment length of reinforcement to assure the composite action of RC members (Cairns &Abdullah, 1996). The interfacial bond behavior is highly related to the durability and serviceability aspects of the structures such as deformation capacity, load carrying, crack distribution and stiffness of RC elements (CEB FIB, 2000).

2.3.1 Bond mechanism of reinforced concrete

The mechanism of bond strength indicates to transferring the forces between steel bars and concrete surrounded (Amleh & Ghosh, 2006). Bond behaviour is mainly determined by three primary mechanisms: chemical adhesion, friction and mechanical interlock. Each one of these contributes to the overall bond behaviour in varying degrees depending on the type of steel bar (ACI 408, 2003). While adhesion and friction are more significant in concrete contains plain bars (FIB, 2000), the mechanical interlock is the main mechanism in concrete containing deformed bars (Bamonte and Gambarova, 2007). Adhesion is a chemical bond forms at a steel-concrete interface at the initial loading, and it is dependent on the roughness of steel and concrete components. It could be collapsed at a small load force owing to the shrinkage or the action of the service loads (Momayez et al., 2005). It is assumed by ACI 408 (2003) that the bond strength formed due to adhesion is between 0.48 to 1.03 MPa. Once adhesion is broken down, friction resistance arises due to the roughness of steel/concrete interface, before the bearing capacity at steel is totally transferred. Friction is mainly dependent on the size and the shape of aggregate as well as the surface characteristics of steel bars (Momayez et al., 2005). It is estimated that up to

35% of the ultimate bond strength could be acquired by a friction mechanism (ACI-408, 2003). Mechanical interlock (wedging effect) is enhanced for deformed bars by the geometry of the ribs along the length of the bar. Bearing against lugs is considered as the main transfer mechanism at higher load levels. The force transfer mechanism is mainly influenced by the mechanical interlocking between the ribs of steel and concrete. When the ultimate bond strength is reached, shear cracks are formed between ribs as interlocking force inducing large bearing stresses around the ribs, and causing the occurrence of the slip. Hence, the ribs restricted the slip movement by bearing against concrete (Wang & Liu, 2003). The mechanism of the bond in reinforced concrete is demonstrated in Figure. 2.5.

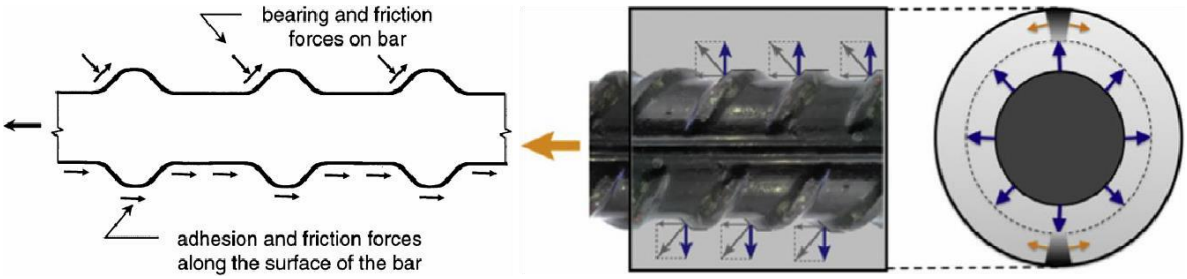

Figure 2.5 Bond mechanisms generated at the rebar–concrete interface (ACI-408, 2003).

2.3.2 Bond failure mechanism

The bond strength is significantly affected by the age of concrete especially in the first three days after casting, and it increases faster than compressive and tensile strengths at these days (Dohou et al ., 2009). Bond failure generally can be shown in two modes, pull-out failure and splitting failure based on some factors such as bonded length and confinement levels. In pull-out failure, reinforcing bar is pulling out from concrete without rupturing reinforcement or crushing concrete by shearing of the interface between reinforcement and surrounding concrete. This mode of failure takes place

when radial forces generated from reinforcement are less than the resistance of concrete, whilst tangential forces are higher. In other words, more energy is required by splitting cracks to reach the outer concrete surface Bond failure typically happens when the reinforcement is adequately confined by a large cover or transverse reinforcements. Specimens can also be pulled out with shorter embedment lengths or those having low strength (ACI 408, 2003). In the case where the cover is relatively small or the concrete is unconfined properly, splitting failure is mostly dominant. Splitting failure occurs due to the radial stresses causing the longitudinal and perpendicular splitting of the concrete surrounding the steel bar, since the concrete cover is not sufficient to resist the pressure, and splitting cracks generate at steel/concrete interface. In other words, it occurs when tensile stresses reach or exceed the tensile strength of concrete, causing a sudden loss in bond stress.

2.3.3 Bond stress – slip behaviour

The relationship between bond stress and slip has a significant influence on the flexural and bending deformation capacity of reinforced concrete structures. Several models have been developed based on the experimental findings to predict the bond stress–slip relationship of reinforced concrete. The BPE Model introduced by Eligehausen et al. (1983) is commonly known as the fundamental model for analysing the bond stress-slip relationship. Afterwards, this model was adopted and developed by the famous model (CEB-FIP,1990) to include the case of splitting failure as well, considering several parameters (i.e. the peak bond stress), the slip corresponding to the peak bond stress, 1, 2, 3, α and β) as shown in Table 2.4.

Table 2.4: Parameters for bond-slip model CEB-FIP Model.

Parameters	Not confined concrete		Confined concrete	
	Bond conditions		Bond conditions	
	Good	Others	Good	Others
1	0.6 mm	0.6 mm	1.0 mm	1.0 mm
2	0.6 mm	0.6 mm	3.0 mm	3.0 mm
3	1.0 mm	2.5 mm	rib spacing	rib spacing
α	0.4	0.4	0.4	0.4
	—	—	—	—
(s)	0.15	0.15	0.40	0.40

According to CEB-FIP Model, the curve bond-slip is composed of different parts based on the influence of some factors such as the strength of concrete, bond conditions and confinement level as presented in the following formulas and Figure 2.6.

$$\tau\ (s) = \tau_{max} \left(\frac{S}{S_1}\right)^{\alpha} \quad \text{for} \quad 0 \le S \le S_1 \qquad (2.14)$$

$$\tau\ (s) = \tau_{max} \quad \text{for} \quad S_1 \le S \le S \qquad (2.15)$$

$$\tau\ (s) = (\tau_{max} - \tau_f \left(\frac{S-S_2}{S_3-S_2}\right) \quad \text{for} \quad S_2 \le S \le S_3 \qquad (2.16)$$

$$\tau\ (s) = \tau_f \quad \text{for} \quad S > S_3 \qquad (2.17)$$

where (s) is the bond strength; $_{max}$ is maximum bond strength; $_f$ is ultimate bond strength and is ultimate displacement.

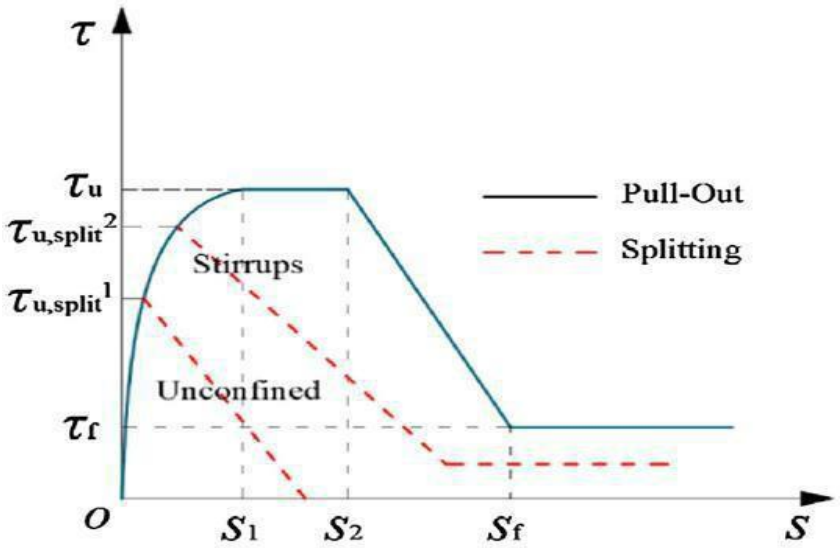

Figure 2.6 Analytical relationship of Bond stress-slip developed by CEP-FIP Model.

On the other hand, research concerning the bond-slip curves of corroded reinforcements is very limited. Investigations done by Yuan et al. (2010) stated that the bond stress-slip model for corroded reinforced concrete is divided into five stages, namely micro-slip, slip, splitting, descending and frictional stage. The area for each stage is controlled by the rate of mass loss and the crack width. Kivell (2012) developed a model for corroded concrete relying on un-corroded steel model as presented in Figure 2.7 (b). On the other hand, a trilinear bond stress-slip model was developed by Feng et al., (2008) based on the regression analysis of database as shown in Figure 2.7(c). The ascending part in this model is very similar with that proposed by Kivell (2012), except for the absence of plateau line at the peak point, while the descending part does not provide any influence of corrosion. The model suggested by Loundgren et al., (2007) was mainly developed based on shifting CEP-FIP model for un-corroded specimens.

As can be seen from Figure 2.7, there is inconsistent amongst these models concerning the corrosion influence on the slip. For instance, Feng et al and Kivell models stated there is no influence of corrosion on the peak slip, whereas Lundgren et al. and Yuan et al presented a consistent decrease in the peak slip with the development of corrosion. On the other hand, Al-Sulaimani et al. (1990) and Mangat & Elgarf (1999) found an opposite phenomenon based on testing beam specimens as the peak slip tends to linearly increase with corrosion.

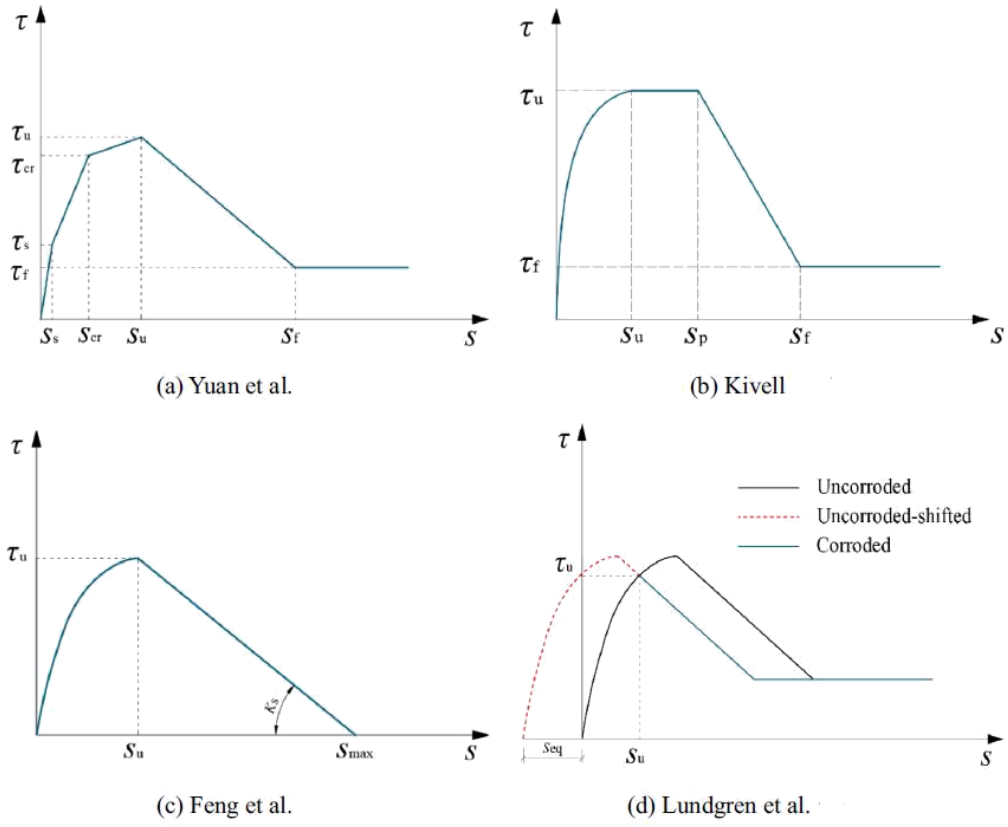

Figure 2.7. Bond-slip models for corroded steel bar.

2.3.4 Factors affecting bond strength

Extensive studies have been conducted to investigate the influence of the main parameters affecting the bond strength in RC members. These parameters are classified by ACI-408 (2003) into three major categories, namely structural characteristics, bar properties and concrete properties. The former group including factors as cover and bar spacing, the bonded length of the bar, and transverse reinforcement. The bar properties cover factors as steel geometry, bar size, steel surface conditions and steel stress, while the latter related to factors such as compressive strength, tensile strength, aggregate quantity and type, and the impact of admixtures. In recent years, reinforcement corrosion has been considered as a very significant parameter influence bonding in reinforced concrete, particularly at severe

environmental conditions. In the following, the effect of the most influential parameters controlling the performance of bond is discussed.

2.3.4.1 Effect of geometry of steel bar

It is generally recognised that the bond of deformed steel is much higher than smooth steel, since higher bursting forces are developed. This is mainly due to the mechanical anchorage in deformed bars that supplied from concrete keys amongst the ribs. Several studies were conducted to investigate the influence of the relative rib area (Rr) on bond behaviour. Bond index or the relative rib area can be defined as the projected rib area normal to the bar axis divided by the nominal bar perimeter multiplied by the centre to centre rib spacing (Metelli & Plizzari, 2014). It is stated that the ultimate load at failure enhanced by 24% when Rr is doubled from 0.08 to 0.16 (Hamad, 1996). The importance of bar geometry (i.e. rib spacing and rib height) lies in enhancing bond strength by assisting by preventing the concrete keys from sliding and enhancing the friction between steel and concrete. It has been confirmed that a minimum bond index is required to guarantee good bond strengths (ACI 408, 2003). Metelli & Plizzari (2014) deduced that when the bond index was doubled from 0.05 to 0.01, the bond strength enhanced by 30-40%. This enhancement owing to lower wedging action created by highly ribbed bars, causing a limitation of the longitudinal splitting crack width, reducing the possibility of bond failure. Conversely, this influence becomes less pronounced in unconfined specimens (ACI 408, 2003; El-Hacha et al., 2006).

2.3.4.2 Effect of bar diameter

It has been recognised that smaller bar diameters embedded in concrete can offer higher bond strength (Esfahani et al., 2013; Baena et al., 2009). This influence may probably be explained by increasing the volume of bleed water trapped pockets between the reinforcements and concrete voids, and therefore the contact area at a

steel-concrete interface would be reduced (Pour & Alam, 2016). However, the relationship between bond strength and diameter cannot always be appreciated as a longer bonded length is needed with increasing the diameter of reinforcement (ACI 408, 2003). On the other hand, the influence of bar diameters might be correlated with the confinement level either; concrete cover thickness or transverse confinement. Wu & Zhao (2013) indicated that bond strength developed with smaller bars when the ratio of cover to bar diameter less than or equal 3, whilst it would not be influenced not above this ratio. On the other hand, higher bond strength is expected for smaller bar diameters in the absence of confinement, whereas the bar influence almost disappeared with high degrees of confinement as reported by Ichinose et al., (2004). The importance of bar diameter might be less pronounced after exposure to highly corrosive environments. This phenomenon could be justified by the erosion of lugs which govern transferring the force between steel and concrete. Based on the author's knowledge, the influence of bar diameter having the same surface area using a pull-out test has not been found in literature, and therefore it would be interesting to examine this parameter in the current study using different types of concrete.

2.3.4.3 Effect of Embedment length

Embedment length is one of the main parameters that influence the bond strength of bars embedded in concrete. It can be generally said that even though the applied tensile load tends to increase with increasing the embedment length of reinforcement, the ultimate bond stress transferred to the surrounding concrete is significantly decreased. This mainly can be explained by increasing non-uniformly distribution of bond stresses along the embedment length of embedment, causing a reduction in the average bond stress (Pour and Alam, 2016; Benmokrane et al., 1996). This nonlinearity distribution of bond stresses is more obvious with longer embedment

lengths, and the tensile stresses decease quickly from the loaded end toward the un-loaded end (Tighiouart et al., 1998).

2.3.4.4 Effect of concrete strength

Bond strength is strongly affected by both tensile and compressive strength of concrete. This is because of the bond strength, in fact, relies on transferred stress between steel and concrete with shear and compression interaction forces. Arel & Yazici, (2012) tested the influence of concrete on bond behaviour using various compressive strengths ranging between 13.46 to 75.40 MPa. They stated that the bond strength is proportional to the square root of concrete strength in addition to affecting the mode of failure, agreeing with other findings (Esfahani& Rangan 1998; Darwin et al., 1992). Representing bond strength by $\sqrt{f'}$ has found to be adequate for concrete below 55 MPa while this normalisation would decrease for those having higher strength concrete (ACI 408, 2003).

The influence of concrete strength can be affected by reinforcement properties and the interaction with concrete (the specific combination of rib spacing and rib height) as indicated by Dahou et al., (2009). To clarify this, the ribs height and the ribs spacing are not exactly the same for different diameter bars, and the bond performance, in fact, is controlled by the blocking of the ribs in the concrete, which depends on compressive strength. Hence, the amount of concrete located between two ribs is lower for smaller Rr. Another factor that should be considered when studying the relationship between concrete strength and bond strength is the influence of concrete cover-steel diameter ratio (c/d) as illustrated by Yalciner et al., (2012). The outcomes obtained from various experiments stated that there the bond strength is proportional to compressive strength up to 3.2 c/d ratio, whilst this correlation was not obvious

above this ratio. For high-strength concrete, reducing in local slippage would presumably occur as reported by some authors (Zuo & Darwin 1998, 2000; Hamad & Itani 1998), as higher bearing capacity is produced to prevent the crushing of concrete keys.

2.3.4.5 Effect of concrete cover

The thickness of concrete cover rete is another key parameter can largely govern to bond behaviour. The increase of concrete cover depth can enhance the bond strength between reinforcement and surrounding concrete in addition to reducing splitting forces since more confinement to reinforcement can be provided before occurring the failure. For instance, Yalcier et al. (2012) tested three different concrete covers (i.e. 15, 30 and 45 mm) with two grades of concrete strength on bond strength. The results highlighted that the bond strength considerably developed by increasing concrete depth. However, this influence seems more sensitive to lower compressive strengths (w/c = 0.75) rather than higher ones (w/c = 0.45) as the bond increased by 43.7% and 6%, respectively, when the cover doubled from 15mm to 30 mm. A similar observation was reported by Lee et al. (2002) and Rashid et al., (2010) relationship between cover thickness and bond strength. The bond failure is also dependent on the depth of cover since the splitting failure can be delayed or prevented in the presence of sufficient concrete cover, whereas those having smaller covers are mostly be failed in pull-out mode, with taking into account the influence of embedment length.

2.3.4.6 Effect of reinforcement corrosion on bond strength

Several research studies have been conducted on the topic of bond degradation due to corrosion. Investigations conducted by Al-Suleiman et al., (1990) are the first work focused on this topic using pull-out and beam test with two parameters: corrosion level

and cover-steel diameter ratio. The outcomes highlighted an improvement in bond strength with low amounts of corrosion (up to 1% weight loss), whilst a significant reduction was measured above this value to record about 50% bond loss at about 5% diameter loss. This phenomenon was later confirmed by other researchers (Cabrera, 1996; Chung et al., 2008; Fang et al., 2004; Ouglova et al., 2008), but with different critical values. For instance, the results from testing cantilever beams under different levels of corrosion conducted by Almsallam et al., (1996) stated a development in bond up to about 5% mass loss. The enhancement bond rate reached up 17% before the bond being consistently decreased with the appearance of outer cracks to reach 80% bond loss at 10% in mass loss. This critical value is far from what was recently reported by Coccia et al., (2016) (0.6% mass loss). Increasing the bond resistance at the initial corrosion stage is likely attributed to the increase of the surface roughness of reinforcements due to the accumulation of corrosion products, causing a development in the frictional forces between reinforcements and the surrounding concrete. Increasing the volume of corrosion products can also lead to developing the radial pressure a steel-concrete boundary, enhancing the bond stress between reinforcements and surrounding concrete. Kivell (2012) stated a decrease in the mechanical bond components occurs even at the initial stage of corrosion, however, the increase in frictional components is more influential, and thence the overall bond is improved as shown in Figure 2. 8. However, the development in bond strength was not recognised with any level of corrosion in a recent study done by Law & Molyneaux (2017), whilst FIB (2000) linked the negative influence of corrosion with the appearance of visible cracks.

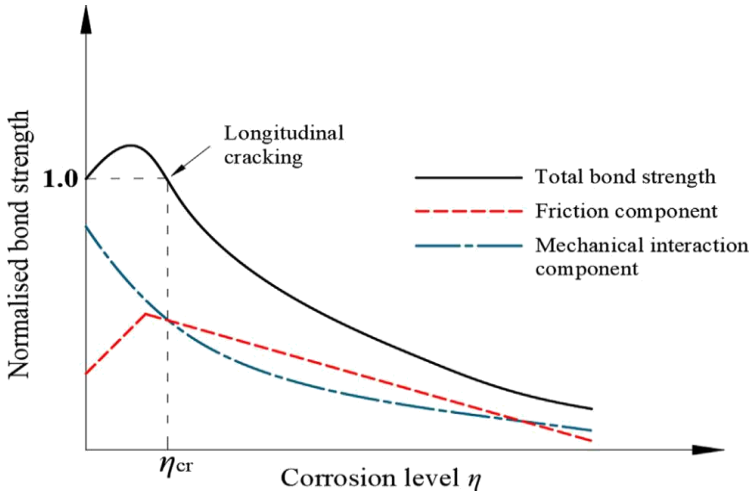

Figure 2.8 Variation of bond strength with corrosion level (Kivell, 2012).

On the other hand, the bond strength begins notably decreasing once the corrosion exceeds the extent value, and consistently decreases at the high levels of corrosion. This may happen due to the fact that the tensile capacity of concrete is almost exhausted, causing a formation of longitudinal cracks. Moreover, the ribs height subsequently drops up to be disappeared at serious corrosion. Nevertheless, it is not necessarily for cracks to be observed, even if reinforcements are severely corroded, which might be correlated to the difference in properties of concrete matrix mainly porosity. A wide experimental programme was applied by Frang et al., (2004) on both smooth and deformed bars, studying four different cases. In the case of un-confined deformed reinforcement, almost two-third of bond strength was lost at just 9% mass loss, whilst the confined specimens showed more ability to encounter the loss in bond and led to a gradual reduction in bond at high corrosion levels. An explanation may be that even though small cracks might have generated due to corrosion, the stirrups could provide enough confinement to prevent those cracks from extensions. This means that the bearing action of the ribs may lead to horizontal bearing and hoops stresses when the load is applied. Therefore, the tension due to cracks is reduced, causing a reduction in the confinement and leading to pull-out failure in most cases.

For unconfined smooth bars, the bond characteristics highly increased with small levels of corrosion to reach about 1.5 times at 2.4% mass loss compared to non-corroded bars, and then a sharp reduction occurred. In the last case, the bond strength enhanced for smooth bars confined by stirrups even with a relatively high degree of corrosion (almost 5% mass loss). In a different investigation, Abosorra et al., (2011) observed the appearance of deep grooves on the bar surface for specimens had high strengths. These grooves may be formed due to the ability of high compressive strengths to detain the rust in narrow areas, and therefore chloride penetration creates these grooves. In addition, using a common type of inhibitors (Calcium Nitrate) did not provide any bond enhancements for both low and high compressive strengths at low levels of corrosion. On the contrary, such inhibitor was highly beneficial to improve bond strength for both high and low compressive strengths at the higher corrosion stages. It can be concluded the bond strength is found to be enhanced at the initial stage of corrosion, whilst further corrosion can cause a significant loss in bond. The difference in the critical value might be ascribed to the difference in test set-up, the type of specimens and current applied to corrode the steel. Whilst high current densities can make corrosion process faster, the diffusion of corrosion products through the steel-concrete interface would be obstructed. However, the performance of the bond looks almost the same when the steel bars being highly corroded.

2.3.5 Methods of bond testing

Even though different types of tests have been used for measuring the bond between steel and concrete, they can be generally classified into two methods, namely pull-out tests, and beam tests. Direct pull-out test is a very effective method used in the laboratories as it is a relatively simple and cost-effective method. This method does not always provide the actual bond existed in the real designed structures, since the

steel bar is pulled in tension, whereas the adjacent concrete would be under compression due to a bearing plate, causing a reduction in cracks formation, and thus increasing the bond strength. However, the results would be accepted and very useful for comparative purposes and studying the impact of different parameters and materials on bond behaviour. One of the earliest set-ups for pull-out test was suggested by Rehm (1961) as shown in Figure 2.9 (a). The same test arrangement has been adopted in many experimental investigations with some modifications to diminish the shortcomings in the test such as the additional confinement provided due to the friction generated between specimens and the bearing plate as it can develop the arch-effect in the centre of the specimen. Therefore, RILEM/CEM/FIP standard recommended using rubber plate between the bearing plate and the concrete block to minimise the friction effects, in addition to moving the embedment length away from the centre of the specimen as presented in Figure 2. 9(b). Details of pull-out test method suggested in some standards and by some researchers are illustrated in Table 2.5. During pull-out test, the bar bonded in concrete is strained at one end due to the tensile load, while the other end is kept unloaded. The tensile loads and the displacement generated between steel and surrounding concrete are measured by linear variable displacement transducers (LVDTs)

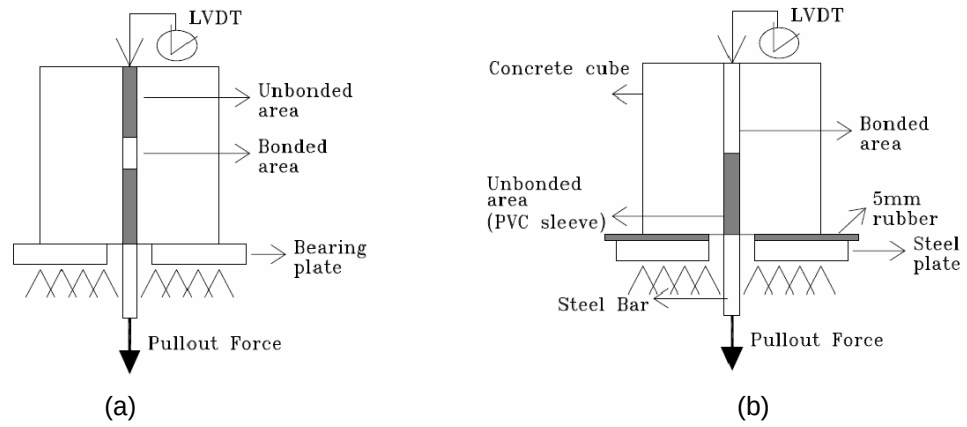

Figure 2.9 Typical pull-out tests: (a) Rehm (1961); (b) RILEM/CEB/FIP (1983).

Table 2.5: A comparison among pull-out test methods according to different researchers.,

Code	Specimen shape	Specimen size (mm)	No. of plastic sleeves	Bonded length (mm)
ASTM-C234 (2000)	Cube	150*150*150	One	150
ACI-440 3R (2012)	Cube	200*200*200	One	5 Ø
GB50152 (1992)	Cube	10 Ø	One	5 Ø
RILEM (1983)	Cube	10 Ø	One	5 Ø
Danish (DS 2082) (2000)	Prism	200*150*150	two	3Ø
Fang (2004)	Prism	140*140*180	One	4Ø
Lee et al., 2000	Cube	8 Ø	One	1.5- 3.5Ø
Auyeung 2000	Prism	175*175*350	Two	5 Ø
IS-2770 (1985)	Cube	100*100*100 for <Ø 12mm 150*150*150 for Ø 12-25mm 225*225*225 for >Ø 25mm	One	5 Ø
Prince & Singh (2013)	Cylinder	100*200	Two	5 Ø

On the other hand, the beam test is more realistic since it can imitate the real bonding mechanism and behaviour under loading due to the similarity in its conditions with those found in real structures. This is mainly because of the concrete in the beam is under tension, causing cracks under low loads (Tigiouart et al., 1998). However, this test is supposed as a time-consuming and costly test because it needs large samples and a lot of effort is required to apply it. Beam test can be applied in different ways, namely end beam, hinged beam, notched beam and splice beam beam-end test and hinged beam test. In the former case, simple support beams are exposed to loading at the end of the cantilevered areas, whilst the sample in the latter case is composed of two unattached beams interconnected by reinforcement steel at the bottom by a steel hinge at the top. Only RILEM/CEB/FIP standard introduced the arrangements for the hinged beam test. Details of beam tests are demonstrated in Figures 2.10-2.11.

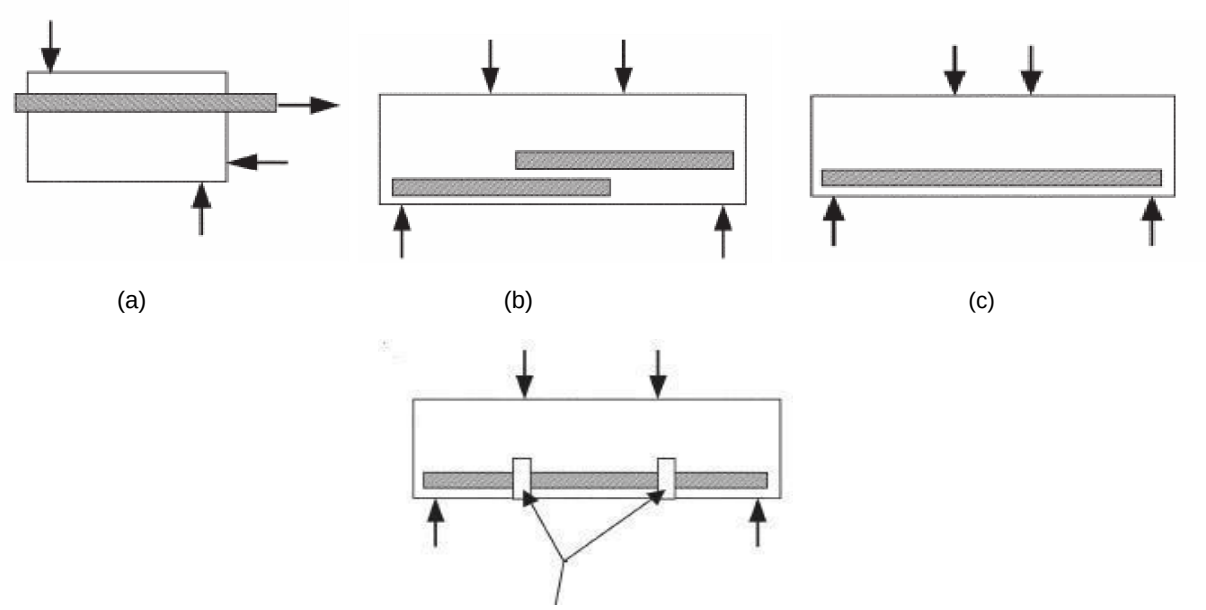

Figure 2.10 - Types of beam test methods: (a) beam-end specimen; (b) simple beam specimen; (c) splice specimen; (d) notched beam specimen.

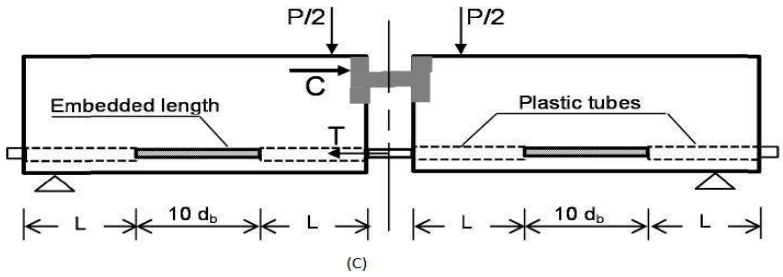

Figure 2.11 Hinged beam sample according to RILEM/CEB/FIP (1982)

2.4 Application of recycled aggregate in concrete

With the increase of concrete utilization, there is a constant increase in the consumption of natural aggregate which is the largest concrete component. It is estimated that the global production of natural aggregate in 2015 was approximately 48.3 billion tons (De Brito et al., 2016). On the other hand, approximately 850 million tons of demolished concrete are generated annually in European countries, which are about 31% of total waste in these countries causing serious environmental issues accompanied by a shortage in landfills (Ferrari et al., 2014). Hence, the use of recycled aggregate obtained from the demolished concrete structures is vital in construction

industry to eliminate these issues and producing alternative aggregates that cannot only be utilized for low-quality applications, but structural applications as well. Therefore, some environmental and economic benefits can be obtained, if RCA is used in concrete structures. However, the use of RCA in the field of construction materials might cause some mechanical and durability problems, since it can perform differently to normal aggregates. Recycled aggregates can be generally produced through two main stages. In the first stage, demolished concrete is crushed to different sizes, while in the second stage the aggregate is screened and cleaned from other materials such as wood, steel and plastic by water cleaning or air-shifting. It is assumed that about 60% of coarse recycled aggregate can be gained from the process of recycling construction and demolition (C & D) wastes (Nagataki et al., 2004).

2.4.1 Challenges facing the use of RCA in structural field

Despite the obvious benefits that can be obtained from recycling construction and demolition (C & D) wastes, the use of RCA in practical applications is still limited due to the presence of some barriers that may restrict using it. The main obstacle is related to the shortcomings in some aspects of its mechanical properties, and more concerns regarding durability properties as the quality of concrete containing RCA might be inferior to those made with natural aggregate. The main reason behind this is the remaining amount of mortar adhering to original concrete causing weak points in concrete and leading to more cracks and porosity. Therefore, the bonding between aggregate and the surrounding matrix can be affected, causing a week interfacial zone in concrete. This attached mortar might directly influence water absorption and specific gravity, which in turn affects the strength and structural performance of RCA. Other possible consequences related to durability are predicted, if this old mortar carries contaminated particles such as water-soluble sulfates or soluble chloride content.

These particles may lead to expansive reactions, and therefore steel reinforcements can be rapidly deteriorated due to corrosion. Further, comparing to normal concrete which contains one interfacial transition zone (ITZ), RCA could contain two ITZs. The old ITZ can be found between the aggregate and the old paste, while the new ITZ located between the old matrix and new paste matrix as demonstrated in Figure 2.12 (Soroushian, 2012). Another obstacle is associated to the inconsistent quality and the difficulty in separating the aggregates that come from old structures as they come from different sources (Marinkovic et al., 2010). The limited usage of RCA might also be related to the lack of knowledge and awareness regarding recycling C & D wastes, especially in developing countries, in addition to the lack of confidence on the produced RCA due to the absence of standard specifications for RCA.

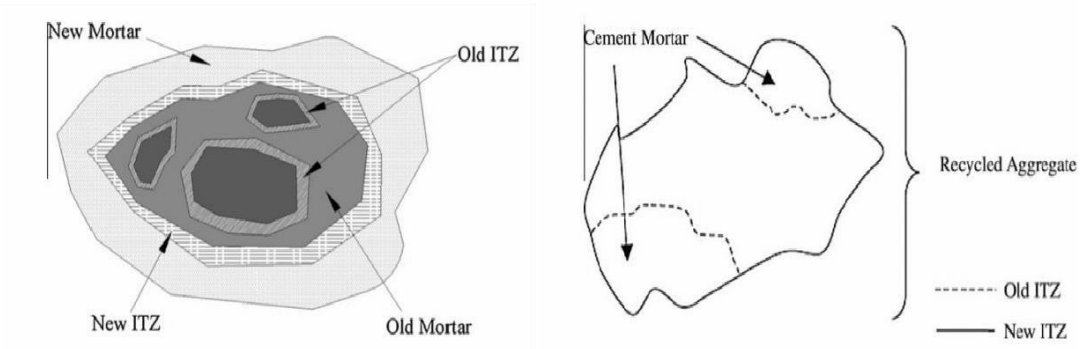

Figure 2.12 The Interfacial Zones recycled aggregate concrete (Soroushian, 2012).

Some investigations focused on determining the amount of attached mortar as it is considered the main problem associated with RCA. For instance, Hansen (2004) investigated different sizes of RCA, and the results revealed that the adherent mortar content ranging between (20-35%) for 16-32 mm size, 40% for size 8-16 mm and 60% for size 4-8mm of RCA. Similar findings were stated by Hesaba et al., (2005) who recorded about 30 % of old mortar attached to gravel with a size between 5-25 mm, and 45-65% for fine aggregate. This is why recycled fine aggregate is not

recommended to use in structures. On the contrary, it is claimed the old cement paste can provide additional hydration to RCA concrete, which probably leads to strengthening the bond between the aggregate and cement (Khalaf & DeVenny, 2004).

2.4.2 Influence of recycled aggregate on concrete properties

As recycled aggregate is a part of this research, it is necessary to explain its effect on the main properties of concrete, especially with a full replacement. The influence of RCA in concrete performance is varied from characteristic to another, as it can be affected by several parameters such as water to cement ratio, RCA percentage and the particle-size distribution of RCA (Tavakoli & Soroushian, 1996). The majority of the available results in the literature showed a reduction in concrete density up to 10% might occur when RCA is fully replaced with normal concrete (Poon & Lam, 2008). On the other hand, the water absorption of concrete prepared with RCA can be mostly found between 3.5 and 8%, which is greatly higher than that typically reported in normal concrete (0.5% - 1.0%) (Poon & Lam, 2008; López-Gayarre et al., 2009). This can lead to more amount of water required during the mixing to achieve similar workability. The workability of RCA concrete is mainly affected by the particle-size distribution of RCA, shape and texture than the quantity of RCA (Manzi et al., 2013). To achieve the same workability, RCA should be used as water-saturated surface dry, or it can be used in dry condition with adding an additional amount of water, calculated based on the difference between the amount of absorbed water by RCA and the water content of RCA. The absorption capacity is mainly controlled by the porosity of cement matrix found in RCA as well as the porosity of concrete cement matrix. On the other hand, additional water can negatively affect the performance of mechanical properties.

2.4.2.1 Mechanical properties of RCA concretes

The majority of previous studies showed that the strength of RCA concrete might be reduced between 10-25% compared to reference concrete (Etxeberria et al., 2007; Ajdukiewicz & Kliszczewicz 2002). This performance of RCA may also be connected with some other factors such as the source of original aggregate, the size of aggregate and water/cement ratios. It has been reported that the smaller aggregate size can probably cause a reduction in concrete strengths accompanied by higher water absorption, which may be associated with the influence of the relatively higher content of weaker paste attached to smaller-sized aggregates (Padmini et al., 2009). The strength of RCA concrete made with high water-cement ratios (0.6 to 0.75) can be probably comparable with normal concrete (Katz, 2003). Rao (2005) confirmed that if w/c is about 55% or more, the compressive strength would be almost similar even at 100% of replacement, whilst a lower w/c (0.4 or less) could decrease the strength by about 25% (Otsuki et al., 2003). This probably because the strength of RCA is mainly controlled by the new ITZ at higher w/c ratios, while the old ITZ controls the strength behaviour of RCA for lower w/c mixtures (Behera et al., 2014). Investigations done on mixtures made with RCA at different ages indicated that un-hydrated old cement and a higher amount of absorbed water inside RCA could extend and enhance the hydration process in long term, eliminating the difference with reference concrete (Gayarre et al., 2014; Abdel-Hay 2015). Li et al., (2012) suggested an additional quantity of cement to acquire the same compressive strength and workability of normal concrete as shown in Figure 2.13.

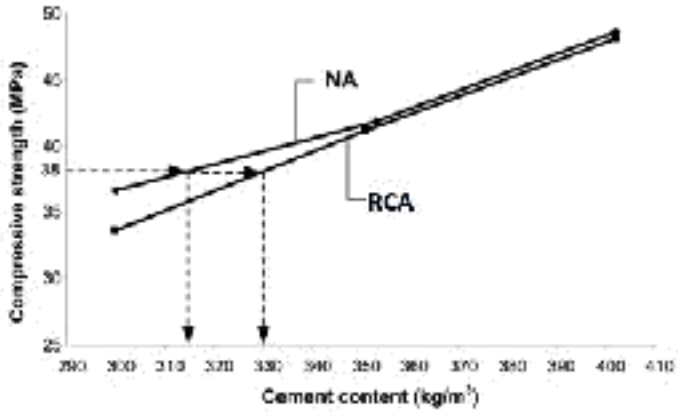

Figure 2. 13 Cement required to improve the compressive strength of recycled aggregate concrete (Li et al., 2012).

The tensile and flexural strengths are found to be probably reduced by 0–10% when normal aggregate is fully substituted with RCA (Hansen, 2004; Ajdukiewicz & Kliszczewicz, 2002; Anderson et al., 2009). However, this effect is generally less than that observed with compressive strength. This might be because these properties are more influenced by the quality of binder rather than the kind of aggregate (Malešev et al. 2010; Thomas et al., 2013).

2.4.2.2 Bond strength of steel and RCA concretes

The bond strength between concrete containing normal aggregate and reinforcing steel bars has been extensively studied, nevertheless, relatively few studies have been carried out to evaluate the bond characteristics between RCA concrete and deformed steel bars. Some of the available results reported that the use of RCA in concrete does not have much effect on the bond strength with a possible reduction of up to 10% compared to normal concrete (Prince & Singh, 2014; Seara-Paz et al., 2014). This reduction owing to the innate micro-crack of the RCA causing a decrease in adhesive force and mechanical interlocks (Yang et al., 2015). Moreover, the bond strength is mainly affected by reinforcement properties such as the surface profile and type of steel rebar rather than those related to aggregate properties (Corinaldesi & Moriconi,

2009; Butler et al., 2011). However, some other researchers reported a development in the bond strength with increasing RCA quantity in concrete (Khalaf & DeVenny, 2004; Kim & Yun, 2013), which might be associated with the increase of friction resulting from the rough surface of RCA (Pandurangan et al., 2016). The bond strength for RCA concrete seems more sensitive to the bar geometry; this can be observed as the bond strength decreased by about 12% for specimens made with plain steel bar, whilst this difference relatively disappeared when the deformed bars were used (Butler et al., 2011). It is also stated that the bond strength between RCA concrete and deformed steel was about 100% higher than that found with plain steel as reported by Xiao & Falkner (2007). The larger size of RCA in concrete might lead to decreasing the bond due to the presence of more air voids in mixtures (Kim & Yun, 2013). Very few studies examined the bond between corroded steel and RCA concrete. The findings reported by Zhao et al., (2013) indicated no significant difference in the bond trend of RCA concrete compared to NCA that had similar strength. The ultimate bond also initially enhanced before being significantly reduced, similar to normal concrete, whilst the influence of corrosion is limited in the presence of stirrups. However, faster bond degradation is recently reported with RCA concrete beams by Yang et al., (2015). Fernandez et al., (2015) stated a delay in cover cracking with the higher levels of RCA replacement, owing to its higher porosity, allowing more spaces to store corrosion products. Therefore, more research is required to achieve a better understanding of the bond behaviour of RCA concrete under corrosion conditions.

2.4.2.3 Durability of RCA concretes

Very limited research has been conducted regarding how corrosion resistance can be affected by the presence of RCA in mixtures. The mechanism of reinforcement corrosion of RCA concrete seems similar to that found in the normal concrete. Friedl et al., (2003) reported that the corrosion might be rapidly accelerated in RCA concrete

due to the presence of chloride contaminated recycled aggregate in the area around steel reinforcement. Ann et al., (2008) found that the corrosion rate in RCA concrete does not seem to be dependent on the type of binder and aggregate for mixtures containing lower levels of chloride (<0.2–0.3% by weight of cement), but significantly changed for higher levels (above 0.5% chloride). It is revealed that if RCA contains more than 0.4 kg/m^3 chloride ions, RCA aggregate should not be used in constructions, which likely can accelerate the corrosion process, and leading to a failure of the structure at early ages (Zhao et al., 2014).

Some experimental studies focused on the relationship between RCA and the carbonation depth, however, there is still no agreement about how the concrete would be affected. Whilst some of these studies suggested the depth of carbonation tends to be diminished by increasing the level of RCA (Xiao et al., 2012; Limbachiya et al., 2000; Kou, 2013), the others reported a contrary trend as the depth of carbonation being increased with increasing RCA, but it becomes slower at longer ages (Yuan et al., 2010). Ryu (2002) suggested that RCA does not have an obvious effect on carbonation.

2.4.3 Available techniques for enhancing RCA concrete properties

In the literature, several techniques and approaches have been adopted for improving the performance of RCA in concrete. However, these techniques can be fundamentally classified in two routes, namely removing the weak surface of RCA, resulting from the existence of old cement mortar or strengthen and modifying the quality of adhered mortar. Removing the old mortar requires one of the following treatments, namely mechanical grinding (Tateyashiki et al., 2001), pre-soaking in acidic solutions (Tam et al., 2007) or ultrasonic cleaning (Katz, 2004). On the other

hand, improving the quality of adhered mortar can be achieved by coating the surface of RCA with different materials such as polymer emulsion, lime powder filler and pozzolanic materials such as silica fume and fly ash (Spaeth & Tegguer, 2013; Wang et al., 2013). These solutions can generally fill up the micro cracks in RCA through the hydration process (Masanori & Takehiro, 2001; Kou et al., 2011). Further, mineral admixtures recorded acceptable results for some properties of RCA concrete. Recently, some researchers suggested that the deficiency in RCA performance can be compensated by using nanomaterials such as nano silica (Hosseini et al., 2009; Mukharjee & Barai, 2014). Nevertheless, information related to this topic is still limited, and therefore more investigations are needed, especially in terms of durability.

2.5 The role of nano silica in concrete

A large number of experimental research have been conducted to improve the sustainability and the performance of concrete. In recent years, emerging nanotechnology has gained considerable attention in concrete industry due to the ability of nanomaterials to considerably enhance the mechanical and durability properties of concrete in addition to the possibility of addressing many technical challenges related to concrete materials (Givi et al., 2013). Amongst these nanomaterials, nano silica (NS) is considered the most effective since it has high pozzolanic activity, besides its ability in filling the micro and nano pores that were left unfilled in the matrix. NS particles are not only an environmentally-friendly material, but they can act as a nucleus to generate an additional calcium-silicate-hydrate (C–S–H), which is the main source of concrete strength (Sanchez & Sobolev, 2010). All these features are primarily attributed to the ability of the tiny small size of its particles which mostly ranges from 5 to 100 nm in filling (Du et al., 2014). Another possible

reason for the high effectiveness of nano silica is the high rate of pozzolanic reaction, which is related to the high surface area of such particles, and therefore the hydration process can be highly enhanced. The difference in particle size between nano silica and other concrete components is described in Figure 2.14.

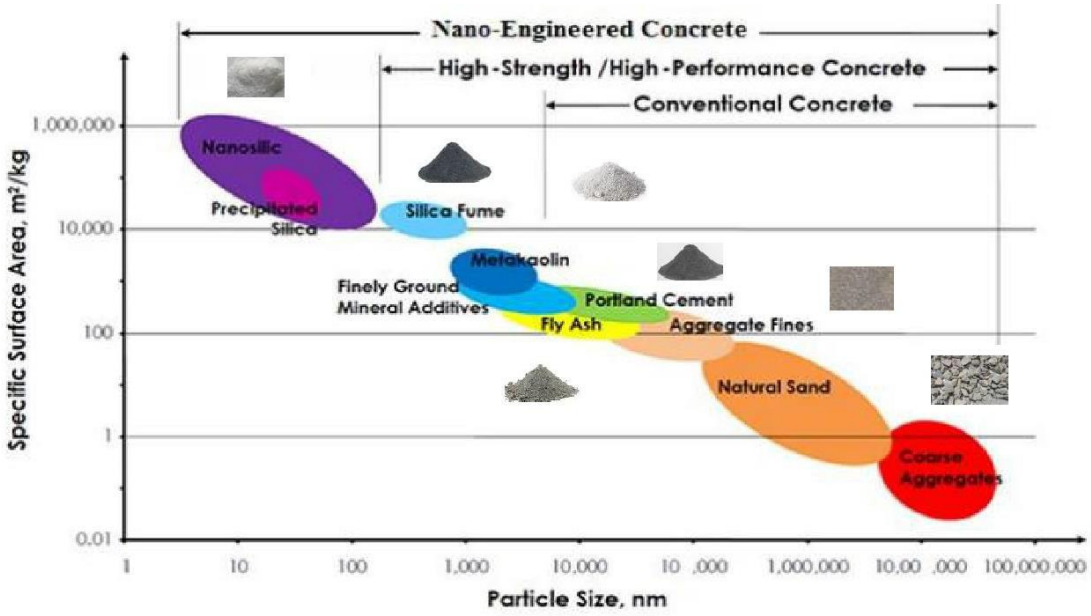

Figure 2.14 Particle size range and specific surface area of concrete ingredients (Sobolev & Gutiérrez, 2005).

NS can be commercially available in two different forms, namely dry grains and colloidal suspension silica. A specific preparation procedure is required before the powdered NS can be used in to ensure the dispersion of the particles during the mixing. However, the colloidal silica is synthetically produced in a dispersive solution, and its particles probably easier to mix and disperse, making them more effective compared to that generated from powders, which is often can be found in the agglomeration state (Zeidan, 2013). However, the potential of agglomeration is still observed, even with colloidal silica (Kong et al., 2012).

Nano silica can be synthesized by different methods such as Sol-gel method, Electric ARC method and biological methodology or it can be directly prepared from bio-waste like rice, husk and ash. However, Sol-gel method is still the most common method used owing to the possibility through this method to control the size of particles and monitoring the size distribution at mild conditions (Bjornstrom, 2004). Ultra-fine productions like nano silica have introduced many incredible benefits to concrete. It has been reportedly demonstrated that NS particle is not only an environmentally friendly material, but also can lead to enhancing concrete strength, improving concrete durability by reducing the pore structure and voids in the mixture (Du et al., 2014). Moreover, NS can easily accelerate the hydration process due to the huge reactive surface of its particles, in addition to the possibility to decrease the segregation and water bleeding of the mixture (Zhang et al., 2011). In comparison with other cementitious materials such as silica fume, NS is found to be more effective in improving concrete strength (Mondal et al., 2010). In addition to the improvement of the physical characteristics, the possibility of enhancing the bond between cement and aggregate is predicted as demonstrated in Figure 2.15.

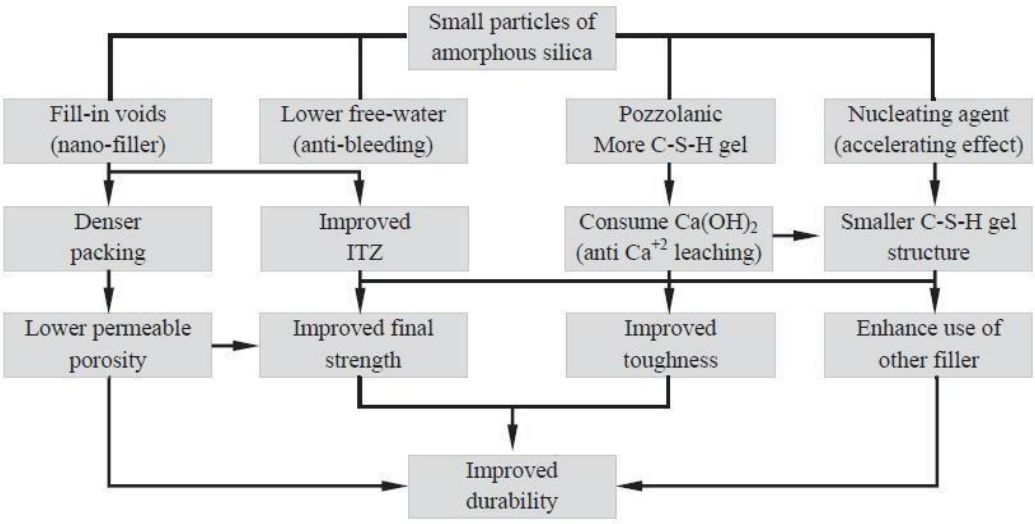

Figure 2.15. The effects of adding nano silica in concrete (Bianchi et al., 2014).

2.5.1 Mechanism of nano silica in concrete

NS particles can significantly contribute to accelerating the hydration of cement. The reaction between cement grains and NS particles leads to forming Silicic-acid (H2SiO4), which subsequently reacts with Calcium to form an additional calcium–silicate–hydrate (C–S–H). The latter then spreads in the water located between cement particles, making concrete more compact. These reactions lead to accelerating the hydration process, simultaneously, consuming free calcium hydroxide Ca(OH)2 by reducing their amount and size. Therefore, making the interfacial transition zone (ITZ) between the hardened paste and aggregates denser, as a result, the concrete strength can be significantly enhanced, especially at the early age (Singh et al., 2013). The difference in the hydration process of nano concrete with other types of concretes (normal and high strength concretes) is shown in Figure 2.16, whilst the main reactions occur during the hydration process are described in the following equations:

$$SiO_2 + H_2O \rightarrow H_2SiO^{2-}_4 \quad (2.18)$$

$$Ca(OH)_2 + H_2O \rightarrow Ca^{2+} + OH^- \quad (2.19)$$

$$H_2SiO^{2-}_4 + Ca^2 \rightarrow \text{C-S-H (additional C-S-H)} \quad (2.20)$$

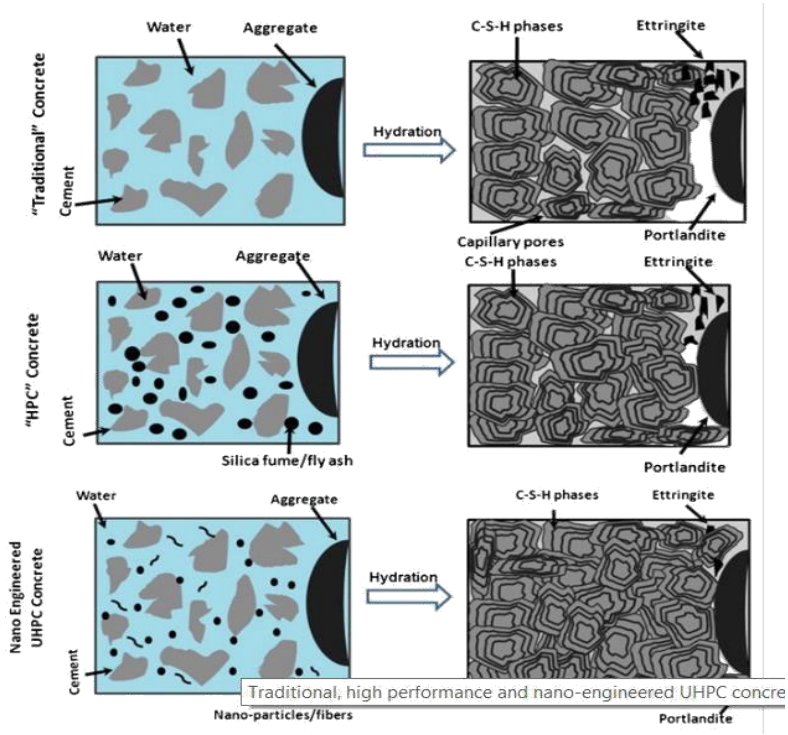

Figure 2.16 Hydration process of normal, high strength and nano concrete (Singh et al., 2013).

2.5. 2 Mechanical properties

Even though the beneficial role of NS particles in concrete has been widely accepted, the use of NS does not always show the same improvement rate. While some studies indicated that the enhancement in compressive strength could reach over 70% compared to normal concrete (Nazari & Riahi, 2011), others showed slight improvements or even some reductions in some cases (Ji, 2005). On the other hand, some researchers concluded that the appropriate percentage of NS ranged between 0.25% and 5 % of binder weight, while others indicated that concrete performance could be enhanced with higher levels up to about 10% (Li, et al., 2006; Gaitero et al., 2008). These differences may be attributed to the difference in NS properties such as surface area, particle size, the state of NS whether dry or colloidal and the dispersion state of the particles. Other reasons could be associated to the microstructure of concrete due to the change in w/b ratios. Table 2.6 demonstrates the variation of

findings of 15 investigations from the literature regarding the effect of NS on concrete compressive strength. Comparing to silica fume, the pozzolanic activity of NS is much higher than that found in silica fume, and therefore a high consumption of CH crystals and their size is predicted (Qing, 2007).

On the other hand, mixtures having large quantities of NS have a huge surface area may result in detrimental effects on concrete performance, causing a higher possibility of agglomeration and poor dispersion (Haruehansapong et al., 2014). The high surface area could influence the fresh properties of concrete due to the high absorption water molecules at their surface (Givi et al., 2013). Furthermore, very small size of its particles would probably increase the possibility of air bubbles entraining through the casting process, which, in turn, prevents the compactness in a proper way (Said et al., 2012). The increase of NS dosage or surface area of its particles may also make the process of dispersion more difficult, and thus specific procedures, for example, ultrasound mixing, are needed, increasing the concrete cost.

Up to now, only two investigations have been available in literature in terms of effecting NS on the bond strength between steel and surrounding concrete. Investigations conducted by Serag et al., (2017) revealed that the highest bond enhancement ratio was obtained at 3% NS, and level of enhancement was much higher for the specimens failed in the pull-out mode (38.5%) compared to those exposed to splitting failure (9%). The other work done by El-Feky et al., (2016) investigated the bond strength of NS concrete after being exposed to corrosive environments. The results revealed that the residual bond strength for the specimens prepared with NS was between 65-79% after being subjected to 15 days of corrosive environments, compared to non-corroded specimens, whilst only 27% of the residual bond was found with the reference

specimens. It is highly recommended to conduct further studies in this area to better understand the bond deterioration of NS concretes.

Table 2.6. List of studies focusing on the effect of NS on concrete strength.

NS Type	NS Size (nm)	SSA (m^2/g)	w/b ratio	Dosage usage (%)	Optimum ratio (%)	Improvement (%)		Reference
						7 d	28 d	
D	13	200	0.48	0.3 and 0.9	0.9	12	12	Du et al., (2014)
D	15	160	0.39	2, 4 and 6	4	-	19	Beigi et al., (2013)
C C	25 5	80 500	0.53 0.53	1.5, 4 and 7 1.5, 4	7 4	28 36	30 34	Bolhassani & Samani, (2015)
D	20-80	-	0.42	1.5, 3 and 4.5	3	4.5	43.5	Serag et al., (2017)
D	12	200	0.35	0.75 and 1.5	1.5	25	12	Khaloo et al., (2016)
C	8-20	-	0.4	0.5,1.5 and 3	3	14	25	Mujkharjee & Barai, (2015)
D	5-40	-	0.35	1, 2, 3, 4, 5, 6, 7 and 8	4	47.9	29.6	Alam Shah et al., (2016)
C	20	- -	0.65 0.50	0.5, 1 and 1.5	1.5 1	30.3 -	41 10.6	Isfahani et al.,(2016)
C	15 80	160 560	0.4	0.5,1, 1.5 and 2	1	21.2	18.5	Najigivi et al., (2010)
D	15	165	0.4	1, 2, 3 ,4 and 5	4	-	74.3	Nazari & Riahi (2011)
D	10	640	0.42	1 and 3	1	-	12.3	Zhang & Li (2011)
C	-	116	0.25	0.5 and 2	2	39	30	Palla et al., (2017)
D	15	640	0.4	0.5,1, 1.5 and 2	1	21.2	21.5	Najigivi et al., (2013)
D	15	160	0.2	1, 2, 3 and 4	3	40	8	Ghafari et al., (2014)
D	20	220	0.45	3, 5 and 7	3	53.2	57.2	Esmaeili & Andalibi (2008)

Note: C = colloidal, D = dry powder, SSA = specific surface area and w/b = water/binder ratio.

2.5. 3 Durability properties

According to previous studies, NS showed a distinct improvement in durability properties when its particles are uniformly dispersed in the matrix. Otherwise, this improvement may be neutralised by the agglomeration of NS particles, especially if they were adjusted into clusters with higher grain size (Li, 2004; Ji et al., 2005). It was found that a very small percentage of NS (0.3%) exhibited a much reduction in water penetration depth, diffusion coefficient and chloride migration coefficient by 45%, 31% and 28.7% respectively, compared to the conventional concrete. This is likely due to

the ability of NS in refining the pore size distribution, particularly at ITZ which can mitigate the ingress of chloride and water ions (Du et al., 2014). On the other hand, 0.9% NS showed a slight improvement compared to 0.3% NS, which is mainly attributed to the agglomerations NS particles, and thus just the particles on the surface of agglomerate may react with portlandite, while those inside the agglomeration will stay without reactions (Zang et al., 2012).

Shaikh & Supit (2015) revealed that NS can obviously help in delaying the appearance of corrosion cracks. The findings showed that more than 1000 h was needed to observe the corrosion cracks for specimens prepared with NS, whilst such cracks were reported at around 700 h for the reference concrete. In another study, El-Feky et al., (2016) found that NS significantly enhanced the concrete resistance against corrosion at all exposure periods (1, 7, and 15 days). However, the best performance observed at early ages (1-7 days), reporting a corrosion reduction between 40-58%, while the high and low percentages of NS showed almost the same influence at 15 days to mitigate the corrosion by about 25%. This reduction can be justified by the reduction of capillary absorption, which in turn partially blocks the pores for chloride and water ions to ingress inside concrete, and hence more protection to steel bars embedded in concrete.

2.6 Existing works of RCA concrete incorporating nano silica

The effectiveness of using small percentages of NS has offered many benefits to concrete such as filling the voids between C–S–H particles, promoting hydration rates and leading to lower permeability. As a consequence, mechanical and durability properties can be significantly improved. More recently, these features have encouraged some researchers to investigate the possibility of NS in compensating the

inferiority in some properties of RCA concrete. In this context, limited information related to the application of nano-silica in RCA concrete has been available in the literature. Hosseini et al., (2011) revealed that adding 3% of NS to 100% RCA concrete showed compressive strength better than normal concrete. Similar improvements were reported by some authors (Mukharjee & Barai, 2014; Erdem, 2018; Shaikh et al., 2014) in different properties (e.g. tensile and flexural strength, water absorption, chloride penetration, microstructure and density). For instance, the water absorption of RCA concrete reduced from 6.52% to 4.17% after NS was added to the mixtures. This reduction in water absorption, especially at an early age is primarily linked to the fact that the ability of NS in a formation of additional C-S-H which can further densify the new mortar matrix and block the interconnected voids in concrete. NS particles are quite effective in filling the pores present in the old adhered mortar of aggregates as well as the new mortar matrix. It is worth mentioning that the addition of superplasticizers to RCA concrete incorporated with NS seems obligatory through the mixing process to achieve acceptable workability. This may because of the high absorption water of RCA and ultra-high specific surface area of NS particles (Hosseini et al., 2011). Based on this information, nano silica is seemingly a promising solution to enhance the inferior performance of RCA in concrete. Nevertheless, investigations on some important properties of this modified concrete such as bond behaviour and corrosion resistance have not been conducted yet.

2.7 Predicting concrete performance using Artificial Neural Network (ANN)

Over the last two decades, artificial neural network (ANN) has been widely developed in different civil engineering applications to deal with complex problems such as concrete durability (Jepsen, 2002), dry shrinkage (Basma et al., 1997), delivery of ready mixed concrete (Graham et al., 2006), predicting the strength of recycled

aggregate concrete (Jiang et al., 2016), assessing the damage and behaviour of concrete structures (Yan and Li, 2016; Chatterjee et al., 2017; García-Segura et al., 2017). In terms of bond strength, Dahou et al., (2009) developed ANN models to predict bond strength by using two inputs (ANN-2) (i.e. compressive strength and bar diameter) and six inputs (ANN-6). The ANN-6 model was more accurate and provided a better correlation with experimental data than ANN-2. This is because the increase of input parameters allows taking into consideration some other effective factors that are not available when just compressive strength and steel bar are used as inputs. In another work, Yan et al., (2017) successfully developed ANN for predicting the bond strength of GFRP reinforced concrete beams. ANN is a powerful computing tool that can use an unlimited number of parameters to precisely predict the performance of different applications, in addition to solving the complicated problems where more conventional analytical methods are not feasible. However, it can be hardly granted a successful extrapolation for parameters that are not involved in the training network since it can only learn from previous examples. Moreover, the accuracy of the developed model can be confused with less training data and a small number of reliable test results, since it is dependent on the available number of database experimental results, and hence ANN needs to be provided by a sufficient number of database. Based on the findings available in the literature, the prediction of bond strength based on pull-out test data for corroded/un-corroded reinforcement embedded in concrete using ANN has not been implemented.

2.8 Concluding remarks

Different topics are directly related to this thesis have been revised and discussed in this chapter, namely reinforcement corrosion, bond strength, and application of both recycled aggregate and nano silica in RC concrete. Based on the previous findings

presented above in this chapter, the following conclusions can be drawn.

- Corrosion can be induced in the laboratories by applying three main techniques, namely wet/drying technique, artificial climate environment technique, and impressed current/voltage, however, the latter seems the most common and effective one.
- The level of corrosion can be determined by different methods, whilst the mass loss and electrochemical measurements are still the main ones, the applicability of the other techniques are still under investigations, and therefore more research in this area is required.
- The bond performance of reinforced concrete is influenced by some of important parameters. Compressive strength, length and diameter of embedment bar, concrete cover and corrosion level are likely the most influential ones.
- The use of RCA in concrete industry introduced many environmental and economic benefits, nevertheless, it is still limited due to the inferiority in some of its properties, especially those related to durability. The consequences associated with the presence of old adhered mortar have been considered as the main reason for the inferior properties of RCA concrete.
- Several approaches have been adopted for improving the performance of RCA concrete, However, they can be mainly classified into two routes; removing the old cement mortar, or strengthen and modifying the quality of such mortar.
- Nano silica incredibly enhanced the majority of concrete characteristics due to its beneficial contributions in filling the tiny voids available in the matrix, enhancing the pozzolanic reaction and acting as a nuclear to produce an additional calcium-silicate-hydrate. Nevertheless, the performance of NS is primarily governed by the properties of its particles (e.g. particle size, specific surface area and the state of agglomeration).

- Little research has been conducted to enhance RCA concrete by NS. The available findings showed that replacing cement with a small quantity of NS can be a very effective solution to compensate for the reduction occurred in the mechanical and microstructural properties of RCA concrete. However, some fundamental properties (i.e. bond strength and corrosion resistance) have not been investigated yet. Therefore, a comprehensive study on these properties and other main properties is essentially needed.
- Finally, artificial neural network is efficiently capable of providing predictions for civil engineering problems it. Thus, it can be developed to predict the bond strength for pull-out specimens under normal and corrosive environmental conditions.

Chapter three

Bond performance between corroded reinforcement and recycled aggregate concrete

3.1 Introduction

Investigations in terms of bond strength between reinforcing steel and RCA concrete under corrosive environments have been scarcely undertaken. Therefore, the main aim of this chapter is to study two distinct phenomena, namely the influence of RCA content on the corrosion resistance of reinforcement embedded in concrete, and the bond performance between RCA concrete and reinforcing steel bars, either corroded or un-corroded using the pull-out test. These aspects were addressed experimentally by performing sixty pull-out specimens considering different parameters, namely RCA content, corrosion level, embedded length of reinforcement and steel bar diameter. The obtained results for RAC concrete were compared to those achieved form normal concretes.

3.2 Experimental program

3.2.1 Materials

The main materials were Portland cement (CEM I/A-LL 52.5R),, fine aggregate (NFA) and 20 mm maximum size natural coarse aggregate (NCA). Recycled coarse aggregate derived from crushed washed construction and demolition waste was used as a replacement to natural with a maximum size 20 mm. Figure 3.1 illustrates the two types of aggregate used in this research, while the typical characteristics of RCA and natural fine and coarse aggregates are listed in Table 3.1. Figure 3.2 shows the

particle distribution for both NCA and RCA, which conforms the requirement of BS EN 882, 1992. Two deformed steel bars with diameters 12 and 20 mm were used in this study, conforming the requirements of BS 4449, 2005 regarding ribs spacing, rib height and relative rib area.

(a) (b)

Figure 3.1. Aggregate types; (a) Natural coarse aggregate, (b) Recycled coarse aggregate.

Table 3.1. Physical characteristics of used aggregate.

Property of aggregate	**Natural fine aggregate**	**Natural coarse aggregate**	**Coarse recycled aggregate**
Maximum grain size (mm)	5	20	20
Specific Gravity	2.60	2.63	2.50
Water absorption (%)	2.10	1.06	4.4
Bulk density (Kg/m^3)	1580	1600	1360
Porosity (%)	-	40	46

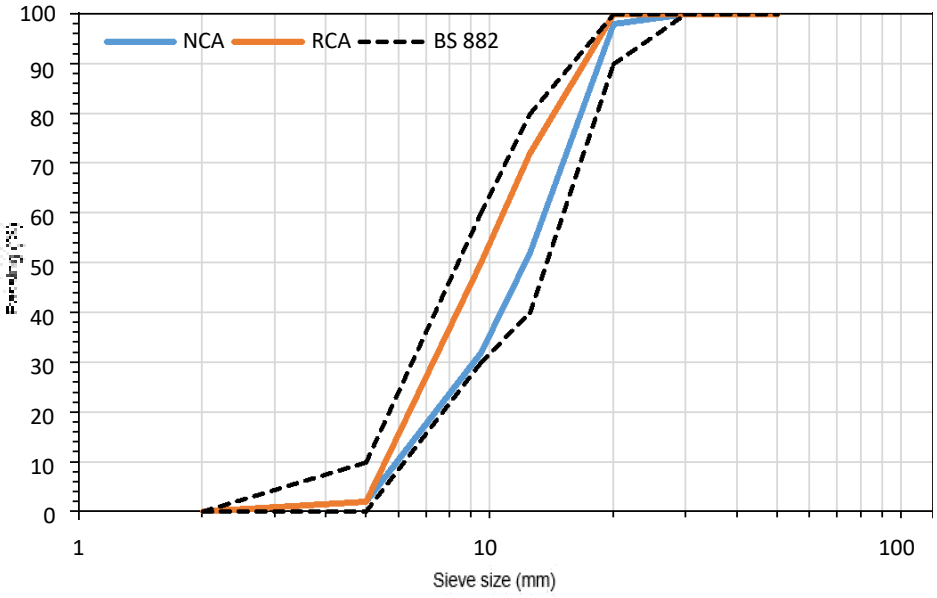

Figure 3.2. Sieve analysis for Natural coarse aggregate and Recycled coarse aggregate.

3.2.2 Specimen details

The pull-out test specimens were conducted according to RILEM CEB FIP (1983) for a total of 60 specimens. The dimensions of the concrete cube specimens were 200mm*200mm*200mm with a single deformed steel bar centrally placed in the cubes. Three different series of pull-out specimens were carried out through this study as presented in Figure 3.3. Whilst the first and second series had a reinforcing bar of 12mm but having different bonded length, the third series was carried out with 20mm diameter bar having the same surface area as bars used in the second series (3650 mm^2). The bonded length of steel bars was selected to be five times of the bar diameter for the first and third series. The remaining length inside the cube was covered by a PVC pipe to ensure this part remained un-bonded. The prominent length from the top was 310mm, while the lower part was isolated to prevent the bar from exposing directly to corrosion.

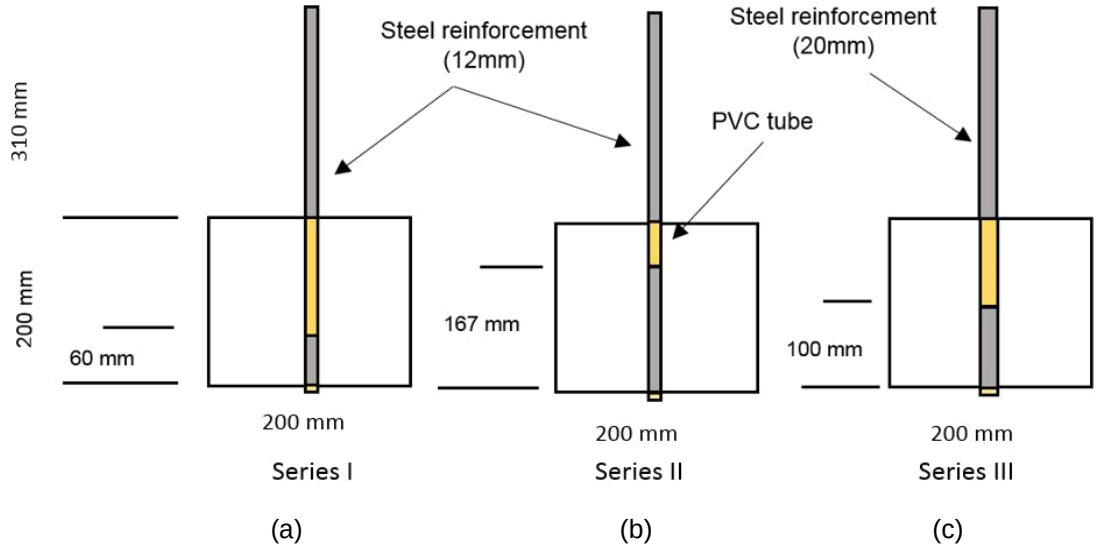

Figure 3. 3 Specimens test details; (a). Ø 12mm, ld= 60 mm; (b). Ø 12mm, ld = 167 mm; (c). Ø 20mm, ld = 100 mm.

3.2.3 Concrete mix design, casting and curing

Four groups of concrete were adopted in this study with a constant w/b ratio but different levels of RCA. Natural coarse aggregate (NCA) was substituted by 0%, 25%, 50% and 100% of RCA to cover all main ratios. Each group of concrete mix consisted of three series of specimens (Figure 3.3), and each series consists of five specimens. The first specimen from each series was tested after 28 days without exposing to any corrosion, whilst the others were tested after 2, 5, 10 and 15 days of corrosion acceleration. These periods were selected after trail tests to represent different stages; 2 days was selected to represent pre-cracking stage, 5 days to illustrate cracking stage, 10 days is chosen to be a presentative for post-cracking stage, and 15 days indicates the period of advanced cracking. All concrete mixtures were made with the same water to binder ratio of 0.4 as demonstrated in Table 3. 2 except for replacing NCA with RCA. The details of all pull-out specimens used in this chapter are illustrated in Table 3.3. It should be noted that the amount of water required for aggregate to be

in a saturated surface dry condition (SSD) was added to the mix by calculating the difference between water absorption and water content. After finishing the cast, the specimens were left 24h at room temperature before they were demoulded. Then, all the specimens were immediately covered by plastic sheets for 28 days until the day of test.

Table 3.2 Mixture proportion of concrete.

w/b	Materials (Kg/m^3)			
	NCA	NFA	Cement	Water
0.4	1180	664	450	180

Table 3.3 Description of tested specimens.

Group	RCA %	Ø	l_d	Period of corrosion (days)
I	0	12	60	0, 2, 5, 10, 15
		12	167	0, 2, 5, 10, 15
		20	100	0, 2, 5, 10, 15
II	25	12	60	0, 2, 5, 10, 15
		12	167	0, 2, 5, 10, 15
		20	100	0, 2, 5, 10, 15
III	50	12	60	0, 2, 5, 10, 15
		12	167	0, 2, 5, 10, 15
		20	100	0, 2, 5, 10, 15
IV	100	12	60	0, 2, 5, 10, 15
		12	167	0, 2, 5, 10, 15
		20	100	0, 2, 5, 10, 15

Figure 3. 4 Casting and curing pull-out specimens.

3.2.4 Corrosion acceleration and testing procedure

Corrosion of steel in concrete is a slow process which may need a long time for reinforcement embedment to be corroded under natural conditions. With the limitation of time in performing the laboratory investigations, different techniques have been proposed to induce corrosion in a short period of time such as wet/drying technique, artificial climate environment technique, and impressed current/voltage acceleration technique (Yuan et al., 2007). Corrosion obtained by the latter is not fully simulative to that occurs in nature due to the difference in the electrochemistry behind the mechanism (Austin et al., 2004), in addition to the possibility of inducing more uniform corrosion along the surface of steel bar than that achieved under a natural environment (Yuan et al., 2007). However, a similar pattern of localized corrosion was obtained by impressed current technique with that occurs in real structures (Caré & Raharinaivo, 2007). The impressed voltage technique has been adopted in this study

owing to its advantages in saving time and cost in addition to the ability to control the corrosion rate through a test period by adjusting the applied voltage. The specimens were placed in plastic tanks containing 3.5% sodium chloride solution by weight of water to simulate the concentration of chloride in seawater (Azad et al., 2007). Pull-out specimens were placed inside plastic tanks, and approximately immersed up to 90% of their volume in NaCl solution. Each group of specimens was connected in parallel with DC power supply as shown in Figure 3. 5, and stainless steel bar was placed inside the tank to work as cathode, while steel reinforcement was used to act as anode. A constant voltage of 12V was applied to each specimen from a DC power supply for 2, 5, 10 and 15 days. As the concrete resistivity varied due to the variation of exposure time, the impressed current intensities ranged between 30mA to 270mA, generating different levels of corrosion. It should be noted that specimens with steel bars having 12mm diameter and 60mm bonded length recorded the lowest corresponding current intensity during all time of exposure, whereas higher current was observed with increasing bonded area, regardless of concrete ingredients. Moreover, the corresponding current for all specimens raised with the increase of exposure time, especially for specimens having longer embedment length during the period between 10-15 days, where some wide cracks were observed.

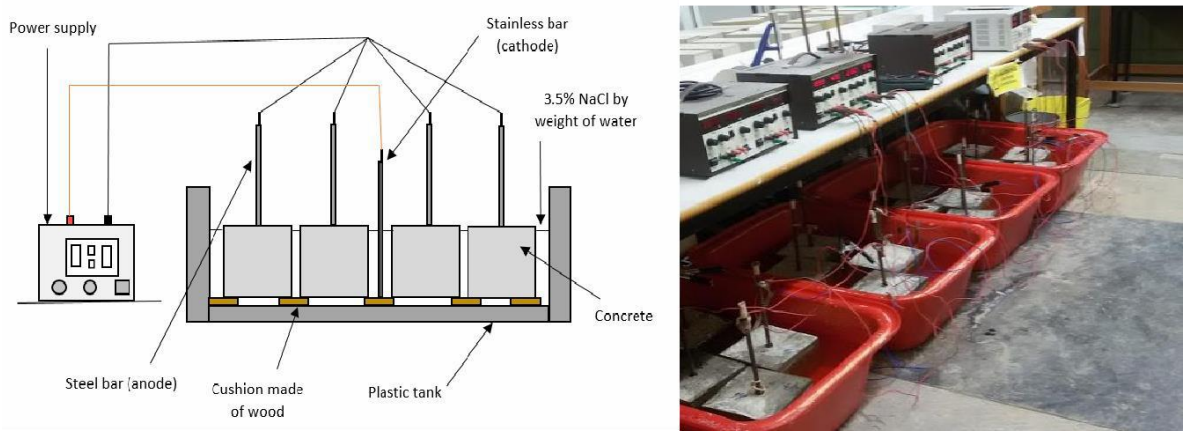

Figure 3. 5 Accelerated corrosion technique.

3.2.5 Concrete properties

Slump test was performed to measure the workability of fresh concrete in accordance with BS EN 12350-2, 2009. The compressive strengths of each mix were measured at 7, 28 and 90 days of curing in accordance with BS EN12390-3, 2009 using (100 mm*100 mm *100 mm) cubes. Tensile test was conducted in accordance with BS EN 12390−6, 2009 using cylindrical samples (300*150mm) and applying compressive loads over the length of cylinder. Two-point loading method was applied to measure the flexural strength at 28 days for beam samples having the dimensions of 500*100*100 mm. Therefore, the span between the two applied loads was 100 mm, while the distance between the two supports was 400 mm. The average of three samples was reported in accordance with BS EN 12390−5, 2009. The water absorption and dry density were simply measured using the specimens of 100 mm cube in accordance with BS1881-122, 1986 and BS EN 12504-1, 2009, respectively.

3.2.6 Pull-out test

Pull-out tests were conducted for both un-corroded and corroded specimens using a Denison machine with a capacity of 500 KN as shown in Figure 3. 6. The specimens were placed between two plates, and a rubber sheet was placed between the plate and the surface of the specimen to ensure that a load stress was uniformly distributed to the face of specimen. A data logger was connected to high precision linear variable differential transducers (LVDTs) to measure the slip of steel bar against the applied load. The axial load was applied up to cause full debonding of specimens, and the slip between the steel bar and concrete was recorded at a constant loading rate of 0.01mm/min. The bond strength, defined as the average bond stress along the bar

length, is calculated by dividing the bond failure load by the bonded surface area of the steel bar as given by Eq. 3.1.

$$\tau_u = P/\pi D L \qquad (3.1)$$

where is the bond strength, *P* is the applied load, *D* is the bar diameter and is the bonded length.

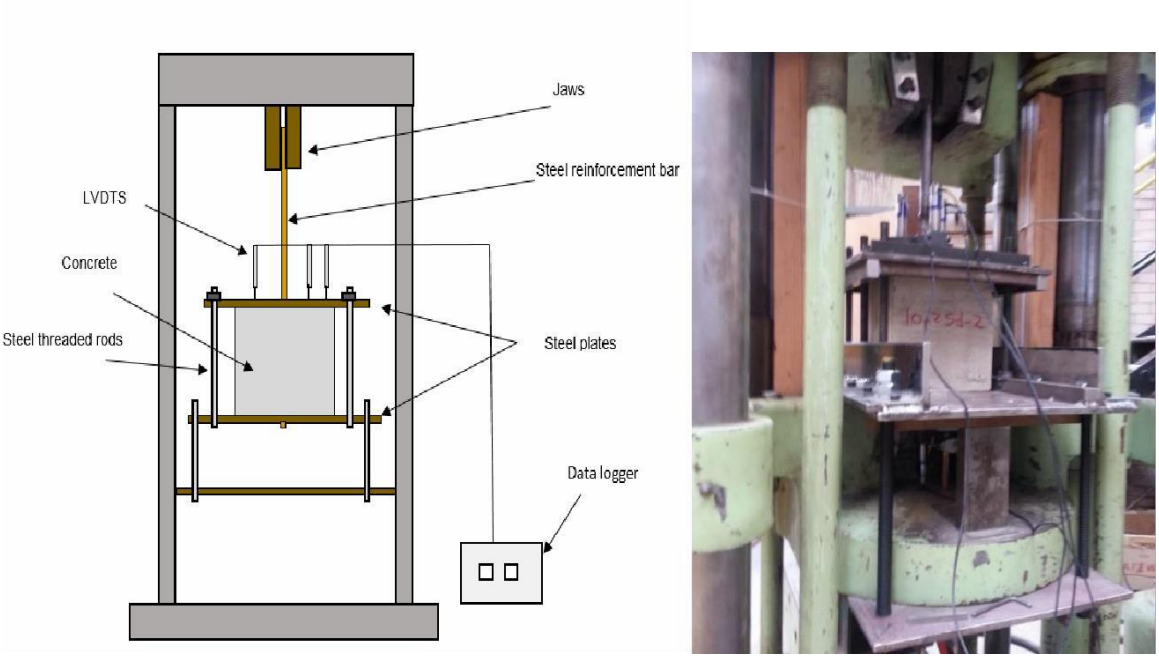

Figure 3. 6 Setup of the pull-out test.

3.2.7 Weight loss measurement

At the end of pull-out test, the corroded bars were taken out from concrete specimens and immersed in a hydrochloric acid solution, and subsequently cleaned by water and an iron brush as recommended by (ASTM G1-03, 2011). The weight of steel bar was recorded after removing the rust and compared to the initial weight of the bar before corrosion. The corrosion level was calculated by Eq. 3.2.

$$\eta = (\ _1 - \ _2)/g_0 * l_d * 100 \qquad (3.2)$$

where η is the corrosion level of reinforcing steel bars, $_1$ and $_2$ are the weights of steel bar before and after corrosion, respectively, g_0 is the weight per unit length of reinforcing bar and l_d is the bonded length.

3.3 Results and discussions

3.3.1 Influence of recycled aggregate on concrete properties

Figure 3. 7 demonstrates the relationship between RCA content and compressive strength of concrete at different ages. It can be observed that there is a gradual reduction in compressive strength with the increase of RCA. As expected, the compressive strength of conventional concrete recorded the highest value at 7 and 28 days compared to other mixes. On average, concrete made with 25% RCA exhibited quite similar results with those obtained by normal concrete, agreeing with other investigations that showed that the use of up to 30% RCA has almost no effect on concrete properties (Rao et al., 2011; Xiao et al., 2012) However, RCA had more contribution to reducing the strength of concrete when the level of replacement increased to 50% and 100% recording approximately 8.5% and 15% reduction, respectively, compared to conventional concrete. Similar trend was reported by others (Butler et al., 2011; Etxeberria et al., 2007), who found that the use of 100% RCA can lead to a reduction between 10% and 30% compared to the conventional concrete. This reduction might be explained by the presence of old cement matrix adhered to the original aggregate, resulting in the formation of another interfacial transition zone (ITZ) between the old and new cement paste, in addition to that located between the natural aggregate and old cement paste. Therefore, two ITZs can be found in RCA concrete, whilst only one ITZ exists in normal concrete. The failure of RCA concrete mainly occurs at these frontier zones, which are considered the weakest areas in

concrete matrix, making the bond between aggregate and the hydrated cementitious matrix weaker (McNeil & Kang, 2013). Micro-cracks and fissures found on the surface of RCA can also contribute to making the concrete more porous, causing more amount of water required to achieve the desirable workability, and as a result compressive strength values would be decreased with the increase of w/b ratio in the matrix. As time of curing extended to 90 days, the rate of strength gain was slightly better for RCA concrete than that achieved by normal aggregate concrete. This can be observed by comparing the improvement achieved over time for concrete made with 50% and 100% RCA (9.5%, 11.5%), respectively, with that found with normal concrete (8%), as similarly observed in previous studies (Evangelista & De Brito, 2007; Kurad et al., 2017). This might be attributed to further cementing action of the remnant un-hydrated mortar adhered to RCA, which may have contributed to improving the strength in the long term. Additionally, the high amount of absorbed water inside RCA particles can further assist in promoting the hydration process by providing internal curing.

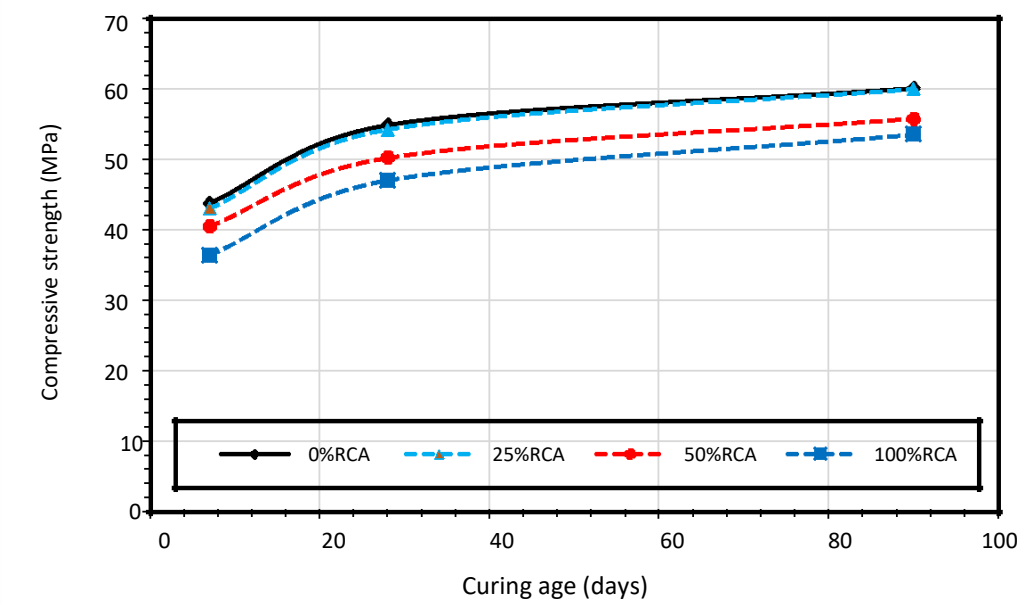

Figure 3. 7. Compressive strength at various ages with different levels of recycled aggregate concrete.

The other main properties of RCA concrete (i.e. tensile strength, flexural strength, water absorption, workability and density) were also investigated. As it can be seen from Table 3.4, the tensile and flexural strengths of RCA concrete were not significantly influenced by the replacement level of RCA. Whilst using 25% and 50% RCA were quite similar to that obtained by normal concrete, 100% RCA led to about 8% and 7% reduction in terms of tensile strength and flexural strength, respectively, following similar trends reported by some authors (Yang et al., 2008; Behera et al., 2014). This is mainly because of these properties are mostly dependent on the surface characteristics of RCA rather than the level of replacement. The water absorption of RCA concrete was significantly affected by the RCA content, reflecting the water absorption capacity of recycled aggregate. As the level of RCA replacement reached 100%, the water absorption increased about 40% compared to the normal one. Therefore, it can be confirmed that the durability properties of concrete are more deteriorated by the content of RCA than the mechanical properties. It is also observed that the density of RCA concrete was approximately 8% lower than that found with normal concrete. From Table 3.4, it can be also noted that the workability of RCA mixes in terms of initial slump was marginally higher than that found in control mixtures, which is consistent with results obtained (Kou & Poon, 2012). This might be explained by the increase of amount of free water required to compensate the higher absorption capacity of RCA, and therefore time was not sufficient for RCA concrete to absorb the extra water at the moment of slump test. However, after about 20 mins, all mixes showed equivalent workability levels, suggesting that the compensating water had been completely absorbed.

Table 3.4. The main properties of concrete mixtures.

Mixture	Compressive Strength (MPa)	Tensile Strength (MPa)	Flexural Strength (MPa)	Water absorption (%)	Density (Kg/m^3)	Slump (mm)
R0	54.66	2.99	4.05	3.74	2404.43	33
R25	54.11	2.95	4.03	3.81	2385.04	33
R50	50.33	2.87	4.0	4.56	2272.12	37
R100	47.08	2.77	3.81	5.26	2193.51	40

3.3.2 Influence of recycled aggregate on reinforcement corrosion

Figure 3. 8 shows the relationship between the corrosion rate of specimens containing different levels of RCA exposed to an electrochemical corrosion for 2, 5, 10 and 15 days. A wide range of corrosion degrees was obtained in this study ranging from 1.34% up to approximately 20% mass loss. It can be observed that the corrosion rate increases by increasing the level of RCA in concrete, especially, when the level of RCA replacement reaches 100%. It can be also noted that all specimens made with 25% RCA showed comparable corrosion rate results to normal concrete at all stages of corrosion exposure. After two days of exposure to corrosion, 100% RCA led to 20%, 20% and 32% increase in corrosion rate for the samples having embedded length 60, 167 and 100 mm, respectively, compared to those containing normal aggregate. This increase continued for 100% RCA concrete with the extension time of corrosion to five days reporting 4.88%, 5.68% and 3.46% mass loss, respectively, whilst the normal concrete reached 3.95%, 4.59% and 2.11% at the same period. The influence of RCA quantity evidently caused more corrosion as the period of corrosion exposure reached 10 and 15 days, reporting an increase in corrosion rate exceeded 50% in some cases, compared to the normal concrete. This is mainly attributed to the high porosity and

water absorption of RCA, resulting from the presence of old adhered mortar on the surface of aggregate. This means that the corrosion rate constantly developed owing to the available of widening cracks on the surface of RCA concrete, allowing more chloride ions to penetrate the concrete. Hence, the rust products readily accumulated on the surface of steel bar. Another possible reason for propagating corrosion might be related to the presence of contaminants in RCA such as chloride, carbonate and sulphate, which can de-passivate the protective layer located around steel bars (Zhao et al., 2015). It is also be observed that more corrosion was spotted for both NCA and RCA concrete with specimens having longer bonded length, making an increase in corrosion rate per unit length. For example, by increaseing the bond length from 60 mm to 167 mm, the corrosion rate per bond length devopled between 5- 20% for RCA concrete.

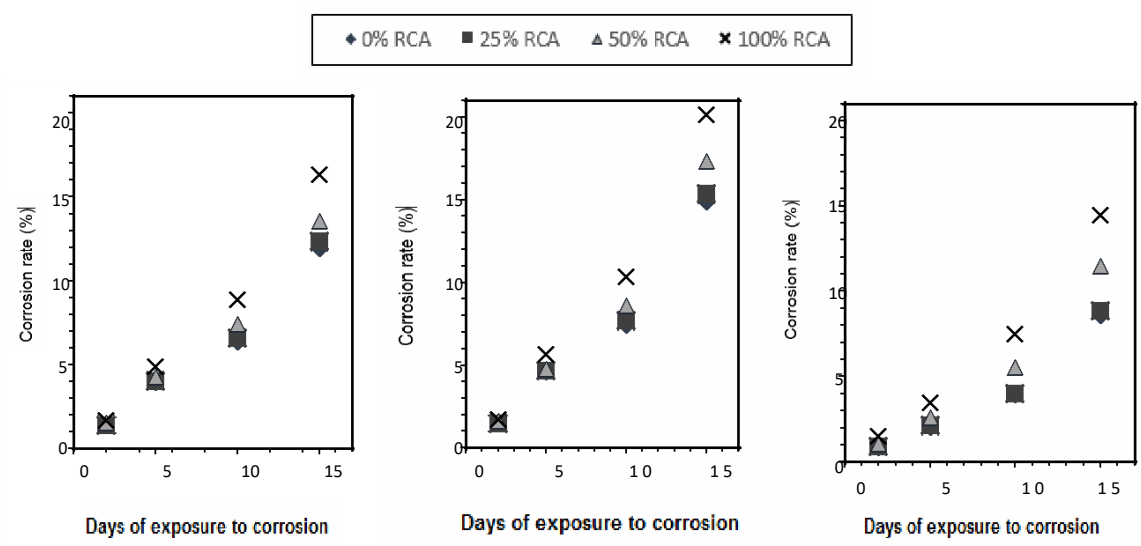

Figure 3. 8. Relationship between recycled aggregate content and corrosion rate for specimens having: (a). Ø 12mm, ld= 60 mm; (b). Ø 12mm, ld = 167 mm; (c). Ø 20mm, ld = 100 mm.

3.3.3 Bond stresses-slip relationships

The measured bond stress versus slip curves for the specimens tested at various degrees of corrosion is drawn in Figures 3.9-3.11. By analysing the relationship between bond stress and slip of steel bars, it can be seen that the behaviour of bond stress of RCA concrete was quite similar to that found with conventional concrete for both cases; corroded and un-corroded, as also reported by (Fernández et al., 2016). For specimens having a short embedment length (60 mm), the relationship between bond stress and slip can be generally divided into three distinguished stages. In the first stage, the bond stress steeply increased with a very little slip ranged between 0 and about 1.5 mm until reaching the ultimate load. The second stage, which represents the first part of descending branch, exhibited a drop in the load after reaching the peak load accompanied by an increase in the bond slip. At the third stage, the bond stress slightly decreases with a rapid increase in the non-recoverable slip until the steel rebar completely pulled out. For specimens having 100 and 167 mm embedment length, the relationship between bond stress and slip showed some differences. This can be observed, especially in the descending branch, showing a sudden drop after reaching the peak stress, resulting from splitting failure. It is also observed that for specimens with 167 mm embedment length either free or had a little amount of corrosion, a slight increase in the bond stress was observed after reaching about 91% of the ultimate stress accompanied by a rapid displacement, corresponding to steel yielding before pulling out from concrete.

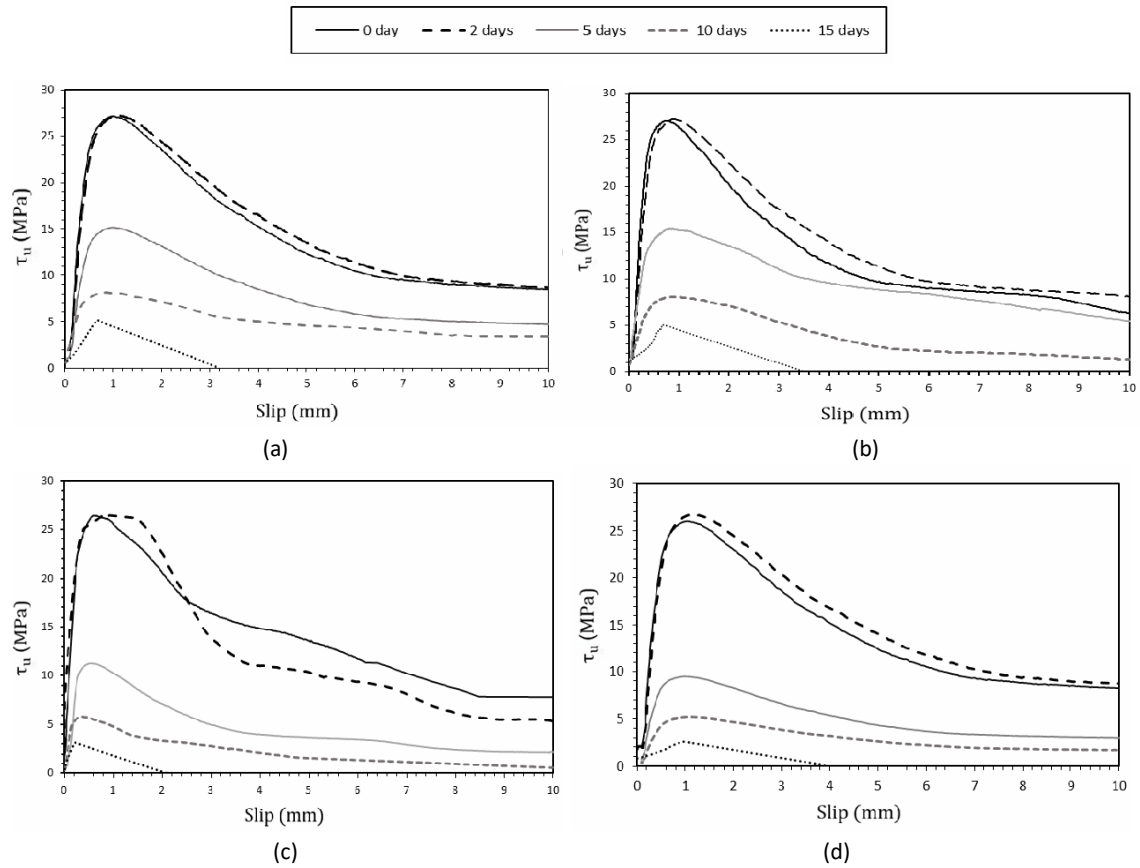

Figure 3. 9. Bond stress versus slip for specimens having Ø 12mm, ld= 60 mm and containing: (a). 0%RCA, (b). 25%RCA, (c). 50%RCA and (d). 100%RCA.

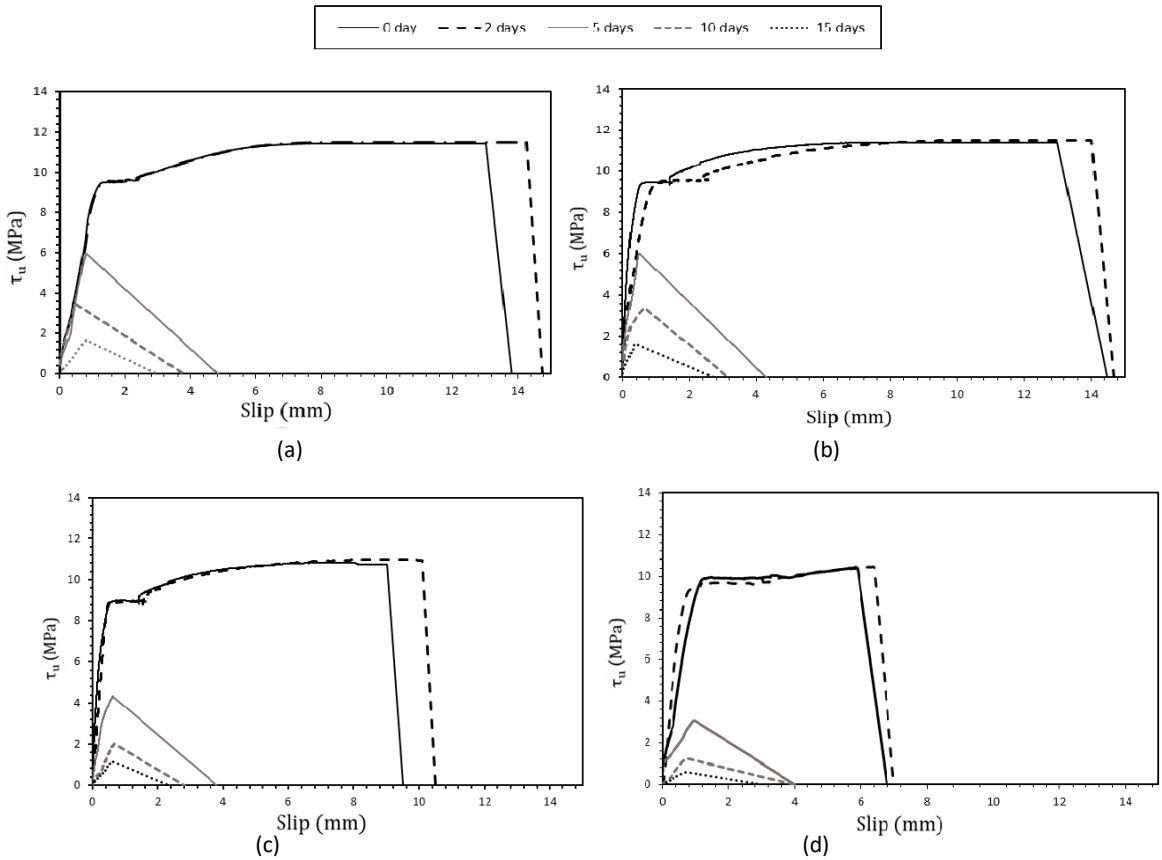

Figure 3. 10. Bond stress versus slip for specimens having Ø 12mm, ld= 167 mm and containing: (a). 0%RCA, (b). 25%RCA, (c). 50%RCA and (d). 100%RCA.

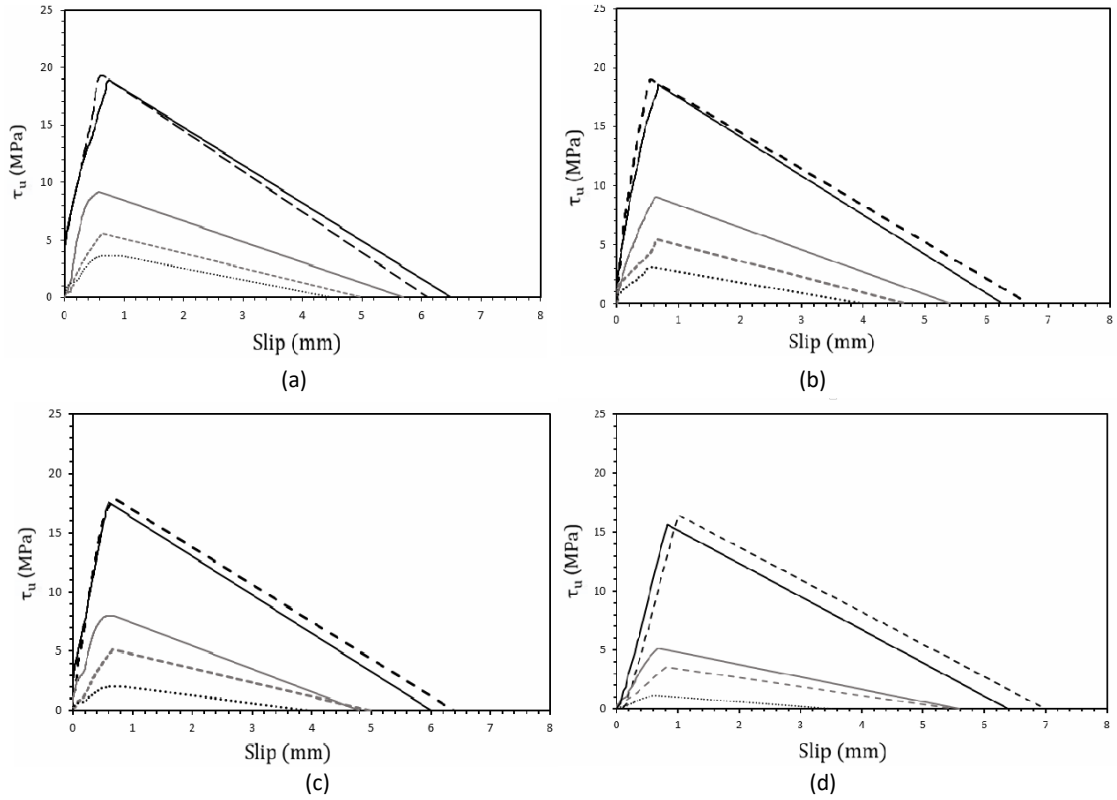

Figure 3. 11. Bond stress versus slip for specimens having Ø 20mm, l_d= 100 mm and containing: (a). 0%RCA, (b). 25%RCA, (c). 50%RCA and (d). 100%RCA.

3.3.4 Influence of recycled aggregate on bond strength

From Figure 3. 12, it can be observed that the bond strength, in general, slightly decreases with the increase of RCA level in concrete. For un-corroded concrete, it can be seen that bond strength between steel reinforcement and concrete containing 25% RCA was comparable to that found in conventional concrete for all specimens. By using 50% RCA in concrete mixture, the bond strength after 28 days reached 26.53 MPa for the samples having 60 mm embedded length, which represents approximately 97% of the bond strength of conventional concrete. Similarly, the other two specimens having embedded length 167mm and 100mm reported about 95% bond strength compared to normal concrete. For 100% RCA, the bond strength between 20mm deformed steel and RCA concrete decreased approximately by 11% compared to normal concrete, whilst those containing 12mm steel bar and having

60mm and 167mm bond length were less affected by reporting 6% and 9% decrease in bond strength, respectively. The possible reason for this reduction might be attributed to the decrease in the mechanical interlock and adhesive force with the increase of RCA ratio due to the presence of micro-crack in RCA surface. Another possible reason for this reduction is the influence of compressive strength on bond strength which is represented by the square root of compressive strength. These results were in agreement with other authors (Rao et al., 2007; Ajdukiewicz & Kliszczewicz, 2002; Yang et al., 2015) who found a reduction in bond strength by up to 10% when NCA is fully replaced by RCA, while the use of both types of aggregate; recycled coarse and fine aggregates leads to about 20% reduction in bond strength (Kim et al., 2012). However, it is stated that the bond strength tends to increase in the presence of RCA. due the roughness of adhered mortar in RCA, which may increase the adhesion and friction mechanisms of bond strength at the steel-concrete interface (Prince & Singh, 2013). In another investigation, it was reported that a slight higher bond for RCA concrete can be obtained when the strength of concrete is similar with normal one (Fernández et al., 2016). It is clearly can be said that the bond strength of un-corroded steel reinforcement is less sensitive to RCA replacement content than other influential factors such as steel surface profile and embedded length.

The influence of RCA content on bond strength continued almost the same after exposing to a short period of an electrochemical corrosion (two days) to lead to about 10% reduction for the full replacement of RCA. It is interesting to mention that through this stage (2 days) the concrete containing 50% and 100% RCA documented a slight better enhancement in terms of bond strength compared to conventional concrete. For example, the bond strength between 167 mm bonded length and 100% RCA enhanced by 4.8%, whilst the normal concrete showed just 2.8% improvement. This

could be explained by the fact that bond strength during this stage was still in improvement due to the low degree of corrosion and the rust products were thicker between steel bar and RCA concrete than that found in conventional one, which was the same observation reported by Fernández et al., (2016).

With the extension of corrosion period to 5 and 10 days, the influence RCA on bond resistance became clearer at 10 days for the samples containing 50% and 100% RCA, especially for larger embedded length (167mm) to obtain 58% and 36% from that stated in conventional concrete. This might be due to higher water absorption and porosity of these concretes, allowing more chloride ions to be easily penetrated into a steel-concrete interface. Hence, more corrosion products are expected to accumulate on the surface of steel causing internal cracks, and consequently affect the performance of bond between steel and concrete. As time reached 15 days which represents harsh corrosive environments, bond strengths were obviously affected by RCA content. For instance, the bond strength between RCA concrete and 60mm bonded length represented about 50% of that found in normal concrete, whereas the degradation of bond between rebar 20mm and the same concrete was approximately 32% of normal concrete. This huge reduction owing to the appearance of widening cracks on the surface of RCA concrete around steel bar, while they were less observed with concrete containing normal aggregate. Nevertheless, the presence of stirrups might reduce the difference between NCA and RCA due to the ability of stirrups on providing enough confinement and controlling the development of cracks resulting from corrosion as found by Zhao et al., (2013).

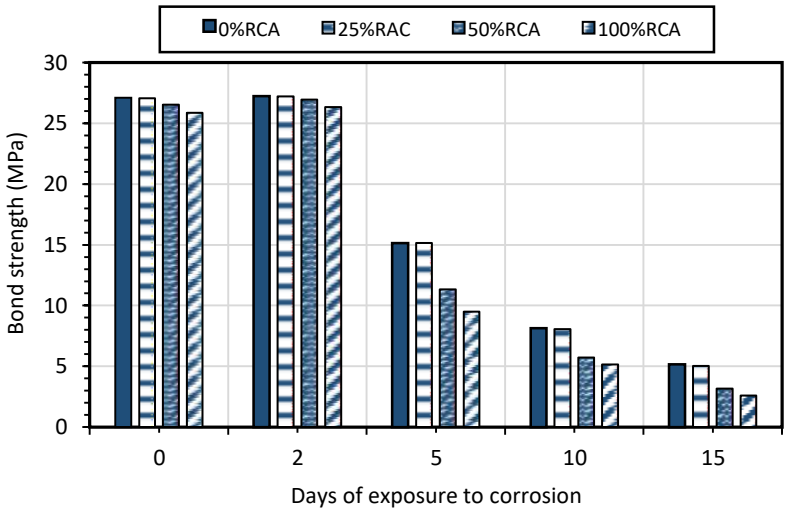

(a)

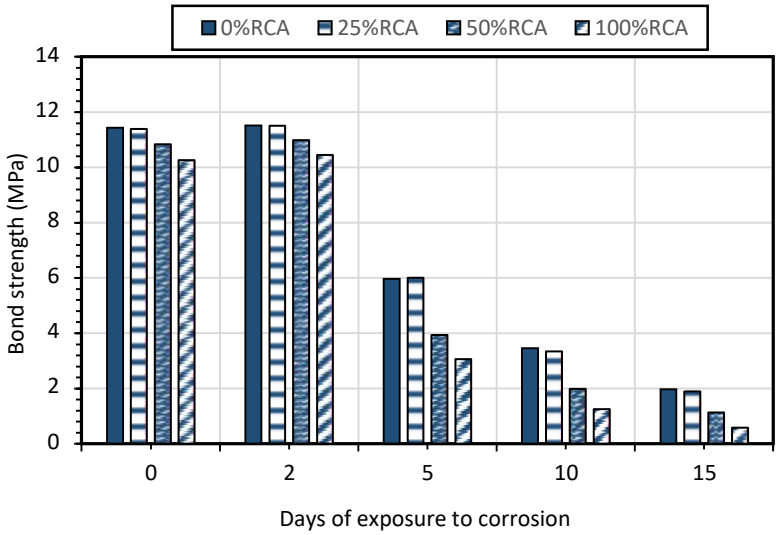

(b)

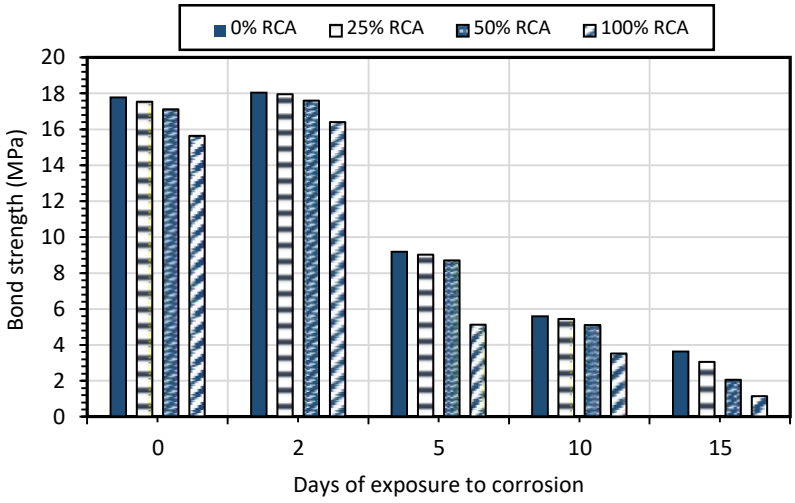

(c)

Figure 3. 12. Relationship between recycled aggregate content and bond strength for specimens having: (a). Ø 12mm, ld= 60 mm; (b). Ø 12mm, ld = 167 mm; (c). Ø 20mm, ld = 100 mm.

3.3.5 Influence of corrosion on bond strength

The variation of bond strength due to corrosion has been investigated for four different periods of exposure starting with 2 days which represents a low amount of corrosion and finishing up with 15 days which represents severe environments. Data related to the influence of corrosion on bond strengths of 60, 167 and 100 mm bonded length are plotted in Figure 3.13. From the obtained results, it can be observed that bond strength is significantly influenced by steel corrosion for both types of concrete; normal and RCA concrete. However, it seems that the bond strength in RCA concrete is more sensitive to corrosion than conventional concrete. Bond strength slightly increased for all specimens after two days of corrosion acceleration when the corrosion rate ranged between 1.34% and 2%. The same observation was reported by other authors for NCA concrete (Ouglova et al., 2008; Auyeung et al., 2000; Fang et al., 2004), who found the corrosion products offer a favourable impact in terms of bond strength at lower corrosion values. This improvement may be explained by the increase of the surface roughness of steel reinforcement due to the creation of a firmly adhered layer of rust on the surface of steel reinforcement, which in turn enhances the radial stresses between the steel and surrounding concrete, and hence improving the frictional forces of bond. However, there is no consensus regarding the critical value of corrosion level as it was reported from 0.5% up to 5% weight loss (Yang et al., 2015; Almusallam et al., 2001). The reason for this difference can be related to the difference in test set-up, the type of tested specimens, details of specimen and current applied to corrode the steel, and therefore parameters used in one experimental work might not be adequate to produce the same behaviour in other experiments.

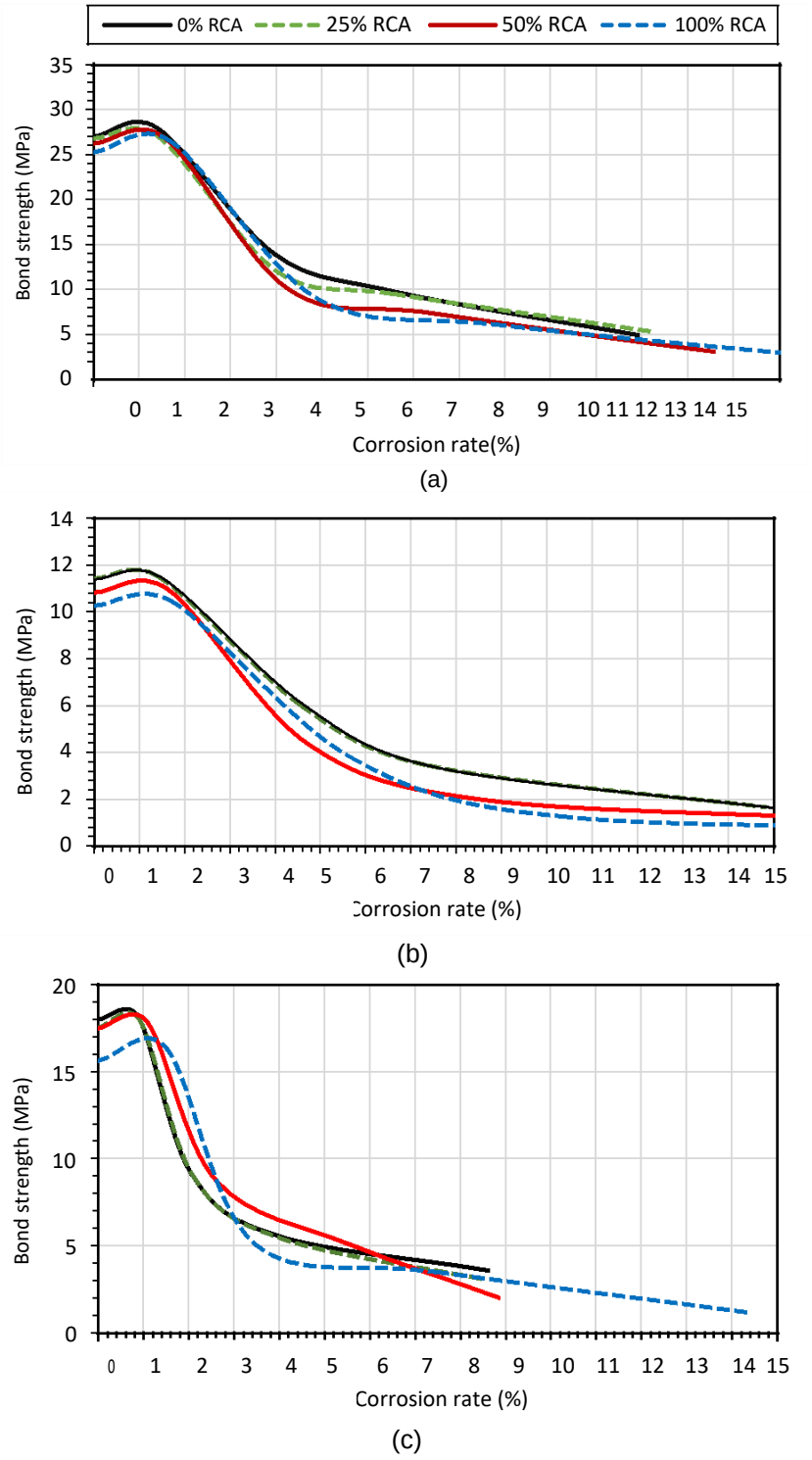

Figure 3.13. Effect of corrosion rate on the bond strength of specimens having: (a). Ø 12mm, l_d= 60 mm; (b). Ø 12mm, l_d = 167 mm; (c). Ø 20mm, l_d = 100 mm.

With a further of corrosion was produced at five days of corrosion, which can be classified as a pre-cracking stage, a loss in bond strength was observed for all specimens due to the development of corrosion rate to be between 2.5% and 5.6%

weight loss. For instance, bond strength between normal concrete and 167 mm bonded length distinctly declined from 11.44 MPa to 6.0 MPa at 4.15% corrosion rate. Similarly, bond strength of 100% RCA concrete with 20mm diameter bar decreased by about 50% as the corrosion rate reached 3.5%. This probably happened due to the lubricating influence of the flaky corroded layer on the steel surface, causing a change in the surface condition of the bar and reducing the friction force of bond strength. Chung et al., (2008) linked the beginning of losing the bond at a steel-concrete interface with the appearance of cracks on the concrete surface. By reaching 10 days of corrosion acceleration, which can be classified as a cracking stage, the passivity of the protective film on the surface of steel was already completely destroyed due to the high rate of corrosion, reaching 10% in some cases. In this advancing levels of corrosion, the ribs height of reinforcing steel began degrading, causing more losing in bond strength, in addition to the appearance of some tight cracks on the external surface of concrete specimens.

Extending time to 15 days, bond strength between 167mm bonded length steel bar and concrete containing 100% RCA was almost lost corresponding to the high rate of corrosion (20%), while less degradation observed with conventional concrete. During this stage, which can be described as a post- cracking stage, some interactive factors may have led to this huge loss in bond at the steel-concrete interface. In addition to the reduction in the bar section, the reinforcement lugs were obviously destroyed up to a significant level in many samples, accompanied by the observation of some longitudinal widening cracks. As a result, the mechanical interlocking force between steel and surrounding concrete was almost lost. It is important to explain that the appearance of cracks on RCA concrete surface could be delayed compared to normal concrete when they were exposed to the same level of corrosion. It is stated that about

30% more time needed for the first crack to be appeared on the surface of RCA concrete compared to normal concrete owing to the high porosity of RCA concrete, which might offer more space for corrosion products to be stored before being cracked (Fernández et al., 2016).

3.3.6 Influence of bar diameter on bond strength

In order to investigate the influence of bar diameter on bond strength, two different bar diameters; 12 and 20 mm were used in this study, while two different cases of bonded length were carried out. In the first case, the influence of bar diameter was investigated using the same surface area of embedment length (6280 mm^2), whilst in the second case, the bonded length for each bar was scaled five times of bar diameter as recommended by RILEM CEB FIP, (1983). From Figure 3. 14, it can be obviously shown that bar diameter significantly influences the performance of bond between reinforcing steel and surrounding concrete. As the bar diameter increases, the bond strength is also increased as long as the surface area of bonded length being constant. Before and after exposure to the initial corrosion, the specimens with 12 mm bar diameter reported about 65% of the bond strength found with 20 mm. This difference is mainly associated to the difference in the relative rib area of steel reinforcement, playing a significant role in bond performance between the bar and its interaction with concrete. The relative bar area, which is mainly governed by the specific combination of bar spacing and ribs height, can be described as a ratio between the bearing area of projections above the core of bar to the shearing area between the ribs (ACI 408, 2003). To clarify this, the ribs height and spacing are not exactly the same for different diameter bars, and the bond resistance, in fact, is controlled by the blocking of ribs in concrete. In the current study, the relative bar rib for 20mm steel bar (0.16) is found to be about 20% higher than that reported for 12mm. This influence can be supported by

the results obtained by Metelli & Plizzari, (2014) who reported 40% enhancement in bond strength when the relative ribs increased from 0.04 to 0.1. The ACI 408 (2003) requirements for the maximum spacing between ribs equal to 70% of bar diameter, and the minimum height of ribs equal to 4% and 5% from the nominal bars (12mm and 20 mm), respectively, whilst the minimum recommendations for relative rib area equal to 1, with favourable values between 1.7 up to 2. The influence of relative bar rib is found to be more pronounced with the presence of transverse confinement. Findings obtained in this study can be supported by Etxeberria et al., (2007) who found about 24% development in the failure load when the relative bar rib increased from 0.08 to 0.16. Another possible factor could be related to this difference is the yielding of 12 mm steel bars before reaching the failure, which in turn might have led to reducing the frictional properties, in addition to the possibility of affecting ribs geometry by reducing relative rib area (CEB-FIB, 2010). It was indicated that a significant reduction in bond stresses for specimens yielded before reaching failure compared to the same samples having a higher strength reinforcement and did not yield (Orangun et al., 1975). However, the findings obtained by Zuo & Darwin, (2000) indicated that just about 2% lower bond strength would occur after yielding. As the corrosion rate develops, the specimens seemingly became less sensitive to this parameter, especially in the advanced stages of corrosion. The likely reason is the erosion of reinforcement lugs of both bars which are responsible for transferring the force between steel and concrete, causing a decrease in transferring this force and making the influence of bar size less effect.

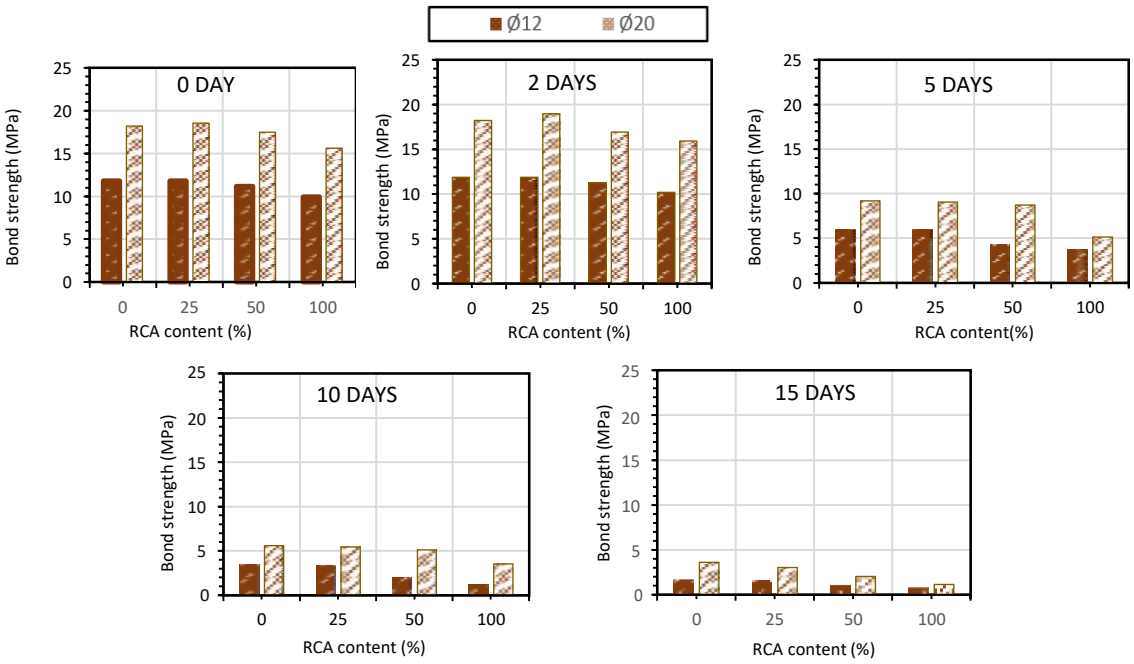

Figure 3.14: Effect of bar size on bond strength of reinforced concrete.

With respect to using two different bonded length based on the size of used bar, the influence of bar diameter showed an opposite trend. From Figure 3. 15, it can be seen that bond strength of RCA concrete decreases as the bar diameter of reinforcing steel increases, similar observation found in normal concrete. For instance, at non-corrosion stage, the bond strength between 20mm reinforcing steel and RCA concrete containing 50% and 100% RCA reported approximately 60% and 63% of that obtained with 12mm, respectively, which can be supported by Pour & Alam (2016). This can be explained by the difference in the surface area of bonded length between these two bars, in addition to the increase of the number and the volume of bleed water trapped pockets between the bars and concrete voids, causing an increment in the number of the voids and decreasing the contact area at a steel-concrete interface (Shang et al., 2017; ACI 408, 2003). The nonlinearity distribution of bond stress is more pronounced in larger bars (which requires a longer embedded length), resulting in a lower bond

strength. By corroding the specimens for different periods, a similar behaviour was noted for both; NCA and RCA concrete. Similarly, Sonebi et al., (2011) stated that bond strength reduced about 45% when the bar diameter increases from 12mm to 20mm, but the reduction being marginal when steel corroded. It is reported that influence of bar diameter on bond strength can be notably observed with low degrees of confinement, however, this impact almost disappeared with high degrees of confinement (Ichinose et al., 2004). Similarly to normal concrete, the bar diameter of RCA concrete had a crucial influence on the failure mode of pull-out test' specimens for both corroded/uncorded steel bars. This can be observed when the samples having larger bar diameter (20mm) failed in splitting instead of pull-out failure observed with smaller bar diameters.

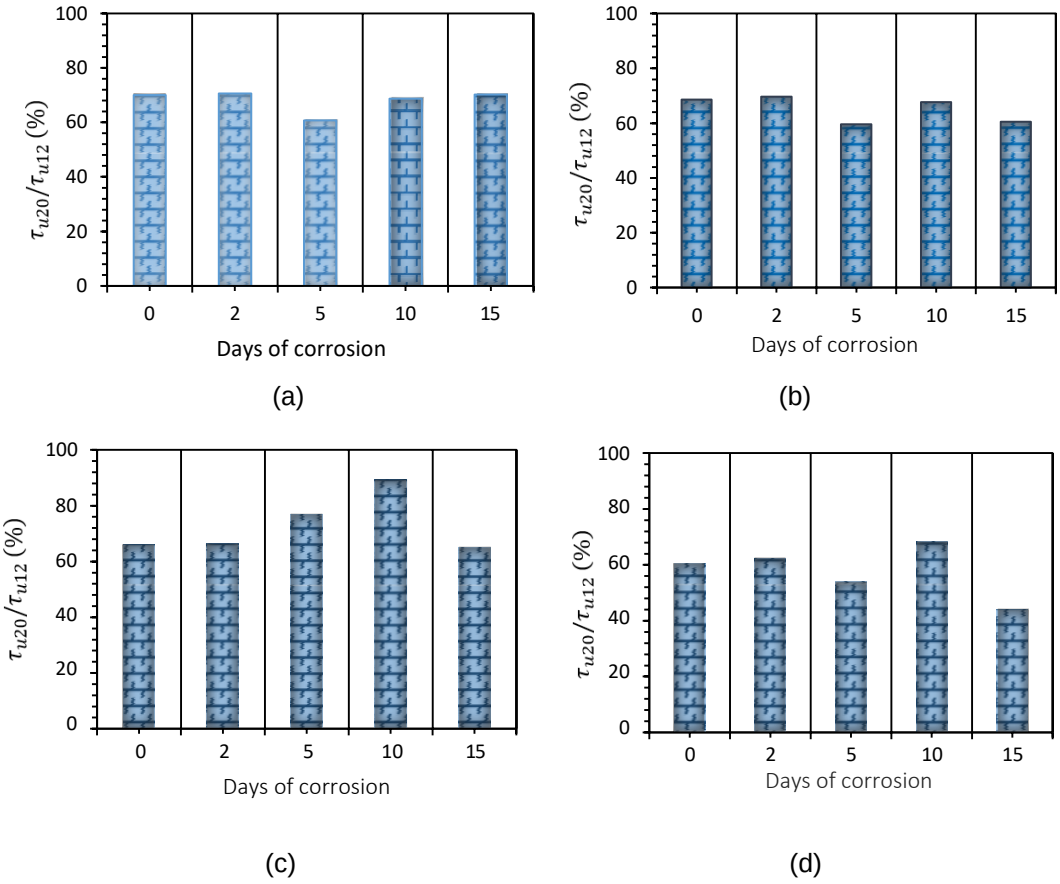

Figure 3.15. Ratio of bond strength between the samples with bar 20mm and bar 12mm for; (a). 0%RCA, (b). 25%RCA, (c). 50%RCA and (d). 100%RCA.

It can be probably concluded that the relationship between rebar diameter and bond strength cannot be always appreciated. This is fundamentally because of the embedment length is needed to be longer as bar diameter increases, while more bond forces are required for larger bars to be failed in the case of a given embedment length (ACI 408, 2003).

3.3.7 Influence of embedded length on bond strength

Based on the test results, it can be said that by increasing the embedment length of reinforcing steel, the ultimate force tends to be higher, however, the ultimate bond strengths obtained from both normal and RCA concrete specimens are clearly decreased. From Figure 3.16, it can be seen that the bond strength of specimens having an un-corroded embalmment length 5 times of bar diameter dropped by about 40% when the length increased to be 13 times of bar diameter. The same scenario was observed with concretes incorporating 50% and 100% RCA, recording approximately 37% and 35% of shorter bonded length, respectively. These findings confirm the earlier results obtained by Pour & Alam (2016), who reported 30-50% reduction in bond strength of RCA concrete when the embedment length doubled. This is mainly because of less bond stress is distributed along the bar when the embedment length increases, in addition to the increase of nonlinear distribution of bond stresses for larger embedment length, causing a reduction in bond strength. The other possible reason is associated with the increase of the number of bleed water trapped between a steel–concrete interfaces. Therefore, this increase in voids led to reducing the contacted area between the rebar and concrete. Hence, the average bond stress transferred to the surrounding concrete reduces when the bonded length increases. It should be noted that increase in bond length will not always lead to an increase in the bond force, since the non-uniformly distribution of applied load reaches a marginal

value close to zero at a certain distance, therefore a further increase in the embedment length will have no influence on the bond performance (Wassouf, 2015; Cairns &. Plizzari, 2003). After exposing to further corrosion, the degradation rate of bonding was higher for longer embedment length, and hence bond strength being more influenced by the change of bonded length. This might occur due to the presence of widening cracks resulting from corrosion along 167mm bonded bar, preventing the force from transferring between steel and concrete preventing the force from transferring between steel and concrete. The difference in embedment length also affected the failure mode of RCA concrete as the most specimens made with 5 Ø bonded length failed by pulling-out the reinforcement, whilst the splitting failure was observed when the contacted area between steel and concrete was longer.

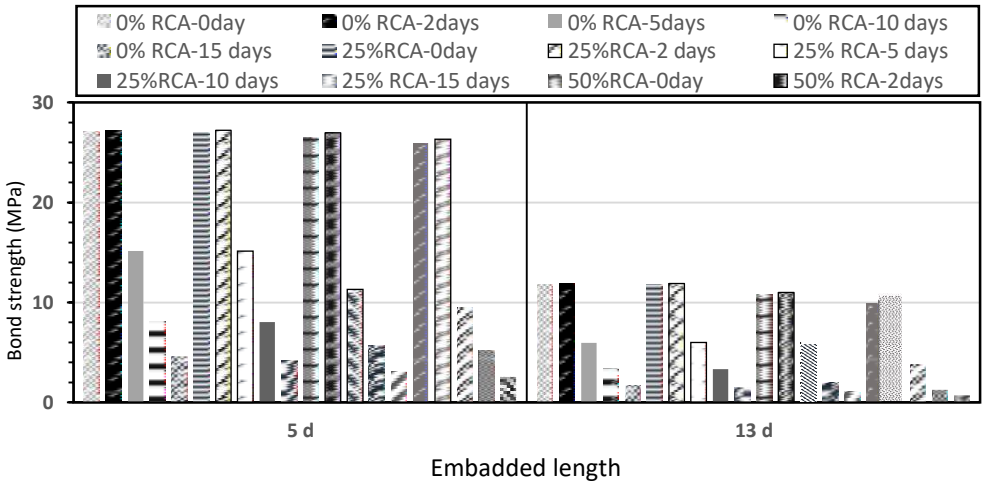

Figure 3.16 Effect of embedded length on bond strength.

From Figure 3.17, it can be seen that there are three types of failure mode were observed during the experiential work. For specimens having 12mm bar diameter, pull-out failure as shown in Figure 3. 17(a) occurred for the majority of those having smaller embedded lengths (60mm) due to the availability of adequate confinement provided by the large cover of concrete (96mm). This type of failure takes place when the shear force generated from concrete exceeds the radial force generated from

concrete force generated from concrete exceeds the radial force of steel bar, allowing steel reinforcement to crush the keys of concrete located between each pair of lugs, and therefore reinforcement easily pulled out without any visible concrete splitting. However, this mode developed to be accompanied by splitting in concrete when the accelerated time for corrosion extended to 10 days as shown in Figure 3. 17(b), because of the formation of some tiny cracks caused by corrosion products, making the confining action almost equiponderant with the radial forces of reinforcement (Tepfers et al., 2000). By reaching 15 days of corrosion, the mode of failure turned into splitting owing to the presence of longitudinal cracks, making concrete to be easily splitted. By increasing the embedment length for the same bar (12mm) to be 13Ø instead of 5Ø (where Ø is the bar diameter), all specimens either; corroded or un-corroded exhibited splitting failure as shown in Figure 3. 17(c), indicating that the confining action generated by the circumferential tensile forces in concrete was smaller than the radial force of steel bar. Therefore, cracks are easily propagated at a steel-concrete interface until reaching the outer concrete surface. By increasing the nominal bar diameter from 12mm to 20mm, the latter pattern failure was observed with all tested specimens. It is important to explain that no differences between NCA and RCA concrete specimens were observed in terms of failure modes, since little change in compressive strength was reported. Therefore, the results confirmed that the failure modes are heavily controlled by concrete strength, bar diameter, embedment length and rate of corrosion, rather than the type of concrete used.

(a) (b) (c)

Figure 3.17. Bond failure modes.

3.3.8 Concrete visual observation after corrosion

This part has only focused on the corrosion damage of reinforced concrete resulting from exposure to aggressive environments (15 days of corrosion acceleration). It is generally accepted that the mechanism of corrosion damage is fundamentally due to the formation of rust products (rustiness) around steel reinforcement, occupying up to six times of original steel volume (Andrade & Alonso, 2001). This expansion could lead to internal tensile stresses in concrete, and as a consequence, cracking and spalling are expected to occur on the surface of concrete (Vidal et al., 2004). Figure 3. 18 shows the difference between the specimens having 100% RCA and those containing only normal aggregate for the three types of used specimens. The visual observations of these samples exhibited a localized rust with a brownish colour along the periphery of embedded length of steel, while a wet orange oxide was spread over the internal surface of concrete. Nevertheless, it can be noticed that the amount of fluid corrosion products for the three types of specimens is more pronounced with RCA concrete, accompanied by a higher rate of steel dissolution, compared to normal concrete specimens. This is primarily attributed to its higher permeability and water absorption, allowing more moisture and chloride ions to reach steel-concrete interface. This may be assigned to the formation of longitudinal cracks along the whole length of the

sample, allowing chloride ions to easily penetrate concrete matrix, and therefore the process of corrosion was speeded up due to the large amount of electrons moving from cathode to anode sites. These visible cracks were less available with the specimens having a shorter bonded length (5 Ø).

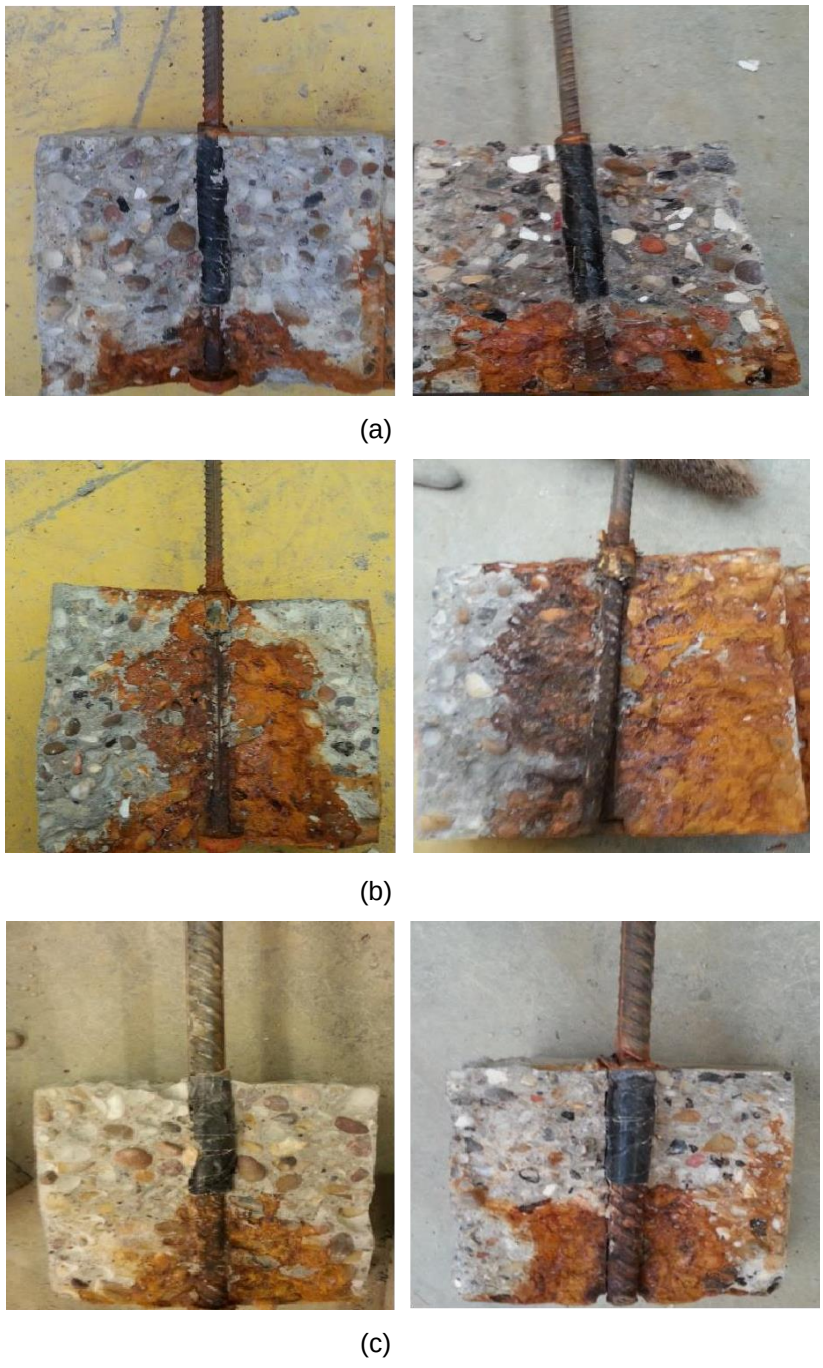

Figure 3. 18. Comparison of corrosion of steel in normal and recycled aggregate concrete for specimens having: (a). Ø 12mm, ld= 60 mm; (b). Ø 12mm, ld = 167 mm; (c). Ø 20mm, ld = 100 mm.

3.5 Conclusions

Experimental investigations were performed to evaluate the influence of recycled coarse aggregate on concrete properties and bond of reinforcing bars embedded in recycled coarse aggregate concrete under different levels of corrosion. Based on the results obtained from this investigation, the following conclusions can be drawn:

- The compressive strength of RCA concrete gradually reduces by increasing the amount of RCA in concrete. At 100% of RCA replacement rate, the compressive strength reduces by approximately 15% at 28 days; however, this effect becomes less pronounced as time of curing extended to 90 days.
- The tensile strength and flexural strength of RCA concrete are not significantly influenced by the replacement level of RCA; an 8% tensile/flexural strength reduction was observed at 100% RCA replacement. However, the water absorption of RCA concrete was considerably affected by the RCA content, reflecting the higher water absorption capacity of recycled aggregate.
- Overall, concrete with 25% RCA replacement level is comparable to normal concrete and did not show a significant change, even in harsh environmental conditions, and therefore, RCA can be recommended to be used up to this limit in structural applications.
- Corrosion of reinforcing steel initiated faster in RCA concrete than NCA, and larger corrosion rate was reported with the increase of the replacement level of RCA due to its high porosity and water absorption.
- The ultimate bond strength of un-corroded steel concrete specimens is slightly affected by the increase of RCA level, but larger steel bar diameters may exhibit more bond strength reduction. Furthermore, the difference of bond strength between NCA and RCA concrete becomes more pronounced as the corrosion rate increases.

- The bond strength of RCA concrete was strongly affected by corrosion products; bond strength slightly enhanced by up to 2% corrosion rate, however, this enhancement reported higher with the increase of RCA level. As the corrosion time further increased, the bond strength is significantly decreased, similar to that of conventional concrete. However, the rate of bond degradation between RCA concrete and corroded steel is much faster than that found in corroded conventional concrete.
- No significant differences between NCA and RCA concrete were observed in terms of bond stress-slip curves and failure mode before and after exposure to corrosion.
- For the same surface area, steel bars having larger diameter showed better bond strength for both NCA and RCA owing to the influence of surface ribs characteristics of steel bars. However, as the corrosion rate increased, this influence has reduced.

Chapter four

Properties of concrete incorporating different nano silica particles

4.1 Introduction

As demonstrated in chapter three, a significant degradation in the bond performance occurred in all tested specimens when RCA used as a replacement to normal aggregate, especially after exposure to severe corrosion conditions. Nano silica is seemingly a promising solution to enhance and compensate for the inferior performance of RCA in concrete. However, available research investigations showed scatter results when NS is used in concrete as illustrated in chapter two. This may be attributed to the difference in NS characteristics such as surface area, particle size and the state of NS whether dry or colloidal. Other reasons could be associated to the microstructure of concrete due to the change in w/b ratio. Therefore, the main aim of this chapter is to evaluate the influence of specific surface area and amount of nano silica on the performance of concrete with different water/binder (w/b) ratios. For this purpose, 63 different mixtures were produced using three different types of colloidal NS having various surface areas (52, 250 and 500 m^2/g) and water/binder ratios (0.4, 0.5, 0.6). By varying the replacement content of NS between 0.25% and 10% by weight of cement, the optimum ratio for each type was determined. Nano silica that shows the best performance in the current chapter will be selected to be added into RCA concretes in chapter five. The main properties were investigated in this chapter, namely compressive strengths, workability and water absorption. Moreover, the microstructure of concrete samples was analysed by the scanning electron microscopy and X-ray diffraction analysis was also carried out for concrete samples.

4.2 Experimental program

4.2.1 Materials

The cement used in this research was Portland cement (CEM I/A-LL 52.5R), manufactured by Hanson UK. Coarse Superplasticizers (Master Glenium 315 C) supplied by BASF was used as needed to maintain the workability of concrete. Three different commercial NS having different properties were utilized in this research. While the first type has a relatively small surface area (51.40 m^2/g), the other two types were obtained from another supplier with larger specific surface areas (250 and 500 m^2/g). These products were named; NS-50, NS-250, and NS-500, respectively based on their specific surface area. All the three NS types were in the colloidal suspension silica form. The main properties of these types of NS are described in Table 4.3, whilst they are chemically compared to cement components as demonstrated in Table 4.4. Moreover, X-ray diffraction analysis (XRD) was carried out using 2 Theta with a step width of 0.02 for these samples and presented in Figure 4.1. The XRD patterns for the three types of NS showed that the broad peak ranged between 11° and 23° on the X-ray scale at 2 Theta, which demonstrates the amorphous structure of NS particles with a very low of crystallinity as well as the presence of chemical compound in nano-form.

Table 4.1 NS physical properties.

Name	Colour	Relative density	Bulk density (kg/m^3)	Average particle size (nm)	SSA (m^2/g)	pH	Solid content of NS (%)
NS-50	Milky	1.2	-	98.7	51.40	9.4	40
NS-250	translucent	1.2	1200	15	250	6.8	30
NS-500	Clear cloudy	1.1	1050	5	500	10	15

Table 4.2 Chemical composition (%) of NS and cement.

Component	SiO_2	CaO	Al_2O_3	FeO_3	MgO	SO_3	Na_2O	R_2O	L.O.I
Cement	20.00	63.00	5.5	0.5	1.0	3.2	0.37	0.12	2.00
NS-50	99.99	-	-	-	-	-	-	-	0.01
NS-250	99.99	-	-	-	-	-	-	-	0.01
NS-500	99.99	-	-	-	-	-	-	-	0.01

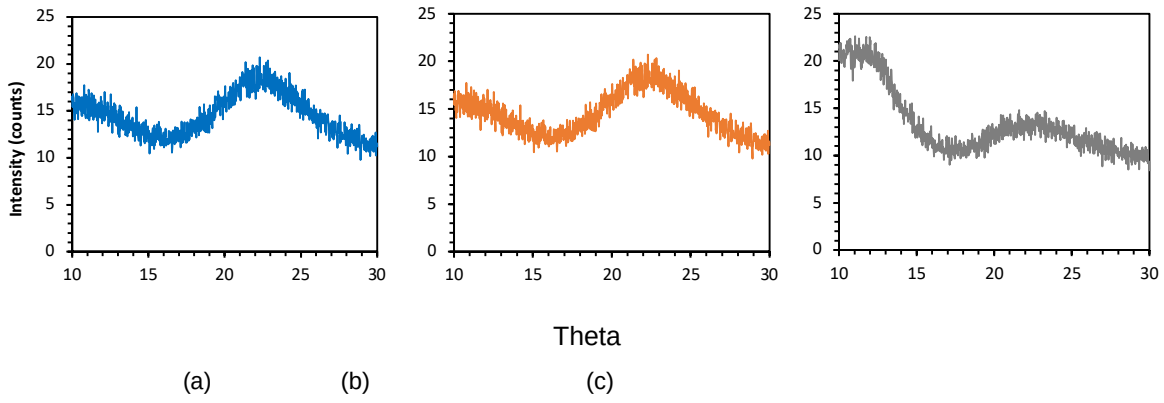

Figure 4. 1 XRD analysis for (a) NS-50, (b) NS-250 and (c) NS-500.

4.2.2 Concrete mix design, casting, and curing

To precisely investigate the influence of above-mentioned parameters, three different water/binder ratios (0.4, 0.5 and 0.6) were considered. The concrete mixing procedures, namely, the preparation of materials, mixing, casting and sampling were performed with accordance to BS 1881−125:1986. A 2001. The mixtures were prepared with various contents of NS including 0.25%, 0.50%, 0.75%, 1%, 1.25%, 1.5%, 2%, 3% for NS-250 and NS- 500, and continued with 5% and 10% for NS-50. Due to the high surface area of NS-250 and NS- 500, it was very difficult to mix concrete with higher NS dosages than 3%, even with SP. Moreover, concrete mixes with NS ratios of 0.25%, 0.75 and 1.25% were excluded for w/b = 0.5 and 0.6 as insignificant changes of compressive strength were recorded for concrete having lower w/b of 0.4 and same NS ratios. Details of concrete mix proportions are given in Table 4.5. In order to achieve a comparative study, all procedures related to mixing and curing were kept the same for all mixes except replacing cement by the required

quantity of NS. It is important to mention that the mixing water was adjusted based on the content of silica and the amount of water present in the solution for each NS type. Initially, NS was mixed separately with the mixing water for 3 mins to assure the particles of NS are uniformly dispersed. Then, the amount required of SP was mixed with the solution for another 1 min in order to maintain the workability. Meanwhile, coarse aggregate, cement and sand were mixed in a rotary mixer for 1 min, then, the solution was immediately added to concrete ingredients and mixed for another 2 mins. After casting, all specimens were covered by polyethylene sheets and left at room temperature for 24 hours before they were demoulded.

Table 4.3 Concrete mix proportions.

w/b ratio	Mix proportions (Kg/m^3)				NS (%)	Superplasticiser (%)		
	Cement	Total water	NFA	NCA		NS-50	NS-250	NS-500
0.4	450	180	664	1180	0	0	0	0
	448				0.25	0	0.125	0.25
	447				0.5	0	0.25	0.5
	446				0.75	0.125	0.375	0.625
	445.5				1	0.25	0.5	0.75
	444.3				1.25	0.3	0.625	0.875
	443.2				1.5	0.35	0.75	1
	441				2	0.55	1	1.5
	436.5				3	0.75	1.5	2
	427.5				5	1.25	-	-
	405				10	2.25	-	-
0.5	400	200	615	1205	0	0	0	0
	398				0.5	0	0.25	0.5
	396				1	0.25	0.5	0.75
	394				1.5	0.35	0.75	1
	392				2	0.55	1	1.5
	388				3	0.75	1.5	2
	480				5	1.25	-	-
	360				10	2.25	-	-
0.6	350	210	610	1210	0	0	0	0
	348.25				0.5	0	0.25	0.5
	346.5				1	0.25	0.5	0.75
	344.75				1.5	0.35	0.75	1
	343				2	0.55	1	1.5
	339.5				3	0.75	1.5	2
	332.5				5	1.25	-	-
	315				10	2.25	-	-

4.2.3 Tests procedures

Experimental testing was mainly focused on the influence of NS on compressive strength as a representative of the mechanical properties of concrete, whilst the transport properties of mixtures was represented by water absorption test. The influence of NS particles on fresh concrete was also discussed in terms of workability by conducting by the slump test according to BS EN 12350−2:2009. The compressive strength of concrete was performed in accordance with BS EN12390-3, 2009 on cubes (100*100*100 mm) after 7 and 28 days of curing. For each mix, three cubes were tested, and the mean value was calculated to represent the compressive strength of concrete. In order to investigate the microstructure of concrete containing NS, samples that showed the highest compressive strength at 28 days for each type of NS were collected from concrete cubes and prepared for scanning electron microscopy (SEM) images and X-ray diffraction. It is important to mention that the samples prepared for SEM images were coated by some gold atoms in order to be conductive surface. The water absorption was simply conducted using 100 mm cube specimens in accordance with BS1881-122, 2011.

4.3 Results and discussions

4.3.1 Workability

The workability of fresh concrete generally decreased with the increase of the specific surface area and content of NS in the mixture. The reduction in workability due to NS particles compared with a control mix was compensated by adding the required amount of superplasticizers (SP), based on the amount and the specific surface area for each type. Several trail mixes were carried out to adjust SP dosages and the required quantity of SP in the mix was considered as an index for the effect of NS on workability as shown in Figure 4. 2.

For w/b = 0.4, the addition of NS-50 needed a negligible amount of SP for most mixes due to the relatively small surface area of NS-50. However, the addition of NS with specific surface area (SSA) of 250 and 500 m^2/g hugely reduced mixes workability compared to the control mix, and thus it was essential to add SP even for small dosages of NS. This can be explained by the generation of a layer of adsorbed water molecules around these particles, causing more need of water to fill up the remaining void fraction. However, it was impossible to mix concrete with 5% and 10% for NS-250 and NS-500 as the required dosage of SP would have highly exceeded the recommended dosage from the manufacturer (1.2%). The highly agglomerated state with the increase of those small particles caused the formation of silanol groups (Si-OH) with firmly-held clusters, may explain the reason behind this remarkable reduction of workability (Hosseini et al., 2011). In addition, the free water in these mixtures was not sufficient to complete the hydration process. The reduction in the amount of lubrication water in concrete due to the increase of NS may also cause more entrapped air inside concrete, especially for high NS dosage (Sneff et al., 2010). It is worth mentioning that the spherical shape of NS particles might slightly minimise frictional forces among the particles (He et al., 2009), nevertheless, this feature was insufficient to encounter the decrease in workability. Results obtained by Li et al., (2018) indicated that the workability of concrete in terms of slump test decreased by 23% and 38% when 1% and 2% NS, respectively, were added to the concrete mixture. As expected, as w/b increased to 0.5 and 0.6, the workability for control mixtures significantly increased to record 80 mm and 160 mm, respectively, however, the addition of NS remarkably affected the workability for these mixes. It seems that less amount of SP was required to attain workability close to that found in the control mix for these w/b ratios compared to that used with w/b = 0.4, as observed by Isfahani et al. (2016).

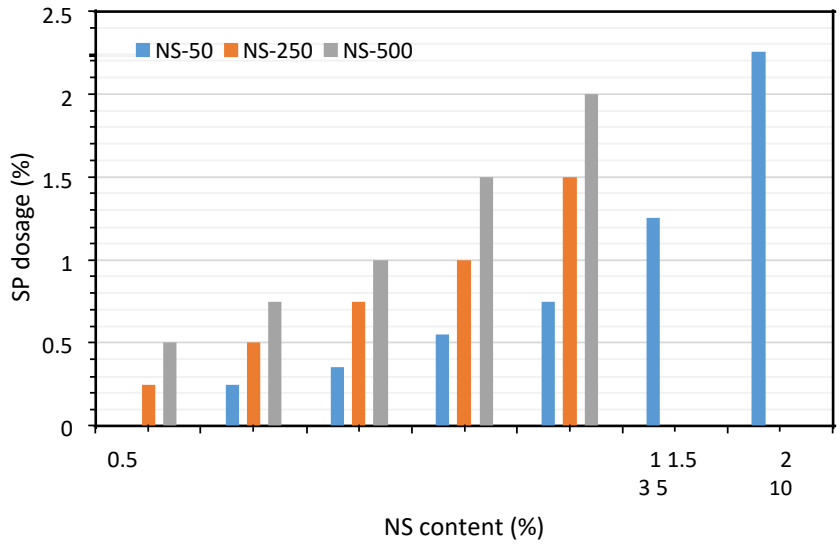

Figure 4. 2 The required amount of superplasticizers (%) against nan silica content (%) in concrete.

4.3.2 Compressive strength of nano silica concrete

4.3.2.1 Effect of nano silica particle size on compressive strength

Compressive strength is considered as the most important property of concrete as it can be an indicator for other properties. The variation of compressive strength at 7 and 28 days with NS content are presented in Figures. 4.3 to 4.5 for different w/b ratios. For w/b = 0.4, it can be observed that the compressive strengths of concrete containing NS at 7 and 28 days were higher than that of control concrete for all mixtures as shown in Figure 4. 3. However, the addition of small dosages of NS (0, 25, 0.50 and 0.75%), NS-50 showed insignificant improvements in compressive strength compared to control mixture, whilst the same dosages of NS-250 significantly enhanced the strength to reach over 16% enhancement at just 0.25%, then, it gradually improved with the increase of NS content. This can be supported by the fact that with smaller silica particles, the rate of cement hydration can also be enhanced due to the increase of the heat release by C3S-accelerated hydration rate (Land & Stephan, 2012).

By adding NS over 1%, more improvements were observed at 7 days for NS-50 to reach the highest strength gain (18.3%) at 3%, then it slightly decreased to record 12.7% and 8.4% at 5% and 10% NS, respectively. This reduction in the performance may be ascribed the excess of NS particles, causing no further chemical reaction, and hence the particles only act as fillers without any more contribution to compressive strength (Givi et al., 2013). Furthermore, the larger quantities of NS (5% and 10%) might enhance the pozzolanic activity, however, the amount of cement in the mixture was not sufficient to complete hydration process. In the other words, by replacing cement by 5 and 10% NS-50, the total quantity of NS in the mixture was more than the amount required for hydration process. Hence, the excess particles would leach out without contributing in further reactions. On the other hand, NS with SSA 250 g/cm^2 exhibited distinct strength enhancements to attain the maximum strength of 57.12 MPa at 7days by using 3% NS, representing approximately 38% compressive strength enhancement, while 31% improvement reported after 28 days compared to the control mix. This improvement reflects the ability of NS in refining the pores and enhancing hydration products distribution, particularly at interfacial transition zone (ITZ) as observed by Du et al., (2014). The findings recorded with NS-500 showed a considerable improvement even with very small dosages, reaching 17.3 and 20.7 % strength gain for concrete have 0.25% and 0.50% NS, respectively, even higher than that obtained by NS-250. This is likely to be explained by the “filling gap materials” principle where smaller size particles were more effective in filling small voids in addition to acting as a nucleus for C-S-H gel when cement particles were replaced by a little amount of NS. However, less improvement was noted with the increase of NS-500 content in concrete, which may be justified by the agglomerated state of NS particles, causing the precipitation of C-S-H gel on the surface of agglomerated NS

particles, preventing the particles from working individually and reacting with cement grains. Therefore, NS particles on the surface of agglomerate might just react with portlandite, while those inside the agglomeration will stay without reactions. Hence a lesser effect is expected with the increase of replacement ratio compared to that produced with those having smaller SSA (250m^2/g) (Kong et al., 2013). On the other hand, NS-50 was less effective on compressive strength at 28days, for example, 3% NS-50 increased the compressive strength to 60.2 MPa compared with that of the control mix (54.8 Mpa). The likely reason seems to be related to the large particle size of this type of NS, making it hard to fill the tiny pores in concrete (w/b = 0.4).

Figure 4.4 demonstrates the influence of the three types of NS on concrete made with w/b = 0.5 after 7 days and 28 days. It can be noted that all concrete containing NS enhanced compressive strength compared to the control mix. Overall, NS-250 was more beneficial for the formation of C-S-H gel than others by achieving the best strength throughout this investigation, whilst NS-50 generally showed the lowest results. However, the enhancement achieved for w/b = 0.5 was better than that for concrete having w/b = 0.4, agreeing with the results of Hossini et al., (2011), who reported that NS particles are more efficient in lower cement content. As depicted in Figure 4.5, the increase of w/b to 0.6 showed the best effects for the three types at both 7 days and 28 days. This can be attributed to the change in the microstructure of concrete matrix corresponding to the change in w/b ratio, thereby the number and size of pores in the matrix would be larger, compared to lower w/b ratios. Consequently, more influence of NS was observed with higher w/b ratios since their pores would be easily filled by NS particles, agreeing with other authors (Beigi et al., 2013; Khaloo et al., 2016). Another reason might be related to the influence of w/b ratio is the formation

of Ca(OH)2 crystal and Ettringite which are abundantly produced in a high w/b ratio, therefore, these unfavourable crystals could be handily absorbed in the existence of NS particles. As a result, more C-S-H gel particles are produced, making concrete matrix denser and more durable (Beigi et al., 2013; Khaloo et al., 2016). It is also observed that the increase of NS dosage did not play the main role in affecting the strength of concrete, however, it is greatly directly influenced by the change in the particle size and surface area of NS.

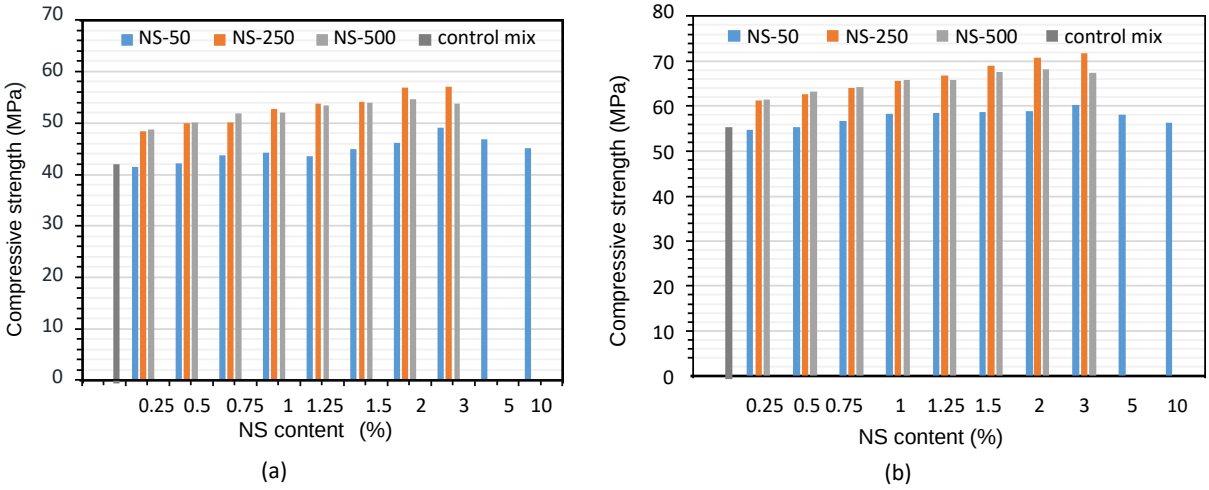

Figure 4. 3 Compressive strength of concrete containing nano silica for water/binder = 0.4 at curing time: (a) 7 days, (b) 28 days.

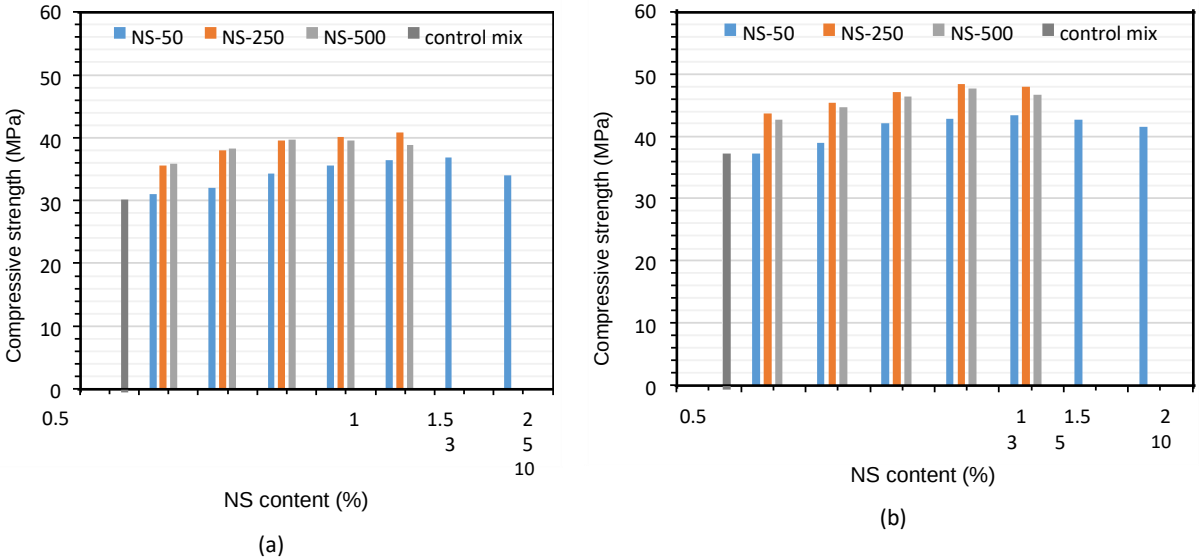

Figure 4. 4 Compressive strength of concrete containing nano silica for water/binder = 0.5 at curing time: (a) 7 days, (b) 28 days.

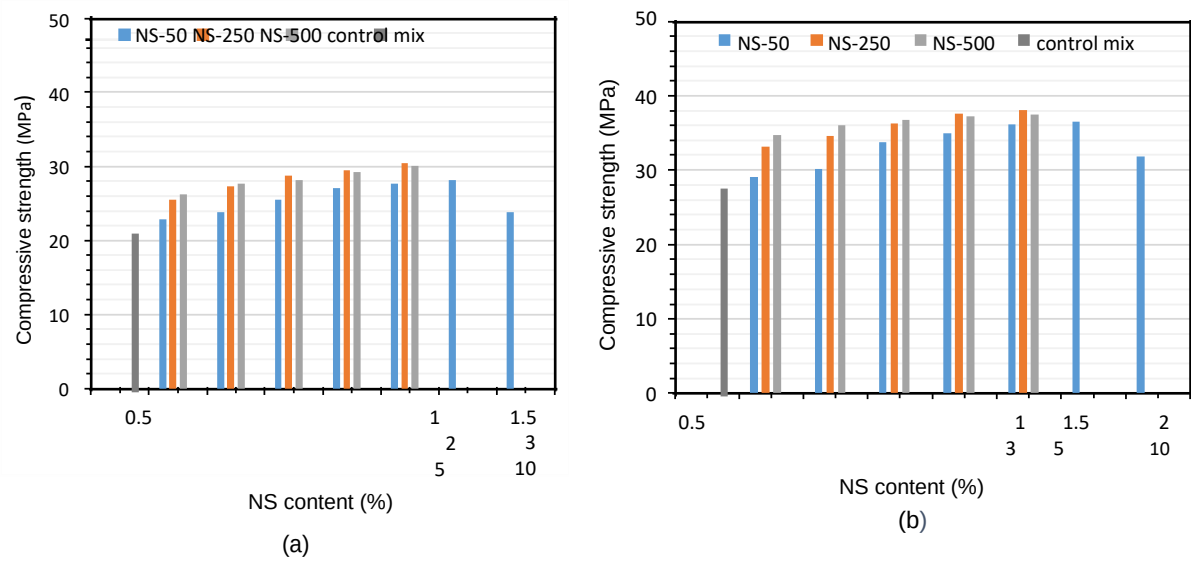

Figure 4. 5 Compressive strength of concrete containing nano silica for water/binder = 0.6 at curing time: (a) 7 days, (b) 28 days.

It can be concluded that amongst the three NS types used, NS-250 achieved the highest enhancement rate for 7 days and 28 days. The possible reason is the suitable size of its particles, which is very efficient in terms of packing ability, pozzolanic activity, and uniform dispersion, and hence the compressive strength distinctly improved for all cases. On the other hand, using a higher w/b showed the best improvement rate with all NS types, which in line with the findings observed by Isfahani et al. (2016), due to the change in concrete microstructure.

4.3.2.2 Optimum dosages of NS in concrete

Whilst the low dosage of NS can slightly improve concrete performance, the high concentrations may cause autogenous shrinkage due to the increase of self-desiccation, and consequently, a higher potential of cracking is predicted. It is stated that the optimum amount of NS is directly dependent on the specific surface area of the silica (Stefanidou & Papayianni, 2012). From Figure 4. 6, it can be noted that the influence of NS-50 on compressive strength was not very strong and did not exceed 18% at w/b = 0.4. However, this effect became more influential at w/b=0.5, to record the largest concrete compressive strength enhancement at 5% NS, achieving 25.75%

and at 7 days, then it reduced to 3% at 28 days. When w/b ratio increased to 0.6, the rate of enhancement significantly raised for both periods, reaching the optimum value at 5% at both periods, indicating that with the increase of w/b, larger amounts of NS have more influence on concrete strength as more NS particles are needed to densify the matrix (Khaloo et al., 2016). It could be also related to the change in the pore size in concrete microstructure, allowing NS with 98 nm particle size to fill these voids. Insignificant improvements with concrete having 10 % NS could be ascribed to the fact that the excess of NS may transform some amorphous C-S-H into tobermorite (C5S6H5), which has lesser strength properties in addition to the increase of unfavourable silica polymerization (Raki et al., 2010).

Regarding NS-250, the optimum ratio of NS ranged between 2-3% NS for all w/b ratios as shown in Figure 4. 7. It can be seen that the highest improvement ratio was also obtained with w/b=0.6 to record an incredible development at 7 days (48.29%), then slightly decreased at 28 days recording 40.4 %, agreeing with previous investigations (Parida, 2015). This can be supported by the fact that NS particles are more effective at early ages due to their high pozzolanic activity, leading to increasing the rate of C3S dissolution in the matrix, and therefore the formation of C-S-H gel would be accelerated (Qing et al., 2007). With respect to NS-500, the small quantity of NS showed a high rate of improvement, while the increase of NS content in concrete was not very beneficial for compressive strength as shown in Figure 4. 8. This could be associated with the agglomeration state of their particles, hindering the mix to obtain the maximum packing, and therefore compressive strength slightly increased with the increase of NS content. It can be probably said that the optimum ratio for NS-500 mostly reported at 2%. On the other hand, by reducing w/b ratio in the mixture, the lower contents of NS (0.5% and 1%) exhibited a better performance compared with

those having a higher w/b ratio (Khaloo et al., 2016). This can be associated with the reduction in hydration degree by decreasing w/b ratio, and therefore smaller amounts of Ca(OH)2 crystals are available to interact with NS particles. In fact, there are two reasons might lead to the reduction in improving the compressive strength when the quantity exceeds the optimum ratio. Firstly, the amount of NS particles in the mixture is higher than that required to react with calcium Hydroxide Ca(OH)2 formed from calcium silicate hydration during hydration process, resulting to leach out the surplus amount of silica (Salami & Behfarnia, 2013; Li & Zhang, 2006).

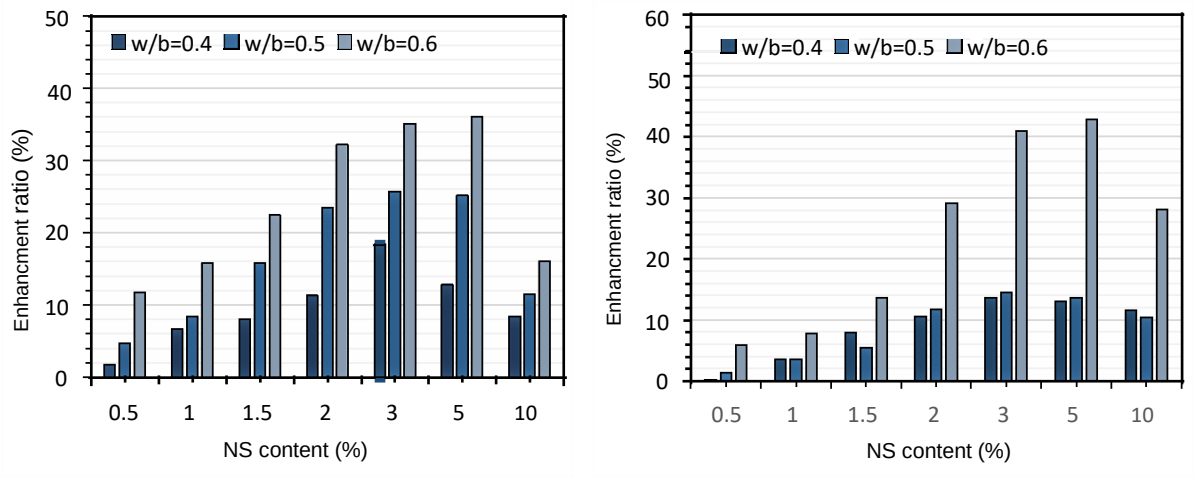

Figure 4. 6 Enhancement ratio of concrete mixed with NS-50 for different water/binder w/b ratios at: (a) 7days, (b) 28 days.

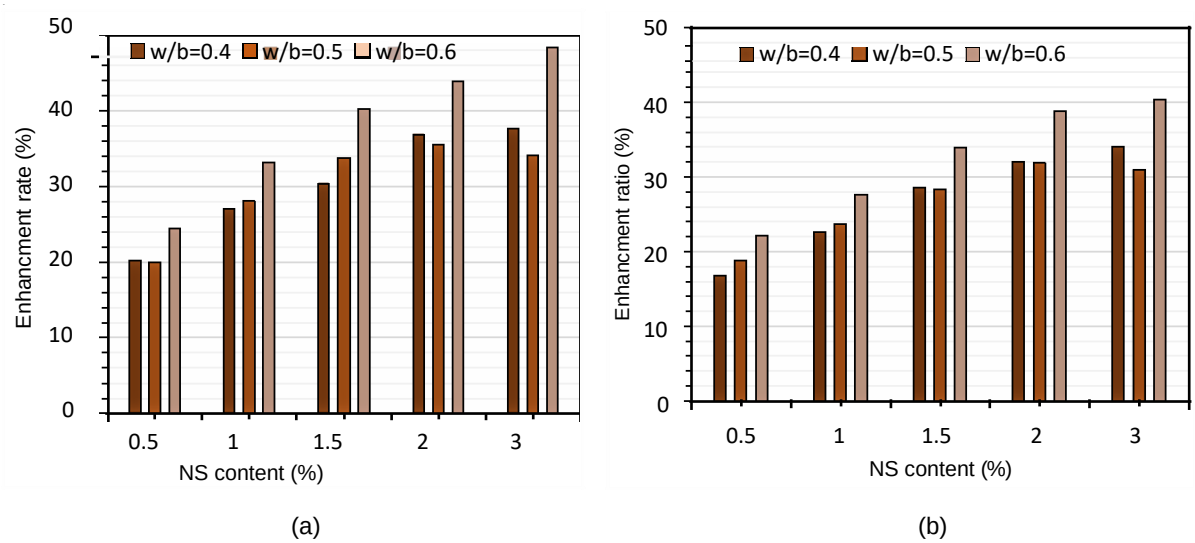

Figure 4. 7 Enhancement ratio of concrete mixed with NS-250 for different water/binder ratios at: (a) 7days, (b) 28 days.

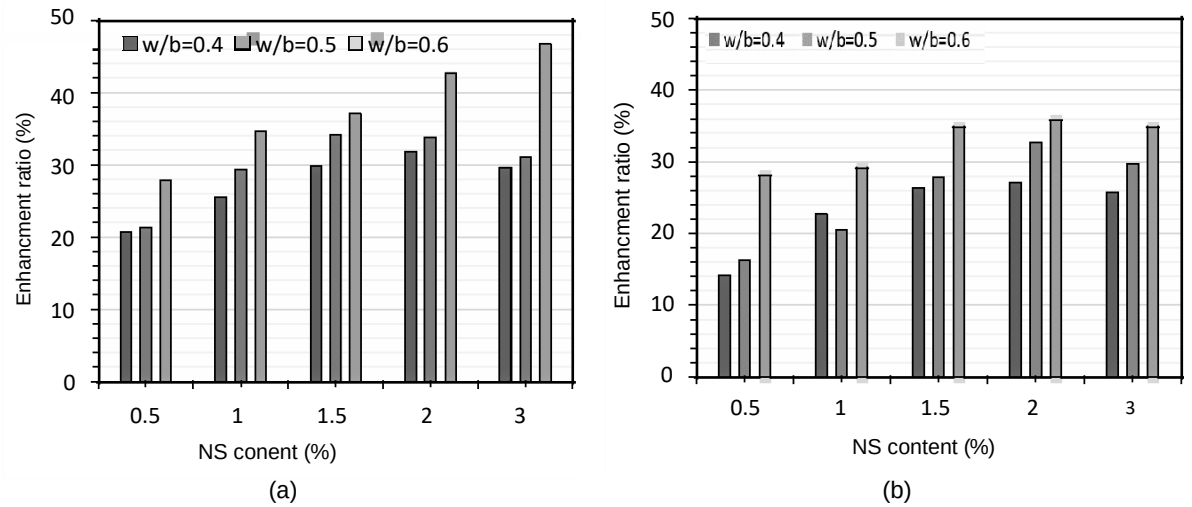

Figure 4. 8 Enhancement ratio of concrete mixed with NS-500 for different water/binder ratios at: (a) 7days, (b) 28 days.

Based on the obtained results, the optimum ratio of NS in concrete ranges between 2 and 5% of cement weight as illustrated in Figure 4. 9, based on its properties and w/b of the mixture. In addition, using a higher quantity of NS over than the optimum ones (2%-5%) might lead to the agglomeration state and the deficiency in dispersion of silica particles in the matrix; hence, the particles may become more difficult to uniformly disperse with the increase of its quantity in the mix, leading to forming a weak zone in the matrix, and therefore the strength of concrete decreases. Other investigations (Singh et al., 2013; Haruehansapong et al., 2014) indicated that the optimum value of NS cannot be constant with a specific surface area but it is affected by some factors such as the state of NS (colloidal or dry) and the production method. The results also indicated that the optimum NS ratio in concrete is found to be reduced corresponding to the decrease in w/b ratio, which might be due to lesser Portlandite available in the matrix.

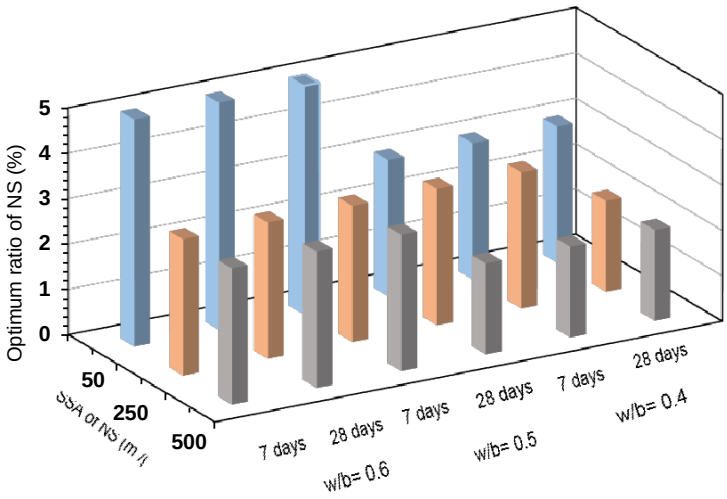

Figure 4. 9 The influence of water/binder ratio on the optimum ratios of nano silica.

4.3.3 Water absorption

Water absorption can be used as a significant indicator for quantifying concrete durability due to the change of pores volume. The variation of water absorption of concrete for the three types of NS considered is demonstrated in Figure 4. 10. At w/b=0.4, all types of NS exhibited an increase in water absorption resistance with the increase of NS content to reach 2.8%, 2.4% and 2.52 at 3% NS compared to 3.7% for control mix. This reduction is primarily due to the ability of NS in refining the pore size distribution, particularly at the interfacial transition zone (ITZ), and therefore the volume pores in matrix are clearly reduced (Du et al., 2014). It is observed that whilst small quantities of NS effectively reduced entering water into concrete matrix, the increase of NS content slightly increased the resistance against water absorption. This phenomenon might be clarified by the reduction in the unfilled voids in concrete with increasing NS content, especially in concrete made with w/b=0.4. As w/b increased to 0.5, the ability of concrete to absorb water became higher, recording 4.9% for control mix. However, the use of NS partially hindered this increase by blocking transport paths for water ions by activated NS particles. Therefore, all mixtures incorporating

NS particles absorbed less water compared to control one due to the improvement of their microstructure, and the ingress of water ions into concrete matrix reduced up to 3.5% in some cases.

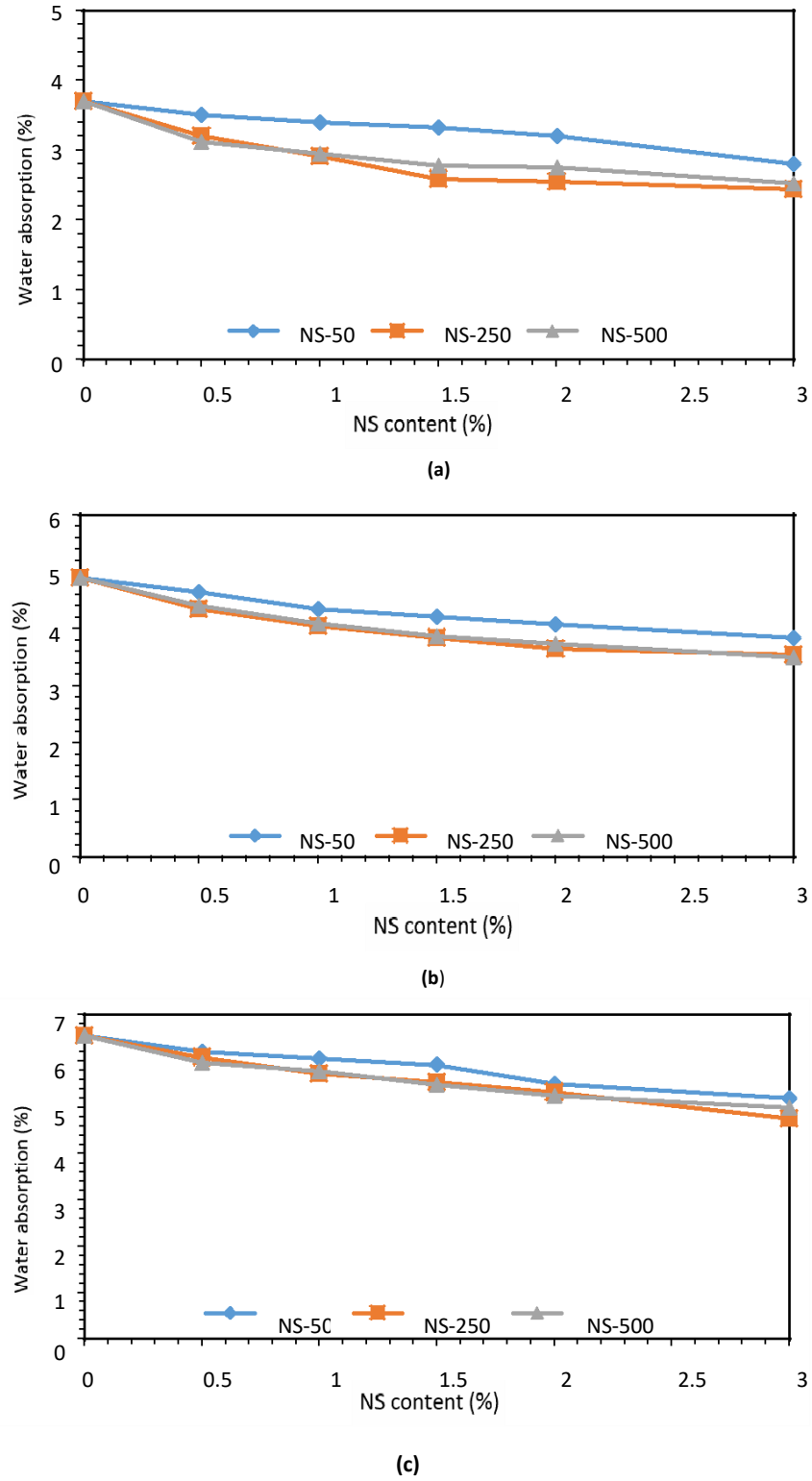

Figure 4. 10. Water absorption of concrete containing different types of nano silica for wate/binder ratios: (a) =0.4, (b) = 0.5 and (c) =0.6

With increasing w/b to 0.6, the microstructure of concrete matrix became poorer and rich by connected voids, and hence, water might easily penetrate concrete surface and reach inside concrete. However, the performance of NS particles in preventing concrete from absorbing water became clearer especially for NS-50 to record almost the same influence obtained by the other types (NS-250 and NS-500).

4.3.4 Microstructural investigations

4.3.4.1 SEM analysis

The microstructure of the samples was analysed by scanning electron microscopy (SEM). The SEM photographs obtained in this study exhibited good correlations with the results obtained for other properties such as compressive strength and water absorption. Figure 4.11 shows some selected morphological characteristics of the microstructure of concrete made without NS. It can be seen that pores and micro-cracks are easily observed in the microstructure of this mixture. Moreover, some unfavourable crystals, such as Ca(OH)2 exist in the matrix. By incorporating 3% of NS-50, it can be observed that concrete microstructure was somewhat improved as shown in Figure 4.12, indicating the ability of these particles in producing an additional C-S-H gel and filling many pores in the matrix. However, some tiny volume of pores still exist, preventing NS-50 particles from occupying these pores. As observed in Figure 4.13 for concrete sample with 3% of NS-250, the amount of capillary pores was remarkably reduced as the use of NS-250 led to a further densification in the microstructure of concrete mixtures, making the matrix rich with C-S-H, which is mainly affected by the shape and size of the particles, particles distribution topology of the matrix and the concentration of particles (Aggarwal & Siddique, 2014). Results obtained by Varghese (2014) revealed that the microstructure of concrete incorporating NS was more uniform, and the high stiffness and chain length of C-S-H

increased almost by 20% compared to the control mix. In comparison with NS-50, the microstructure of NS-250 samples led to a denser microstructure, especially at the interfacial transition zone (ITZ) between aggregate and paste. The SEM investigations of NS particles with 2% of a high specific surface area (NS-500) showed almost similar results with that found in concrete incorporating NS-250 as presented in Figure 4.14, however, agglomeration state was spotted in some areas due to their ultra-high surface area.

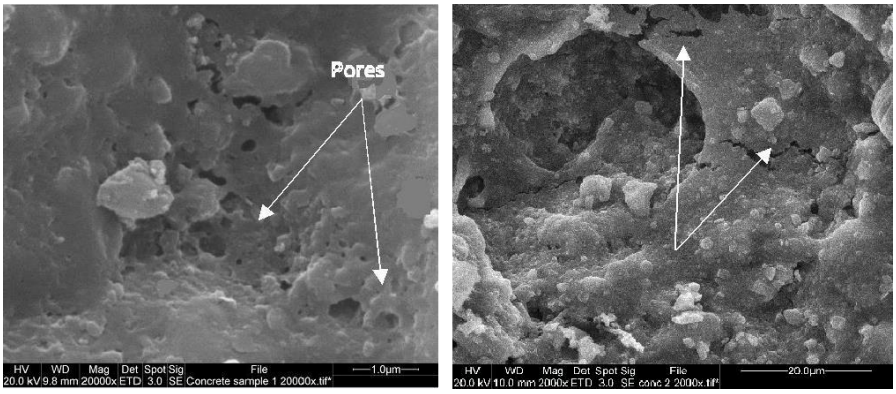

Figure 4.11 Scan microscope photographs of concrete made without Nano silica.

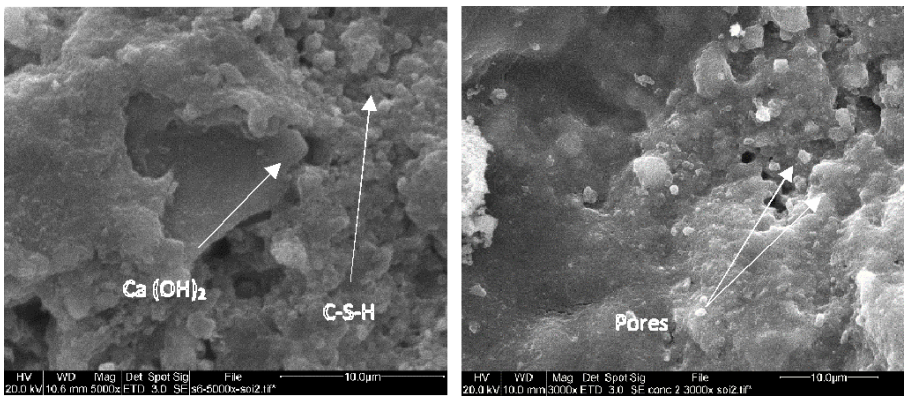

Figure 4.12 Scan microscope photographs of concrete made with 3% of NS-50.

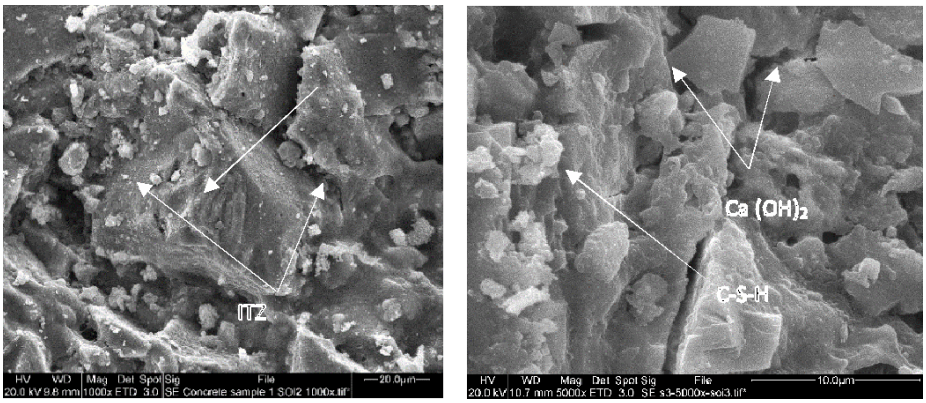

Figure 4.13 Scan microscope photographs of concrete made with 3% NS-250.

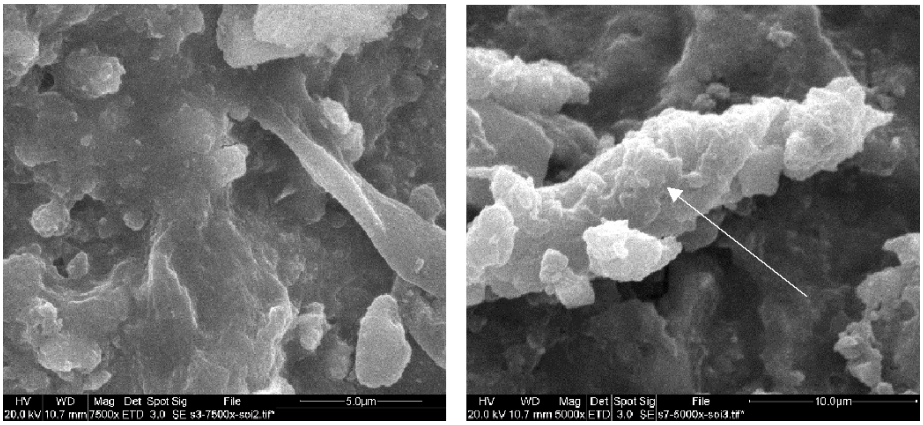

Figure 4.14 Scan microscope photographs of concrete made with 2% of NS-500.

4.3.4.2 XRD

XRD analysis was carried out for concrete made with and without NS at the age of 28 days. In order to apply XRD analysis, samples with the highest compressive strength were collected from concrete cubes for each type of NS, and finely grounded. These selected samples had 3%, 3% and 2% of NS-50, NS-250 and NS-500, respectively. As observed from Figure 4.15, it can be clearly seen that the main crystallization components found in concrete were as follows: quartz, portlandite Ca(OH)2, in addition to un-hydrated grains including Alite (C2S) and Belite (C3S). Generally, it is not possible to identify directly the peaks of C-S-H which is the main source of concrete strength by XRD due to the low crystallinity of C-S-H, making it difficult for the radiations to be diffracted into peaks. However, portlandite Ca(OH)2 which has an

inverse relation with C-S-H can be used to quantify the performance of concrete; if C-S-H is decreased, more CH would be spotted in XRD results (Shaikh et al., 2014). Evidently, the peaks intensity of Portlandite, Alite and Belite were deceased when NS used in concrete for all samples containing NS compared to the control one. This is mainly attributed to the high pozzolanic activity of NS particles, in addition to its ability in consuming Ca(OH)2 particles producing an additional amount of C-S-H gel, which is the main source of concrete strength (Khaloo et al., 2016). The reduction in the peaks of un-hydrated grains (C3S and C2S) indicated the efficiency of NS particles in the reaction with these grains and improving hydration process. It can be also noted that NS-250 showed the lowest intensity values of Ca(OH)2, confirming the previous results obtained from compressive strength test. The main peaks for all samples were identified as quartz peaks due to the large number of aggregate particles whether fine or coarse containing quartz. The increase of quartz peaks was noticeable when NS added to the matrix, especially with NS-250 and NS-500 indicating the presence of NS in the matrix.

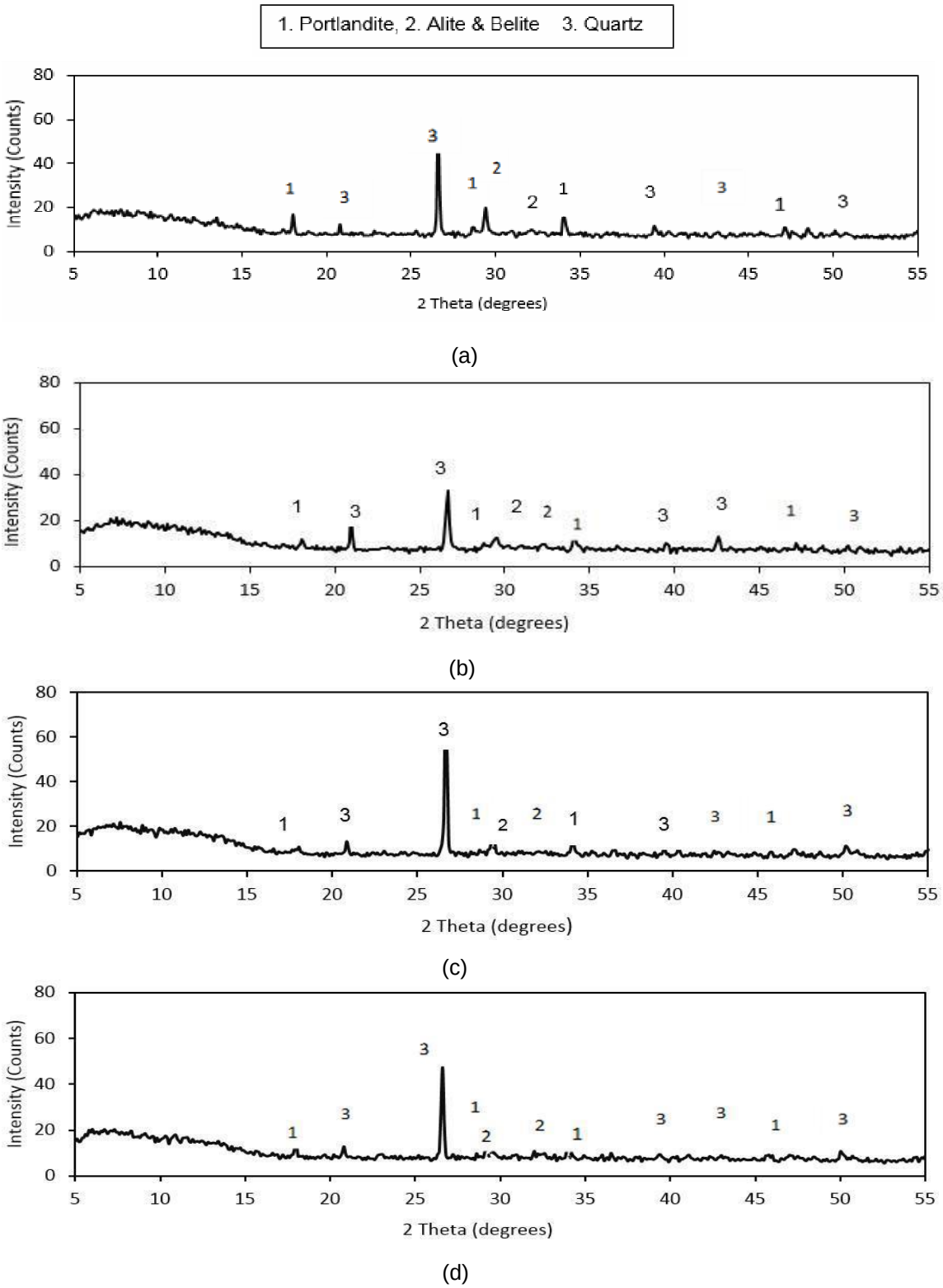

Figure 4.14 X-ray diffraction spectra of concrete made with and without different types of nano silica at 28 days: (a) without NS, (b) NS-50, (c) NS-250 and (d) NS-500.

4.4 Conclusions

This paper presented the influence of surface area and dosage of NS on concrete properties. The following conclusions may be drawn from the experimental results:

- Influence of NS on concrete workability is mainly governed by the specific surface area of NS and partially affected by the w/b ratio of concrete mix. While the increase of specific surface area could hugely decrease concrete workability, the increase of w/b seemingly leads to reducing the demand water for mixing concrete incorporating NS through hydration process.
- The influence of NS on concrete compressive strength was more pronounced at the early age (7 days) for all mixes compared with that at 28 days, corresponding to the acceleration of hydration process due to the ultra-high surface area of these materials.
- The compressive strength of concrete is directly influenced by the change of the specific surface area of NS. Amongst the three used types of NS, NS with SSA of 250 m^2/g showed the highest enhancement rate of compressive strength at 7 and 28 days, followed by NS with SSA of 500 m^2/g, whilst using NS with SSA of 51.4 m^2/g was less advantageous for all mixes.
- The optimum replacement ratio for each type of NS is greatly associated with the particles reactivity and agglomeration state. Apparently, it becomes higher since the size of NS particles is larger, however, it is found to be ranging between 2% and 5%. The optimum ratio of NS also related to w/b ratio; it is found to be increased with the increase of w/b ratio corresponding to the growth of pores and calcium hydroxide in the matrix.
- The increase of w/b ratio leads to improving the performance of NS particles in the matrix due to the accessibility of NS in filling the voids available in concrete made with higher w/b ratio. The water absorption considerably

decreased when NS particles were used in concrete, especially with higher w/b ratios.

- Results obtained by XRD analysis and SEM investigation confirmed the contribution of the use of NS as a partial replacement to cement in improving the performance of concrete by enhancing the pore structure of concrete.

Chapter five

Bond strength between corroded steel and recycled aggregate concrete incorporating nano silica

5.1 Introduction

Limited information related to the application of nano silica in recycled aggregate concretes has been available in the literature. However, investigations on the effect of nano silica on the bond performance of reinforcement embedment length in recycled aggregate concrete have not been conducted yet. Therefore, in this chapter, the selected nano silica in chapter four has been added into both normal and RCA concretes to investigate the bond strength and corrosion rate for recycled aggregate concretes incorporating nano silica under different levels of corrosive environments. The experimental work consisted of testing 120 pull-out specimens prepared from different mixtures to be compared with those made without NS (chapter three). The main parameters studied were the amount of recycled aggregate (i.e. 0%, 25%, 50% and 100%), nano silica (1.5% and 3%), embedment length (5 and 13Ø) as well as reinforcement diameter (12 and 20mm). Different levels of corrosion were electrochemically induced for 2, 5, 10 and 15 days. The experimental findings were compared to available equations for predicting the bond strength of un-corroded/corroded steel embedded in concrete, whilst a new formula for predicting the normalized bond was proposed. Finally, the economic impact of using nano silica in RCA concrete was discussed.

5.2. Experimental program

The same materials presented in test specimens in chapter four were used in this chapter including cement, fine aggregate, normal and coarse aggregate and steel reinforcement, whilst the colloidal nano silica (NS-250) exhibited the best enhancement ratios in all tested conducted in chapter four was selected to be only used in this chapter. Superplasticisers (SP) (Master Glenium 315 C) was used in accordance with BS EN 12,350 − 2:2009. Similarly, all procedures associated to the details of pull-out specimens, accelerating corrosion, pull-out test set-up, and mass loss measurement were kept the same as performed in chapter four. The same mix design was also conducted; however, small dosages of cement was replaced by nano silica (1.5% and 3%), and SP was added to compensate the decrease occurred in the mixtures' workability. The results obtained from the trail mixes showed that about 0.75% and 1.5% of SP were needed for mixes prepared with 1.5% and 3% NS, respectively, to obtain almost similar slump value, since the workability significantly decreases with increasing the quantity of NS in the mix. Therefore, new eight different mixtures containing NCA, RCA and NS were performed in this chapter to be compared with those prepared without NS (Chapter four) as presented in Table 5.1, whilst the details of all tested specimens in this research was demonstrated in table 5.2.

Table 5.1 Concrete mixture proportions (Kg/m^3).

Series	NCA	RCA	NFA	Cement	Water	NS	SP
R0	1180	-	664	450	180	-	-
R25	885	255	664	450	180	-	-
R50	590	510	664	450	180	-	-
R100	-	1120	664	450	180	-	-
R0-NS1.5	1180	-	664	443.25	180	6.75	3.75
R25 NS1.5	885	255	664	443.25	180	6.75	3.75
R50- NS1.5	590	510	664	443.25	180	6.75	3.75
R100- NS1.5	-	1120	664	443.25	180	6.75	3.75
R0-NS3	1180	-	664	436.5	180	13.5	7.5
R25-NS3	885	255	664	436.5	180	13.5	7.5
R50-NS3	590	510	664	436.5	180	13.5	7.5
R100-NS3	-	1120	664	436.5	180	13.5	7.5

Note: NCA= normal coarse aggregate; RCA= recycled coarse aggregate; NFA= normal fine aggregate; NS= nano silica; SP= superplasticizers.

Table 5.2 Description of tested specimens.

Series	Group	NS %	RCA %	Ø (mm)	l_d (mm)	Period of corrosion (days)
Series I	RO	0	0	12	60	0, 2, 5, 10, 15
	R25	0	25			
	R50	0	50			
	R100	0	100			
	RO-NS 1.5	1.5	0			
	R25-NS 1.5	1.5	25			
	R50-NS 1.5	1.5	50			
	R100-NS 1.5	1.5	100			
	RO-NS3	3	0			
	R25-NS3	3	25			
	R50-NS3	3	50			
	R100-NS3	3	100			
Series II	RO	0	0	12	167	0, 2, 5, 10, 15
	R25	0	25			
	R50	0	50			
	R100	0	100			
	RO-NS 1.5	1.5	0			
	R25-NS 1.5	1.5	25			
	R50-NS 1.5	1.5	50			
	R100-NS 1.5	1.5	100			
	RO-NS3	3	0			
	R25-NS3	3	25			
	R50-NS3	3	50			
	R100-NS3	3	100			
Series III	*RO*	*0*	*0*	*20*	*100*	*0, 2, 5, 10, 15*
	R25	0	25			
	R50	0	50			
	R100	0	100			
	RO-NS 1.5	1.5	0			
	R25-NS 1.5	1.5	25			
	R50-NS 1.5	1.5	50			
	R100-NS 1.5	1.5	100			
	RO-NS3	3	0			
	R25-NS3	3	25			
	R50-NS3	3	50			
	R100-NS3	3	100			

5.3 Results and discussions

5.3.1 Mechanical properties

The compressive strengths of NCA and RCA concretes made with and without nano silica at the ages of 7, 28 and 90 days are exhibited in Figure 5.1. From the presented results, it can be seen that the compressive strength tends to decrease as the replacement content of RCA in the mixture increases at all test ages. The use of 50%

and 100% RCA resulted in 8.5% and 15% reduction of compressive strength at 28 days, respectively, in comparison with normal concrete. It is documented that the strength of concrete is mainly dependent on aggregates' strength, cement and the weak interfacial transition ITZ between aggregate and cement mortar. The reduction in strength of RCA concrete is commonly linked to the ITZ located between the old and new cement, resulting from the presence of attached old mortar on aggregates' surface. However, as the time of curing reached 90 days, the development of strength for 50 and 100 RCA concretes were slightly higher than that found in conventional concrete reporting 9.5% and 11.5% enhancement, respectively, whilst the normal concrete just enhanced 8%.

By incorporating 1.5% NS in mixtures, it can be clearly seen that the compressive strength for both normal and recycled aggregate concretes greatly enhanced, especially at an early age (7days) achieving 30% and 43%, respectively, of their respective compressive strengths without NS, owing to the extremely high specific surface area of nano silica, which in turn accelerates the hydration rate and facilitate the reaction with calcium hydroid Ca(OH)2, producing an additional calcium silicate hydrate. However, the effect of NS became less for both NCA and RCA concretes in terms of strength development as time of curing increases, reporting just 17% and 18.3% enhancement, respectively at 90 days compared to those made without NS, agreeing with the results obtained by other authors (Li et al., 2017). Moreover, the addition of 1.5% nano silica to fully RCA concretes was sufficient and even better than the conventional concrete in terms of compressive strength at all age tested.

Regarding the effect of NS content, it can be seen that by doubling the replacement content of NS to be 3%, the strength of concrete continually promoted, making 29.5% and 37.5% enhancement at 28 days for NCA and RCA concrete, respectively, which

are between 7-13% higher than that reported with 1.5% NS. This slight improvement might have occurred as a result of agglomeration state, preventing some NS particles from reacting with cement particles. The results also indicated that the substitution 25% of NCA by RCA showed almost the same trend with the obtained in normal concrete at all test ages, regardless of the replacement dosage of nano silica, which in agreement with previous research (Rao et al., 2011). With respect to strength gain, the findings showed that the 100% RCA concrete incorporating NS achieved higher strength gain ratio, in comparison with conventional concrete at all curing ages. This increased gain ratio is mainly attributed to the higher capillary spaces and larger pores available in the microstructure of RCA concrete. Therefore, NS particles can easily fill up these spaces, in addition to the ability of such particles in reacting with the large amount of Ca(OH)2 found in RCA concrete, producing more C-S-H gel, which is similar to that reported in recent investigations done by Li et al., (2017).

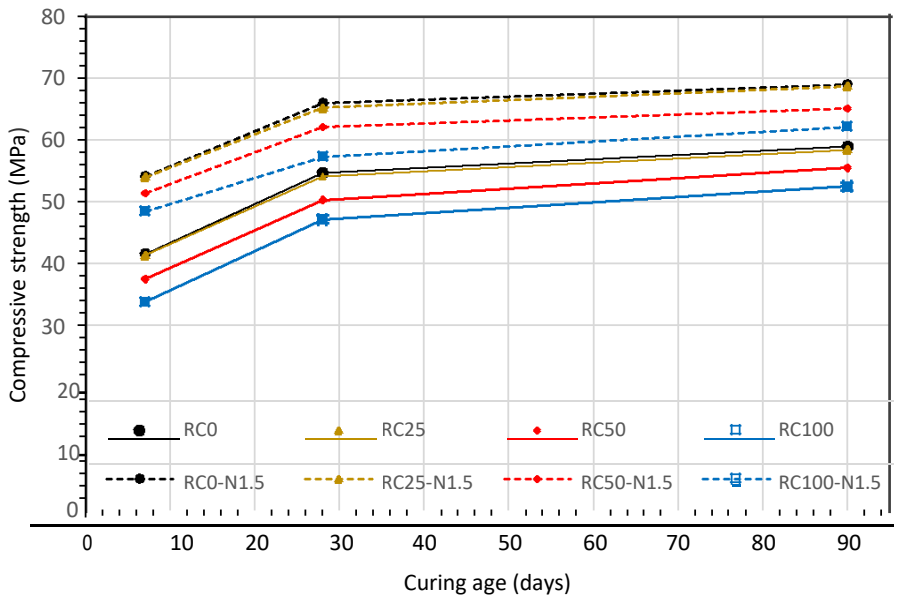

(a)

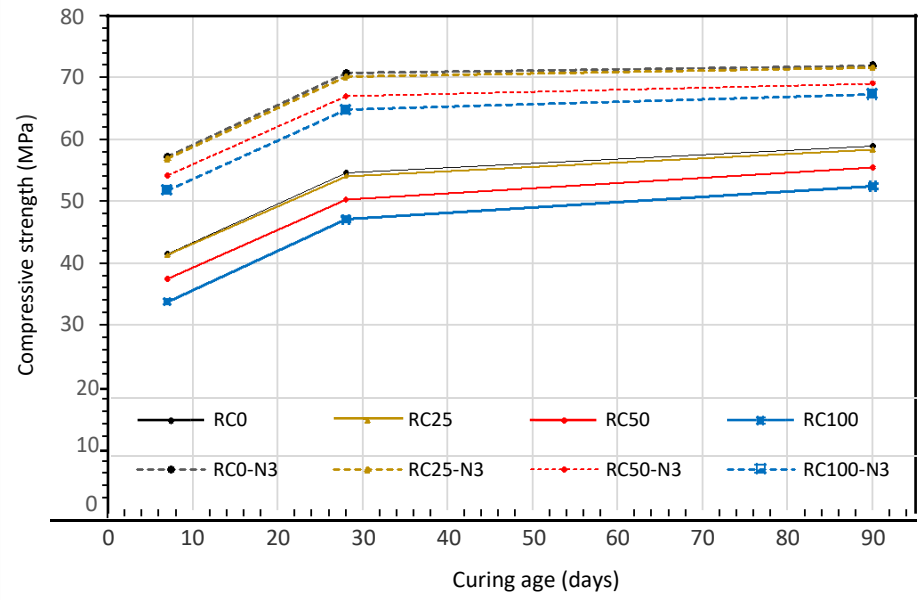

(b)

Figure 5.1 Compressive strength of concrete mixtures made with: (a) 1.5% and (b) 3% nano silica.

The influence of nano silica on the other important concrete properties was also investigated and presented in Figure 5.2. As exhibited in Figure 5.2 (a) and (b), the tensile strength and flexural strength showed almost the same trend and they were less affected by using RCA compared to compressive strength, causing a reduction of not more than 10% for a fully replacement concrete, indicating that these properties are heavily dependent on the binder effect rather than the type of aggregate (Mukharjee & Barai, 2014).

The incorporation of NS was more than enough to compensate the reduction occurred in RCA mixtures by enhancing the bond between aggregate and cement paste at ITZ, and achieving a development in tensile and flexural strengths ranged between 10-16%. Similarly, the density of concrete tends to decrease up to about 8% based on the amount of RCA in concrete, agreeing with the findings of Verian, (2012); Xiao et al., (2005). This reduction is mainly attributed to the lower specific gravity of RCA in addition to the presence of attached old mortar on RCA surface, making concrete more concrete porous and lightweight. The density of all concrete mixtures was slightly improved by the addition of 1.5% and 3% NS by filling the voids present between old and new mortars at ITZ. Nevertheless, the density of 100R-3NS is still lower than that found in the control mix, which might be explained by the presence of some lightweight aggregate grains (gypsum) in RCA. On the other hand, the absorption capacity was clearly risen by increasing the percentage of RCA in concrete mixtures, reaching about 40% higher for 100% RCA concrete compared to the corresponding concrete. This unfavourable increase in water absorption is mainly reflected the higher water absorption capacity of RCA. As shown in Figure 5. 2 (d), the water absorption capacity was hugely dropped for all mixtures, especially for those prepared with fully recycled aggregate, reporting about 25% and 36% reduction at 1.5% and 3% NS, respectively.

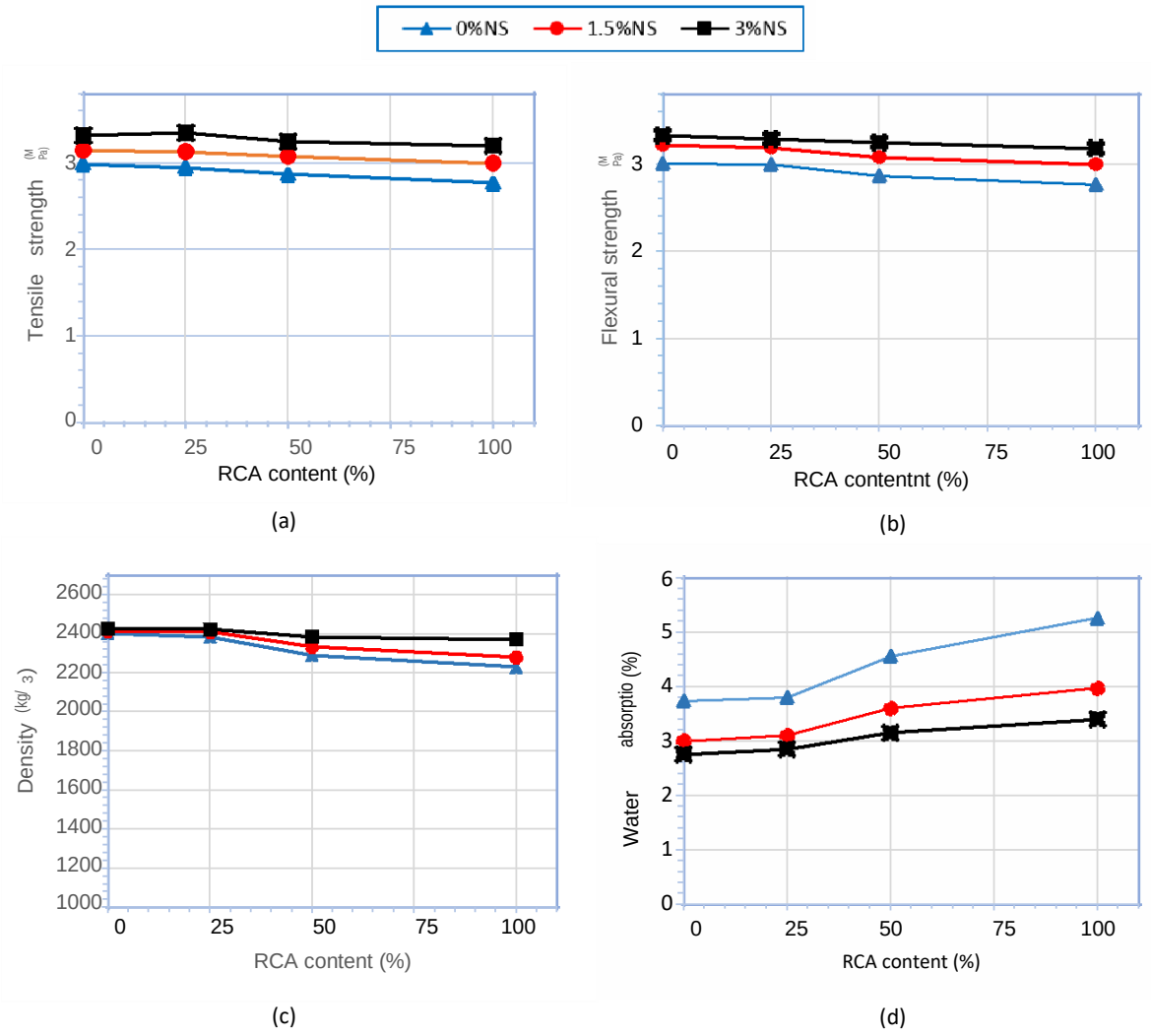

Figure 5.2 Properties of concrete properties made with different ratios of nano silica.

5.3. 2 Influence of nano silica on corrosion resistance

The corrosion rates resulted from applying impressed voltage technique for each exposure period (2, 5, 10 and 15 days) are presented together in Figure 5.3. A wide range of corrosion rate in terms of mass loss was obtained during the current investigation ranging between 0.7% up to about 20%. As can be seen from Figure 5.3, higher mass loss was reported with specimens having larger embedment length (Ø 12mm, ld = 167 mm), since some longitudinal cracks were spotted with such specimens, allowing chloride ions to readily reach steel surface. From the presented results, it can be recognised that the corrosion rate has significantly raised for the three

different types of specimens when NCA was substituted by 50% and 100% RCA, whilst the replacement of quarter quantity showed comparable results. For instance, the average mass loss after two days for specimens made with 100%RCA specimens having 167mm bonded length was about 20% higher than those free of RCA. This influence developed over exposure time to be about 23% and 37% higher corrosion, respectively, compared to reference concrete, and became more apparent by reaching 15 days, reporting more than 20% weight loss, which approximately 40% higher compared to normal concrete. This is fundamentally ascribed to the high water absorption and permeability of RCA, which are directly related to the presence of old paste mortar on aggregate' surface. The higher corrosion rates might be also linked to the presence of contaminants in RCA (e.g. sulphate, chloride and carbonate), which facilitate the de-passivation of protective film around steel reinforcement (Behera et al., 2014). Nevertheless, the addition of 1.5% NS to mixtures considerably enhanced the resistance of specimens against corrosion for both normal and RCA concretes. For example, the average corrosion rate for R0-NS1.5 is reduced by about 31%, 36%, 45% and 48% at 2, 5, 10 and 15 days, respectively owing to the pore filling ability of nano-silica, as it fills the pores up to nano size, and thereby making concrete less permeable. This improvement in corrosion resistance was more obvious with the increment of RCA content, reporting lower corrosion rates of 40%, 42%, 45% and 52% for 100%RCA at the same periods. This might be explained by the higher capillary spaces and larger pores available in the microstructure of RCA concretes. It is also observed that the incorporation of 1.5% NS with 100RCA concrete reduced the growth of corrosion and showed a slightly better resistance at all ages, in comparison with control specimens made without NS. By doubling the quantity of NS to 3%, lower corrosion products were accumulated around steel reinforcements for all mixes;

however, the corrosion rate reduced by just 5-25%, in comparison with those containing 1.5% NS.

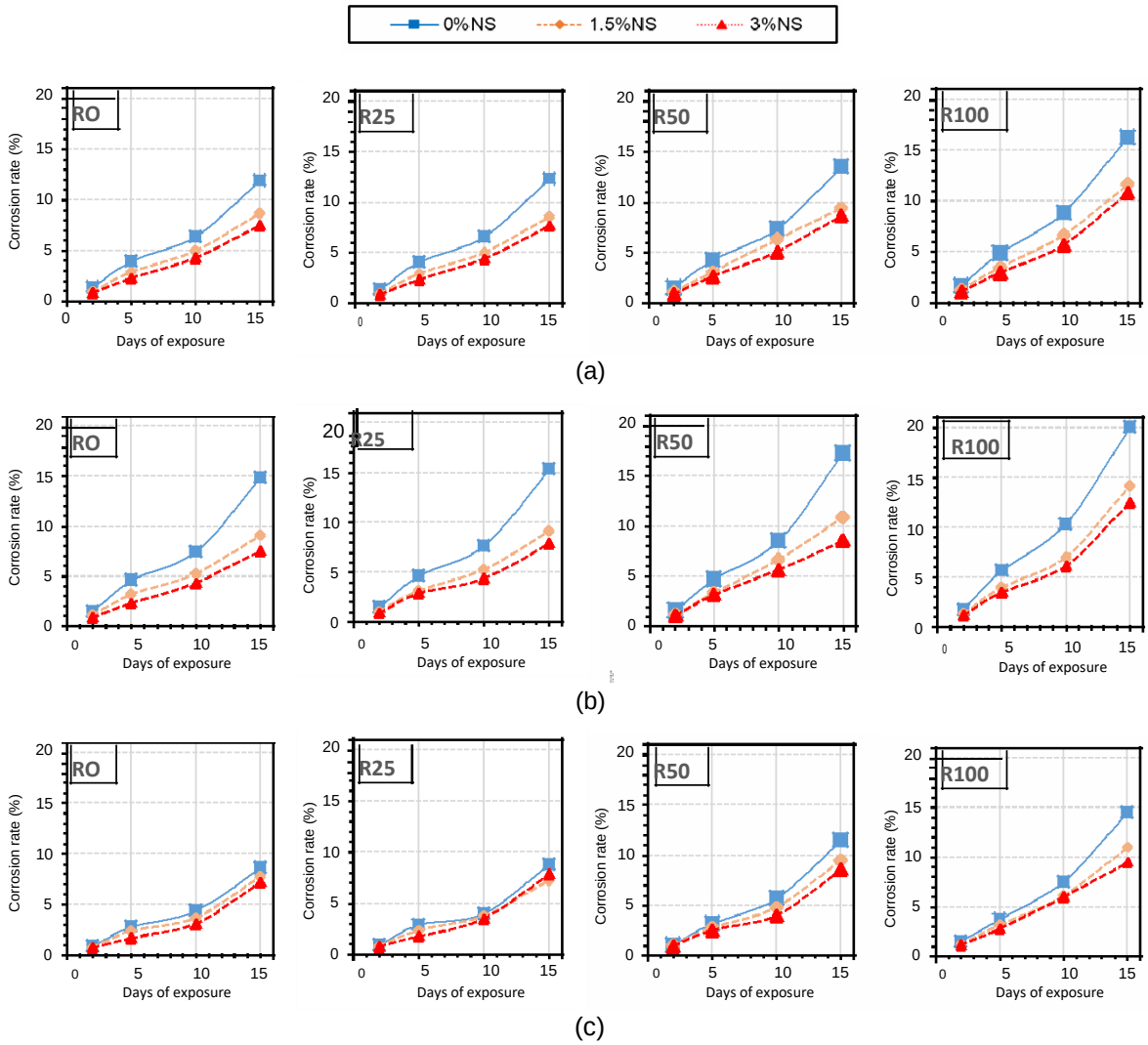

Figure 5.3 Variation of corrosion levels for specimens having; (a). Ø 12mm-l_d = 60mm; (b). Ø 12mm-l_d =167mm; (c). Ø 20mm-l_d =100mm.

Figure 5.4 shows the visual observations for the three types of specimens having 100% RCA made with and without NS. For those prepared without NS, it can be seen that the specimens were deeply corroded and brownish rust was noticed along the vicinity of steel embedment, whereas fluid corrosion oxides with an orange colour were spread over the internal concrete surface, nevertheless, these products became less pronounced when NS was added to concrete. It can also obviously noticed that nano silica contributed to improving concrete protection against the propagation of steel

corrosion for the three types of specimens as concrete mixtures became less impermeable. Another observation from Figure 5.4 is the higher corrosion products available with specimens having larger embedment length (Ø 12mm, ld = 167 mm), since longitudinal cracks were spotted with such specimens, allowing chloride ions to readily reach steel surface, and hence corrosion process was accelerated and more electrons moved between cathodes and anodes sites.

Figure 5.4 Comparison of steel corrosion in recycled aggregate concretes incorporating nano silica for specimens having: (a). Ø 12mm-ld= 60mm; (b). Ø 12mm-ld =167mm; (c). Ø 20mm-ld =100mm.

5.3. 3 Bond strengths of reinforced concretes made with nano silica

5.3. 3. 1 Bond stress- slip relationship

Due to the large number of specimens tested in this work, only the bond stress-slip relationships for 100% RCA concrete made without and with 3%NS were selected to be presented in this section, whilst the results for all specimens tested are presented in Appendix A. Figures 5.5-5.7 show the bond stress versus slip for the three types of specimens (Ø 12mm-ld= 60mm, Ø 12mm-ld =167mm and Ø 20mm-ld =100mm) before and after adding NS. As shown in Figure 5.4, the bond stress-slip curves can be divided into 3 stages, and possibly 4 stages in some cases. A marginal slip between steel and concrete occurred in the first stage, whilst the stress is rapidly increased up to reach the peak value. It should be noted that the bond stress of specimens containing NS (free and had a little corrosion) slightly increased accompanied by a rapid increase in slip displacement after reaching steel reinforcement to yielding, whilst this part was not observed with those made without NS. Thereafter, the bond stress began decreasing with a gradual increase in displacement, resulting from the occurrence of pull-out failure. In the last stage, the residual stress became almost constant when it reached about 30% of the stress peak. For specimens having 167 mm embedment length as shown in Figure 5.6, slow development in bond stress was observed for those un-corroded/slightly corroded accompanied by a speed displacement after reaching about 10 MPa, resulting from yielding of steel, which continued until the peak point. Then, the bond stress suddenly dropped due to the occurrence of splitting failure for those free of NS, whilst unexpected failure occurred for specimens made with NS before reaching the peak due to the rupture occurred in reinforcement prior to bond failure. As shown in Figure 5.7, all specimens made with 100 mm embedment length showed the same trend regardless of corrosion rate and

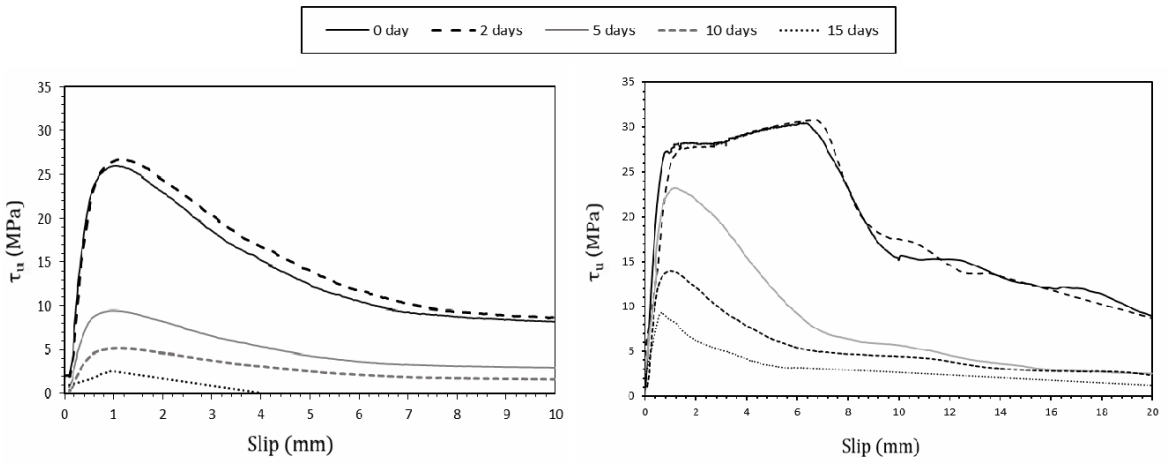

(a) (b)

Figure 5.5 Bond stress versus slip for specimens having Ø 12mm-l_d= 60mm and (a). R100 and (b). R100-NS3.

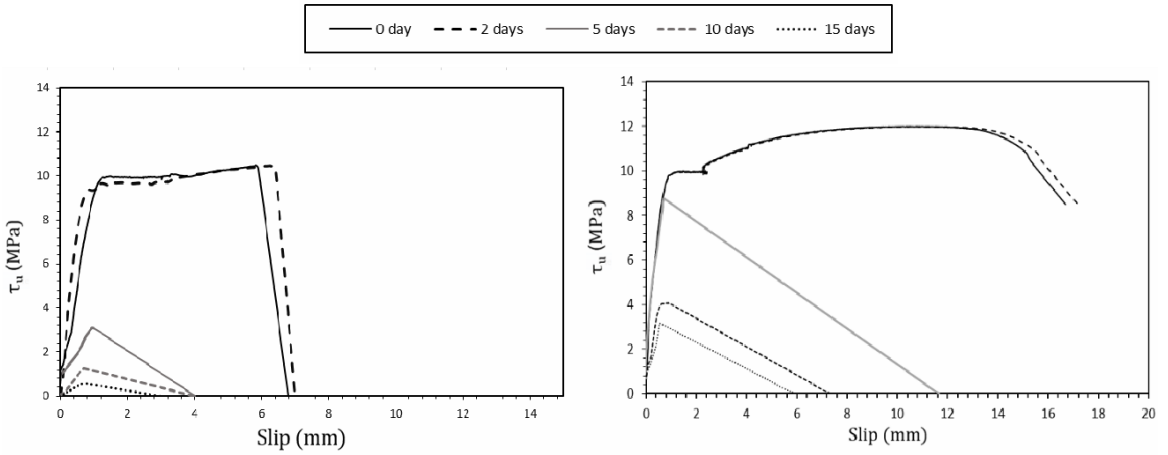

(a) (b)

Figure 5.6 Bond stress versus slip for specimens having Ø 12mm-l_d= 167mm and (a). R100 and (b). R100-NS3.

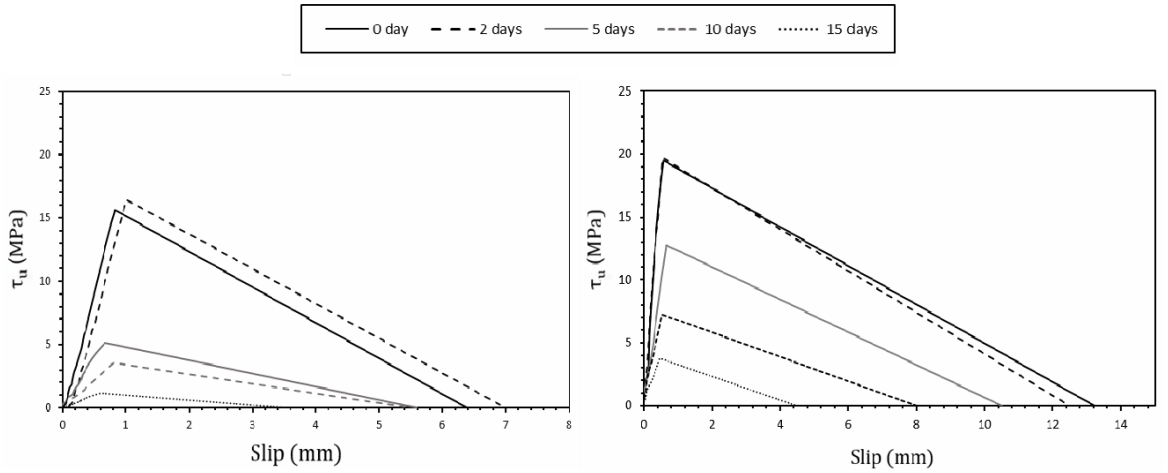

(a) (b)

Figure 5.7 Bond stress versus slip for specimens having Ø 20mm-l_d=100mm and (a). R100 and (b). R100-NS3.

NS content. This can be observed as the bond stress speedily increased with a slight increase in slip till reaching the peak, then a sudden drop in bond stress was observed.

5.3. 3. 2 Influence of nano silica on bond strength

Figure 5.8 presents how the bond strength can be influenced by adding NS to both normal and RCA concretes at various corrosive periods. As it can be seen that the bond strength slightly reduced for non-corroded specimens when normal aggregate was replaced by RCA, reporting between 6% and 11% bond decrease. This reduction probably related to the presence of cracks on the surface of RCA, affecting the adhesive force and the mechanical interlock of RCA concrete. Nevertheless, much more bond degradation was observed for RCA concretes after being exposed to corrosive environmental conditions to reach less than half at 15 days of corrosion, in comparison to conventional concrete. This was supported by the results presented in a recent study (Fernandez et al., 2016).

By partially replacing cement in normal concrete with 1.5% NS, the bond strength for un-corroded specimens (Ø 12mm-ld= 60mm, Ø 12mm-ld=167mm, Ø 20mm-ld=100mm) increased by 11%, 8% and 12%, respectively. Better bond enhancements were stated after adding the same quantity of NS to fully RCA concretes, 9-21%. However, the influence of adding 1.5% NS became more pronounced after exposure to corrosion, especially with the increase of RCA contents. For instance, the bond strength for R100- NS1.5 having 100mm bonded bar length achieved over three times higher bond, after 15 days corrosion, compared to the same mixture without NS, achieving about 2% higher than conventional concrete. This huge difference at this stage might be ascribed to the availability of wide cracks in RCA specimens, while those cracks were almost disappeared in NS mixtures. Therefore, the addition of 1.5% NS was evidently sufficient to recover the poor bond performance occurred after being

subjected to chloride severe conditions. The superior performance of NS is primarily attributed to the double effect of NS in enhancing the bond strength as well as corrosion resistance. This probably can be attributed to the enhancement of compressive strengths resulting from the formation of supplemental C-S-H gels, in addition to the effectiveness of NS particles in retarding the ingress of chloride ions into steel/concrete interface by acting as a filler to the tiny pores available in the matrix. Thus, the degradation of bond during the progression of corrosion process was impeded and delayed. By increasing the level of NS from 1.5% to 3%, the bond enhancement ratio increased in a narrow range (4%-9%) for all specimens free from corrosion, On the other hand, the bond resistance of using the same quantity (3%) was markedly promoted with increasing both RCA content and exposure period to salt solutions. Therefore, NS particles were more efficient in terms of bond performance with fully RCA replacement rather than normal concrete, likewise the observations obtained from other properties (i.e. compressive strength and corrosion resistance). This is primarily attributed to the higher capillary spaces and larger pores available in the microstructure of RCA concrete. Therefore, NS particles can easily fill up these spaces, in addition to the ability of such particles in reacting with a large amount of Ca(OH)2 found in RCA concrete, and producing more C-S-H gel. It is also observed that the majority of NS specimens made with longer bonded length (167mm) and did not expose to corrosion or slightly corroded failed due to steel bar rupture, rather than bond failure; for those specimens, no bond strength is reported. Another observation from these results is that the specimens having Ø 20mm-ld=100mm were more sensitive to the influence of RCA and NS contents in terms of bond strength rather than others since higher relative rib areas were reported with such specimens, enhancing the transfer of force between steel and surrounding concrete.

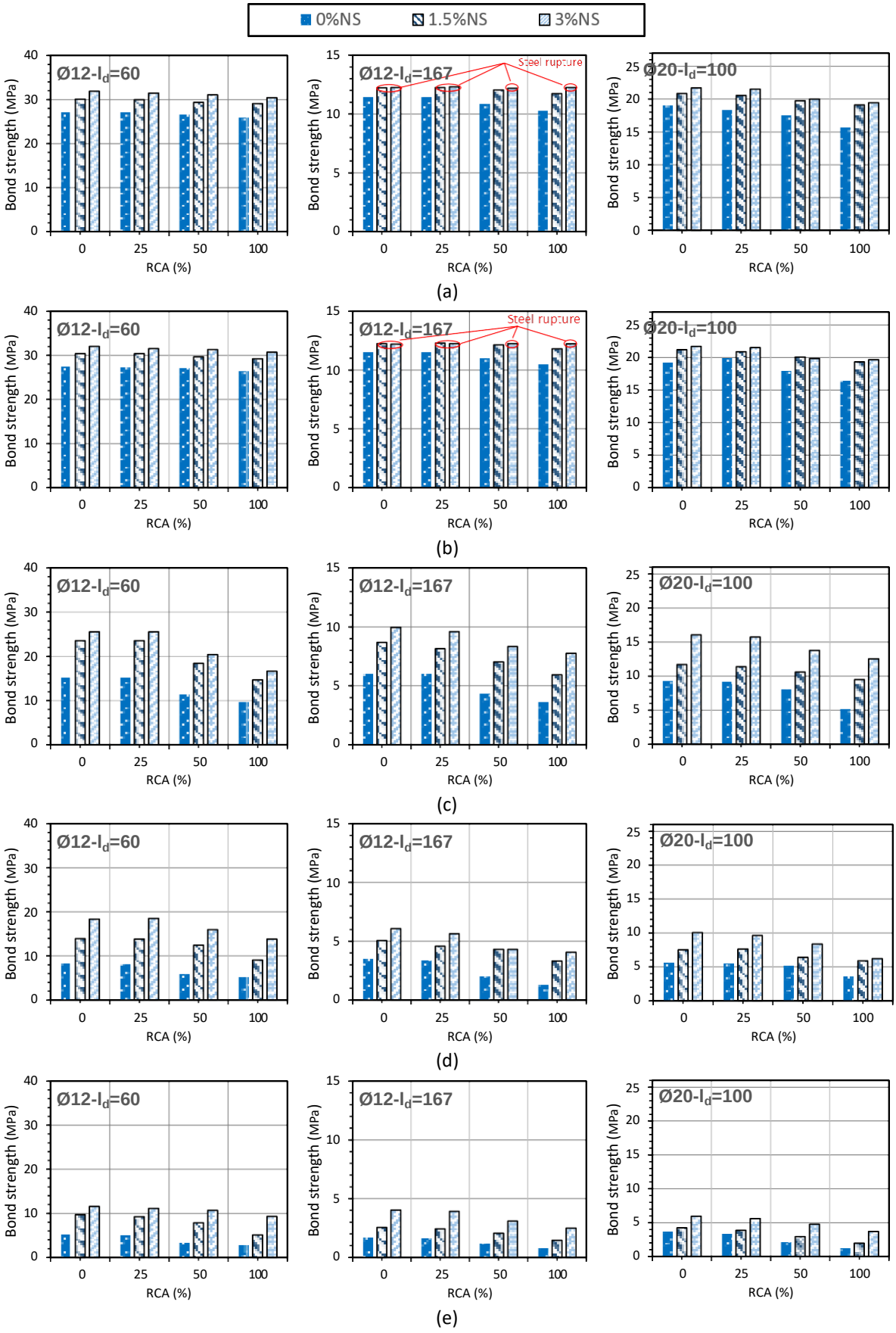

Figure 5.8 Bond strengths of specimens exposed to corrosion for: (a) 0 day, (b) 2 days, (c) 5 days, (d) 10 days, (e) 15 days.

5.3. 3. 3 Effect of corrosion level on bond strength

This section is mainly focused on how the ultimate bond between steel reinforcement and concrete can be influenced by corrosion products, regardless of mixtures components (i.e. RCA or NS). Even though several studies have been conducted on this area, varying levels of effect were reported in addition to disagreement regarding the critical corrosion value (Yang et al., 2016; Coccia et al., 2016; Auyeung et al., 2000). Figure 5.9 presents the effect of corrosion on bond strength for 60mm, 167mm and 100 mm embedment length specimens as a ratio of the bond strength of corroded bars to that without corrosion. From the presented results, it can be obviously seen that the bond strength slightly promoted up to about 6% enhancement with a little amount of corrosion products, agreeing with the similar observations reported by other authors for normal concrete specimens as well as RCA concrete (Fernandez et al., 2016). However, this improvement seems much smaller than that obtained in other studies as the improvement exceeded 20% (Wei-liang et al., 2001) and reached 40% (Al-Sulaimani et al., 1990), which might be explained by the larger concrete cover used in the current work (90-94mm) as well as higher compressive strength, leading to reduction of stresses from corrosion products. It is important to note that there is still no consensus about the critical corrosion rate as it has been reported between 0.5% and 2.4%, associated to the difference in details of specimens' tested as well as the direct current applied for accelerated steel corrosion. Accordingly, the enhancement in the current study was reported up to almost 2% corrosion rate, while further corrosion resulted in a significant reduction in the bond strength. The increased roughness of steel surface and the development of radial stresses at steel-concrete interface due to the formation of a small layer of rust around the bar could explain why the frictional bond forces increase. A considerable loss in bond was observed with the

propagation of corrosion, reporting between 10-80% degradation at corrosion level 2.5-10%. This likely happened due to the appearance of internal cracks, which could extend up to the external surface of concrete. During this stage, the passivity protective layer around reinforcement was destroyed in addition to the decay of ribs height. In the highly advancing levels of corrosion (above 10% weight loss), the residual bond resistance did not exceed 20% for the majority of specimens. This serious degeneration is primarily attributed to the appearance of longitudinal cracks on accompanied by the losing of reinforcement lugs.

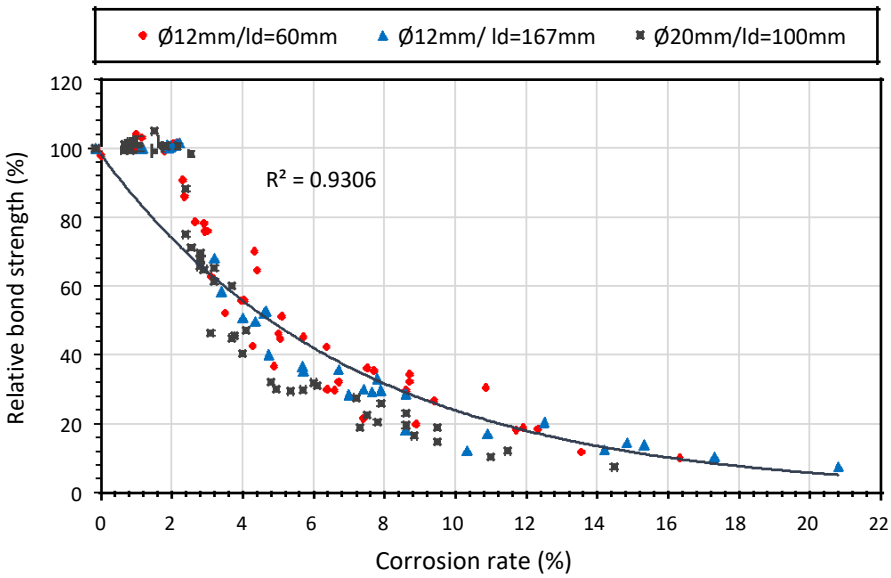

Figure 5.9 Relationship between corrosion rate and relative bond strength.

5.3. 3. 4 Effect of embedment length on bond strength

Figure 5.10 (a-b) exhibits the influence of bonded length for specimens prepared with 12mm bar diameter before and after exposure to corrosive environments (15 days). As shown in Figure 5.10 (a), by increasing the un-corroded bonded length from 5 to 13 times of bar diameter, the ultimate bond strengths considerably decreased by 37% and 35 % for R50 and R100 mixture, respectively. These findings are supported by a previous work (Pour et al., 2016) that stated between 30-50% reductions in bond

resistance of RCA concrete as the bonded length was doubled to be 10 times of bar size. The increase of non-linear distribution of bond stresses along larger embedment length might explain the drop in bond resistance, and therefore lower bond stresses were distributed with the increase of bar length. This distribution could reach a neglected value (almost zero) at a certain point, and hence the increase of bonded length beyond this point would not cause any difference on the bond performance (Wassouf, 2015). On the other hand, no exact reduction rates were reported for the majority of specimens made with NS due to steel rupture with the longer embedment length (13 Ø). In the advancing levels of corrosion (15 days), more degradation in bonding was observed with longer bonded length, especially for mixtures made without NS as shown in Figure 5.10 (b), owing to the presence of longitudinal cracks, restricting force transfer between reinforcement and surrounding concrete, whereas those containing NS showed almost the same rate. By increasing the embedment length from 5 to 13 times of bar diameter, the mode of failure was also changed from pull-out mode to splitting in concrete.

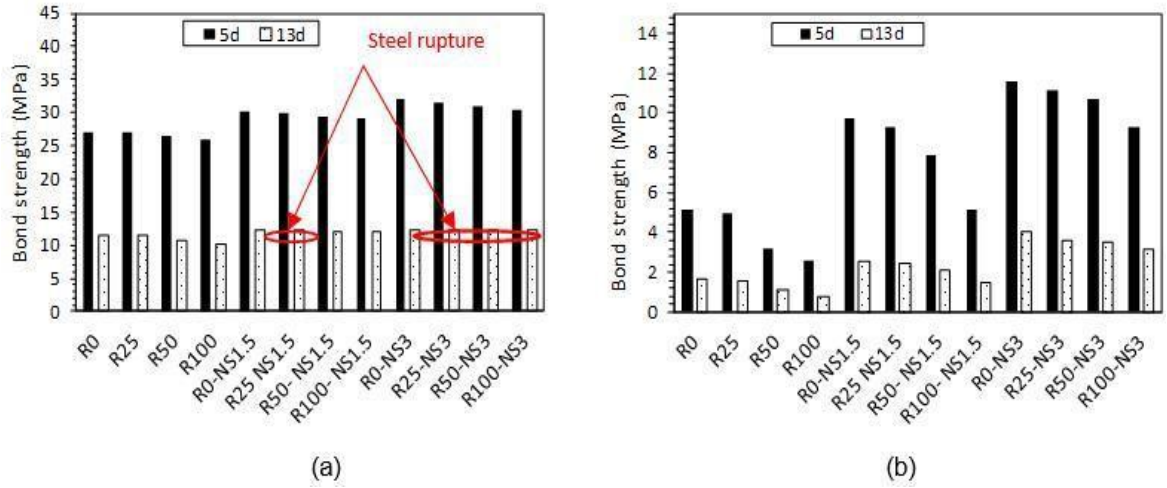

Figure 5.10 Effect of embedment length on bond strength: (a) before corrosion (b) after corrosion.

5.3. 3. 5 Effect of bar diameter on bond strength

In the present study, the influence of bar diameter was investigated for bars (12mm and 20mm) using two different cases of bond length. Whilst in the first case the comparison was made using the same bonded area (6280mm^2), in the second case the embedment length was chosen to be five times of bar diameter, as recommended by RILEM specification (1983). By using the same bonded area, the results indicated that the bond resistance provided by Ø12mm reported 60-65% of the bond obtained from larger bars (20mm) as shown in Figure 5.11(a). Even though a similar trend was anticipated for un-corroded NS specimens, nevertheless, the comparison was not obtained as bar rupture occurred in 12mm steel reinforcement before de-bonding. These results might be explained by the influence of relative rib area of steel as it plays an influential role in enhancing bond mechanism by blocking the ribs in concrete. The relative rib area ( ) can be simply described by the specific combination of ribs height and bar spacing (ACI-408, 2003), which can be found different from bar diameter to another. In this study, the relative rib area for Ø 20mm (0.16) reported approximately 20% higher than found in Ø 12mm, agreeing with other authors (Al-Sulaimani et al., 1990) who reported 40% higher bond when raised from 0.04 to 0.1, whereas another study (Hamad, & Itani, 1998) stated 24% higher bond resistance as doubled from 0.08 to 0.16. The difference in bond load might be also affected by reaching Ø12mm to the yielding stage before the occurrence of bond failure, and therefore the frictional properties and ribs geometry would be affected (Hamad, & Itani, 1998). Specimens probably became less sensitive to bar diameter after being progressively corroded, which can be justified by the erosion of steel lugs for both bars, and therefore the transferred force between reinforcement and concrete would be reduced. The change

in bar diameter from 12mm to 20mm also directly caused a change in the failure mode from pull-out to be split.

The results obtained from the other situation (5 times of bar diameter) showed a notable reduction in the maximum bond strength for larger bar diameter (20mm) for all specimens tested either corroded or un-corroded. As depicted in Figure 5.11(b), the bond strength for 20mm non-corroded bars reported about 63% of those made with 12mm, in agreement with previous investigations (Pour et al., 2016). This phenomenon is attributed to the increase of bleeding water trapped underneath the reinforcement, resulting in larger numbers of voids, which in turn caused a reduction in the contact area between steel and surrounding concrete, and therefore the bond strength would be eventually reduced (Shang et al., 2017). Almost similar behaviour was observed after exposure to aggressive environments as reported by others (Sonebi et al., 2011).

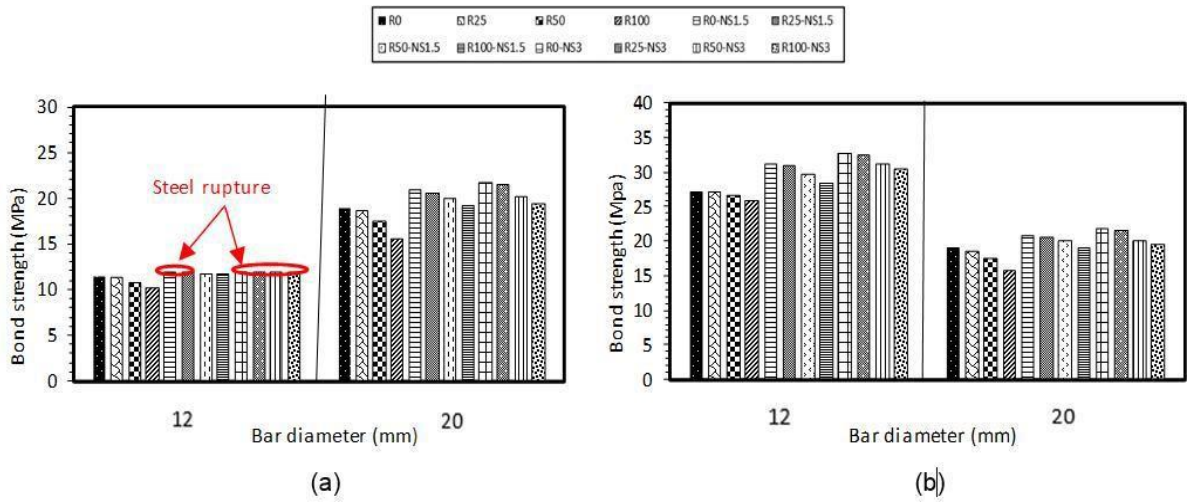

Figure 5.11 Effect of bar diameter on bond strength using: (a) the same bonded area; (b) l_d= 5Ø.

5.3. 3. 6. Bond failure mechanism

According to the obtained results, four types of failure were observed from pull-out test during the present study as shown in Figure 5.12, based on concrete strength, corrosion level in addition to the bonded length and bar diameter of steel. Pull-out

failure mode was dominant for specimens having Ø12mm and smaller embedded length (60mm), before and after being slightly corroded, owing to the availability high level of confinement provided by the large concrete cover (94mm). In this case, the shear force resulted from concrete surpassed the radial force generated from reinforcement, and therefore the steel ribs would crush concrete keys placed between steel lugs. After ten days of corrosion acceleration, some specimens interestingly failed in pull-out mode accompanied by splitting mode as shown in Figure 5.12(b). This might occur due to the presence of narrow cracks making the radial forces of reinforcement almost equal with the confining action. However, the mode of failure changed to splitting for specimens that highly corroded due to the existence of wide cracks. As the embedment length increased from 5 to13Ø, two types of failure were observed; steel bar rupture or concrete splitting failure. Whilst the former mode was dominant for non-corroded NS specimens and those slightly corroded as shown in Figure 5.12(c), splitting mode was observed with medium and highly corroded specimens as well as those made without NS, indicating that the radial force generated from steel reinforcement overcame the confining action resulting from the tensile strength of concrete (See Figure 5.12(d)). In the case of specimens having Ø20mm, l_d=100mm, the latter mode was predominant on all specimens tested regardless of corrosion rate

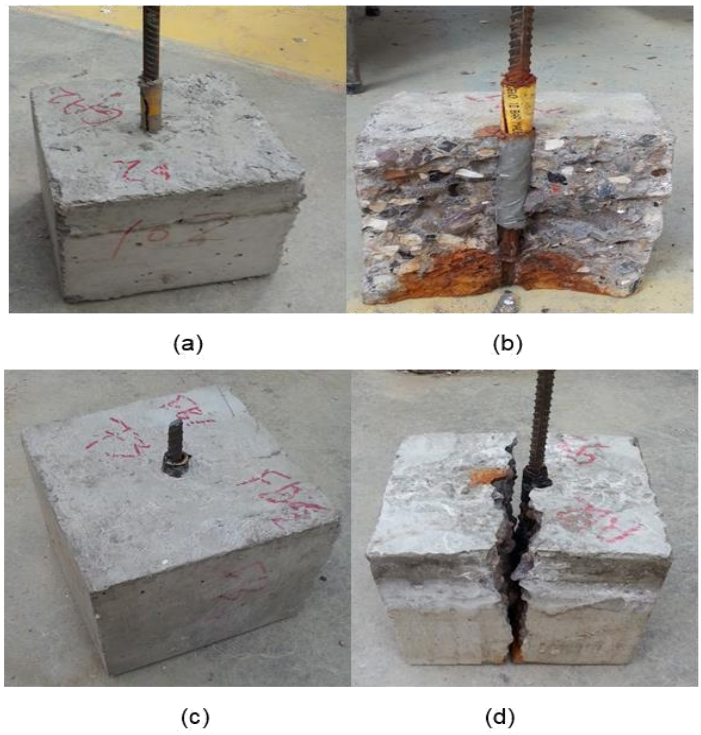

Figure 5.12 Bond failure modes obtained from pull-out tests.

5.4 Bond strength equations in code provisions and empirical equations

5.4.1 Comparison of experimental bond strength of un-corroded bars with existing models

For comparison purposes, several equations have been proposed to estimate the bond strengths between steel and concrete taking into consideration the influence of main parameters (i.e. compressive strength, concrete cover, bar diameter and embedment length). These models are summarised in Table 5.3, and compared with the experimental results to evaluate the performance of these models as presented in Figure 5.13, whilst a 45^{o} line was plotted to represent the same experimental and predicted bond values. It should be noticed that such models were mainly proposed for normal concrete specimens. In order to properly compare the results with these models, a correction factor was adopted (0.8-0.82) for converting the strength of cube into cylinder strength (Neville, 2006).

Table 5.3 Existing models for predicting bond strengths.

Reference	Model
CEB-FIP (2010)	$\tau_u = 2.5\sqrt{f'_c}$ at pull-out failure; $\tau_u = 7.0\left(\frac{\sqrt{f'_c}}{25}\right)^{0.25}$ at splitting failure
Australian Standard 3600 (2004)	$\tau_u = 0.265\sqrt{f'_c}.\left(\left(\frac{c}{d_b}\right) + 0.5\right)$
Orangun et al., (1977)	$\tau_u = 0.083045\sqrt{f'_c}\left(1.2 + 3.0\left(\frac{c}{d_b}\right) + 50\frac{d_b}{l_d}\right)$
Darwin et al., (1992)	$\tau_u = 0.083045\sqrt{f'_c}\left(1.06 + 2.12\left(\frac{c}{d_b}\right)\right).\left(0.92 + 0.08\left(\frac{C_{max}}{C_{min}}\right) + 75\left(\frac{d_b}{l_d}\right)\right)$ where c_{min} = min (C_x, C_y, $C_s/2$), while c_{max} = max (min (C_x, $C_s/2$), C_y), which C_x is the side cover, C_y is the bottom cover, and C_s is the spacing between the bars
Esfahani & Rangan (1998)	$\tau_u = 8.6\frac{C/d+0.5}{C/d+5.5}f_{ct}$ where f_{ct} (*MPa*) is the tensile strength of concrete taken as $0.55\sqrt{f'_c}$.

As can be seen from Figure 5.13 that varying levels of performance were obtained by applying these equations. It can be noticed that the equation suggested by Darwin et al., (1992) showed the closest correlation with the experimental results, with a mean ratio of 1.06 and a standard deviation (S.D) of 0.189. Esfahani & Rangan model was less accurate, especially in the case of higher bonded length with a mean value of 1.08 and S.D of 0.43, since the variation in embedment length was not considered in this equation. The equation proposed by Orangun et al. (1977) showed under-predicted values for specimens made with a short embedment length (5 times of Ø) for either bar diameter 12mm or 20mm; however, the results were over-estimated for longer embedment length (13 times of Ø), presenting 0.86 mean value and 0.27 S.D. The predicted values obtained from CEB-FIP model (2010) showed conservative results (Mean=0.75, S.D=0.146), showing under-predicted values in the case of smaller bar diameter, while better predictions were obtained with larger bar diameter (20mm). The Australian Standard (AS3600) presents a reasonable correlation with the experimental

results (Mean =0.82, S.D=0.37), since the influence of compressive strength, concrete cover and bar diameter were only considered in the equation. The over-estimation observed with the most of these models in the case of longer bonded length may be attributed to the nonlinear distribution of bond stresses along the bonded length of bars.

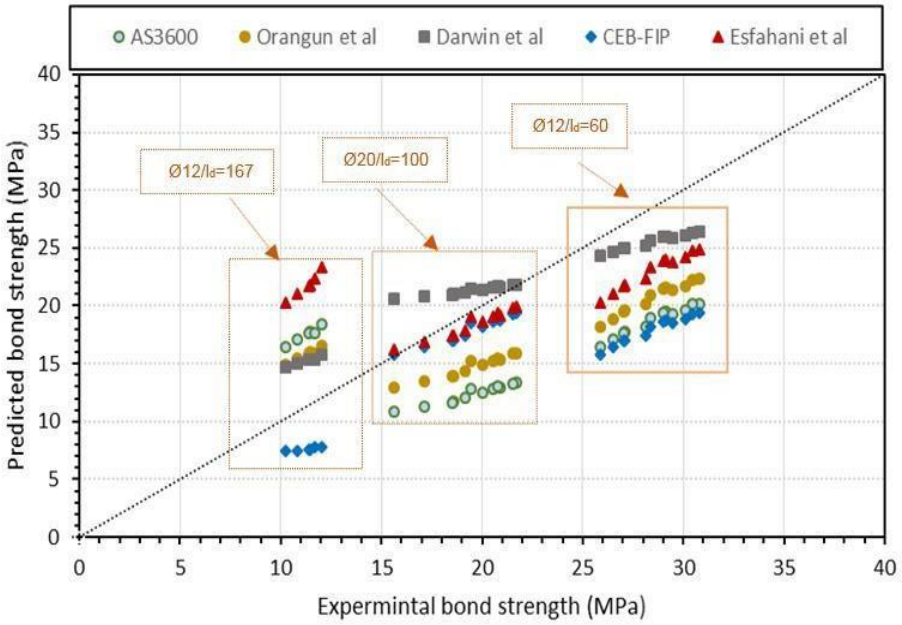

Figure 5.13 Experimental versus predicted bond strengths.

5.4. 2 Predicting bond degradations due to corrosion

The effect of corrosion on bond strength has been assessed by several researchers (Cabrera, 1996; Bhargava et al., 2007); Kivell, 2012) and has been expressed as a ratio between bond after exposure to corrosion products to the original bond (without corrosion) as follow:

$$K_t = \frac{\tau_c}{\tau_0}$$

where *Kt* is the relative bond strength, τ_0 is the reference bond strength of un-corroded steel bars, and τ_c is the bond strength of steel bars exposed to corrosion.

In the present work, six models were used for predicting the relative bond (Kt) as demonstrated in Table. 5.4, and the results calculated from these formulas were

compared with those experimentally obtained as shown in Figure 5.14.

Table 5.4 Models for predicting the relative bond strengths due to corrosion.

References	Normalised equation
Cabrera (1996)	K_t = 1-5.6 η,
Auyeung et al. (2000)	$K_t = e^{-32.51\,\eta}$
Lee et al. (2002)	*If* $f_c' \leq$ *21 MPa,* K_t = 1, for $\eta < -\frac{\ln((0.34f_c'-1.93)/5.21)}{-0.0561}$ % $K_t = \frac{5.21e^{-0.0561\eta}}{0.34f_c'-1.93}$ for $\eta > -\frac{\ln((0.34f_c'-1.93)/5.21)}{-0.0561}$ % *If* $f_c' >$ *21 MPa,* $K_t = \frac{5.21e^{-0.0561\eta}}{5.21}$
Chung et al., (2008)	K_t = 1 for $\eta \leq$ *2.0%* $K_t = \frac{24.7\eta^{-0.55}}{16.87}$ for $\eta >$ *2.0%*
Bhargava et al., (2007)	$K_t = 1.192\,\eta^{(-0.117\,\eta)}$, η >1.5% K_t = 1.0 for $\eta \leq$ *1.5%*
Kivell (2012)	$K_t = e^{-7.61\,(\eta\,-2.4\%)}$, $\eta \leq 1.0$ $K_t = 1.2\,e^{-0.076\,\eta}$, η >1.0

Note: K_t = relative bond strength; η = corrosion rate.

From Figure 5.14, it is apparent that none of these models exhibited a high accuracy in predicting the relative bond strength, in particular, Lee et al., (2002) and Kivell et al. (2012) models, which are highly over-estimating *Kt* with a mean value of 0.68 and 0.64, respectively. The over-estimation was also observed with the formulas proposed by Chung et al.,(2008), Bhargava et al, (2007) and Cabrera et al,(1996) with a coefficient of determination 0.73, 0.76 and 0.74, respectively, since the suggested loss in bond due to corrosion tends to gradually decrease by increasing the level of corrosion. This trend does not appropriately match the significant degradation occurred with the experimental specimens, especially after the appearance of tiny cracks on specimens' surface. On the other hand, the findings obtained from Auyeung et al., (2000) formula show under-estimated values compared to the actual results, giving the best performance with a coefficient of determination of 0.81.

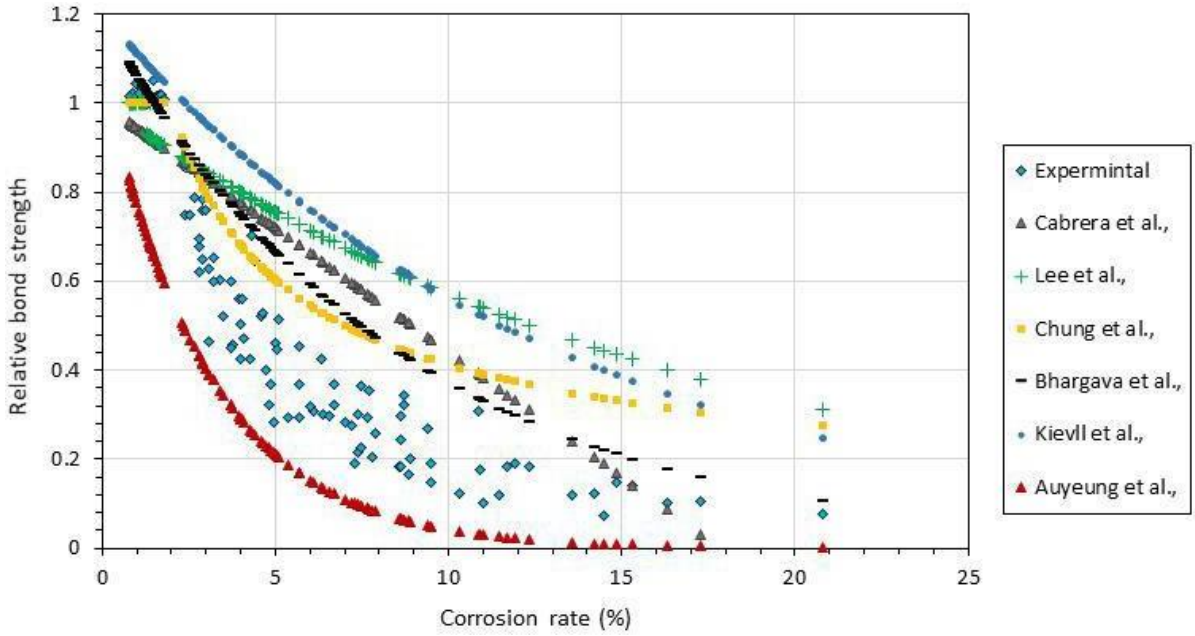

Figure 5.14 Comparison of relative bond strength calculated by models to the experimental results.

To improve the theoretical prediction of the effect of the corrosion rate on bond strength, a regression analysis was performed to obtain a new relative bond strength coefficient, K_t, using the experimental data obtained in this study as well as the database collected by Fig et al, (2016). The experimental data collected by Fig et al. (2016) cover variations of parameters, including concrete specimen size, bar diameter, concrete cover thickness, concrete strength, and corrosion level. However, it should be noted that all specimens collected in the database were prepared for natural aggregate and the bond strength was obtained from pull-out test. Therefore, the following formula is proposed to predict the normalised bond strength, assuming that the increase in bond strength up to 2% mass loss is negligible:

$$K_t = 1, \text{ for } \eta \leq 2.0\%; \qquad K_t = =1.69\times\eta^{(0.913)}, \text{ for } \eta > 2.0\%$$

where η is the corrosion rate, and K_t (= / $_0$) is the bond strength of steel bars exposed to corrosion relative to the reference bond strength of un-corroded steel bar.

The proposed formula has been validated through a comparison with the current experimental results as shown in Figure 5.15. It can be clearly seen that the proposed formula closely predicts the bond degradation due to corrosion with a mean ratio of predicted to experimental bond strengths of 0.99, a standard deviation of 0.17 and a coefficient of variation of 0.17.

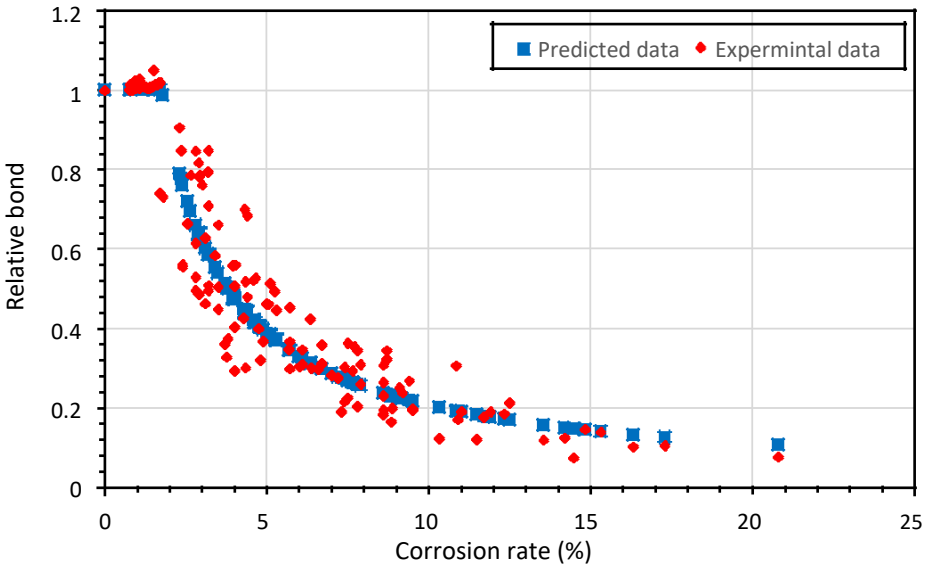

Figure 5.15 Comparison of the predicted relative bond to the experimental results.

5.5 Economic impact of using nano silica in recycled aggregate concrete

Although the use of NS enhanced many mechanical properties of RCA concrete as observed in the current investigation and others (Erdem et al., 2108; Li et al., 2017), the initial cost of concrete is likely to be increased due to the addition of NS. Other economic and environmental matters of adding NS to concrete that are expected to over-weight such initial cost increase are discussed below:

- Firstly, the cost of nano silica is not too expensive compared with other nano materials as emphasised by the widespread use of nano silica in recent years due to its known beneficial properties.
- As a little amount of NS is mostly used in concrete (less than 3%), the total cost of concrete would not be significantly affected.

- The cost of RCA is cheaper than that of normal aggregate that can partially mitigate the increase of initial cost due to the addition of NS.
- The transportation cost of RCA becomes more economical than normal aggregate, since RCA is mostly transported from local quarries, whilst transporting normal aggregate is dependent on the location of its source.
- Another factor is associated to the escalated cost of landfilling of RCA if not used due to stricter environmental regulations, especially in areas of increasingly scarce landfills.
- Furthermore, the addition of NS to RCA concrete is likely to enhance the concrete durability in comparison with the control concrete, as observed from the current results, and therefore the life cycle of such concrete structures would be probably extended, reducing the life-cycle cost of RCA concrete with NS.
- Moreover, the use of RCA can further contribute to mitigating the expected increased price of natural aggregate as about 60% of natural limestone resources could be saved (Xiao et al., 2012), accompanied by reducing the cost required to address the emissions of CO2 since about 15-20% of these emissions would be reduced (Gou et al., 2018).
- Finally, the price of NS is expected to become cheaper with their mass production.

5.6 Conclusions

In this chapter, the influence of adding NS to concretes prepared with various levels of RCA was experimentally investigated in terms of bond strength with steel bars at various levels of corrosion as well as corrosion resistance under corrosive conditions. Based on the obtained results, the following conclusions can be drawn:

➢ The addition of nano silica to normal and RCA concretes showed an improvement of compressive strength up to 40% at 28 days, however, the strength gain obtained by adding NS to RCA concretes was higher than that for conventional concretes. In addition, NS was appreciably sufficient to recover the decrease occurred due to RCA content and achieved even higher strength, in comparison to control concrete.

➢ The corrosion level significantly propagated with the increase of RCA quantity in concrete, especially under advancing levels of corrosion exposure, owing to its higher permeability and water absorption, nevertheless, NS particles evidently recuperated this phenomenon by considerably minimising the pores available in mixtures.

➢ The use of a small quantity of NS (1.5%) showed between 8-21% bond enhancements with both normal and RCA concretes in non-corrosive conditions; however, much better influence (more than three times) was observed with increasing corrosion period, reflecting the double counting effect of NS particles in enhancing the bond strength as well as corrosion resistance.

➢ NS particles were more effective with RCA concrete mixtures compared with normal concretes, achieving higher enhancement rate in terms of bond and corrosion resistance due to the accessibility of NS in dealing with the larger pores available in RCA concretes

➢ NS was superbly effective in recovering the poor performance in bond strength and corrosion resistance for RCA concretes, achieving higher values than the reference concrete.

➢ By doubling the content of NS (3%), the bond resistance slightly enhanced for non-corroded specimens, whilst its influence becomes more pronounced by increasing RCA content as well as exposure time to corrosion.

➢ The bond performance of RCA and NS concretes was seriously influenced by the level of corrosion; while the bond resistance slightly increased up to about 6% enhancement with a small amount of corrosion (2% mass loss), further corrosion led to a significant bond degradation.

➢ The effect of bar diameter is directly related to the bonded length; unexpectedly, higher bond strengths obtained with larger diameters for all mixtures in the case of using the same surface area due to the influence of relative ribs area. On the other hand, an opposite trend was observed when the bonded length was taken as a ratio

of bar diameter. Higher decreasing rates in bond strength were observed when the embedment length increased from 5 to 13 times of bar diameter.

➢ Darwin' Model exhibited the highest accuracy for predicting the bond strength of un-corroded bars embedded in concrete, whilst the formula suggested by Auyeung et al., provided a better predicting of bond degradation due to corrosion.

➢ The new formula proposed to predict the bond degradation due to corrosion showed a high accuracy with the experimental results.

➢ Different environmental and economic benefits can probably be obtained by incorporating NS intro recycled aggregate concretes.

Chapter six

Evaluation of reinforced concrete corrosion using impact-echo method

6.1 Introduction

Most deterioration of reinforced concrete structures are commonly related to corrosion of steel reinforcement. Non-destructive testing (NDT) has been developed for detecting the internal conditions and identifying different kinds of damages in RC members, in addition to helping the prediction of their future performance. Although some of non-destructive techniques have been applied for detecting corrosion, the obtained results from these methods show either complicated findings or they cannot be easily interpreted. Therefore, there is still an increase demand for applying an effective method for detecting corrosion in RC structures. In this context, very little research has been reported on the application of the impact-echo technique in detecting steel corrosion in RC structures. Hence, this chapter investigates the feasibility of using the impact echo-method for identifying corrosion of steel reinforcement in concrete structures. For this purpose, all specimens conducted in chapter five (180 reinforced concrete specimens) were tested by impact-echo method, and the impact-echo results were correlated against the actual corrosion levels obtained by the mass loss method.

6.2 Principle of impact-echo method

The impact-echo (IE) technique, belonging to the elastic wave propagation family, has been primarily used for flaw detection in concrete structures. The impact-echo method was introduced by Carino and Sansalone in 1980, and it is based on the analysis of

reflected stress waves generated from a transient impact. The impact-echo method has been successfully used in different applications in concrete, for example detecting delamination in bridge decks (Tawhed & Gassman, 2002), voids behind tunnel lining (Aggelis et al., 2008), and voids in grouted tendon ducts (Jaeger et al., 1996). The main attractive features of this technique are related to its relatively low cost and rapid inspection. Even though the impact-echo method was developed for detecting defects in plate-like structures, this method is successfully applied to detect flaws in other members of structures (e.g. columns and beams) (Lin & Sansolone, 1992). Recently, the application of IE technique has been employed to detect corrosion damage in reinforced concrete beams (Šamárková et al., 2014). The findings indicated that dominant frequencies resulting from this technique can be effectively used for detecting corrosion in reinforced concrete. However, further research is necessary to establish the validity of such technique for detecting corrosion of steel in concrete structures.

Impact-echo technique is an acoustic technique based on introducing a transient stress wave into the structure by applying low energy elastic impact at a point on the surface of structure, and monitoring the dynamic displacements caused by the arrival of stress waves reflected from internal defects and external boundaries. The displacement waveforms then are analysed in the frequency domain (Carino, 2001). After applying the impact from the surface of the structural element, three types of waves are generated during the impact-echo test, as shown in Figure 6.1, namely Shear wave (S-wave), Rayleigh surface wave (R-wave) and Pressure wave (P-wave). The P and S-waves propagate into the solid along spherical wave fronts, whereas the R wave move away from the impact point along the surface (Carino, 2001). These waves are refracted or reflected at internal interfaces (i.e. air-concrete interface and

steel-concrete interface). P-wave is the main importance in the impact-echo testing and it provides the most significant information related to the quality of the medium as well as the impedance contrast at any internal interface. This is might be explained as the vertical displacements resulted from P-waves are much larger than those obtained from others. The distinct peaks in the amplitude spectrum represent the dominant frequencies in the waveform. The amplitude of the refracted and reflected waves is mainly dependent on the impedance contrast between the structural element and the material contacted with such element (Carino, 2001). For a normal incidence of P-wave, the reflection coefficient (R) is used to characterise the amplitude of those waves and it can be calculated as shown below:

$$R = \frac{Z_t - Z_i}{Z_t + Z_i} \tag{6.1}$$

where is the acoustic impedance of the structural element, and is the acoustic impedance of the internal interface or boundary.

At a concrete-air interface, almost all of the energy resulted from the incident wave is reflected, and therefore the compressive stress wave generated on the top of structure is reflected as tensile stress wave and propagates back into the surface of structure. On the other hand, the stress waves resulted from other interfaces (concrete-steel interface) are partially reflected and partially refracted from the interface (Lin et al., 2004). This is mainly due to the acoustic impedance of reinforcing steel is higher than that of concrete (Carino, 1986). Thus, the reflected waves are still under the same phase (compressive waves).

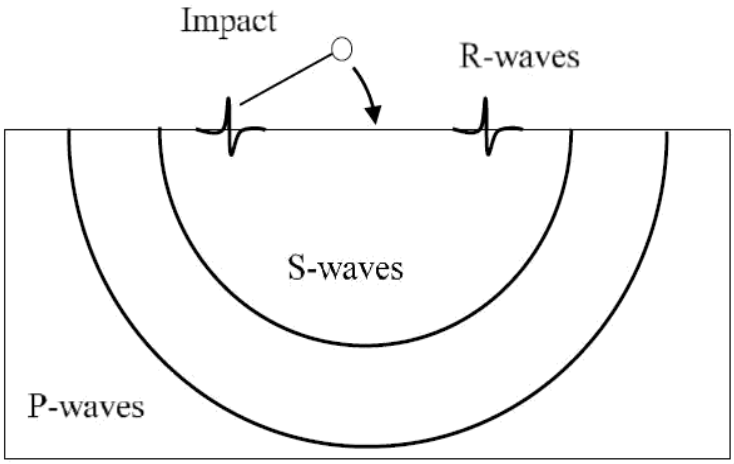

Figure 6.1 Stress waves caused by impact echo (Carino, 2001).

In general, the wavelength, wave speed, and frequency of propagating waves can be related through the following relationship:

$$C = f\lambda \qquad (6.2)$$

where C = wave velocity, f = frequency and □ = wavelength.

P wave speed (C_P) can be calculated from equation (6.2)

$$C_P = \sqrt{\frac{E(1-V)}{\rho\,(1+V)(1-V)}} \qquad (6.3)$$

where E is the Young's modulus of elasticity, and ρ and V are the Poisson's ratio and mass density of the body.

The S-wave speed (C_S) can be calculated from equation (6.3).

$$C_S = \sqrt{\frac{E}{2P(1-V)}} \qquad (6.4)$$

On the other hand, the R-wave speed (C_R) can be calculated by equation (6.5).

$$C_C = \frac{0.87 + 1.12C}{1+C} * C \qquad (6.5)$$

6.3 Frequency analysis

In the development of impact-echo method, the time domain analysis was used initially to evaluate the time from the onset of the impact up to the return of the P-wave (Carino, 2001). However, time domain analysis was found to be time-consuming and the results could not be easily interpreted. Thereafter, Fast Fourier transform (FFT) is designed for transforming the waveforms resulting from time-domain into frequency domain, revealing the predominant frequency components, which appear as peaks in the amplitude spectrum. The maximum frequency is dependent on the duration of impact, which in turn associated to the contact time and the size of impact source (Lin et al., 1992). Therefore, as the contact time decreases, the frequency content of the impact becomes more-broad band. After applying impact on the sample surface, P-waves are generated due to the multiple reflections of impact between the surface of the sample and the reflecting interface. When the P-wave reaches the test surface, it produces a displacement at the surface of specimen. Hence, the periodic pattern of the waveform is depended on the round-travel distance of P wave. If the transducer is placed near to the impact echo point, the round–trip distance will be about 2T, where T is the space between the test surface and reflecting interface. The frequency of reflected wave arrival at the receiver depends on the wave speed and the distance between the test surface and the reflecting interface. The travel time and frequency can be calculated from the following equations:

$$t = \frac{2T}{C_P} \tag{6.7}$$

$$f = \frac{1}{t} \tag{6.8}$$

where t = time of arrival of P-wave; T = reflecting interface; C_P= P-wave speed; and f = frequency.

Equations 6 and 7 can be combined to produce equation 8, where represents the shape factor correction and its value corresponds to the change in specimen dimensions. This equation represents the fundamental equation for the impact-echo method.

$$f = \beta \frac{C_P}{2T} \quad (6.9)$$

6.4 Experimental program

The same test specimens presented in chapter five (180 specimens were made from twelve different mixtures containing NCA, RCA and NS) were tested by the impact-echo method to investigate the capability of such method in detecting corrosion in reinforced concrete. As shown in chapter five, a wide range of corrosion level was obtained in this study ranging from 0.85% up to over 20% mass loss.

6.4.1 Impact-echo method

The success of the IE technique, as any other NDT technique, relies on the skills of applying the method as well as the judgment and interpretation of the results (Carino, 2001). The impact-echo test apparatus is composed of three main components: an impact source; a receiving transducer; and a data acquisition-signal analysis system, which is used to receive the output of the transducer connected with a computer. The impactor can be a hardened steel sphere attached to steel rod. In order to achieve accurate measurements, the Bruel & Kjear calibrator was used for calibrating the impact device each time before the onset of measurement. Figure 6.2 demonstrates the impact device manufactured by Buerl & Kjear, whilst the data analyser used in this study is the WinMLS program.

Figure 6.2 Impact echo device.

Figure 6.3 shows the testing set up using the impact-echo technique. In this arrangement, the accelerometer is placed on the upper surface of concrete specimen using a double-sided tape, while the impact was applied to the lateral surface of concrete cube by a pendulum from a predetermined height from a predetermined height. This procedure was applied since the steel bar was placed at the centre of specimen, and the signal to noise ratio was high in the configuration tested. The accelerometer was connected to the data acquisition system that was connected to a computer, which was used to transform the time domain to the frequency domain using the stated software. Measurements were repeated three times for each specimen and average value was taken to avoid measurement uncertainty. It should be noted that the contact time of the impacts for all specimens was below 600 ms. The time domain waveforms obtained from the impact-echo were recorded and transformed into the frequency domain. It should be noted that the distance between the pendulum and concrete surface needs to be kept constant for all specimens to produce an impact of the same amplitude for each test. Before applying the test, the specimens were disconnected from a DC power and taken out from water and left to dry as the frequencies obtained from impact echo are sensitive to the moisture content of concrete and the results could be disturbed.

Figure 6.3 Impact echo test.

In addition, two specimens having different nominal diameter bars (12mm and 20mm) were selected to evaluate the response of impact echo in terms of amplitude in detecting the internal defected areas (i.e. voids in concrete) by marking out a grid pattern on the specimen surface. Each grid contains 100 different locations located at 4 cm^2 and the measurement was conducted at each grid point using an accelerometer as shown in Figure 6.4. The results then were plotted as a 2D surface map to aid the identification of any defected areas.

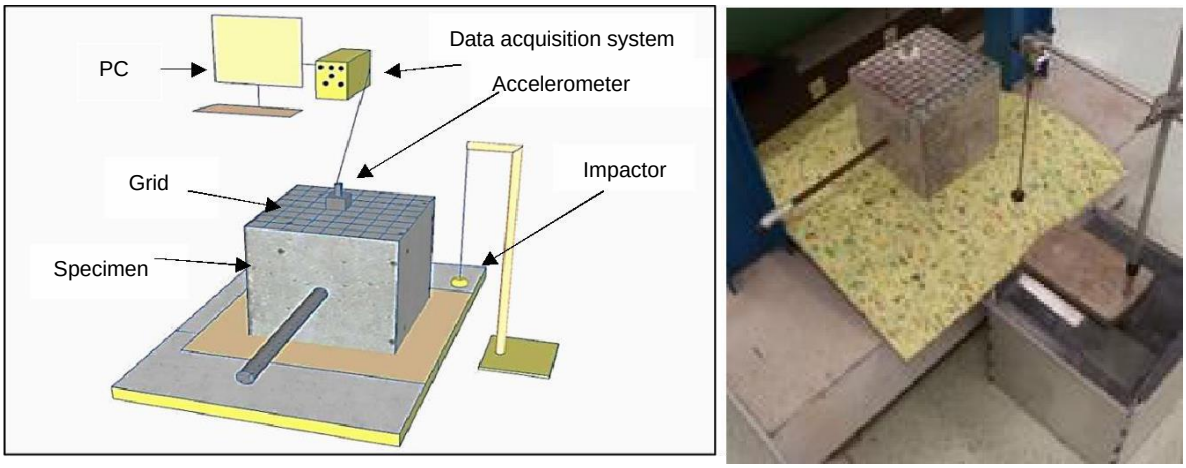

Figure 6.4 Detecting the damage in reinforced concrete by applying the impact-echo method.

6.5 Results and discussion

6.5.1 Evaluation Faraday's law equation in predicting corrosion

The theoretically estimated mass loss of reinforcing steel due to corrosion can be expressed by using Faraday's law as shown in equation (6.10).

$$\text{mass loss } (\eta) = \frac{t*I*M}{Z*C_F} \qquad (6.10)$$

where is time (seconds), is the initial current applied (Ampere), is atomic weight (for reinforcing steel = 55.847 g/mol), is valence charge of iron (2 moles for electron) and is Faraday' constant, which represents the amount of electrical charge in one mole of electrons (F= 96487 c/mol).

Figure 6.5 shows the theoretical corrosion rate based on Faraday's law versus the measured gravimetric mass loss for all specimens tested. Faradays' equation has been widely accepted for anticipating the degradation in reinforcing steel due to corrosion (El Maaddawy et al., 2006). The values obtained from equation (6.9) need to be converted into percent, and therefore the mass loss calculated from equation (6.9) were divided by the original mass of the exposed portion of the bar. It can be seen that even though different parameters were related to weight loss measurements (i.e. bar diameter, embedded area, exposure time, current applied), the theoretical findings based on Faraday's showed a good correlation with those obtained from mass loss, with a residual standard deviation of 0.51, and a coefficient of determination of 89.3%. The performance of Faraday's law might be associated to the voltage applied to accelerate corrosion. Results obtained by El Maaddawy et al., (2006) revealed that the loss in steel reinforcement can be well-predicted by Faradays' law when a low voltage (15V) is applied to accelerate corrosion. Conversely, the measured corrosion rate would be considerably lower compared to those theoretically predicted by

Faraday's law when a high voltage (60V) is applied. This might be related to hindering the diffusion of Fe^{2+}/OH^- ions when a high voltage is applied, leading to loses in the impressed current efficiency, and therefore less corrosion would occur compared to that predicted.

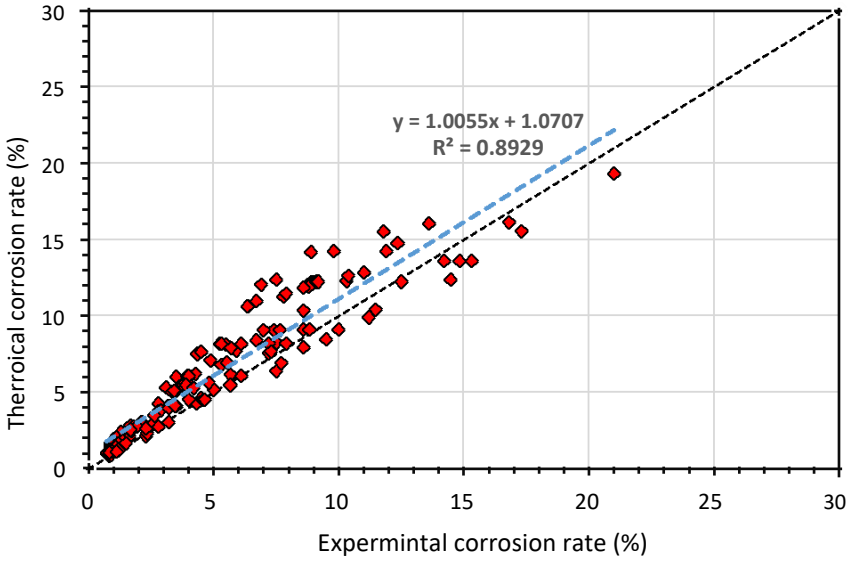

Figure 6.5 Theoretical corrosion rate obtained from Faradays' law vs. the experimental corrosion rate.

6.5.2 Corrosion detection using impact-echo technique

Even though the impact-echo method was mainly developed for detecting defects in plate-like structures, this method was successfully applied to detect flaws in other members of structures (Lin & Sansolone, 1992). The dominant frequencies in the response signal are considered as the main key to reveal information about material characteristics and internal defects (Ohtsu & Uddin, 2008). Figure 6.6 shows the variations in frequency peak values for all specimens over different durations of corrosion acceleration. For non–corroded specimens, it can be observed that the frequency peak obtained from impact echo measurements ranged between 9000 and 9500 Hz for all specimens having 12 mm bar diameter, confirming previous works that indicated the frequency of impact-echo of concrete structures is typically ranged between 5000-40000Hz (Schubert & Köhler, 2008). This slight difference is

considered acceptable, corresponding to the variations in density, elastic modulus and the heterogeneous nature of concrete mixtures. For the larger bar diameter of 20mm, frequencies tended to decline to be about 8500Hz for the majority of specimens, regardless of concrete components. This reduction probably might be explained as more energy might have leaked into the surrounding area of larger steel bars after applying impact waves, and therefore less energy could be reflected to the receiver. In the case of exposure to a short period of corrosion acceleration (2 days), the peak values of frequency slightly are reduced for some of the specimens, while the others showed a slight increase or unchanged, indicating that the IE measurements cannot evaluate the damage in reinforced concrete at the initial stage of corrosion. This matches the earlier observation (Liang & Su, 2001), that suggested the onset of corrosion cannot be identified by the impact-echo method. It must be noted that corrosion would not induce immediately on the surface of steel bars after applying the current. The initiation of corrosion can just only actually occur when the protective film on the steel surface is lost (Ohtsu & Uddin, 2008).

At five days of corrosion acceleration, more corrosion products were induced in all specimens, however, no cracks were observed at the majority of specimens' surface. The findings obtained at this stage, which represents the moderate level of corrosion, showed a clear reduction in the predominant frequencies as they shifted to be ranged between 6000 Hz and 8000 Hz for specimens made without nano silica. The possible reason for shifting frequencies during this stage could be related to the presence of internal micro-cracking around steel bar due to rust occurrence, causing a reduction in the density of specimen, and hence the frequencies of reflective waves tend to decrease. The reduction in frequency peaks might also reflect the decrease in wave energy, which might be explained by the change of rebar geometry due to the

formation of corrosion products at the surface of steel bars, making the surface of bar much rougher, and hence the wave energy would be refracted at the rough surface of corroded area in many directions (Miller, 2010). The accumulation of rust at the surface of rebar leads to making the mass of bar larger, which in turn might result into slowing down the speed of waves. As a consequence, more energy might have absorbed by the rust and the intensity of wave decreased compared to those free of corrosion. The formation of hydrated ferric oxide ($Fe^{+3}O3H2O$) at the surface of steel reinforcing, might also explain why a reduction in frequency peaks occurred as this rust product is known as a porous material (Miller, 2010), and thus more wave energy could be absorbed compared to non-porous materials. On the other hand, the majority of those containing nano silica were less affected, showing frequencies above 8000 Hz, which seems reasonable as less rust products are anticipated in nano silica concretes due to the effectiveness of nano silica in reducing the electrical conductivity of concrete (El-Feky et al., 2016). As a result, the corrosion resistance of such concretes is significantly enhanced.

By extending the period of corrosion to ten days, the frequency peaks decreased for the majority of specimens to around 4000 Hz. For instance, the frequency peak of normal concrete having 20 mm steel bar shifted to 4300 Hz compared with 8700 Hz for the intact specimens. This drop in frequency values probably corresponding to the growth of corrosion-induced cracking. Some of these cracks can be observed at the outer surface of concrete due to the volumetric expansion of corrosion products at a steel/concrete interface. The increase in corrosion volume induces strains at the interface, exceeding the critical tensile capacity of concrete and creating cracks, which might have reduced the rigidity of the cube, and eventually reduced the resonant frequency. After 15 days of corrosion exposure, which represents severe corrosive

conditions, the frequency peaks generated from stress wave propagation were considerably reduced to correspond to the high level of corrosion. At this stage, it can be observed that the frequency of specimens made with fully recycled aggregates barely reached 1000 Hz as shown in Figure 6. 6(b), and reported the lowest obtained value, indicating that the rebar reached a very high level of corrosion. It is also found that the specimens having Ø 12 mm, ld = 167 mm showed lower frequency peaks compared to others, suggesting that higher mass loss is expected with those specimens. This low frequency might be explained by the presence of longitudinal cracks due to the high permeability of RCA, and therefore chloride ions can be easily reached the steel surface.

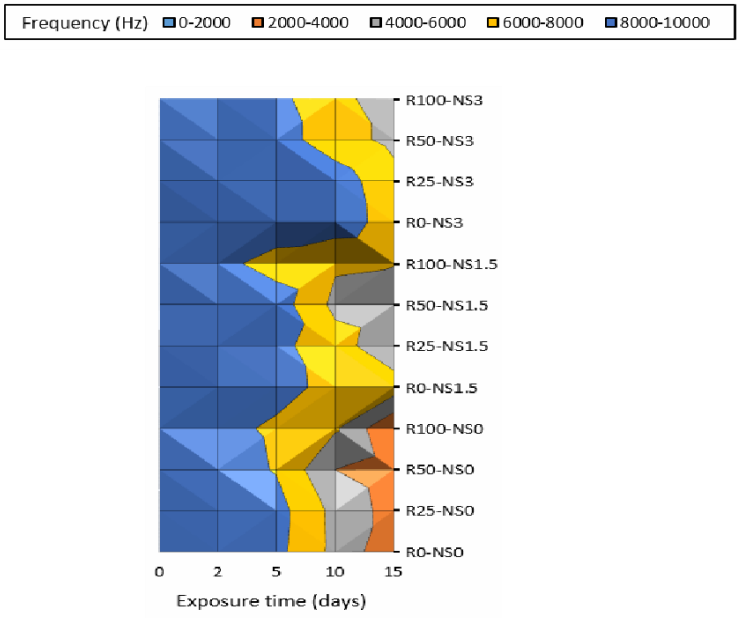

(a) Ø 12mm, l_d= 60 mm

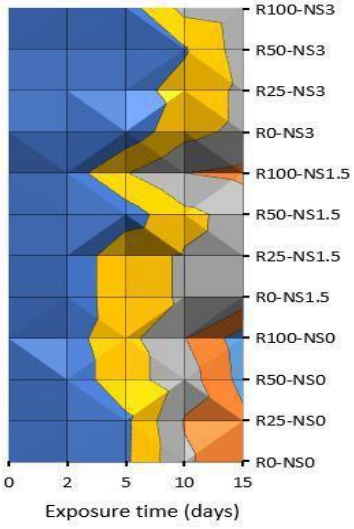

(b) Ø 12mm, ld= 167 mm

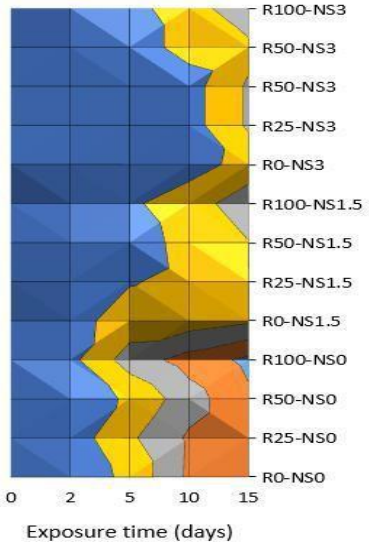

(c) Ø 20mm, l_d = 100 mm

Figure 6.6 Relationship between frequency peak values versus corrosion time for different specimens.

Figure 6.7 exhibits the shift in the frequency peaks for the selected series (normal concrete having Ø 12 mm and ld= 60 mm) to demonstrate how the frequency peak resulting from impact echo can be affected by increasing rust products in reinforced concrete.

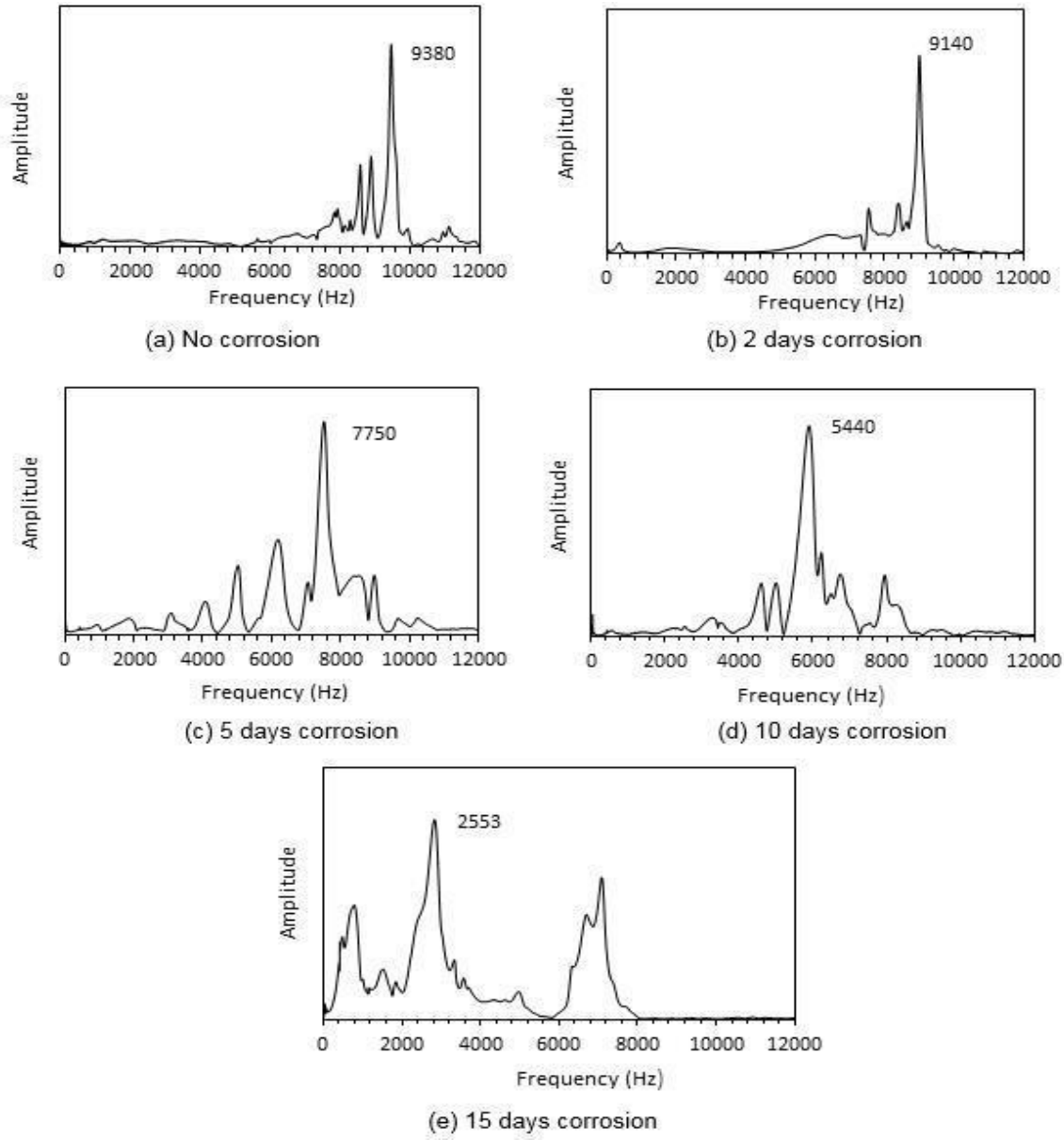

Figure 6.7 Amplitude spectra obtained from impact-echo tests for normal concrete specimens having Ø 12mm, l_d= 60 mm.

R0-NS0 specimen having Ø 12 mm and ld=167 mm was selected to observe the influence of corrosion (before and after exposure to corrosion) in a two-dimensional

time-frequency plane as presented in Figures 6. 8 and 9, respectively. These two-dimensional time-frequency graphs were visualised using Wavelet Toolbox in MATLAB to show how the frequency varies across the image and helps to reveal the patterns in a noisy image. The impact signal was cut to show only the localized part of signal, and therefore the 2D frequency response possibly can be used for separating the target echoes in a noisy the impact-echo signal (Shokouhi, 2006). Therefore, it is possible for the time within waveforms to be identified at each frequency (unlike Fourier transform that provides information about the frequency of the entire signal) (Aggelis et al., 2008). From the contour plot, it can be seen that there is not a decisive difference in the response of Wavelet transforms before and after exposure to corrosion, since the low frequency can be seen in both conditions. However, it can be observed that the frequency seems more linear for the whole duration of time before corrosion occurred, whereas the linear pattern in the frequency response for the same specimen is interrupted over the duration of time due to corrosion creating voids as shown in Figure 6.9, and thus the waves after corrosion are distorted, especially between the frequency regions 1000Hz to 8000Hz.

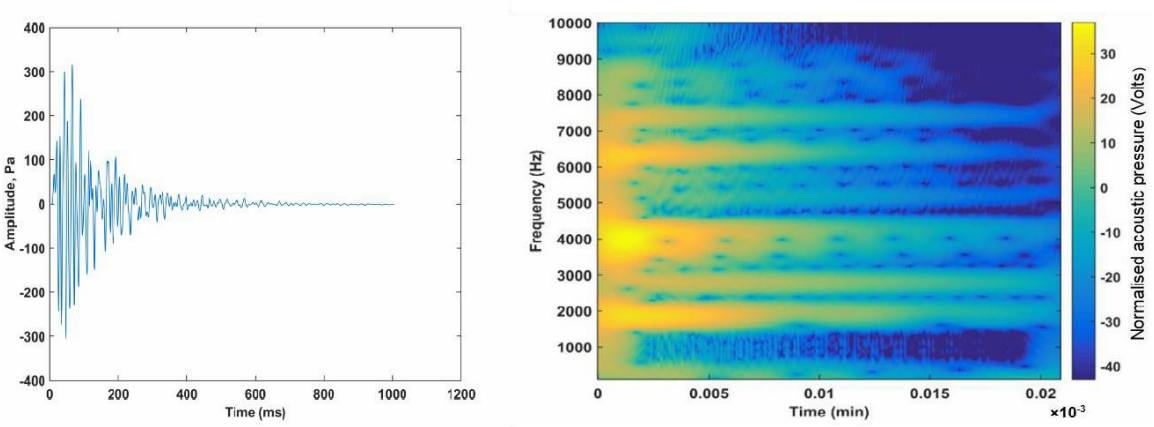

Figure 6.8 The contour plot of normal concrete specimen before exposure to corrosion.

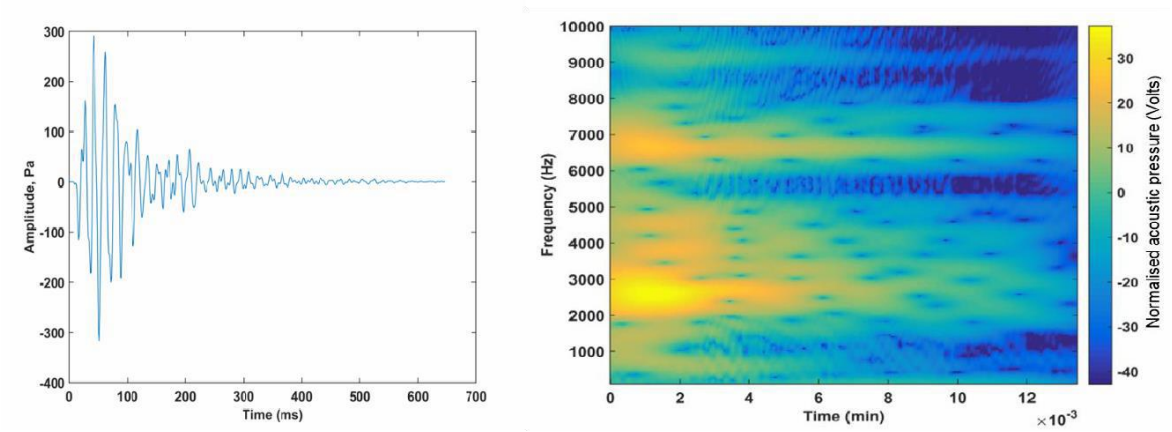

Figure 6.9 The contour plot of normal concrete specimen after exposure to corrosion.

6.5.3 Visual observations

The influence of time on the development of corrosion was visually observed to generally compare with the findings obtained by the impact-echo test. For instance, specimen having 100% RCA concrete (RC100-NS0) exhibited a small amount of corrosion along the steel bar after two days of corrosion as shown in Figure 6.10 (a). When accelerated corrosion time extended to 5 days, there was significant rust on the steel surface and surrounding concrete as shown in Figure 6.10 (b). At ten days of corrosion, a higher amount of steel dissolution was observed due to the formation of narrow longitudinal cracks parallel to steel reinforcement on the surface of concrete, allowing more moisture and chloride ions to reach the steel-concrete interface. After 15 days, there was exhibited localized corrosion with a brownish colour that were deeply spread around the bar and adjacent area, while a wet orange oxide was spread through the sound concrete as depicted in Figure 6.10 (d), allowing chloride ions to easily penetrate concrete matrix. Hence, the rust products readily accumulated on the surface of steel bar and the process of corrosion was speeded up due to the presence of cracks, allowing the large amount of electrons moving from cathode to anode sites.

(a) 2 days (b) 5 days (c) 10 days (d) 15 days

Figure 6.10 Comparison of reinforcement corrosion for R100-NS0 specimens having Ø 12mm, l_d =167mm after different periods of accelerated corrosion.

6.5.4 Correlations between weight loss and impact echo

A total of specimens were tested in the current experimental investigations, however, 36 specimens were not exposed to corrosion testing, whilst 144 specimens were exposed to different periods of accelerated corrosion. Most of data obtained from the experimental work (90%) were used to develop the relationship between of the impact echo measurements and mass loss, and the remaining (10%) was used for testing the relationship. The dividing process was selected randomly to ensure all parameters would be involved. A wide range of corrosion degrees was obtained in this study ranging from 0.85% up to approximately 20% mass loss. Figure 6.11 shows the corrosion rate in terms of weight loss versus the peak frequency obtained from the impact-echo technique at different degrees of corrosion damage. From this plot, it can be noted that the peak of frequency clearly deceases with increasing of mass loss for the majority of specimens. The coefficient of determination of the best-fit line is approximately 79%, with a standard of deviation of 0.24. This best-fit line was used to estimate the corrosion rate for 14 specimens having different variables (i.e. compressive strength, corroded area, bar diameter and corrosion time) as summarised in Table 6.1. It can be seen that while some results showed a high accuracy in estimating mass loss (0.989, 1.025 and 1.07) ratio estimated/measured, the others

exhibited a conservative estimation compared to those obtained from the experimental results with a ratio of estimated/measured between 0.79 and 1.4. The regression relation between the corrosion rate, η, and the frequency peak, , is presented below:

$$\eta\ (\%) = 16.94\text{-}0.0017*(\square) \tag{6.11}$$

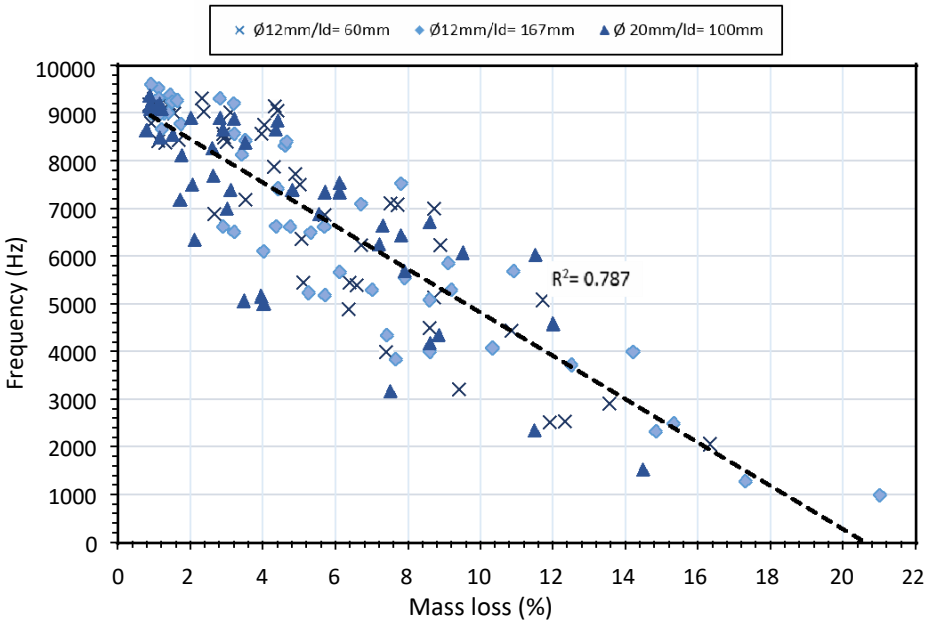

Figure 6.11 Correlation between peak frequencies obtained from impact echo and mass loss.

Table 6.1 Comparison of corrosion rate obtained by impact-echo with mass loss.

Specimen group	*Corrosion time (days)*	*Steel bar (mm)*	*Bonded length (mm)*	*Frequency peak (Hz)*	*Predicted corrosion rate (%)*	*Experimental corrosion rate (%)*	_____
R0-NS0	2	12	60	9120	1.426	1.39	1.025
R0-NS0	10	12	60	5446	8.072	6.375	1.26
R100-NS0	10	12	60	6230	6.74	8.88	0.76
R100-NS1.5	5	12	60	7196	5.096	3.5	1.46
R25-NS0	2	12	60	9267	1.312	1.62	0.80
R100-NS3	10	12	167	7420	4.71	4.4	1.07
R25-NS0	10	12	167	3850	10.78	7.65	1.4
R100-NS1.5	5	12	167	6114	6.93	5	1.38
R100-NS3	15	12	167	3728	10.99	12.5	0.88
R100-NS3	2	20	100	9100	1.59	1.2	1.33
R50-NS0	10	20	100	6886	5.62	5.54	1.01
R0-NS3	10	20	100	7400	4.75	4.8	0.989
R50-NS3	10	20	100	7350	4.83	6.1	0.792
R25-NS3	15	20	100	5700	7.9	7.37	1.07

Results obtained from the impact-echo measurements at the grid points were exhibited in the form of contour maps of the peak frequency. The technique used involved drawing a 10 x 10 grid on the surface of the specimen and the transmission level of amplitude was calculated for each of the grid points before and after corrosion, and expressed as decibels in logarithmical units (dB) using the following formula:

$$dB = 20 \log_{10} (amplitude \times 10^{-6}) \quad (6.12)$$

Figure 6.12-13 and 14 show the readings of amplitude for a 100 point grid concrete blocks containing 12 mm and 20 mm steel reinforcements, respectively, before and after corrosion exposure. Plotting the transmission level of amplitude for each grid point as a 2D contour plot aims to aid the identification of defected areas. Amplitude is normally higher in the internal defected areas i.e. voids created due to corrosion (yellow regions in Figures 6.12b & 13b). It can be clearly observed that more noise regions can be found in both specimens after exposure to corrosion acceleration compared to the same measurements recorded before corrosion, indicating that more voids and cracks would be created in such areas due to the development of radial stresses at steel-concrete interface caused by rust products. From the plots, it can also be seen that the noise levels, which are represented by amplitude values shifted to be higher after exposure to corrosion, raising to be about 86 dB for the specimen with 12mm diameter steel bar, compared 80 dB reported for the same specimen before being corroded. Similarly, the amplitude value for the specimen having 20mm diameter steel bar developed from 81 dB to be approximately 84 dB.

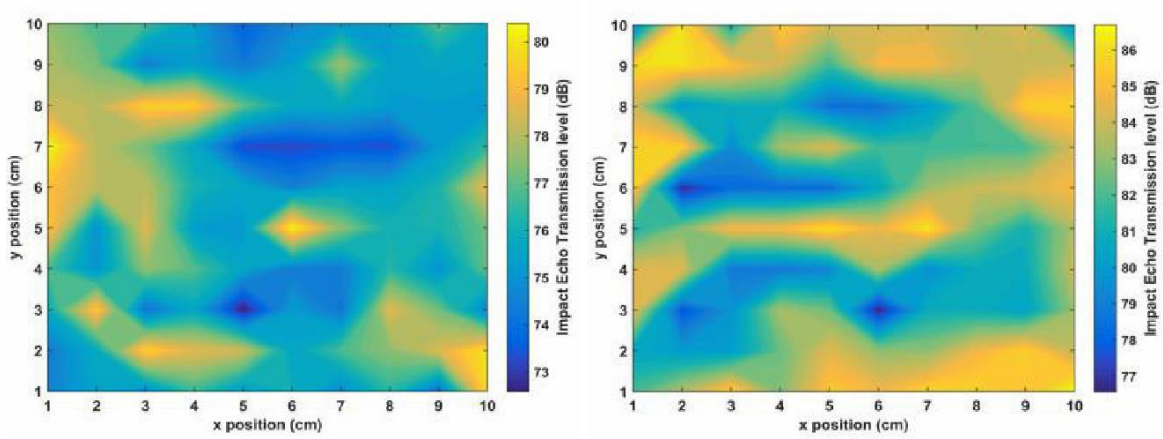

(a) Before corrosion (b) After corrosion

Figure 6.12 2D surface map of amplitude for the specimen having 12mm steel bar.

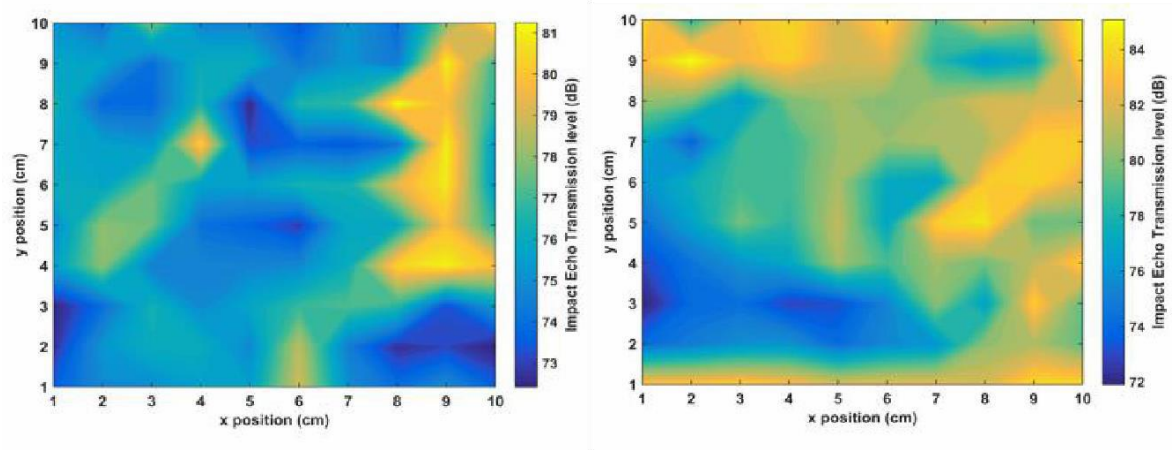

(a) Before corrosion (b) After corrosion

Figure 6.13 2D surface map of amplitude for the specimen having 20mm steel bar.

6.6 Conclusions

In this paper, the corrosion damage in different reinforced concrete mixtures was experimentally evaluated using the impact-echo technique based on the analysis of frequency domain at different stages of corrosion. The results showed that the impact echo testing can be effectively used to qualitatively detect the damage caused by corrosion in reinforced concrete structures. The following conclusions can be drawn:

- The loss in steel reinforcement predicted by Faraday's law exhibited a good correlation with the measured gravimetric mass loss.

- The un-corroded specimens prepared with larger bar diameters exhibited lower response in terms of frequency peaks after being reflected to the surface of concrete.
- A significant difference in the response of impact echo was observed for the majority of the specimens after exposure to corrosion environments.
- The dominant frequencies in the amplitude tended to clearly decrease with the progression of corrosion damage.
- No clear trend was observed in terms of frequency peak at the initial stage of corrosion.
- The results obtained by the impact-echo technique showed a reasonable agreement with the results of mass loss method.

Chapter seven

Prediction of bond strength for un-corroded/corroded steel bars in concrete using Artificial Neural Networks

7.1 Introduction

Accurate prediction of bond strength between steel reinforcement and concrete is of great importance to design RC members, and the bond performance can be affected by some primary parameters as demonstrated in section 2.5. However, predicting bond strength with a high degree of accuracy based on the rational methods is hardly obtained. Thus, Artificial Neural Network (AAN) has been introduced in this chapter to model the bond strength between un-corroded/corroded steel and concrete using the results obtained in chapter five in addition to two sets of data collected from the literature. The main parameters considered for developing ANN models are compressive strength, embedment length, concrete cover, steel bar diameter and corrosion rate. Furthermore, a parametric study was performed to investigate the generalization ability of the proposed models and the influence of such parameters on bond strength.

7.2 Principle of Artificial Neural Network

Artificial Neural Network (ANN) modelling is a computational system simulates the biological neurons existing in the human brain. In recent years, there has been a growing interest in using ANN in many civil engineering applications. This mainly owing to its features such as non-linearity, analysing, solving complicated problems and predicting the behaviour of systems where more conventional analytical methods

are not feasible. ANN can also be used even with an unlimited number of parameters, however, its performance is mainly dependent on the available number of database exerted from experimental results as it can be confused with a small number of training data. The randomly selected values for initial biases and weights can be considered as another drawback of ANN. Furthermore, ANN can also experience from over-fitting since it is not able to generalize new data within the range of inputs.

The neural network is fundamentally developed through five processes, namely data acquisition and analysing the problem, determining the architecture, determining the learning process, and training, validating and testing the network the network (Pala et al. 2007). The typical neural network system is composed of three major layers, namely input layers which represent the effective parameters, an output layer representing the target variable, and one or more hidden layers, showing in neurons form and connected by biases, weights and transfer functions. Neural network has a large number of nodes connecting with varying weights. Weight and bias are controlling the transmission of information between input and output. The number of neurons in each layer varies and it is primarily dependent on the problem. Whilst the neurons found in the input layer are representing the main effective factors and the output layer is composed of one neuron corresponds the experimental results, there is no a specific principle to determine the exact number of hidden layers and the number of neurons in the hidden layer. The selection of neurons is dependent on different factors such as the number of input and output units, the number of training samples, and the complexity of the functions (Alshihri et al., 2009). Therefore, the ideal number of hidden layers and neurons should be sufficient to correct the model, which only can be confirmed through a number of trails (Atici, 2011). The hidden layer is composed of two main parts: sum function and activation function. Back-Propagation

Neural Network is the most powerful technique used for training the network based on updating the weights and minimising the errors between calculated outputs and targets (Jadid, et al., 1996). These errors are backwardly propagated from the output layer, and thus weights and biases are modified based on the information that has learned. This process should be duplicated for a number of epochs until achieving the desired accuracy. The schematic diagram of Artificial Neural Network is presented in Figure 7.1.

The correlation between the inputs and the outputs can be mathematically expressed as follows:

$$y = f(S) = f(\sum_{i=0}^{n} w_{ij}.\, x_i + b)\ , i = 0, 1, 2, 3\ , 4, \ldots\ldots, n \qquad (7.1)$$

where x_i the input, y is the output, x_i is a bias, w_{ij} the weight of inputs for j neuron, b is the bias of j neuron, f is the transfer function.

The new bias and weights are expressed by Equations 7.2 and 7.3, which are repeated till the error of network is minimised.

$$b_{i+1} = b_i - \delta \nabla E_{i/b} \qquad (7.2)$$

$$w_{i+1} = w_i - \delta \nabla E_{i/w} \qquad (7.3)$$

where designates the root mean square error (RSME) for a repetition , which is expressed by:

$$\delta \nabla E_{i/w} = \frac{\partial E_i}{\partial w} \qquad (7.4)$$

$$E_i = \sqrt{\frac{1}{N}} \sum_{0=1}^{n} |e_n|^2 \qquad (7.5)$$

where is the absolute error between experimental and predicted values and *N* is the number of database.

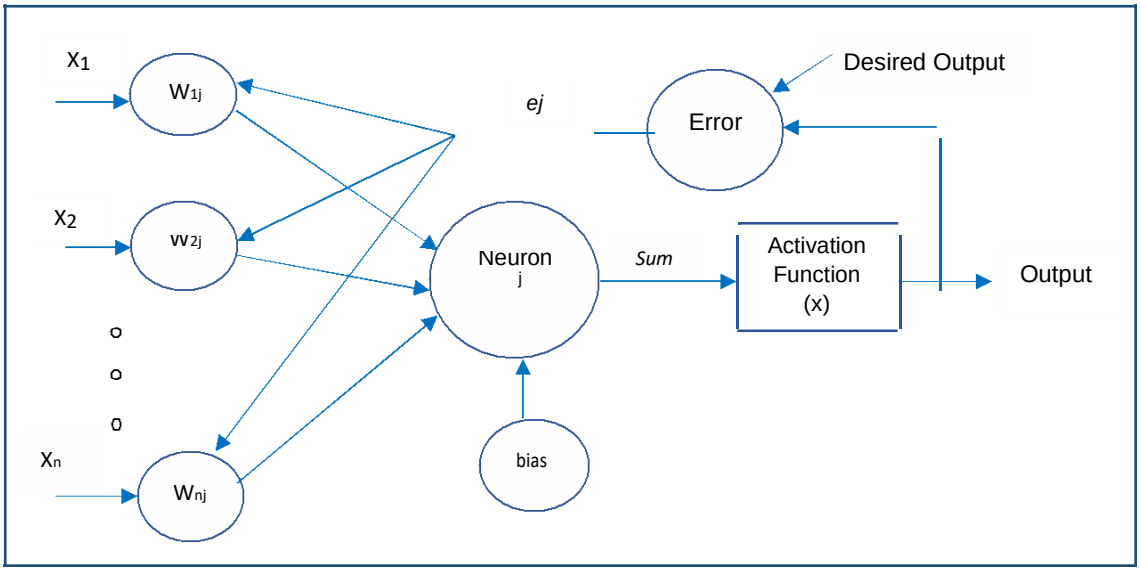

Figure 7.1. The system used in Artificial neural network models for transferring information.

7.3 Artificial neural network modelling

7.3.1 Description of the models

In the current study, ANN has been adopted to predict the bond strength between (corroded and un-corroded) steel bars and concrete had different properties using MATLAB 2018. Two different simulations have been performed to predict the bond strength of reinforced concrete, namely (ANN-4) and (ANN-5) using two sets of data. In the former model (ANN-4), four parameters were considered as inputs including compressive strength, bond length, concrete cover and bar diameter, whilst the output was expressed by one neuron referred to the value of bond strength of reinforced concrete. The latter model (ANN-5) was designed to predict the bond strength between corroded steel and concrete considering the same parameters used in the first simulation in addition to the influence of corrosion rate. It must be noted that the influence of RCA replacement level and NS content was involved within other parameters (i.e. compressive strength and corrosion level). Figure 7.2 exhibits the

Architecture of ANN model, whereas the main stages applied for the proposed ANN models are demonstrated in Figure 7. 3.

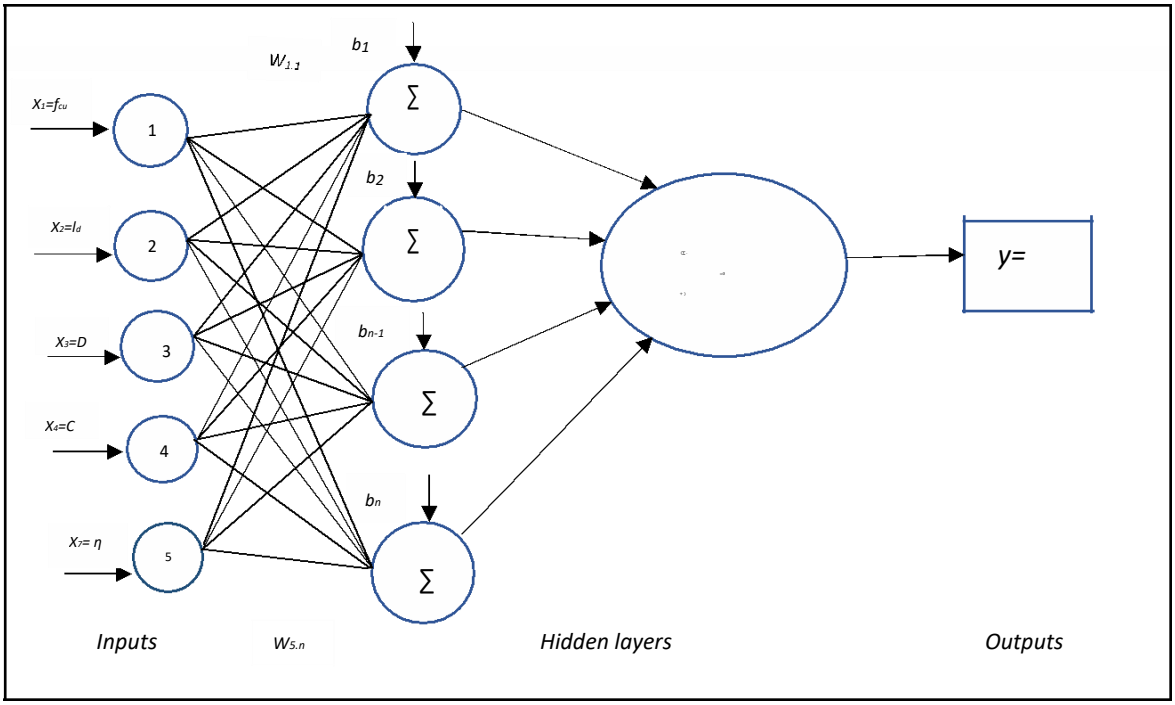

Figure 7. 2. Architecture of Artificial neural network model.

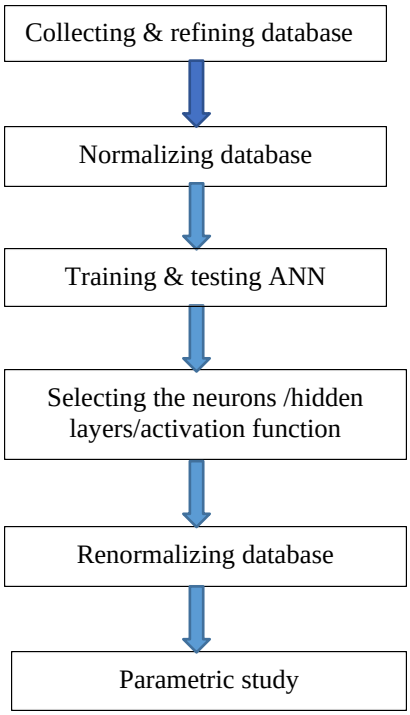

Figure 7. 3. Main stages applied for the proposed Artificial neural network models.

7.3.2 Experimental database

In the current study, two sets of data were collected from the literature in addition to author's findings. The first database consists of 147 specimens to predict the bond strength for un-corroded reinforced concrete, whilst 381 specimens were collected for the second database to predict the bond strength of corroded reinforced concrete. The database presented in the current investigation was refined from the available data in the literature to fulfil the following requirements:

- Limited to deformed steel bars.
- Corrosion was induced only by electrochemical acceleration technique and the corrosion rate was measured by weight loss method.
- Specimens produced without any stirrups since the presence of stirrups can provide additional confinements.
- All specimens prepared for pull-out test, so the data obtained from beams' specimens was excluded.
- The bond at zero corrosion was available as the change in bond due to corrosion is defined from this reference point.

Therefore, 11 data sets collected from the literature (Almusallam et al.,1996; Alsulamani et al., 1990; Yalciner et al., 2013; Fang et al., 2006; Cabrera & Ghoddoussi,1992; Fernandez et al., 2016; Yang et al., 2015; Coccia et al., 2016; Siempu & Pancharti, 2017; Serag et al, 2017, and Kim et al., 2014) were used to develop ANN-4 for predicting the bond strength between non-corroded bars and concrete as shown in Table B.1 in Appendix B. For ANN-5 model, 23 data sets from 8 experimental investigations (Almusallam et al., 1996; Alsulamani et al., 1990; Yalciner et al., 2013; Fang et al., 2006; Cabrera & Ghoddoussi, 1992; Fernandez et al., 2016; Yang et al., 2015; and Coccia et al., 2016) were used to predict the bond strength of

corroded reinforcement embedded in concrete in addition to the results obtained through the current work as presented in Table B. 2 in Appendix B. It should be noted that 73 data values from the total data in ANN-5 were free from corrosion as they were needed for comparison reasons. In addition, 154 data sets were containing RCA, while 108 data collected from specimens containing NS. The frequency distribution of each parameter used for training, validating and testing of the developed ANNs is presented in Figures. 7.4 and 7.5, whilst the statistical properties of these parameters for both models are exhibited in Tables 7.1 and 7.2.

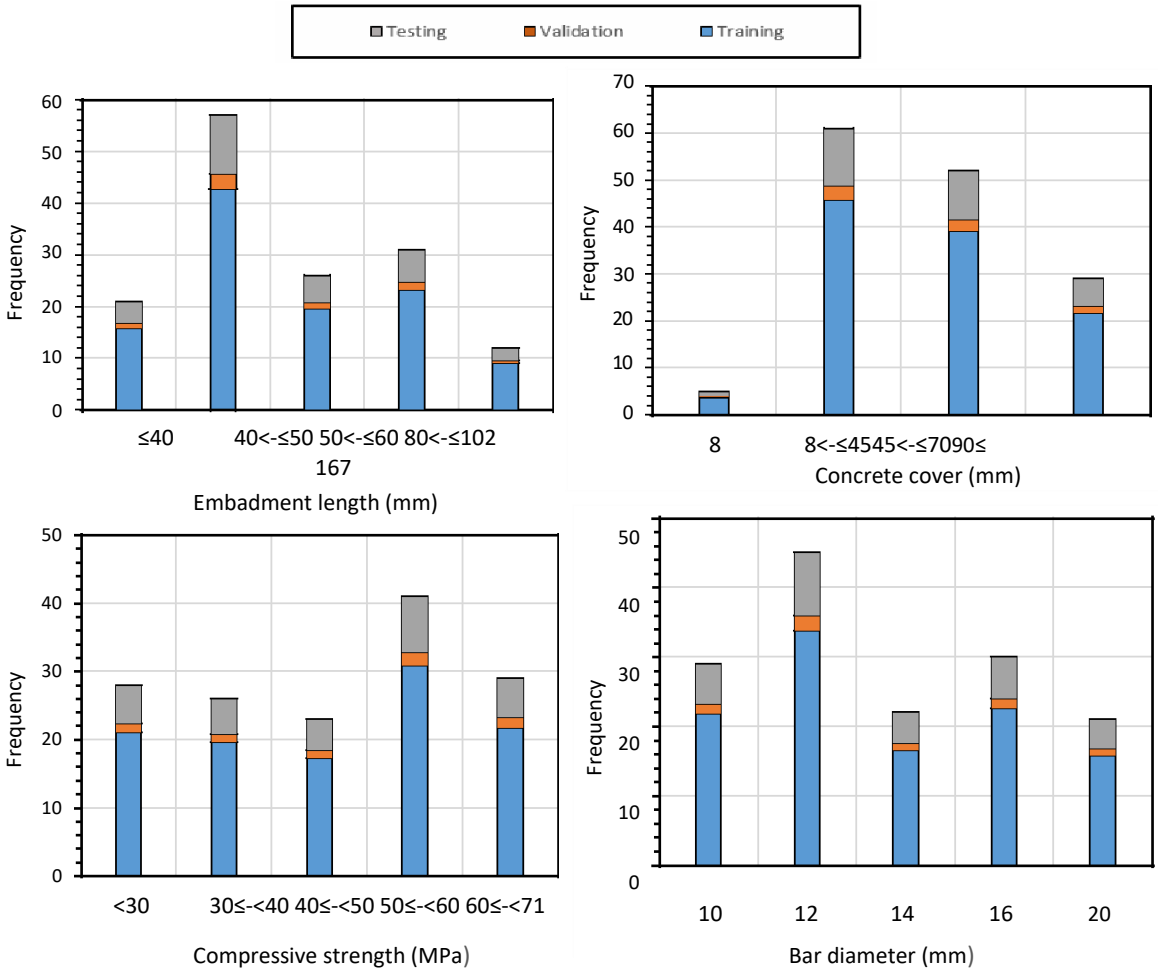

Figure 7. 4. Distribution of different parameters in non-corroded pull-out database.

The refined database was divided into three sets, namely, training, validation and testing. Whilst the majority of database used for training the model (75%) to create a more accurate model, just 5% used for the validation and the remaining (20%) applied

for testing. During the training stage, the network is modified based on the obtained errors and the used data is processed to optimise the network and minimise the deviation. Validation is mainly utilised to measure the generalisation of network as well as to cease training when generalization stops improving. Testing is fundamentally applied to inspect the ability of ANN in predicting properly the output, using data that has not been used during the training phase.

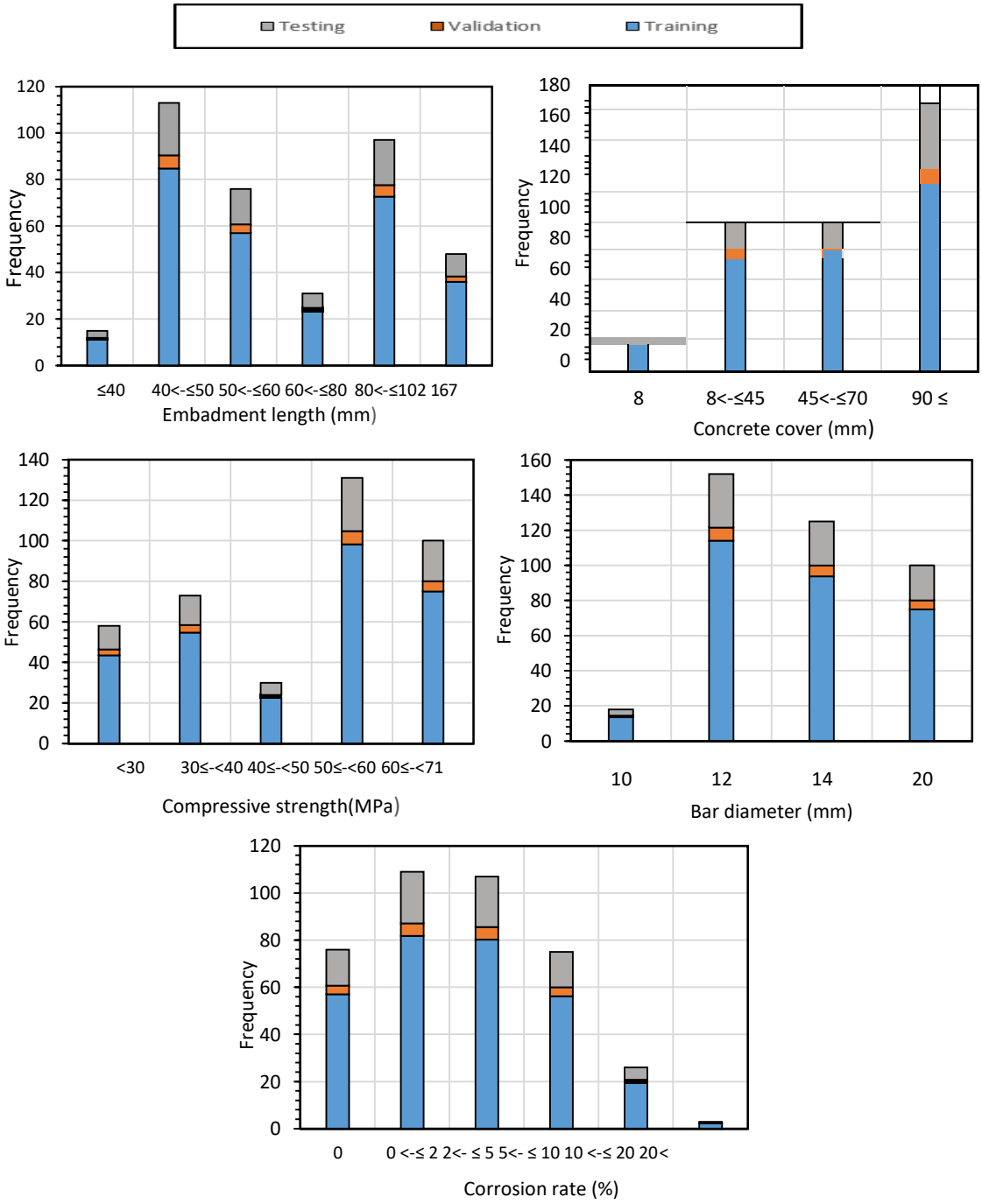

Figure 7. 5. Distribution of different parameters in corroded/un-corroded pull-out database.

Table 7. 1. Statistical properties of un-corroded pull-out specimens (ANN-4).

Neural network input parameters	Minimum	Maximum	Mean	S.D	COV%
Embedment Length, l_d (mm)	25	167	72.4	34.12	47.13
Compressive strength of concrete, fcu (MPa)	20.7	70.8	45.59	14.96	32.23
Concrete cover, c (mm)	8	94	59.53	22.19	37.27
Bar diameter (mm)	10	20	13.86	43.75	23.25
Bond strength (MPa)	9.1	34.99	20.0	6.10	30.33

Note: SD is the standard deviation and COV is the coefficient of variation.

Table 7. 2. Statistical properties of corroded pull-out specimens (ANN-5).

Neural network input parameters	Minimum	Maximum	Mean	S.D	COV%
Corrosion level (%)	0	49.4	3.86	4.8	89.12
Embedment Length, l_d (mm)	40	167	81.16	38.54	47.43
Compressive strength of concrete, fcu (MPa)	23	70.8	47.29	15.61	33.0
Concrete cover, c (mm)	8	94	66.55	28.34	42.53
Bar diameter (mm)	10	20	14.62	3.36	23.04
Bond strength (MPa)	0.78	34.94	13.01	7.95	61.12

7. 3.3 Normalisation of database

To improve the efficiency of NN training and enhance the learning ability of the neural network, data values were normalised to be suitable for training process prior to be implemented in the network. Data values were scaled in order to eliminate the influence of bias in the neural network in addition to accelerating the process time of training by starting within the same interval. Different types of activation functions can be applied in the network, however, log sigmoid and tan sigmoid functions are the most common transfer functions used to normalise data for non-linear applications. Log sigmoid function can be applied to scale the data between 0 and 1 range, whereas tan sigmoid function is scaled data within the interval (-1 and +1). The algorithm for normalisation data can be demonstrated using the following equation:

$$x_n = \frac{y_{max} - y_{min}}{x_{max} - x_{min}} (x - x_{min}) + y_{min} \qquad (7.6)$$

Where is the scaled input, and are the minimum and maximum of the normalized variables, respectively, and are the minimum and maximum target values, respectively. In the current work, tan sigmoid function was adopted to normalize the values within the interval [-1, 1], and therefore and are equivalent -1 and +1, respectively, and equation 7.6 is adjusted to be in the following form:

$$x_{scaled} = \frac{2*(x_{actual-x_{min}})}{x_{max}-x_{min}} - 1 \qquad (7.7)$$

7. 3.4 Neural network training

ANN modelling was developed utilising the multi-layered feed forward neural network with a back-propagation algorithm available in MATLAB version 9.4 (R2018a). A wide range of learning techniques, transfer functions, network architectures and training functions are available in this version (Ashour & Alqedra, 2005). Levenberg–Marquardt algorithm is found the preferred choice of back propagation algorithm for training the network due to its fast learning ability compared to other types of algorithms (Suratgar et al., 2005). Four parameters are used for training of Levenberg–Marquardt algorithm, namely, the maximum number of repetitions, target performance, in particular, the tolerance between the actual output and the prediction obtained from ANN, the minimum allowed gradient and the maximum run time. It should be noted that 1000 epochs were selected as a maximum number for training, while the initial biases and weight were randomly appointed by NN toolbox.

7. 3.5 Topology of ANN

It has been stated that one hidden layer is found sufficient for predicting the target (Ni et al., 2000; Siddique et al., 2011; Duan et al., 2013), and hence one hidden layer was

adopted to develop ANN model in the current study. Even though many research studies have been carried out to optimise the procedures regarding the calculation of neurons number in the hidden layer, there is still no specific approach for determining the architecture of BPNN. Boger et al., (1997) revealed that using about 0.66 of input layer size might probably give the best neurons number in the hidden layer. Furthermore, the number of neurons in the hidden layer should not exceed one more than the double of inputs as reported by Atici (2011). Accordingly, the optimum neurons number can be only confirmed based on a trial and error method. Therefore, a total of 11 NNs with different neurones were created and tested for each database (i.e. 2, 3, 4, 5, 6, 7, 8, 9, 10, 11 and 12 neurons), and the highest accurate one was adopted to measure the independent parameters. The more closely R value approaches to 1, the robustness of NN is expected, In addition, the mean squared error (MSE) is carried out for monitoring the performance of training network. As a value of MSE is smaller and closer to zero, a better performance is predicted. MSE can be calculated using the following formula:

$$\mathrm{MSE} = \frac{\sum_{i=1}^{n} (T_i - A_i)^2}{n} \qquad (7.7)$$

where is the target value, is actual value and n is the number of training dataset. A trial and error method was applied, and the process of training was ceased after reaching the maximum number of epochs as well as when the MSE for validation data begins to exceed the selected epochs.

7.3.6 Performance of the trained ANNs

Five statistical parameters were used to assess the performance of networks prepared with different architectures, namely, mean value, coefficient of variation (COV%), standard deviation (SD) and mean squared error (MSE) and correlation coefficient (*R*).

The statistical findings performance of the trained architectures of neural network for the two sets of databases are presented in Tables 7. 3 and 7. 4. The variation between the experimental results and the output obtained from NN was calculated for each point, and MSE was used for monitoring the performance of network during training phase. As can be observed from Tables 7.3 and 7.4, the statistical parameters for the trained 4*8*1 NN exhibited the best performance amongst NNs used for predicting the bond strength for non-corroded steel bars (ANN-4). Therefore, one hidden layer with 8 neurones is decided to be utilised for ANN-4. On the other hand, one hidden layer with 10 neurones (5*10*1) NN achieved the best performance for those containing different levels of corrosion (ANN-5). The selection of a reasonable number of neurones as found during the current training can also help in avoiding the possibility of overfitting that might occur with using larger neurons in the hidden layer.

Table 7.3 Statistical results of the models created for un-corroded reinforced specimens (ANN-4).

NN architecture	Mean	SD	COV (%)	R	MSE
4*2*1	1.015	0.126	12.63	0.905	37.22
4*3*1	1.013	0.12	12.55	0.924	31.51
4*4*1	1.014	0.104	10.32	0.955	27.28
4*5*1	1.013	0.104	10.29	0.959	15.4
4*6*1	1.019	0.081	8.04	0.968	14.51
4*7*1	1.012	0.079	7.86	0.973	13.4
4*8*1	1.006	0.056	4.17	0.985	10.23
4*9*1	1.007	0.065	6.42	0.982	11.8
4*10*1	1.019	0.063	6.28	0.981	13.99
4*11*1	1.014	0.063	6.33	0.980	14.5
4*12*1	1.019	0.067	6.629	0.969	17.8

Table 7.4 Statistical results of the models created for corroded reinforced specimens (ANN-5).

NN architecture	Mean	SD	COV (%)	R (%)	MSE
5*2*1	1.013	0.126	12.63	91.1	39.2
5*3*1	1.017	0.12	12.55	91.9	33.5
5*4*1	1.014	0.104	10.32	93.2	29.4
5*5*1	1.013	0.104	10.29	94.16	20.1
5*6*1	1.019	0.081	8.04	94.8	18.9
5*7*1	1.012	0.079	7.86	94.92	17.5
5*8*1	1.019	0.067	6.629	95.97	14.95
5*9*1	1.018	0.065	6.42	97.127	13.34
5*10*1	1.003	0.063	6.28	97.624	12.89
5*11*1	1.046	0.073	6.33	97.38	14.62
5*12*1	1.014	0.056	5.54	95.29	20.51

A comparison between the predicted values obtained from the selected NN models and experimental findings for training and testing and all data sets are presented in Figures. 7.6 and 7.7, respectively. From these figures, it can be observed that the selected NNs showed a high degree of fitness, indicting a high agreement between the predicted values and the experimental results. The mean ratio between predicted and experimental values for training, testing and all data sets of non-corroded reinforced specimens achieved 0.976, 0.936 and 0.968, respectively. On the other hand, the predicted bond strengths for corroded specimens were slightly less accurate with a coefficient of determination is equal 0.957, 0.956 and 0.956 for training, testing and all data, respectively. The most important Information derived from Matlab software for the developed models including a comparison between the “target” and “output” parameters in terms of Pearson’ correlation coefficient (R), training state, training error histogram and best validation performance of network training is displayed in Figures B.1-6 in Appendix B.

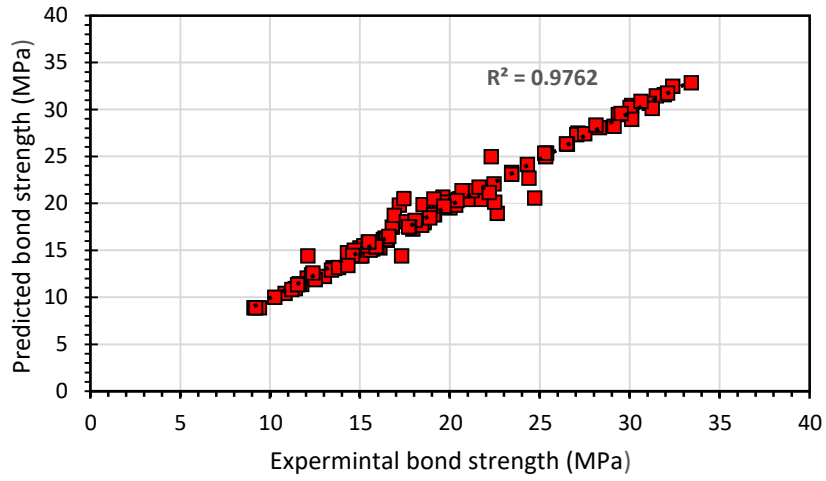

(a)

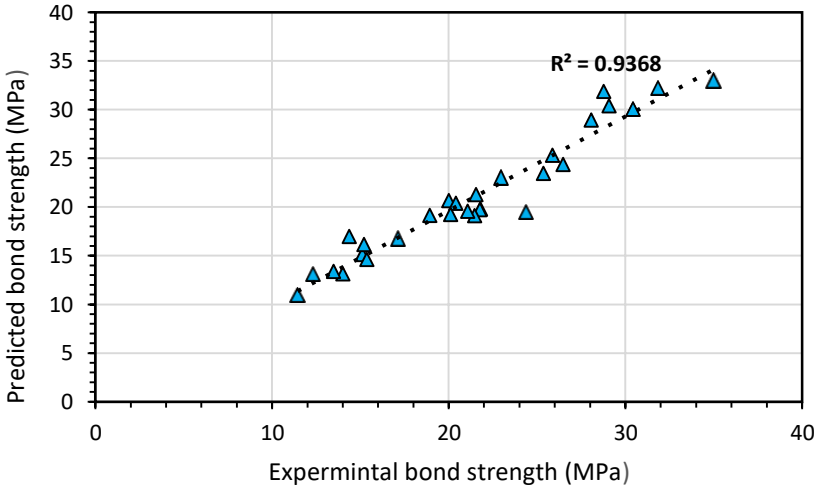

(b)

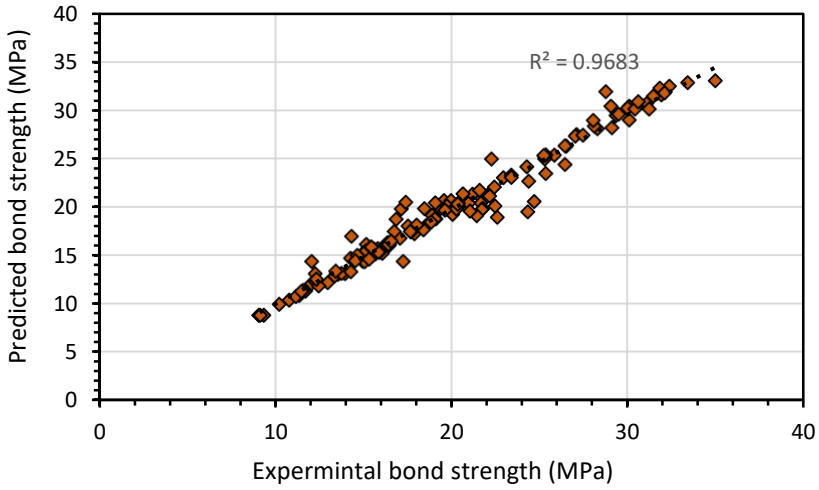

(c)

Figure 7.6 Comparison of experimental and predicted bond strengths for ANN-4: (a) training, (b) testing and (c) all data sets.

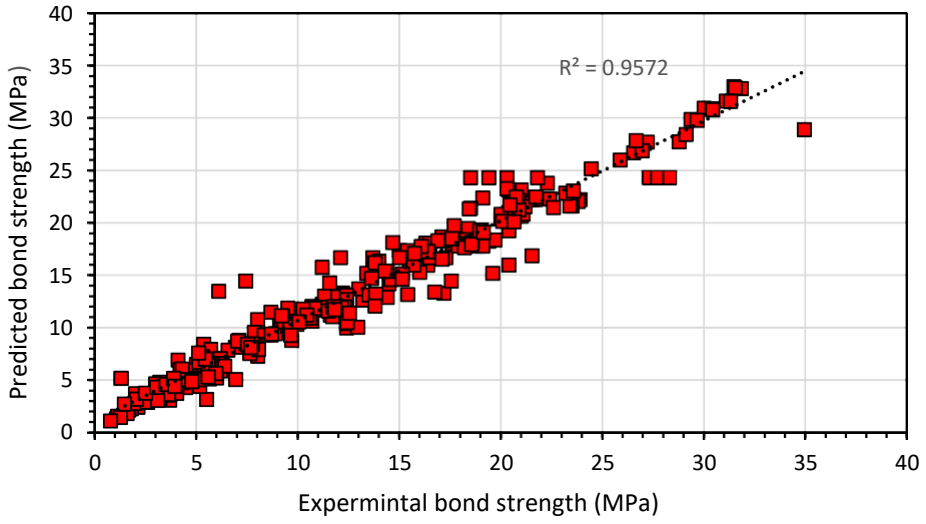

(a)

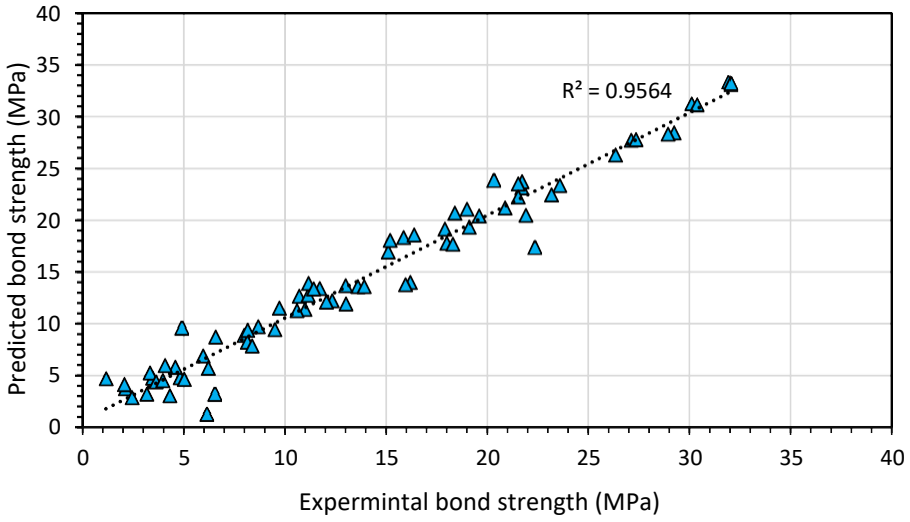

(b)

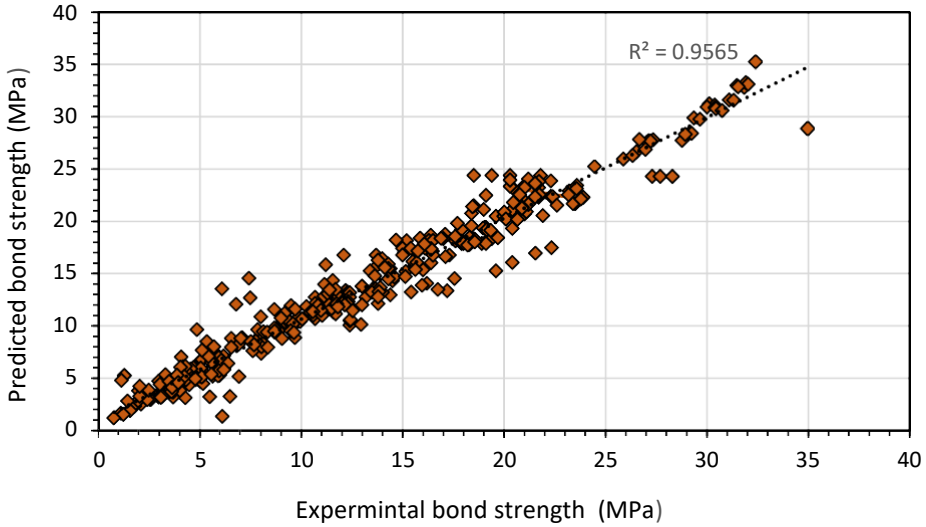

(c)

Figure 7.7 Comparison of experimental and predicted bond strengths for ANN-5: (a) training, (b) testing and (c) all data sets.

7.4 Parametric analysis using developed ANNs

The trained 4*8*1 network is employed to conduct a parametric study for quantifying the influence of input parameters on the bond strength of non-corroded specimens, whilst 5*10*1 architecture was used to analyse the effect of the parameters on the bond strength for corroded and un-corroded specimens. It should be noted that only the values within the ranges having a high frequency were involved in the parametric study to obtain appreciable trends, whilst those at the extremes were neglected. To apply the parametric study and analyse the influence of main parameters on bond strength, one parameter was changed within the range of frequency while the others were kept constant.

7.4.1 Effect of embedment length on bond strength

Figure 7.8 exhibits how the bond strength can be affected by the change in the embedment length of reinforcement. Experimental findings (Siempu & Pachautic, 2017) were plotted in Figure 7.8(a) and the current findings were plotted in Figure 7.8 (b) to compare with the predicted results obtained from ANN4 and ANN5, respectively. As it can be seen that by increasing the bonded length, the bond strength decreases owing to the nonlinear distribution of the bond stresses over the bonded length, indicating that the trained ANN-4 and ANN-5 are adequately identified this parameter. However, it can be noted that the influence of un-corroded embedment lengths longer than 100mm showed less decrease in the bond strength, whilst those corroded continuously decreases with the increase of bonded length owing to the appearance of longitudinal cracks along steel bars resulting from corrosion propagation, making concrete to be easily split. The influence of bonded length was also acknowledged by the majority of existing models for predicting bond strength, however, the Canadian code ignores the embedment length in their bond strength equations.

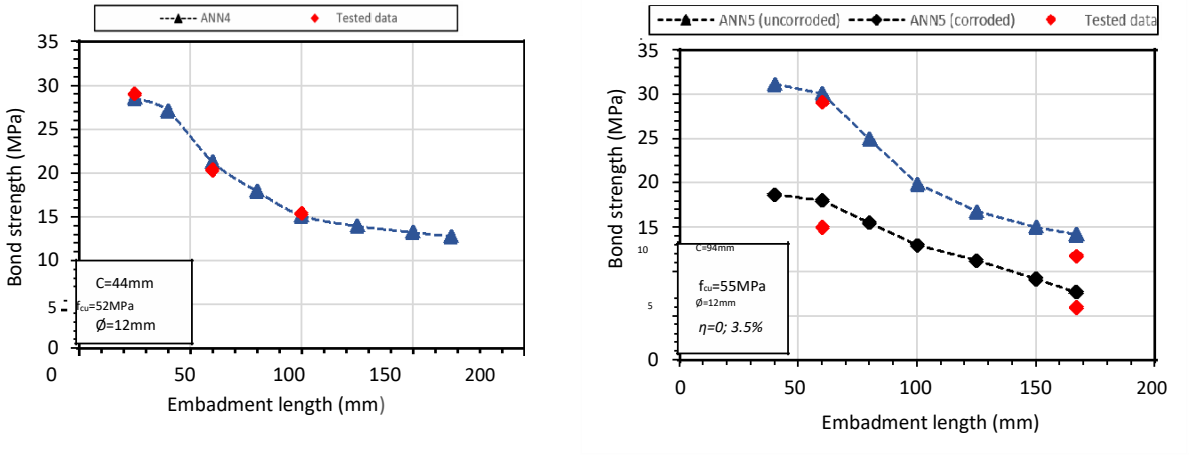

(a) (b)

Figure 7. 8 Effect of embedment length on the predicted bond strength obtained by (a) ANN-4, (b) ANN-5.

7.4.2 Effect of bar diameter on bond strength

Using larger bar diameters result in less bond strengths as predicted by ANN-4 and ANN-5 shown in Figure 7.9. This trend in agreement with the findings reported in previous studies (Pour et al., 2016; Serag et al., 2017). This tendency is probably because of the generation of voids underneath the diameters resulted from the bleeding of water, causing less contact area between steel and adjusted concrete. Nevertheless, the findings obtain from the developed ANNs showed that the effect of this parameter seemingly became less pronounced in corroded bars embedded in concrete as shown in Figure 7.9 (b). This likely can be clarified by the erosion occurred in reinforcement ribs, which control transferring the force between steel and concrete, making the impact of using different diameters less influential. The influence of bar diameter has been involved in all design codes used for predicting the bond strength.

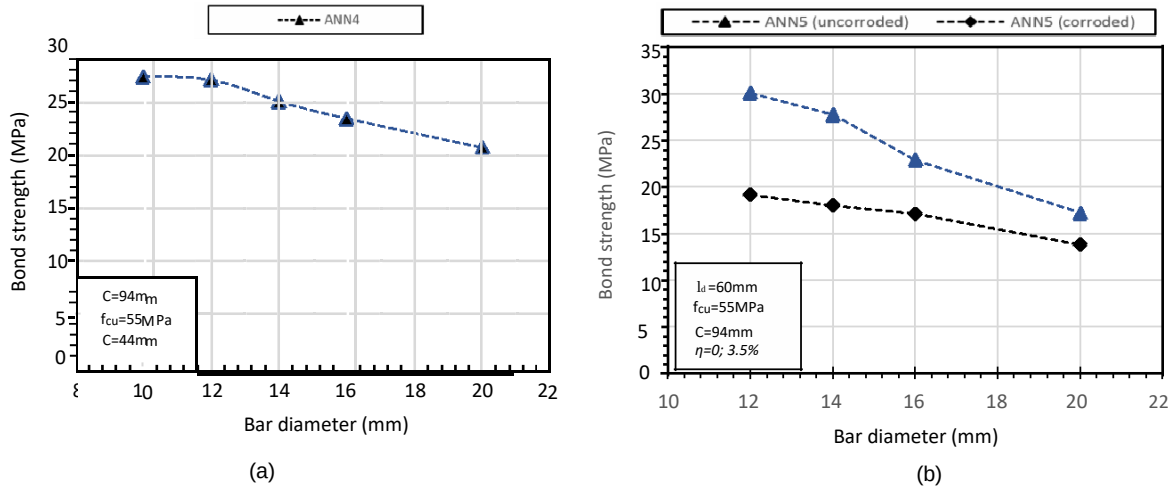

Figure 7. 9 Effect of bar diameter on the predicted bond strength obtained by (a) ANN-4, (b) ANN-5.

7.4.3 Effect of compressive strength on bond strength

Figure 7.10 illustrates the influence of changing concrete strength on the ultimate bond strength for both corroded and un-corroded specimens as predicted by ANN-4 and ANN-5, respectively. As can be seen from Figure 7.10 (a), the bond strength linearly developed with increasing concrete strengths for specimens having a small cover (44mm). However, the influence of concrete strength on the bond resistance is more pronounced with those having larger covers (94mm) as well as after exposing to corrosion.as shown in Figure 7.10 (b). Providing higher confinements with lager covers might explain the importance of increasing concrete strengths, whilst more protection against corrosion would be acquired with those having higher strengths, providing higher resistance against bond degradation due to corrosion. It must be stated that the influence of compressive strength on the bond strength was acknowledged in all existing codes by being involved in their equations.

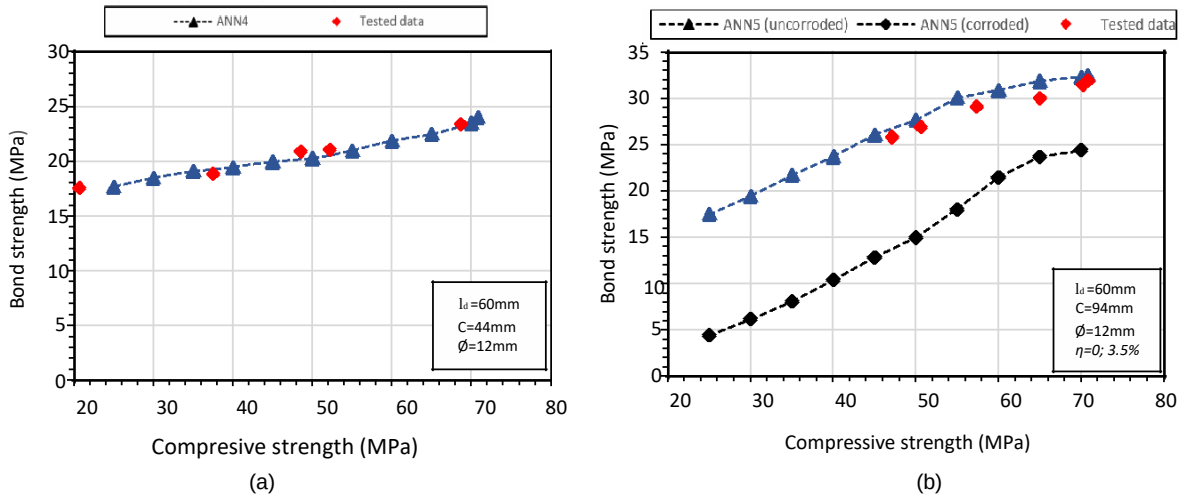

Figure 7. 10 Effect of compressive strength on the predicted bond strength obtained by (a) ANN-4, (b) ANN-5.

7.4.4 Effect of concrete cover on bond strength

To study the influence of concrete cover, all other parameters were kept constant, while the change in concrete cover was tested from 8 to 94 mm. As depicted in Figure 7.11, the predicted bond strengths for un-corroded specimens by the developed ANNs tend to be highly increased with larger concrete cover up to about 60 mm, then the impact of concrete cover became less importance, agreeing with the results reported in a previous work (Yalciner et al., 2013). From Figure 7.11(b), it can be stated that the increase of cover becomes more significant for those exposure to higher corrosion levels since more protections against corrosion are required in addition to the development in confinements. The influence of concrete cover has been considered in the majority of existing models as one of the main parameters for predicting the bond strength.

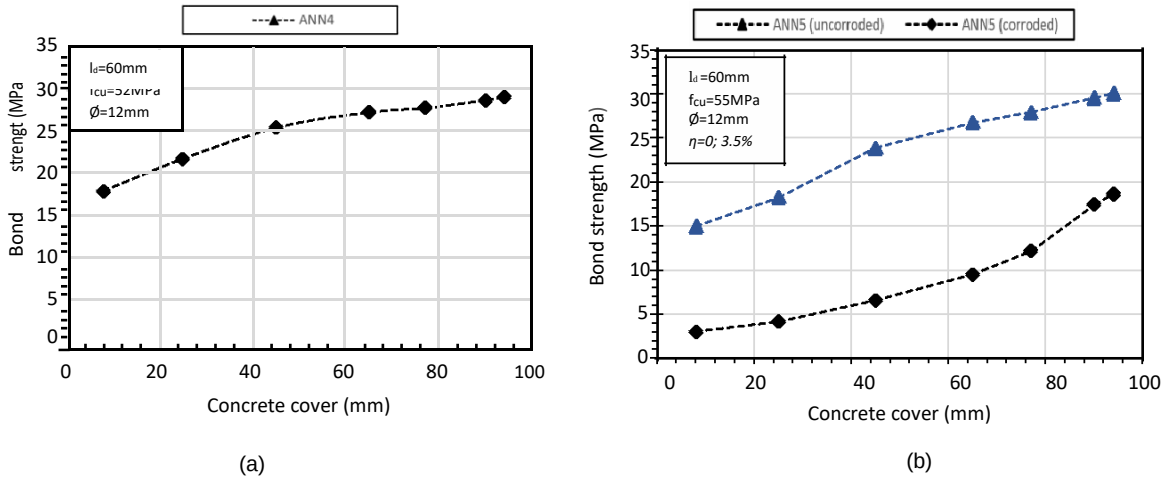

Figure 7.11 Effect of concrete cover on the predicted bond strength obtained by: (a) ANN-4, (b) ANN-5.

7.4.5 Effect of corrosion on bond strength

Figure 7.12 demonstrates the influence of corrosion on bond strength as predicted by ANN-5. It can be noted that the trend of bond strength slightly enhanced with a small quantity of corrosion due to the generation of the internal stresses between steel and surrounding concrete produced by the accumulation of rust products around steel bar, agreeing with the findings stated by previous researchers (Auyeung et al., 2000; Fang et al., 2004). From Figure 7.12, it is also can be observed that the propagation in of corrosion causes a sudden reduction in the bond resistance, which might be justified by the generation of internal cracks with increasing rust products volume, agreeing with previous studies (Auyeung et al., 2000; Coccia et al., 2016). As can be observed from the plotted results, the bond strengths predicted by ANN-5 are well correlated with the experimental findings. For instance, at about 3.5% corrosion rate was almost the half of bond strength for un-corroded specimens.

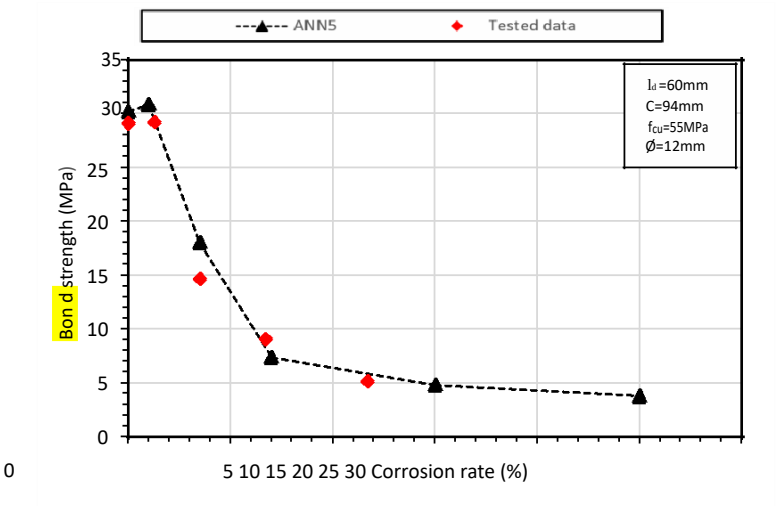

Figure 7.12 Effect of corrosion rate on the predicted bond strength.

7.5 Comparison between the prediction given by ANN-4 model and different existing models

In this section, the developed model for non-corroded specimens (ANN-4) was compared with five existing predictive models presented in chapter five using a147 of database. The summery statistical results of these models are presented in Table 7.5, whilst the comparisons between predicted and experimental results for these models are shown in Figure 7.13. It can be observed that the bond strength estimated by ANN-4 exhibited much higher accuracy in prediction the bond strength compared to other suggested models. In general, these models underestimate most of bond strength values, however, the performance of these models was uneven from one to another. The Australian Standard (AS3600) model exhibited the poorest estimation and significantly underestimated the values with a mean of 0.51, and MAPE and MSE of 52.5% and 66.21%, respectively. On the other hand, Darwin' model exhibited the best estimation of bond strength amongst other models with the lowest S.D, MSE and MAPE of 0.18, 17.08 % and 17.25 %, respectively.

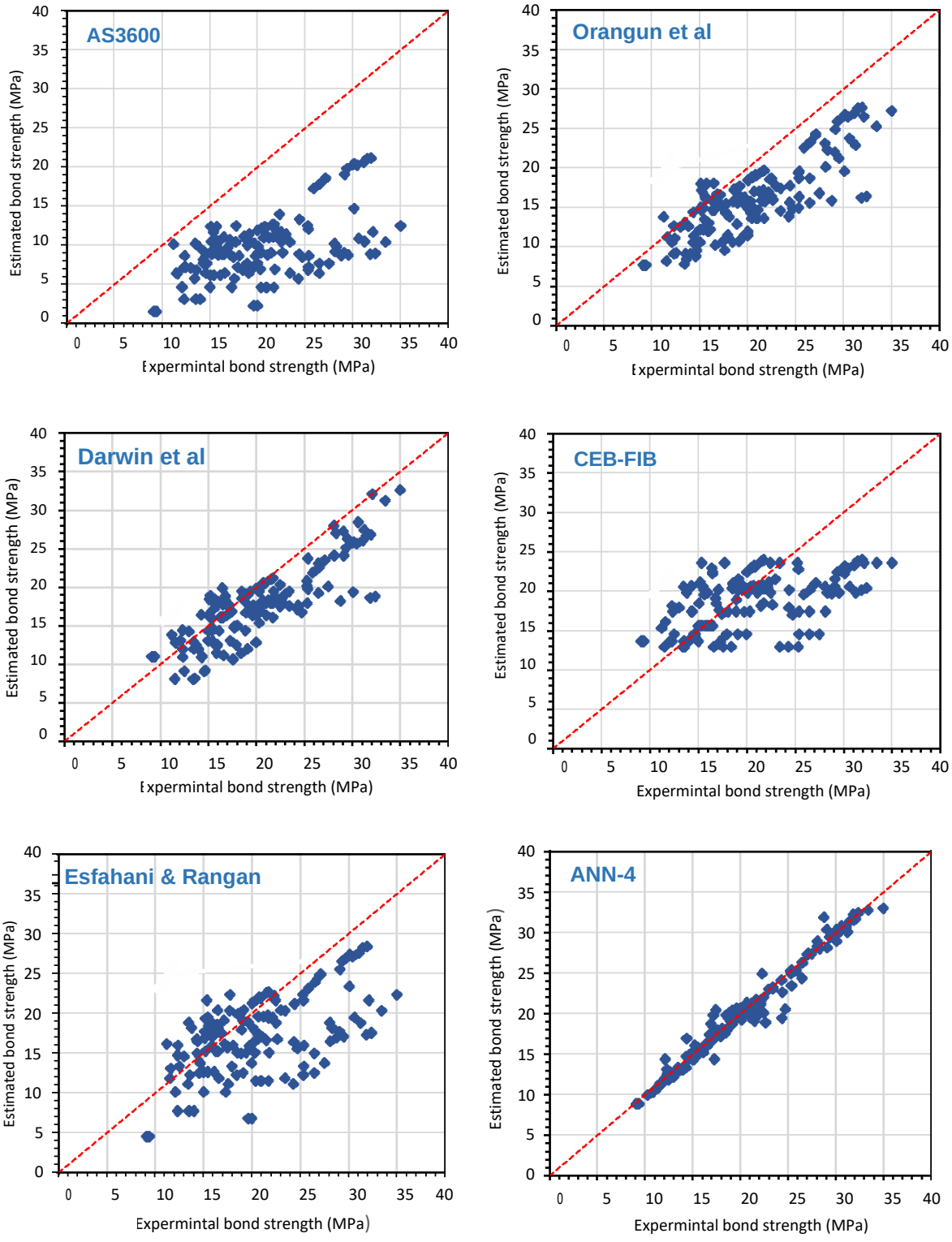

Figure 7.13 Comparison between predicted and experimental bond strengths using ANN-4 and the existing models.

Table 7. 5 Summary of statistical results for bond strength predicted by ANN-4 and the existing models

Predicted model	Mean	S.D	MAPE (%)	MSE (%)
Australian Standard 3600 (2004)	0.51	0.257	52.2	66.21
Orangun et al., (1977)	0.80	0.216	23.53	31.64
Darwin et al., (1992)	0.87	0.180	17.08	17.25
CEB-FIP (2010)	0.77	0.280	22.02	31.29
Esfahani & Rangan (1998)	0.88	0.325	25.59	42.07
ANN-4	0.98	0.056	8.42	10.23

7.6 Conclusions

Artificial Neural Network was successfully developed to predict the bond strength for un-corroded/corroded steel bars embedded in concrete based on several parameters, using two sets of databases collected from the literature in addition to the current experimental results. A parametric study was conducted to analyse the impact of input parameters of the proposed NN models. The following conclusion have been drawn from this study:

- Levenberg–Marquardt algorithm is found the preferred choice of back propagation algorithm for training the network. The trained 4*8*1 NN exhibited the best performance in ANN-4 model for predicting the bond strength in non-corroded reinforcement specimens. On the other hand, one hidden layer with 10 neurones (5*10*1) NN achieved the best performance for those containing different levels of corrosion (ANN-5).
- The developed ANN-4 and ANN-5 provide a high accuracy in predicting bond strength for un-corroded and corroded specimens, respectively, indicating that ANN models have learned well the bond strength and the affecting parameters. However, ANN-4 exhibited a better performance in terms of predicting the bond strength for un-corroded specimens.
- The performance of the developed ANNs is heavily dependent on the volume of collected database as well as its readability. The developed ANN models can be

only perfectly valid within the ranges of inputs involved in the current study, whereas less accuracy of prediction might be obtained beyond these ranges.

- The parametric study conducted using the proposed ANN models revealed that the bond strength is directly proportional to concrete cover for un-corroded specimens up to about 60mm, then the influence becomes less pronounced. However, the increase of concrete cover seems more significant in the case of exposure to corrosion.
- The predicted bond strength is linearly proportional to concrete compressive strength for specimens prepared with small concrete covers, whilst more influence was observed with larger covers and advanced levels of corrosion.
- The trends obtained from the proposed models exhibited inverse relationships between the bond strength and both parameters: the bonded length and bar diameter, agreeing with the actual results.
- ANN-5 presented a slight bond development with a small amount of corrosion, while a significant degradation was observed with further corrosion rates, showing a consistent agreement with those obtained from experimental investigations.
- The bond prediction obtained from the developed NN is in a better agreement with the database than obtained from the existing models, followed by the model proposed by Darwin, whilst the Australian Standard (AS3600) model exhibited the poorest estimation.

Chapter eight

Conclusions and future work

8.1 Summary

The bond performance between corroded/uncorroded steel reinforcement and concrete containing recycled aggregate and nano silica was thoroughly investigated in this thesis. The research work is composed of five main stages. In the first stage, the experimental investigation was performed on the effect of replacing normal aggregate by RCA on the bond strength at different levels of exposure to corrosive conditions as presented in chapter 3. Different investigations were conducted in the second stage to select the most effective type of nano silica based on its characteristics in addition to determining the optimum dosages for each type. In third stage, the selected nano silica was incorporated with both normal and RCA concrete to investigate how corrosion and bond resistance can be enhanced under different levels of corrosive environmental conditions. Fourthly, the feasibility of the impact-echo method for identifying the corrosion identifying was evaluated and compared to the corrosion obtained by mass loss method. Finally, Artificial Neural Network was developed to predict the bond strength between corroded/un-corroded steel and concrete.

The experimental part includes testing 180 pull-out specimens prepared from 12 different mixtures, in addition to 63 different mixtures were produced using three different quantities and types of colloidal NS having various surface areas. The main parameters studied were the amount of recycled aggregate (i.e. 0%, 25%, 50% and 100%), nano silica (1.5% and 3%), embedment length as well as the steel bar diameter

(12 and 20mm). Different levels of corrosion were electrochemically induced by applying impressed voltage technique for 2, 5, 10 and 15 days. The experimental observations mainly focused on the corrosion level in addition to the ultimate bond, failure modes and slips occurred.

A numerical study was carried out using the neural network toolbox available in MATLAB 2018 to predict the bond strength for corroded and corroded reinforced concrete. A parametric study was conducted using the main influencing parameter to investigate the generalization ability of the proposed models and the influence of such parameters on bond strength.

The main aim of this chapter is to summarize the principal findings of the research carried out in this study and provide a number of recommendations and suggestions for future work.

8.2 Conclusions

The full details of findings obtained from each section in the current research were reported at the end of each chapter. Therefore, this section summarises the principal findings drawn from this research work as follows:

1. The compressive strength of RCA concrete gradually reduces by increasing the amount of RCA in concrete. At 100% of RCA replacement rate, the compressive strength reduces by approximately 15% at 28 days; however, this effect becomes less pronounced as time of curing extended to 90 days.

2. Concrete made with 25% RCA replacement is very comparable to normal concrete and did not show a significant change, even under harsh environmental conditions, and therefore RCA can be recommended to be used up to this limit in all structural applications.

3. Corrosion of reinforcing steel initiated faster in RCA concrete, and higher corrosion rates were reported with increasing the level of RCA in mixtures.

4. The ultimate bond strength of reinforced concrete specimens is slightly affected by the increase of RCA level under normal conditions, but the difference becomes more pronounced after exposure to harsh corrosive conditions. In other words, the rate of bond degradation between RCA concrete and corroded steel is much faster than that found in corroded conventional concrete.

5. No significant differences between NCA and RCA concrete were observed in terms of bond stress-slip curves and failure mode before and after exposure to corrosion.

6. The performance of concrete is directly influenced by the change of the surface area of nano silica. Amongst the three used types of nano silica, NS with SSA of 250 m^2/g showed the highest enhancement rate in terms of compressive strength, water absorption and microstructure analysis, followed by NS with SSA of 500 m^2/g, whilst NS with SSA of 51.4 m^2/g was less advantageous for all mixtures.

7. The optimum ratio of nano silica is greatly associated to the particles reactivity and agglomeration state, in addition to the issue where the best packing is obtained for each type; it becomes higher for larger NS particles, however, it is found to be ranging between 2% and 5%. The optimum nano silica ratio in concrete is also affected by the water to binder ratio; it tends to increase corresponding to the increase in w/b ratios. More efficiency of NS particles is noted by using higher ratios of w/b.

8. A considerable enhancement in concrete strength was observed up to 40% after adding nano silica to all concrete mixtures, however, the strength gain was slightly higher with RCA concretes. In addition, NS was appreciably sufficient to recover the decrease occurred with RCA concrete and achieved even higher strength, in comparison to control concrete.

9. NS particles evidently recovered the significant corrosion propagation occurred in RCA concretes, especially under advancing levels of corrosion exposure by considerably minimising the pores available in mixtures.

10. The use of a small quantity of NS (1.5%) showed between 12-17% bond enhancements with both; normal and RCA concretes under non-corrosive conditions, however, much better influence was observed with increasing corrosion periods, reflecting the double effect of NS particles in enhancing the bond strength as well as corrosion resistance.

11. More efficiency of NS particles was observed with RCA concretes than found in conventional concretes in terms of enhancing bond and corrosion resistance, and therefore NS was superbly effective in recovering the poor performance in bond for RCA concretes.

12. By doubling the content of NS (3%), the bond resistance slightly enhanced for non-corroded specimens, while more influence was observed with larger quantities of RCA as well as longer periods of corrosion exposure.

13. The bond performance of RCA and NS concretes was seriously influenced by corrosion products; while the bond resistance slightly increased up to about 6% enhancement with a small amount of corrosion (2% weight loss), further corrosion led to a significant bond degradation.

14. The influence of bar diameter is directly related to the bonded length; by using similar reinforcement areas, higher bond strengths was reported for all tested specimens with larger diameters due to the influence of relative ribs area. An opposite trend was observed when the bonded length was taken as a ratio of bar diameter. Higher decreasing rates in bond strength were also observed when the embedment length increased from 5 to 13 times of bar diameter.

15. A significant difference in the response of impact echo was observed for the majority of the specimens after exposure to the high and moderate levels of corrosion as the dominant frequencies tended to clearly decrease with the progression of corrosion damage. However, no clear trend was observed at the initial stage of corrosion.

16. Impact-echo testing can be effectively used to qualitatively detect the damage caused by corrosion in reinforced concrete structures. Comparing to results obtained from weight loss method, the impact-echo technique showed a reasonable agreement with a regression coefficient of 0.79.

17. The existing models for predicting the bond strength of uncorroded specimens showed a good accuracy with experimental findings, especially that proposed by Darwin. However, the available models to predict the degradation in bond strength due to corrosion exhibited conservative correlation with the experimental findings.

18. A new formula was proposed to predict the bond degradation due to reinforcement corrosion based on regression analysis, showing a good agreement with the experimental results.

19. Different environmental and economic benefits was discussed by incorporating NS intro recycled aggregate concretes.

20. Artificial Neural Network was successfully developed to predict the bond strength for un-corroded/corroded steel bars embedded in concrete, and the performance of the proposed ANN models was confirmed by conducting a parametric study.

8.3 Recommendations for future work

1. Despite several approaches have been adopted to control the variability occurred during the production of RCA, further studies are still required in order to establish standard procedures for classifying the quality of RCA. The critical characteristics to assorting RCA need to be clearly identified.

2. One of the major drawbacks of RCA concrete is associated to the performance of durability properties, therefore a comprehensive study for assessing the other important durability properties of RCA concrete incorporating NS (i.e. shrinkage, freezing and thawing, sulphate attack, and alkali-silica reaction) is significantly needed.

3. Investigations on the full-scale structural elements for RCA concrete with the inclusion of NS are required. Experimental investigations on the serviceability, especially crack propagation also urgent to meet engineering demands. The long-term mechanical and durability properties of such concrete are also encouraged to be thoroughly investigated.

4. It is of great importance to perform a life cycle cost analysis for the modified RCA concrete in order to quantify the economic impact and analyse the cost effectiveness.

5. The bond deterioration under natural corrosion has not been sufficiently studied since the majority of existing investigations were conducted based on artificial corrosion. Thus, it is recommended to perform more investigations based on naturally corroded

specimens. Moreover, the majority of bond models are unsuitable for practical application. Therefore, it is highly recommended to develop realistic numerical models to achieve a better understanding of the bond strength of corroded structures.

6. In the current investigation, the optimum quantity of nano silica was found varying based on nano silica characteristics. Therefore, a model identifies the relationship between the optimum quantity and the characteristics of NS needs to be developed.

7. Research regarding the bond stress- slip relationship under steel corrosion is very limited and contradicted, and hence it is suggested to further improve the current models.

8. Despite impressed current is the most common technique for inducing corrosion, procedures for speeding the laboratory test need to be standardized since great varying levels of current density have been stated in the literature. These variations can probably affect obtaining the required level of corrosion. Thus, applying similar current and voltages can help in predicting the level of corrosion.

9. Assessing reinforcement corrosion by infrared thermography, electromagnetic and optical sensing methods are still new in corrosion field. Hence, more investigations need to be conducted since very few studies are available in this area.

10. Further investigations on the bond deterioration of reinforcing steel bar under the coupled effects of cyclic loading and reinforcement corrosion are highly encouraged since very limited research is available in the literature.

11. The promising results obtained from the impact-echo method indicated the high possibility of such method for evaluating corrosion in reinforced concrete, and therefore, more investigations need to be implemented for field large applications.

12. Other artificial intelligence approaches, namely support vector regression, fuzzy logic, genetic algorithm and M5P model tree, as well as hybrid modelling strategy are recommended to predict the bond strength of corroded bars embedded in concrete.

References

ABOSRRA, L., ASHOUR, A. & YOUSEFFI, M. 2011. Corrosion of steel reinforcement in concrete of different compressive strengths. *Construction and Building Materials,* 25**,** 3915-3925.

AGGELIS, D. G. 2013. Wave propagation through engineering materials; assessment and monitoring of structures through non-destructive techniques. *Materials and Structures,* 46**,** 519-532.

AHMAD, S. 2003. Reinforcement corrosion in concrete structures, its monitoring and service life prediction—a review. *Cement and concrete composites,* 25**,** 459-471.

AHMAD, S. 2009. Techniques for inducing accelerated corrosion of steel in concrete. *Arabian Journal for Science and Engineering,* 34**,** 95.

AJDUKIEWICZ, A. & KLISZCZEWICZ, A. 2002. Influence of recycled aggregates on mechanical properties of HS/HPC. *Cement and concrete composites,* 24**,** 269-279.

AKIYAMA, M. & FRANGOPOL, D. M. 2014. Long-term seismic performance of RC structures in an aggressive environment: Emphasis on bridge piers. *Structure and Infrastructure Engineering,* 10**,** 865-879.

AL-SULAIMANI, G., KALEEMULLAH, M. & BASUNBUL, I. 1990. Influence of corrosion and cracking on bond behavior and strength of reinforced concrete members. *Structural Journal,* 87**,** 220-231.

ALMUSALLAM, A. A., AL-GAHTANI, A. S. & AZIZ, A. R. 1996. Effect of reinforcement corrosion on bond strength. *Construction and building materials,* 10**,** 123-129.

AMLEH, L. & GHOSH, A. 2006. Modeling the effect of corrosion on bond strength at the steel–concrete interface with finite-element analysis. *Canadian Journal of Civil Engineering,* 33**,** 673-682.

ANDERSON, K. W., UHLMEYER, J. S. & RUSSELL, M. A. 2009. Use of recycled concrete aggregate in PCCP: literature search.

ANDRADE, C. & ALONSO, C. 2001. On-site measurements of corrosion rate of reinforcements. *Construction and building materials,* 15**,** 141-145.

ANN, K. Y., MOON, H., KIM, Y. & RYOU, J. 2008. Durability of recycled aggregate concrete using pozzolanic materials. *Waste Management,* 28**,** 993-999.

ANN, K. Y. & SONG, H.-W. 2007. Chloride threshold level for corrosion of steel in concrete. *Corrosion Science,* 49**,** 4113-4133.

AREL, H. Ş. & YAZıCı, Ş. 2012. Concrete–reinforcement bond in different concrete classes. *Construction and building materials,* 36**,** 78-83.

ASSOULI, B., BALLIVY, G. & RIVARD, P. 2008. Influence of environmental parameters on application of standard ASTM C876-91: half cell potential measurements. *Corrosion Engineering, Science and Technology,* 43**,** 93-96.

AUDENAERT, K., MARSAVINA, L. & DE SCHUTTER, G. Influence of cracks on the service life of concrete structures in a marine environment. Key Engineering Materials, 2009. Trans Tech Publ, 153-160.

AUYEUNG, Y., BALAGURU, P. & CHUNG, L. 2000a. Bond behavior of corroded reinforcement bars. *Materials Journal,* 97**,** 214-220.

AUYEUNG, Y., BALAGURU, P. & CHUNG, L. 2000b. Influence of Corrosion on Bond Behavior of Reinforcement Bars. *Special Publication,* 193**,** 1051-1074.

AZAD, A. K., AHMAD, S. & AZHER, S. A. 2007. Residual strength of corrosion-damaged reinforced concrete beams. *ACI Materials Journal,* 104**,** 40.

BADAWI, M. & SOUDKI, K. 2005. Control of corrosion-induced damage in reinforced concrete beams using carbon fiber-reinforced polymer laminates. *Journal of Composites for Construction,* 9**,** 195-201.

BAEK, S., XUE, W., FENG, M. Q. & KWON, S. 2012. Nondestructive corrosion detection in RC through integrated heat induction and IR thermography. *Journal of Nondestructive Evaluation,* 31**,** 181-190.

BAENA, M., TORRES, L., TURON, A. & BARRIS, C. 2009. Experimental study of bond behaviour between concrete and FRP bars using a pull-out test. *Composites Part B: Engineering,* 40**,** 784-797.

BALLIM, Y., REID, J. & KEMP, A. 2001. Deflection of RC beams under simultaneous load and steel corrosion. *Magazine of Concrete Research,* 53**,** 171-181.

BEHERA, M., BHATTACHARYYA, S., MINOCHA, A., DEOLIYA, R. & MAITI, S. 2014. Recycled aggregate from C&D waste & its use in concrete–A breakthrough towards sustainability in construction sector: A review. *Construction and building materials,* 68**,** 501-516.

BEIGI, M. H., BERENJIAN, J., OMRAN, O. L., NIK, A. S. & NIKBIN, I. M. 2013. An experimental survey on combined effects of fibers and nanosilica on the mechanical, rheological, and durability properties of self-compacting concrete. *Materials & Design,* 50**,** 1019-1029.

BERKELEY, K. & PATHMANABAN, S. 1990. *Cathodic protection of reinforcement steel in concrete*.

BHARGAVA, K., GHOSH, A., MORI, Y. & RAMANUJAM, S. 2007. Corrosion-induced bond strength degradation in reinforced concrete—Analytical and empirical models. *Nuclear Engineering and Design,* 237**,** 1140-1157.

BIANCHI, G. Q. 2014. *Application of nano-silica in concrete*, University Press.

BJÖRNSTRÖM, J., MARTINELLI, A., MATIC, A., BÖRJESSON, L. & PANAS, I. 2004. Accelerating effects of colloidal nano-silica for beneficial calcium–silicate–hydrate formation in cement. *Chemical Physics Letters,* 392**,** 242-248.

BOLHASSANI, M. & SAMANI, M. 2015. Effect of type, size, and dosage of nanosilica and microsilica on properties of cement paste and mortar. *ACI Materials Journal,* 112.

BS, B. 1997. Structural Use of Concrete, Part 1: Code of Practice for Design and Construction. *British Standards Institution, UK*.

BUTLER, L., WEST, J. & TIGHE, S. 2011. The effect of recycled concrete aggregate properties on the bond strength between RCA concrete and steel reinforcement. *Cement and Concrete Research,* 41**,** 1037-1049.

CABRERA, J. 1996. Deterioration of concrete due to reinforcement steel corrosion. *Cement and concrete composites,* 18**,** 47-59.

CAIRNS, J. & ABDULLAH, R. B. 1996. Bond strength of black and epoxy-coated reinforcement-a theoretical approach. *Materials Journal,* 93**,** 362-369.

CAIRNS, J., DU, Y. & LAW, D. 2008. Structural performance of corrosion-damaged concrete beams. *Magazine of Concrete Research,* 60**,** 359-370.

CHATTERJEE, S., SARKAR, S., HORE, S., DEY, N., ASHOUR, A. S. & BALAS, V. E. 2017. Particle swarm optimization trained neural network for structural failure prediction of multistoried RC buildings. *Neural Computing and Applications,* 28**,** 2005-2016.

CHEUNG, M. M. & CAO, C. 2013. Application of cathodic protection for controlling macrocell corrosion in chloride contaminated RC structures. *Construction and Building Materials,* 45**,** 199-207.

CHUNG, L., KIM, J.-H. J. & YI, S.-T. 2008. Bond strength prediction for reinforced concrete members with highly corroded reinforcing bars. *Cement and concrete composites,* 30**,** 603-611.

COCCIA, S., IMPERATORE, S. & RINALDI, Z. 2016. Influence of corrosion on the bond strength of steel rebars in concrete. *Materials and structures,* 49**,** 537-551.

COMMITTEE, A. 2003. Bond and Development of Straight Reinforcing Bars in Tension (ACI 408R-03). *American Concrete Institute, Detroit, Michigan, US***,** 49.

COMMITTEE, A. Building code requirements for structural concrete (ACI 318-05) and commentary (ACI 318R-05). 2005. American Concrete Institute.

COMMITTEE, J. C. 2007. Standard Specifications for Concrete Structures-2007 ‘‘Design’’. *Japanese Society of Civil Engineering (JSCE), JSCE Guidelines for Concrete*.

DAHOU, Z., SBARTAÏ, Z. M., CASTEL, A. & GHOMARI, F. 2009. Artificial neural network model for steel–concrete bond prediction. *Engineering Structures,* 31**,** 1724-1733.

DU BÉTON, F. I. FIB (2000). *Bond of Reinforcement in Concrete*.

DU, H., DU, S. & LIU, X. 2014. Durability performances of concrete with nano-silica. *Construction and Building Materials,* 73**,** 705-712.

EL-FEKY, M. S., SERAG, M. I., YASIEN, A. M. & ELKADY, H. 2016. Bond strength of nano silica concrete. subjected to corrosive environments. *ARPN Journal of Engineering and Applied Sciences,* 11**,** 13909-13924.

EL MAADDAWY, T., CHAHROUR, A. & SOUDKI, K. 2006. Effect of fiber-reinforced polymer wraps on corrosion activity and concrete cracking in chloride-contaminated concrete cylinders. *Journal of Composites for Construction,* 10**,** 139-147.

EL MAADDAWY, T., SOUDKI, K. & TOPPER, T. 2005. Long-term performance of corrosion-damaged reinforced concrete beams. *ACI Structural Journal,* 102**,** 649.

EL MAADDAWY, T. A. & SOUDKI, K. A. 2003. Effectiveness of impressed current technique to simulate corrosion of steel reinforcement in concrete. *Journal of materials in civil engineering,* 15**,** 41-47.

ELBUSAEFI, A. A. 2014. *The effect of steel bar corrosion on the bond strength of concrete manufactured with cement replacement materials.* PhD thesis, Cardiff University.

ELSENER, B., WOJTAS, H. & BÖHNI, H. Galvanostatic Pulse Measurements-Rapid on Site Corrosion Monitoring. CORROSION AND CORROSION PROTECTION OF STEEL IN CONCRETE. PROCEEDINGS OF INTERNATIONAL CONFERENCE HELD AT THE UNIVERSITY OF SHEFFIELD, 24-28 JULY 1994. VOLUME 1, 1994.

ERDEM, S., HANBAY, S. & GÜLER, Z. 2018. Micromechanical damage analysis and engineering performance of concrete with colloidal nano-silica and demolished concrete aggregates. *Construction and Building Materials,* 171**,** 634-642.

ESFAHANI, M. R., RAKHSHANIMEHR, M. & MOUSAVI, S. R. 2013. Bond strength of lap-spliced GFRP bars in concrete beams. *Journal of composites for construction,* 17**,** 314-323.

ESFAHANI, M. R. & RANGAN, B. V. 1998. Bond between normal strength and high-strength concrete (HSC) and reinforcing bars in splices in beams. *Structural Journal,* 95**,** 272-280.

ETXEBERRIA, M., VÁZQUEZ, E., MARÍ, A. & BARRA, M. 2007. Influence of amount of recycled coarse aggregates and production process on properties of recycled aggregate concrete. *Cement and concrete research,* 37**,** 735-742.

FANG, C., LUNDGREN, K., CHEN, L. & ZHU, C. 2004. Corrosion influence on bond in reinforced concrete. *Cement and concrete research,* 34**,** 2159-2167.

FERRARI, G., MIYAMOTO, M. & FERRARI, A. 2014. New sustainable technology for recycling returned concrete. *Construction and Building Materials,* 67**,** 353-359.

FRIEDL, L., VOLKWEIN, A. & SCHIEBL, P. 2003. The risk of corrosion of steel in recycled aggregate concrete. *Special Publication,* 212**,** 1055-1072.

GAITERO, J., CAMPILLO, I. & GUERRERO, A. 2008. Reduction of the calcium leaching rate of cement paste by addition of silica nanoparticles. *Cement and Concrete Research,* 38**,** 1112-1118.

GAO, J., WU, J., LI, J. & ZHAO, X. 2011. Monitoring of corrosion in reinforced concrete structure using Bragg grating sensing. *NDT & E International,* 44**,** 202-205.

GARCÍA-SEGURA, T., YEPES, V. & FRANGOPOL, D. M. 2017. Multi-objective design of post-tensioned concrete road bridges using artificial neural networks. *Structural and Multidisciplinary Optimization,* 56**,** 139-150.

GAYARRE, F. L., PEREZ, C. L.-C., LOPEZ, M. A. S. & CABO, A. D. 2014. The effect of curing conditions on the compressive strength of recycled aggregate concrete. *Construction and Building Materials,* 53**,** 260-266.

GENG, J., WU, J. & ZHAO, X. Simulation of fiber Bragg grating sensor for rebar corrosion. Second International Conference on Smart Materials and Nanotechnology in Engineering, 2009a. International Society for Optics and Photonics, 74931I.

GENG, O., YUAN, Y. & LI, F. 2009b. Study on the corrosion rate of steel bars in concrete under high humidity conditions. *International Journal of Modelling, Identification and Control,* 7**,** 155-159.

GHOSAL, M. & CHAKRABORTY, A. K. 2015. A Comparative Assessment of Nano-SiO2 & Nano-TiO2 Insertion in Concrete. *European Journal of Advances in Engineering and Technology,* 2**,** 44-48.

GIVI, A. N., RASHID, S. A., AZIZ, F. N. A. & SALLEH, M. A. M. 2010. Experimental investigation of the size effects of SiO2 nano-particles on the mechanical properties of binary blended concrete. *Composites Part B: Engineering,* 41**,** 673-677.

GIVI, A. N., RASHID, S. A., AZIZ, F. N. A. & SALLEH, M. A. M. 2013. Influence of 15 and 80 nano-SiO2 particles addition on mechanical and physical properties of ternary blended concrete incorporating rice husk ash. *Journal of Experimental Nanoscience,* 8**,** 1-18.

GONZALEZ, J., LOPEZ, W. & RODRIGUEZ, P. 1992. Corrosion mechanisms and kinetics controlling factors in reinforced concrete. *Revista de Metalurgia (Madrid),* 28**,** 297-305.

GRAHAM, L. D., FORBES, D. R. & SMITH, S. D. 2006. Modeling the ready mixed concrete delivery system with neural networks. *Automation in construction,* 15**,** 656-663.

HA, T.-H., MURALIDHARAN, S., BAE, J.-H., HA, Y.-C., LEE, H.-G., PARK, K.-W. & KIM, D.-K. 2007. Accelerated short-term techniques to evaluate the corrosion performance of steel in fly ash blended concrete. *Building and Environment,* 42**,** 78-85.

HANSSON, C. M. 1984. Comments on electrochemical measurements of the rate of corrosion of steel in concrete. *Cement and Concrete Research,* 14**,** 574-584.

HARUEHANSAPONG, S., PULNGERN, T. & CHUCHEEPSAKUL, S. 2014. Effect of the particle size of nanosilica on the compressive strength and the optimum replacement content of cement mortar containing nano-SiO 2. *Construction and Building Materials,* 50**,** 471-477.

HONG, S.-X., LAI, W. & HELMERICH, R. Monitoring accelerated corrosion in chloride contaminated concrete with ground penetrating radar. 2012 14th International Conference on Ground Penetrating Radar (GPR), 2012. IEEE, 561-566.

HOSSEINI, P., BOOSHEHRIAN, A. & MADARI, A. 2011. Developing concrete recycling strategies by utilization of nano-SiO 2 particles. *Waste and Biomass Valorization,* 2**,** 347-355.

ICHINOSE, T., KANAYAMA, Y., INOUE, Y. & BOLANDER JR, J. 2004. Size effect on bond strength of deformed bars. *Construction and building materials,* 18**,** 549-558.

JAFFER, S. J. & HANSSON, C. M. 2009. Chloride-induced corrosion products of steel in cracked-concrete subjected to different loading conditions. *Cement and Concrete Research,* 39**,** 116-125.

JEPSEN, M. T. 2002. Predicting concrete durability by using artificial neural network. *Published in a special NCR-publication*.

JI, T. 2005. Preliminary study on the water permeability and microstructure of concrete incorporating nano-SiO 2. *Cement and Concrete Research,* 35**,** 1943-1947.

KATZ, A. 2003. Properties of concrete made with recycled aggregate from partially hydrated old concrete. *Cement and concrete research,* 33**,** 703-711.

KATZ, A. 2004. Treatments for the improvement of recycled aggregate. *Journal of materials in civil engineering,* 16**,** 597-603.

KHALAF, F. M. Recycling of clay bricks as aggregate in asphalt concrete. Proceedings of International RILEM Conference on the Use of Recycled Materials in Buildings and Structures, Barcelona, Spain, 2004. 56-65.

KHALAF, F. M. & DEVENNY, A. S. 2004. Recycling of demolished masonry rubble as coarse aggregate in concrete. *Journal of materials in civil engineering,* 16**,** 331-340.

KHALOO, A., MOBINI, M. H. & HOSSEINI, P. 2016. Influence of different types of nano-SiO 2 particles on properties of high-performance concrete. *Construction and Building Materials,* 113**,** 188-201.

KIM, S.-W. & YUN, H.-D. 2013. Influence of recycled coarse aggregates on the bond behavior of deformed bars in concrete. *Engineering Structures,* 48**,** 133-143.

KONG, D., DU, X., WEI, S., ZHANG, H., YANG, Y. & SHAH, S. P. 2012. Influence of nano-silica agglomeration on microstructure and properties of the hardened cement-based materials. *Construction and Building Materials,* 37**,** 707-715.

KWON, S.-J., XUE, H., FENG, M. Q. & BAEK, S. Nondestructive corrosion detection in concrete through integrated heat induction and IR thermography. Nondestructive Characterization for Composite

Materials, Aerospace Engineering, Civil Infrastructure, and Homeland Security 2011, 2011. International Society for Optics and Photonics, 79831R.

LEE, H.-S., NOGUCHI, T. & TOMOSAWA, F. 2002. Evaluation of the bond properties between concrete and reinforcement as a function of the degree of reinforcement corrosion. *Cement and Concrete research,* 32**,** 1313-1318.

LEI, B. Bond behaviour between recycled aggregate concrete and corroded steel rebars. Applied Mechanics and Materials, 2012. Trans Tech Publ, 1391-1394.

LI, X., CAO, Z., ZHANG, Z. & DANG, H. 2006. Surface-modification in situ of nano-SiO 2 and its structure and tribological properties. *Applied Surface Science,* 252**,** 7856-7861.

LÓPEZ-GAYARRE, F., SERNA, P., DOMINGO-CABO, A., SERRANO-LÓPEZ, M. & LÓPEZ-COLINA, C. 2009. Influence of recycled aggregate quality and proportioning criteria on recycled concrete properties. *Waste management,* 29**,** 3022-3028.

LOPEZ, W. & GONZALEZ, J. 1993. Influence of the degree of pore saturation on the resistivity of concrete and the corrosion rate of steel reinforcement. *Cement and concrete research,* 23**,** 368-376.

LOUNIS, Z. & AMLEH, L. 2004. Reliability-based prediction of chloride ingress and reinforcement corrosion of aging concrete bridge decks. *Life-Cycle Performance of Deteriorating Structures: Assessment, Design and Management.*

MANGAT, P. & ELGARF, M. 1999. Strength and serviceability of repaired reinforced concrete beams undergoing reinforcement corrosion. *Magazine of concrete research,* 51**,** 97-112.

MANGUAL, J., ELBATANOUNY, M. K., ZIEHL, P. & MATTA, F. 2013. Acoustic-Emission-Based Characterization of Corrosion Damage in Cracked Concrete with Prestressing Strand. *ACI Materials Journal,* 110.

MANSFELD, F., SUN, Z., HSU, C. & NAGIUB, A. 2001. Concerning trend removal in electrochemical noise measurements. *Corrosion Science,* 43**,** 341-352.

MANZI, S., MAZZOTTI, C. & BIGNOZZI, M. 2013. Short and long-term behavior of structural concrete with recycled concrete aggregate. *Cement and Concrete Composites,* 37**,** 312-318.

MARINKOVIĆ, S., RADONJANIN, V., MALEŠEV, M. & IGNJATOVIĆ, I. 2010. Comparative environmental assessment of natural and recycled aggregate concrete. *Waste management,* 30**,** 2255-2264.

MEHTA, P. K. & MONTEIRO, P. 1993. Durability. *P. K. Mehta.--Concrete, microstructure, properties and materials.--Westerville: JP Skalny (Ed)***,** 113-155.

METELLI, G. & PLIZZARI, G. A. 2014. Influence of the relative rib area on bond behaviour. *Magazine of Concrete Research,* 66**,** 277-294.

MOMAYEZ, A., EHSANI, M., RAMEZANIANPOUR, A. & RAJAIE, H. 2005. Comparison of methods for evaluating bond strength between concrete substrate and repair materials. *Cement and concrete research,* 35**,** 748-757.

MONDAL, P., SHAH, S., MARKS, L. & GAITERO, J. 2010. Comparative study of the effects of microsilica and nanosilica in concrete. *Transportation research record: journal of the transportation research board***,** 6-9.

MONTEMOR, M., SIMOES, A. & FERREIRA, M. 2003. Chloride-induced corrosion on reinforcing steel: from the fundamentals to the monitoring techniques. *Cement and Concrete Composites,* 25**,** 491-502.

NAGATAKI, S., GOKCE, A., SAEKI, T. & HISADA, M. 2004. Assessment of recycling process induced damage sensitivity of recycled concrete aggregates. *Cement and concrete research,* 34**,** 965-971.

NAZARI, A. & RIAHI, S. 2011. The effects of SiO2 nanoparticles on physical and mechanical properties of high strength compacting concrete. *Composites Part B: Engineering,* 42**,** 570-578.

OTIENO, M., ALEXANDER, M. & BEUSHAUSEN, H.-D. 2010. Corrosion in cracked and uncracked concrete–influence of crack width, concrete quality and crack reopening. *Magazine of Concrete Research,* 62**,** 393-404.

OTSUKI, N., MIYAZATO, S.-I. & YODSUDJAI, W. 2003. Influence of recycled aggregate on interfacial transition zone, strength, chloride penetration and carbonation of concrete. *Journal of materials in civil engineering,* 15**,** 443-451.

OUGLOVA, A., BERTHAUD, Y., FOCT, F., FRANÇOIS, M., RAGUENEAU, F. & PETRE-LAZAR, I. 2008. The influence of corrosion on bond properties between concrete and reinforcement in concrete structures. *Materials and Structures,* 41**,** 969-980.

PADMINI, A., RAMAMURTHY, K. & MATHEWS, M. 2009. Influence of parent concrete on the properties of recycled aggregate concrete. *Construction and Building Materials,* 23**,** 829-836.

PAGE, C. & TREADAWAY, K. 1982. Aspects of the electrochemistry of steel in concrete. *Nature,* 297**,** 109.

PALLA, R., KARADE, S., MISHRA, G., SHARMA, U. & SINGH, L. 2017. High strength sustainable concrete using silica nanoparticles. *Construction and Building Materials,* 138**,** 285-295.

PANDURANGAN, K., DAYANITHY, A. & PRAKASH, S. O. 2016. Influence of treatment methods on the bond strength of recycled aggregate concrete. *Construction and Building Materials,* 120**,** 212-221.

POLDER, R., ANDRADE, C., ELSENER, B., VENNESLAND, O., GULIKERS, J., WEIDERT, R. & RAUPACH, M. 2000. RILEM TC 154-EMC: electrochemical techniques for measuring metallic corrosion. *Materials and structures,* 33**,** 603-611.

POON, C. S. & LAM, C. S. 2008. The effect of aggregate-to-cement ratio and types of aggregates on the properties of pre-cast concrete blocks. *Cement and Concrete Composites,* 30**,** 283-289.

POUR, S. M. & ALAM, M. S. Investigation of compressive bond behavior of steel rebar embedded in concrete with partial recycled aggregate replacement. Structures, 2016. Elsevier, 153-164.

POURSAEE, A. & HANSSON, C. 2009. Potential pitfalls in assessing chloride-induced corrosion of steel in concrete. *Cement and Concrete Research,* 39**,** 391-400.

PRINCE, M. J. R. & SINGH, B. 2013. Bond behaviour of deformed steel bars embedded in recycled aggregate concrete. *Construction and Building Materials,* 49**,** 852-862.

PRINCE, M. J. R. & SINGH, B. 2014. Bond behaviour between recycled aggregate concrete and deformed steel bars. *Materials and structures,* 47**,** 503-516.

QING, Y., ZENAN, Z., DEYU, K. & RONGSHEN, C. 2007a. Influence of nano-SiO2 addition on properties of hardened cement paste as compared with silica fume. *Construction and building materials,* 21**,** 539-545.

QING, Y., ZENAN, Z., DEYU, K. & RONGSHEN, C. 2007b. Influence of nano-SiO 2 addition on properties of hardened cement paste as compared with silica fume. *Construction and building materials,* 21**,** 539-545.

RAO, A., JHA, K. N. & MISRA, S. 2007. Use of aggregates from recycled construction and demolition waste in concrete. *Resources, conservation and Recycling,* 50**,** 71-81.

RASHID, M. H., KHATUN, S., UDDIN, S. & NAYEEM, M. 2010. Effect of strength and covering on concrete corrosion. *European Journal of Scientific Research,* 40**,** 492-499.

REHM, G. 1961. The fundamentals of bond between steel reinforcement and concrete. *Deutsche association for steel reinforcement-concrete,* 138**,** 59.

REVIE, R. W. 2011. *Uhlig's corrosion handbook*, John Wiley & Sons.

RYU, J. 2002. An experimental study on the effect of recycled aggregate on concrete properties. *Magazine of Concrete Research,* 54**,** 7-12.

SADOWSKI, Ł. 2010. New non-destructive method for linear polarisation resistance corrosion rate measurement. *Archives of Civil & Mechanical Engineering (Oficyna Wydawnicza Politechniki Wroclawskiej),* 10.

SAID, A. M., ZEIDAN, M. S., BASSUONI, M. & TIAN, Y. 2012. Properties of concrete incorporating nano-silica. *Construction and Building Materials,* 36**,** 838-844.

ŠAMÁRKOVÁ, K., CHOBOLA, Z., ŠTEFKOVÁ, D. & KUSÁK, I. Impact-echo methods to assessment corrosion of reinforced concrete structures. Applied Mechanics and Materials, 2014. Trans Tech Publ, 268-271.

SCHIESSL, P. & RAUPACH, M. Influence of temperature on the corrosion rate of steel in concrete containing chlorides. Proceedings of the First International Conference on Reinforced Concrete Materials in Hot Climates, 1994. 537-549.

SEARA-PAZ, S., GONZÁLEZ-FONTEBOA, B., EIRAS-LÓPEZ, J. & HERRADOR, M. F. 2014. Bond behavior between steel reinforcement and recycled concrete. *Materials and structures,* 47**,** 323-334.

SERAG, M. I., YASIEN, A. M., EL-FEKY, M. S. & ELKADY, H. 2017. EFFECT OF NANO SILICA ON CONCRETE BOND STRENGTH MODES OF FAILURE. *International Journal,* 12**,** 2892-2899.

SHAH, M. M. A., BALAJI, E. & PANDIAN, G. A. M. 2016. Experimental study on mechanical properties of high strength concrete using Nano-Silica.

SHAIKH, F., SUPIT, S. & SARKER, P. 2014. A study on the effect of nano silica on compressive strength of high volume fly ash mortars and concretes. *Materials & Design,* 60**,** 433-442.

SINGH, L., KARADE, S., BHATTACHARYYA, S., YOUSUF, M. & AHALAWAT, S. 2013. Beneficial role of nanosilica in cement based materials–A review. *Construction and Building Materials,* 47**,** 1069-1077.

SOBOLEV, K. & GUTIÉRREZ, M. F. 2005. How nanotechnology can change the concrete world. *American Ceramic Society Bulletin,* 84**,** 14.

SONG, H.-W., PACK, S.-W., NAM, S.-H., JANG, J.-C. & SARASWATHY, V. 2010. Estimation of the permeability of silica fume cement concrete. *Construction and Building Materials,* 24**,** 315-321.

SOROUSHIAN, P. 2012. Strength and durability of recycled aggregate concrete containing milled glass as partial replacement for cement. *Construction and Building Materials,* 29**,** 368-377.

SPAETH, V. & TEGGUER, A. D. 2013. Improvement of recycled concrete aggregate properties by polymer treatments. *International Journal of Sustainable Built Environment,* 2**,** 143-152.

TAM, V. W., TAM, C. M. & LE, K. N. 2007. Removal of cement mortar remains from recycled aggregate using pre-soaking approaches. *Resources, Conservation and Recycling,* 50**,** 82-101.

TATEYASHIKI, H., SHIMA, H., MATSUMOTO, Y. & KOGA, Y. 2001. Properties of concrete with high quality recycled aggregate by heat and rubbing method. *Proc. JCI,* 23**,** 61-66.

TAVAKOLI, M. & SOROUSHIAN, P. 1996. Strengths of recycled aggregate concrete made using field-demolished concrete as aggregate. *Materials Journal,* 93**,** 178-181.

THOMAS, C., SETIÉN, J., POLANCO, J., ALAEJOS, P. & DE JUAN, M. S. 2013. Durability of recycled aggregate concrete. *Construction and Building Materials,* 40**,** 1054-1065.

TORABIAN ISFAHANI, F., REDAELLI, E., LOLLINI, F., LI, W. & BERTOLINI, L. 2016. Effects of nanosilica on compressive strength and durability properties of concrete with different water to binder ratios. *Advances in Materials Science and Engineering,* 2016.

VIDAL, T., CASTEL, A. & FRANCOIS, R. 2004. Analyzing crack width to predict corrosion in reinforced concrete. *Cement and concrete research,* 34**,** 165-174.

WANG, H.-L., WANG, J.-J., SUN, X.-Y. & JIN, W.-L. 2013. Improving performance of recycled aggregate concrete with superfine pozzolanic powders. *Journal of Central South University,* 20**,** 3715-3722.

WANG, X. & LIU, X. 2003. A strain-softening model for steel–concrete bond. *Cement and Concrete Research,* 33**,** 1669-1673.

WEBSTER, B., WERNER, S., WELLS, D. & BREMER, P. 2000. Microbiologically influenced corrosion of copper in potable water systems—pH effects. *Corrosion,* 56**,** 942-950.

WINSTON, R. 2000. Uhlig's corrosion handbook.

XIAO, J. & FALKNER, H. 2007. Bond behaviour between recycled aggregate concrete and steel rebars. *Construction and Building Materials,* 21**,** 395-401.

XIAO, J., LI, W. & POON, C. 2012. Recent studies on mechanical properties of recycled aggregate concrete in China—A review. *Science China Technological Sciences,* 55**,** 1463-1480. YALCINER, H., EREN, O. & SENSOY, S. 2012. An experimental study on the bond strength between reinforcement bars and concrete as a function of concrete cover, strength and corrosion level. *Cement and Concrete Research,* 42**,** 643-655.

YANG, H., DENG, Z., QIN, Y. & LV, L. 2015. A study on the bond behavior of corroded reinforced concrete containing recycled aggregates. *Advances in Materials Science and Engineering,* 2015.

YOON, S., WANG, K., WEISS, W. J. & SHAH, S. P. 2000. Interaction between loading, corrosion, and serviceability of reinforced concrete. *Materials Journal,* 97**,** 637-644.

YUAN, C., LUO, Z., DING, T., WANG, H., HAO, Y. & ZHANG, H. 2010. Orthogonal experiment of carbonation resistance for recycled aggregate concrete. *Journal of Wuhan University of Technology,* 21**,** 9-12.

ZAKI, A., CHAI, H. K., AGGELIS, D. G. & ALVER, N. 2015. Non-destructive evaluation for corrosion monitoring in concrete: A review and capability of acoustic emission technique. *Sensors,* 15**,** 19069-19101.

ZEIDAN, M. S. 2013. Performance of concrete incorporating colloidal nano-silica.

ZHANG, M.-H. & ISLAM, J. 2012. Use of nano-silica to reduce setting time and increase early strength of concretes with high volumes of fly ash or slag. *Construction and Building Materials,* 29**,** 573-580.

ZHANG, M.-H. & LI, H. 2011. Pore structure and chloride permeability of concrete containing nano-particles for pavement. *Construction and Building Materials,* 25**,** 608-616.

ZHAO, Y., LIN, H., WU, K. & JIN, W. 2013. Bond behaviour of normal/recycled concrete and corroded steel bars. *Construction and building materials,* 48**,** 348-359.

ZUO, J. & DARWIN, D. Bond slip of high relative rib area bars under cyclic loading. 2000. American Concrete Institute.

Appendix A

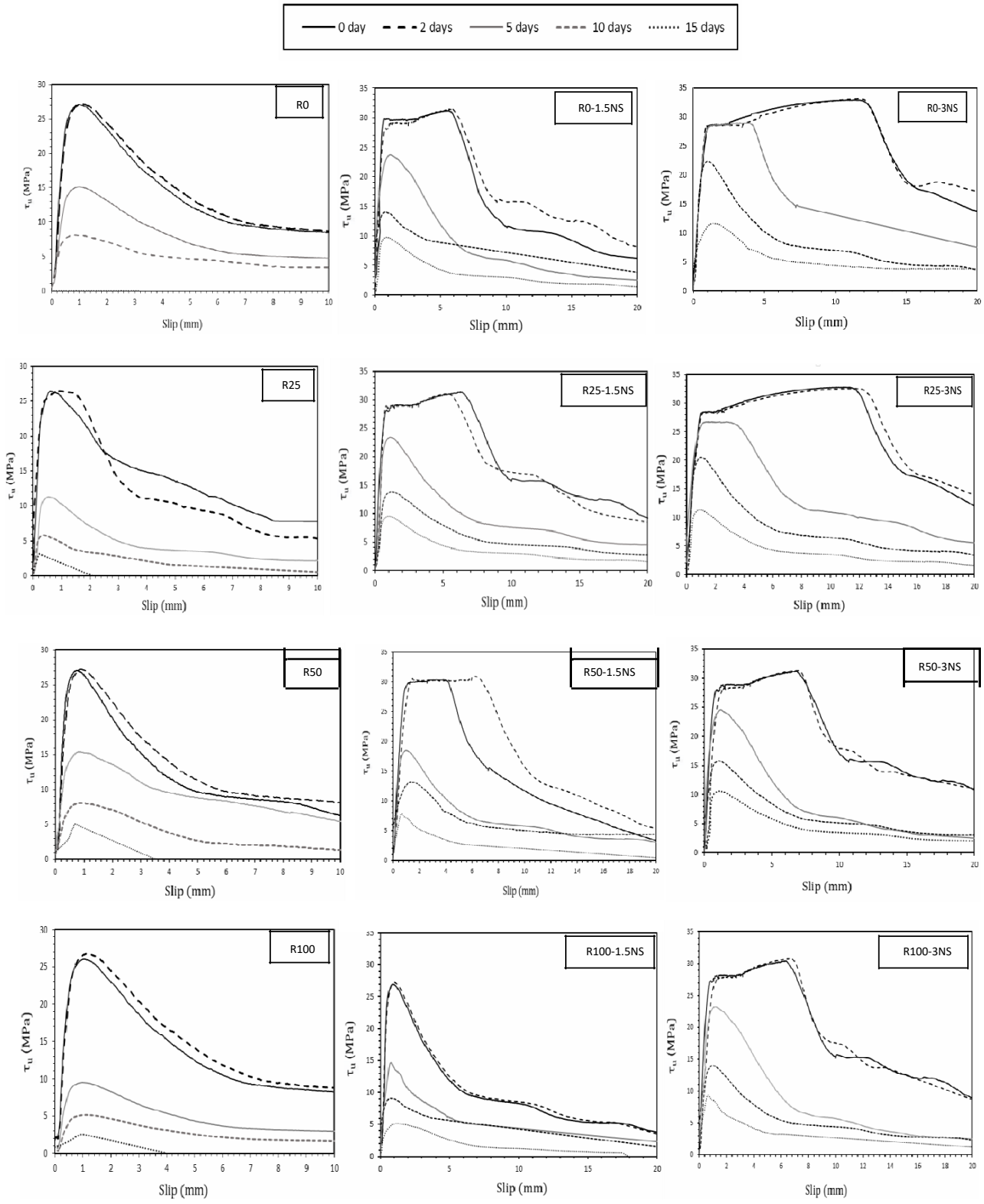

Figure A. 1 Bond stress versus slip for specimens having Ø 12mm, ld= 60 mm.

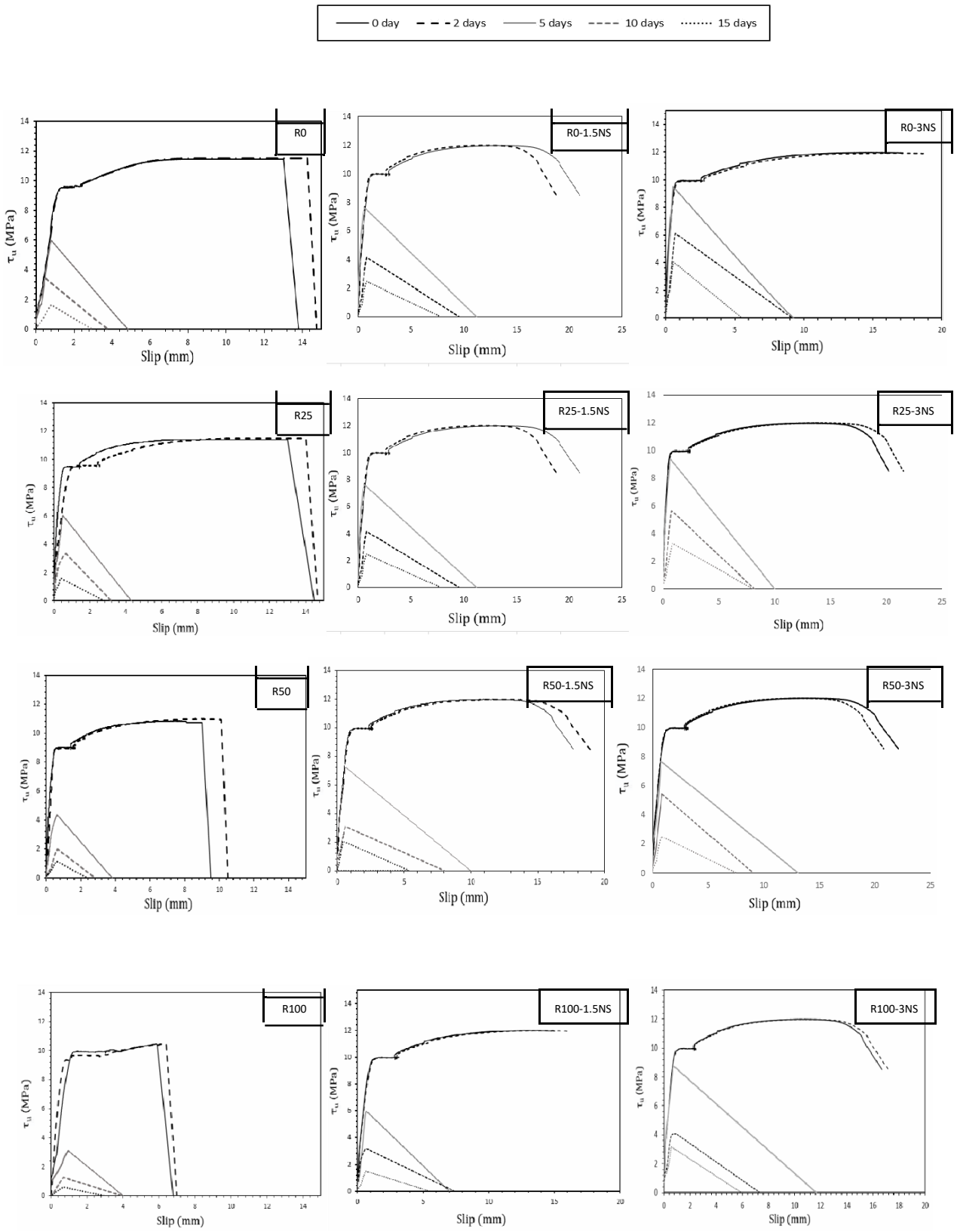

Figure A. 2 Bond stress versus slip for specimens having Ø 12mm, ld= 167 mm.

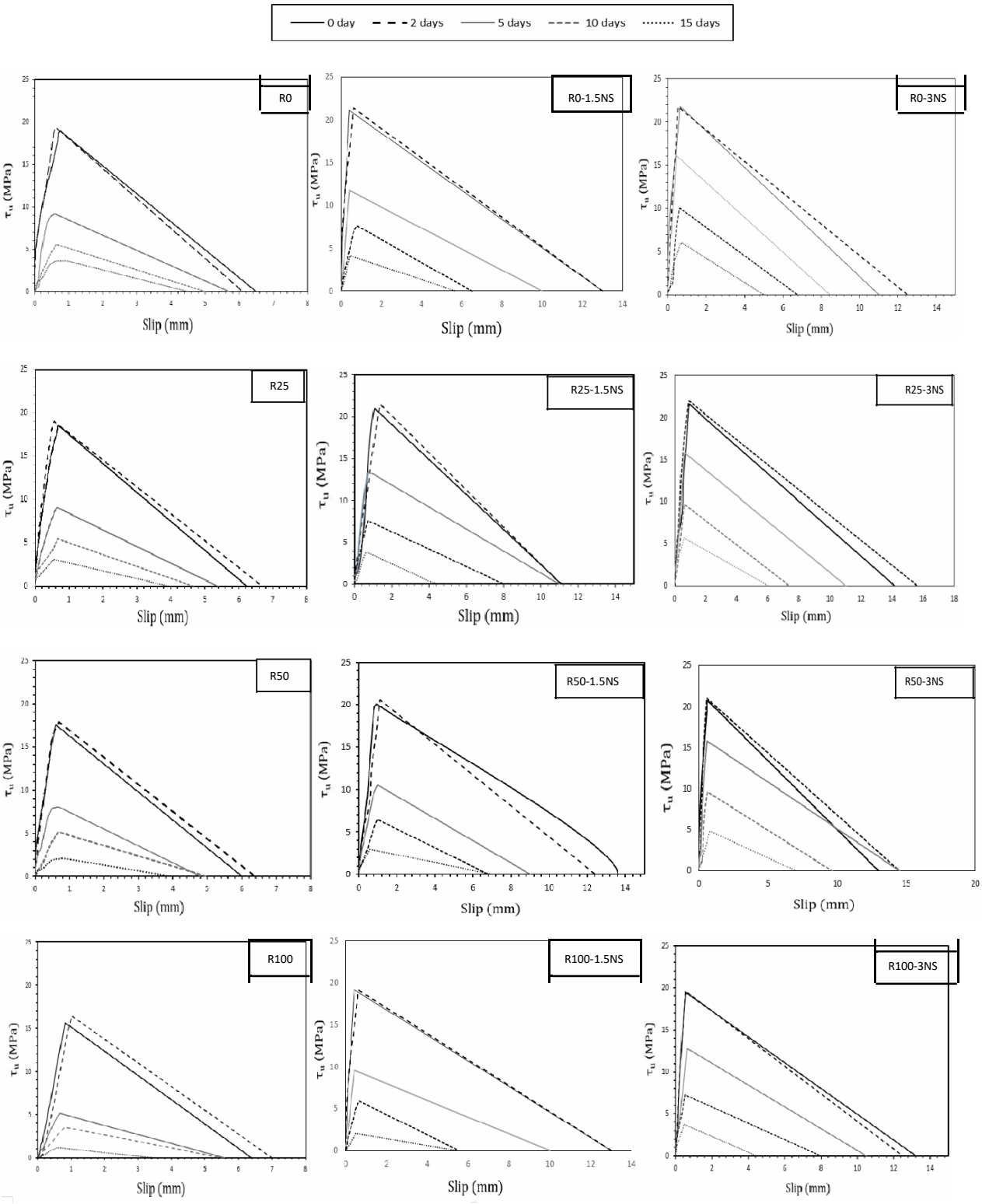

Figure A. 3. Bond stress versus slip for specimens having Ø 20mm, ld= 100 mm.

Appendix B

Table B.1 - Experimental database of 147 pull-out specimens used for ANN-4.

Reference	l (mm)	C (mm)	f_{cu} (MPa)	d_b (mm)	RCA (%)	NS (%)	f_y (MPa)
Author	60	94	54.66	12	0	0	27.12
	60	94	54.11	12	25	0	27.05
	60	94	50.33	12	50	0	26.53
	60	94	47.1	12	100	0	25.87
	60	94	66	12	0	1.5	30.11
	60	94	65.2	12	25	1.5	30.01
	60	94	62.15	12	50	1.5	29.36
	60	94	57.3	12	100	1.5	29.12
	60	94	70.8	12	0	3	31.92
	60	94	70.2	12	25	3	31.47
	60	94	67	12	50	3	31.09
	60	94	64.8	12	100	3	30.44
	167	94	54.66	12	0	0	11.44
	167	94	54.11	12	25	0	11.39
	167	94	50.33	12	50	0	10.83
	167	94	47.1	12	100	0	10.26
	167	94	62.15	12	50	1.5	12.05
	167	94	57.3	12	100	1.5	11.75
	100	90	54.66	20	0	0	18.58
	100	90	54.11	20	25	0	18.55
	100	90	50.33	20	50	0	17.11
	100	90	47.1	20	100	0	15.63
	100	90	66	20	0	1.5	20.87
	100	90	65.2	20	25	1.5	20.56
	100	90	62.15	20	50	1.5	20.01
	100	90	57.3	20	100	1.5	19.14
	100	90	70.8	20	0	3	21.72
	100	90	70.2	20	25	3	21.53
	100	90	67	20	50	3	20.77
	100	90	64.8	20	100	3	20.45
Almusallam et al.,1996	102	64	30	12	0	0	15.86
	40	70	30	10	0	0	15.1
	40	70	30	10	0	0	15.7
	40	70	30	10	0	0	15.1
	56	68	30	14	0	0	16.3
Alsulamani et al., 1990	56	68	30	14	0	0	15.2
	56	68	30	14	0	0	16.5
	80	65	30	20	0	0	15
	80	65	30	20	0	0	16.1
	80	65	30	20	0	0	15.6
Yalciner et al., 2013	50	8	23	14	0	0	9.1
	50	8	23	14	0	0	9.4
	50	8	23	14	0	0	9.2
	50	23	23	14	0	0	14
	50	23	23	14	0	0	12.3
	50	23	23	14	0	0	13.5
	50	38	23	14	0	0	12.1
	50	38	23	14	0	0	17.3
	50	38	23	14	0	0	15
	50	8	51	14	0	0	19.6
	50	8	51	14	0	0	20
	50	23	51	14	0	0	20.9
	50	23	51	14	0	0	21.7
	50	23	51	14	0	0	21
	50	23	51	14	0	0	20.4
	50	38	51	14	0	0	21.8
	50	38	51	14	0	0	18.5
	50	38	51	14	0	0	19.4
	50	38	51	14	0	0	20.3

Fang et al., 2006	50	44	51.2	12	0	0	32.38
	50	44	47.8	12	50	0	28.77
	50	44	49.95	12	100	0	31.84
	100	65	61.8	20	0	0	16.5
	100	65	64.9	20	50	0	16.4
Cabrera and Ghoddoussi,1992	100	65	52.6	20	100	0	14.3
	100	65	39.7	20	0	0	13.01
	100	65	40.6	20	50	0	12.3
	100	65	32	20	100	0	11.61
Serag et al., (2017)	70	69	29	12	0	0	11.21
	75	69	42	12	0	0	21.75
	75	69	50	12	0	1.5	24.4
	75	69	61	12	0	3	30.1
	75	69	55	12	0	4.5	22.3
	75	67	42	16	0	0	15.1
	75	67	50	16	0	1.5	15.56
	75	67	61	16	0	3	16.45
	75	67	55	16	0	4.5	15.2
Kim et al., (2014)	64	67	45.1	16	0	0	16.79
	64	67	41.27	16	30	0	22.63
	64	67	39.5	16	60	0	24.36
	64	67	35.7	16	100	0	24.71
	64	67	40.7	16	0	0	21.46
	64	67	38.41	16	30	0	17.18
	64	67	37.4	16	60	0	19.77
	64	67	35.97	16	100	0	17.43
Fernandez et al., (2016)	50	45	64.13	10	0	0	25.32
	50	45	57.19	10	20	0	22.97
	50	45	52.74	10	50	0	21.22
	50	45	44.2	10	100	0	18.93
	50	45	53.85	10	0	0	21.62
	50	45	52.83	10	20	0	20.67
	50	45	49.85	10	50	0	19.11
	50	45	42.04	10	100	0	16.9
Siempu & Pancharti, (2017)	25	45	26.1	10	0	0	27.49
	50	45	26.1	10	0	0	19.99
	100	45	26.1	10	0	0	14.68
	30	44	26.1	12	0	0	26.47
	60	44	26.1	12	0	0	19.09
	100	44	26.1	12	0	0	14.58
	40	67	26.1	16	0	0	25.37
	80	67	26.1	16	0	0	17.93
	150	67	26.1	16	0	0	12.5
	25	45	20.7	10	100	0	25.31
	50	45	20.7	10	100	0	18.43
	100	45	20.7	10	100	0	13.59
	30	44	20.7	12	100	0	24.3
	60	44	20.7	12	100	0	17.57
	100	44	20.7	12	100	0	13.41
	40	67	20.7	16	100	0	23.43
	80	67	20.7	16	100	0	16.6
	150	67	20.7	16	100	0	11.52
	25	45	48.5	10	0	0	31.24
	50	45	48.5	10	0	0	22.49
	100	45	48.5	10	0	0	15.93
	30	44	48.5	12	0	0	29.51
	60	44	48.5	12	0	0	21.07
	100	44	48.5	12	0	0	15.89
	40	67	48.5	16	0	0	28.31
	80	67	48.5	16	0	0	20.1
	150	67	48.5	16	0	0	13.8
	25	45	37.53	10	100	0	28.12
	50	45	37.53	10	100	0	20.31
	100	45	37.53	10	100	0	14.37
	30	44	37.53	12	100	0	26.47
	60	44	37.53	12	100	0	18.88
	100	44	37.53	12	100	0	14.32

Siempu & Pancharti, (2017)	40	67	37.53	16	100	0	25.38
	80	67	37.53	16	100	0	18.06
	150	67	37.53	16	100	0	12.37
	25	45	68.67	10	0	0	34.99
	50	45	68.67	10	0	0	25.26
	100	45	68.67	10	0	0	17.75
	30	44	68.67	12	0	0	33.42
	60	44	68.67	12	0	0	23.43
	100	44	68.67	12	0	0	17.7
	40	67	68.67	16	0	0	32.1
	80	67	68.67	16	0	0	22.46
	150	67	68.67	16	0	0	15.36
	25	45	52.19	10	100	0	30.62
	50	45	52.19	10	100	0	22.18
	100	45	52.19	10	100	0	15.46
	30	44	52.19	12	100	0	29.07
	60	44	52.19	12	100	0	20.39
	100	44	52.19	12	100	0	15.49
	40	67	52.19	16	100	0	28.07
	80	67	52.19	16	100	0	19.65
	150	67	52.19	16	100	0	13.47

Table B.2 - Experimental database of 381 pull-out specimens used for ANN-5.

Reference	η (%)	l (mm)	C (mm)	cu (MPa)	(mm)	RCA (%)	NS (%)	, (MPa)
Almusallam et al.,(1996)	0	102	64	30	12	0	0	15.86
	2.22	102	64	30	12	0	0	16.38
	2.67	102	64	30	12	0	0	17.9
	3.44	102	64	30	12	0	0	18.4
	3.89	102	64	30	12	0	0	17.1
	4`.56	102	64	30	12	0	0	16.4
	5	102	64	30	12	0	0	13.6
	5.56	102	64	30	12	0	0	10.7
	6.67	102	64	30	12	0	0	5
	7.5	102	64	30	12	0	0	4.49
	11.7	102	64	30	12	0	0	3.37
	15.6	102	64	30	12	0	0	3.17
	20	102	64	30	12	0	0	2.97
	31.9	102	64	30	12	0	0	2.6
	49.4	102	64	30	12	0	0	2.2
	0	40	70	30	10	0	0	15.1
	0	40	70	30	10	0	0	15.7
	0	40	70	30	10	0	0	15.1
	0.3	40	70	30	10	0	0	20.4
	0.5	40	70	30	10	0	0	21.9
	0.87	40	70	30	10	0	0	23.9
	1.5	40	70	30	10	0	0	22.3
	1.83	40	70	30	10	0	0	21.2
	2.66	40	70	30	10	0	0	19.1
	3.25	40	70	30	10	0	0	17.7
	4.24	40	70	30	10	0	0	14.5
	4.52	40	70	30	10	0	0	14.4
	4.81	40	70	30	10	0	0	10.9
	6.67	40	70	30	10	0	0	9.7
	6.7	40	70	30	10	0	0	7.1
	0	56	68	30	14	0	0	16.3
	0	56	68	30	14	0	0	15.2
	0	56	68	30	14	0	0	16.5
	0.3	56	68	30	14	0	0	19.1
	0.76	56	68	30	14	0	0	21
	0.9	56	68	30	14	0	0	21.1
	1.22	56	68	30	14	0	0	19
	1.36	56	68	30	14	0	0	20.4
	1.62	56	68	30	14	0	0	18.4
	2.75	56	68	30	14	0	0	15.5
	2.89	56	68	30	14	0	0	16
	3	56	68	30	14	0	0	14.6

Alsulamani et al., (1990)	3.33	56	68	30	14	0	0	13.2
	3.33	56	68	30	14	0	0	10.7
	4.29	56	68	30	14	0	0	7.9
	5.45	56	68	30	14	0	0	4.1
	0	80	65	30	20	0	0	15
	0	80	65	30	20	0	0	16.1
	0	80	65	30	20	0	0	15.4
	0.3	80	65	30	20	0	0	19.1
	0.5	80	65	30	20	0	0	19.4
	0.65	80	65	30	20	0	0	19.7
	0.78	80	65	30	20	0	0	18.3
	1.16	80	65	30	20	0	0	17.6
	1.67	80	65	30	20	0	0	13.7
	1.86	80	65	30	20	0	0	15.7
	2	80	65	30	20	0	0	14.4
	2.69	80	65	30	20	0	0	11.8
	2.87	80	65	30	20	0	0	11.4
	3.08	80	65	30	20	0	0	11.6
	3.13	80	65	30	20	0	0	11.7
	3.6	80	65	30	20	0	0	9.6
	4.25	80	65	30	20	0	0	8
	4.35	80	65	30	20	0	0	8
Yalciner et al., (2013)	0	50	8	23	14	0	0	9.1
	0	50	8	23	14	0	0	9.4
	0	50	8	23	14	0	0	9.2
	2.47	50	8	23	14	0	0	11.2
	2.72	50	8	23	14	0	0	11.7
	4.09	50	8	23	14	0	0	13
	4.1	50	8	23	14	0	0	13
	4.32	50	8	23	14	0	0	12.2
	4.33	50	8	23	14	0	0	12.2
	6.51	50	8	23	14	0	0	3.2
	8.91	50	8	23	14	0	0	3.7
	8.9	50	8	23	14	0	0	3
	14.5	50	8	23	14	0	0	2.1
	14.7	50	8	23	14	0	0	2
	18.8	50	8	23	14	0	0	4.3
	0	50	23	23	14	0	0	14
	0	50	23	23	14	0	0	12.3
	0	50	23	23	14	0	0	13.5
	1.37	50	23	23	14	0	0	18
	1.4	50	23	23	14	0	0	17.9
	1.6	50	23	23	14	0	0	17
	1.69	50	23	23	14	0	0	16.9
	3.45	50	23	23	14	0	0	9.6
	3.57	50	23	23	14	0	0	8.9
	5.36	50	23	23	14	0	0	3.7
	5.36	50	23	23	14	0	0	3.3
	6.4	50	23	23	14	0	0	5.5
Yalciner et al., (2013)	6.87	50	23	23	14	0	0	6.5
	16.7	50	23	23	14	0	0	2.13
	17.3	50	23	23	14	0	0	1.8
	0	50	38	23	14	0	0	12.1
	0	50	38	23	14	0	0	17.3
	0	50	38	23	14	0	0	15
	0.66	50	38	23	14	0	0	18.9
	0.68	50	38	23	14	0	0	17.9
	0.68	50	38	23	14	0	0	18
	0.69	50	38	23	14	0	0	19.1
	0.84	50	38	23	14	0	0	18.3
	0.88	50	38	23	14	0	0	18.2
	1.6	50	38	23	14	0	0	13.7
	1.69	50	38	23	14	0	0	13.4
	2.66	50	38	23	14	0	0	12.4
	3.81	50	38	23	14	0	0	1.3
	3.81	50	38	23	14	0	0	1.3
	6.27	50	38	23	14	0	0	3.2
	0	50	8	51	14	0	0	19.6
	0	50	8	51	14	0	0	20
	0.77	50	8	51	14	0	0	22.3
	0.8	50	8	51	14	0	0	22.4

	0.9	50	8	51	14	0	0	21.7
	0.94	50	8	51	14	0	0	21.5
	1.33	50	8	51	14	0	0	18.5
	3.3	50	8	51	14	0	0	7.5
	3.41	50	8	51	14	0	0	6.8
	4.47	50	8	51	14	0	0	6.3
	7.48	50	8	51	14	0	0	3.5
	7.56	50	8	51	14	0	0	3.5
	8.95	50	8	51	14	0	0	3
	0	50	23	51	14	0	0	20.9
	0	50	23	51	14	0	0	21.7
	0	50	23	51	14	0	0	21
	0	50	23	51	14	0	0	20.4
	0.65	50	23	51	14	0	0	23.8
	0.77	50	23	51	14	0	0	23.5
	0.77	50	23	51	14	0	0	23.4
	1.7	50	23	51	14	0	0	14
	1.72	50	23	51	14	0	0	13.8
	4.45	50	23	51	14	0	0	4.2
	5.14	50	23	51	14	0	0	6.2
	9.9	50	23	51	14	0	0	5.9
Fang et al., (2006)	0	50	38	51	14	0	0	27.3
	0	50	38	51	14	0	0	27.7
	0	50	38	51	14	0	0	28.3
	2.69	50	38	51	14	0	0	7.43
	3.08	50	38	51	14	0	0	6.1
	0	50	38	51	14	0	0	21.8
	4	50	38	51	14	0	0	11.9
	6.1	50	38	51	14	0	0	6
	0	50	38	51	14	0	0	18.5
	0	50	38	51	14	0	0	19.4
	0	50	38	51	14	0	0	20.3
	0.31	50	38	51	14	0	0	20.3
	0.56	50	38	51	14	0	0	20.3
	0.71	50	38	51	14	0	0	23.2
	1.09	50	38	51	14	0	0	22.6
	2.28	50	38	51	14	0	0	20.4
	2.48	50	38	51	14	0	0	19.6
	4.46	50	38	51	14	0	0	17.2
	4.87	50	38	51	14	0	0	16.2
	6.41	50	38	51	14	0	0	14.3
	6.8	50	38	51	14	0	0	14.3
	7.95	50	38	51	14	0	0	12.4
	8.16	50	38	51	14	0	0	12.4
	9.35	50	38	51	14	0	0	10.6
	10	50	38	51	14	0	0	12.4
	11.6	50	38	51	14	0	0	8.68
	12.1	50	38	51	14	0	0	4.87
Fernandez et al., (2016)	0	50	44	51.2	12	0	0	32.38
	1.65	50	44	51.2	12	0	0	5.36
	2.6	50	44	51.2	12	0	0	4.73
	5.75	50	44	51.2	12	0	0	4
	0	50	44	48.28	12	0.2	0	34.94
	1.65	50	44	48.28	12	0.2	0	6.93
	2.6	50	44	48.28	12	0.2	0	5.65
	5.75	50	44	48.28	12	0.2	0	4.81
	0	50	44	47.8	12	0.5	0	28.77
	1.65	50	44	47.9	12	0.5	0	6.57
	2.6	50	44	47.1	12	0.5	0	5.72
	5.75	50	44	47.11	12	0.5	0	4.29
	0	50	44	49.95	12	1	0	31.84
	1.65	50	44	49.95	12	1	0	8.03
	2.6	50	44	49.95	12	1	0	6.12
	5.75	50	44	49.95	12	1	0	4.2
Cabrera and Ghoddoussi,1992	0	100	65	61.8	20	0	0	16.5
	1.96	100	65	61.8	20	0	0	12.96
	2.9	100	65	61.8	20	0	0	5.31
	0	100	65	64.9	20	0.5	0	16.4
	0.75	100	65	64.9	20	0.5	0	13.64
	1.71	100	65	64.9	20	0.5	0	11.04
	2.54	100	65	64.9	20	0.5	0	6.57

	0	100	65	52.6	20	1	0	14.3
	0.67	100	65	52.6	20	1	0	12.33
	1.37	100	65	52.6	20	1	0	9.87
	2.7	100	65	52.6	20	1	0	7.63
	0	100	65	39.7	20	0	0	13.01
	0.44	100	65	39.7	20	0	0	7.98
	1.42	100	65	39.7	20	0	0	6.19
	2.63	100	65	39.7	20	0	0	4.8
	0	100	65	40.6	20	0.5	0	12.3
	1.7	100	65	40.6	20	0.5	0	5.31
	2.54	100	65	40.6	20	0.5	0	4.79
	0	100	65	32	20	1	0	11.61
	0.73	100	65	32	20	1	0	5.75
	2.1	100	65	32	20	1	0	5.02
	2.9	100	65	32	20	1	0	4.49
Coccia et al., (2016)	0	70	69	29	12	0	0	11.21
	0.1	70	69	29	12	0	0	14.13
	0.46	70	69	29	12	0	0	17.56
	0.8	70	69	29	12	0	0	16.74
	0.88	70	69	29	12	0	0	15.42
	0.94	70	69	29	12	0	0	11.74
	1	70	69	29	12	0	0	11.14
	1.24	70	69	29	12	0	0	9.51
	1.34	70	69	29	12	0	0	8.68
	1.52	70	69	29	12	0	0	8.02
	2.8	70	69	29	12	0	0	4.7
	3.2	70	69	29	12	0	0	6.95
	3.92	70	69	29	12	0	0	5.17
Author	0	60	94	54.66	12	0	0	27.12
	1.39	60	94	54.66	12	0	0	27.35
	3.95	60	94	54.66	12	0	0	15.15
	6.375	60	94	54.66	12	0	0	8.14
	11.9	60	94	54.66	12	0	0	5.15
	0	60	94	54.11	12	0.25	0	27.05
	1.4	60	94	54.11	12	0.25	0	27.22
	4.03	60	94	54.11	12	0.25	0	15.14
	6.58	60	94	54.11	12	0.25	0	8.06
	12.325	60	94	54.11	12	0.25	0	5
	0	60	94	50.33	12	0.5	0	26.53
	1.55	60	94	50.33	12	0.5	0	26.96
	4.28	60	94	50.33	12	0.5	0	11.32
	7.39	60	94	50.33	12	0.5	0	5.72
	13.55	60	94	50.33	12	0.5	0	3.16
	0	60	94	47.1	12	1	0	25.87
	1.68	60	94	47.1	12	1	0	26.34
	4.88	60	94	47.1	12	1	0	9.5
	8.88	60	94	47.1	12	1	0	5.16
	16.32	60	94	47.1	12	1	0	2.61
	0	60	94	66	12	0	0.015	30.11
	0.986	60	94	66	12	0	0.015	30.38
	2.9	60	94	66	12	0	0.015	23.58
	5	60	94	66	12	0	0.015	13.91
	8.7	60	94	66	12	0	0.015	9.72
	0	60	94	65.2	12	0.25	0.015	30.01
	0.99	60	94	65.2	12	0.25	0.015	30.4
	2.92	60	94	65.2	12	0.25	0.015	23.57
	5.05	60	94	65.2	12	0.25	0.015	13.84
	8.6	60	94	65.2	12	0.25	0.015	9.24
	0	60	94	62.15	12	0.5	0.015	29.36
	1.15	60	94	62.15	12	0.5	0.015	29.66
	3.1	60	94	62.15	12	0.5	0.015	18.44
	6.35	60	94	62.15	12	0.5	0.015	12.44
	9.4	60	94	62.15	12	0.5	0.015	7.86
	0	60	94	57.3	12	1	0.015	29.12
	1.3	60	94	57.3	12	1	0.015	29.24
	3.5	60	94	57.3	12	1	0.015	14.68
	6.7	60	94	57.3	12	1	0.015	9.06
	11.7	60	94	57.3	12	1	0.015	5.13
	0	60	94	70.8	12	0	0.03	31.92
	0.85	60	94	70.8	12	0	0.03	32.03
	2.3	60	94	70.8	12	0	0.03	28.93

Author	4.32	60	94	70.8	12	0	0.03	22.34
	7.5	60	94	70.8	12	0	0.03	11.56
	0	60	94	70.2	12	0.25	0.03	31.47
	0.85	60	94	70.2	12	0.25	0.03	31.53
	2.35	60	94	70.2	12	0.25	0.03	26.67
	4.4	60	94	70.2	12	0.25	0.03	21.54
	7.7	60	94	70.2	12	0.25	0.03	11.16
	0	60	94	67	12	0.5	0.03	31.09
	0.9	60	94	67	12	0.5	0.03	31.31
	2.65	60	94	67	12	0.5	0.03	24.46
	5.1	60	94	67	12	0.5	0.03	15.96
	8.7	60	94	67	12	0.5	0.03	10.7
	0	60	94	64.8	12	1	0.03	30.44
	1.1	60	94	64.8	12	1	0.03	30.74
	3	60	94	64.8	12	1	0.03	23.17
	5.7	60	94	64.8	12	1	0.03	13.8
	10.85	60	94	64.8	12	1	0.03	9.32
	0	167	94	54.66	12	0	0	11.44
	1.427	167	94	54.66	12	0	0	11.51
	4.59	167	94	54.66	12	0	0	5.97
	7.4	167	94	54.66	12	0	0	3.45
	14.83	167	94	54.66	12	0	0	1.67
	0	167	94	54.11	12	0.25	0	11.39
	1.47	167	94	54.11	12	0.25	0	11.5
	4.65	167	94	54.11	12	0.25	0	6
	7.65	167	94	54.11	12	0.25	0	3.34
	15.32	167	94	54.11	12	0.25	0	1.59
	0	167	94	50.33	12	0.5	0	10.83
	1.62	167	94	50.33	12	0.5	0	10.98
	4.74	167	94	50.33	12	0.5	0	4.33
	8.59	167	94	50.33	12	0.5	0	1.98
	17.3	167	94	50.33	12	0.5	0	1.13
	0	167	94	47.1	12	1	0	10.26
	1.72	167	94	47.1	12	1	0	10.45
	5.68	167	94	47.1	12	1	0	3.56
	10.32	167	94	47.1	12	1	0	1.26
	20.8	167	94	47.1	12	1	0	0.78
	3.2	167	94	66	12	0	0.015	8.7
	5.25	167	94	66	12	0	0.015	5.06
	9.1	167	94	66	12	0	0.015	2.57
	3.18	167	94	65.2	12	0.25	0.015	8.15
	5.3	167	94	65.2	12	0.25	0.015	4.58
	9.18	167	94	65.2	12	0.25	0.015	2.44
	0	167	94	62.15	12	0.5	0.015	12.05
	1.25	167	94	62.15	12	0.5	0.015	12.15
	3.4	167	94	62.15	12	0.5	0.015	7.04
	6.7	167	94	62.15	12	0.5	0.015	4.32
	10.9	167	94	62.15	12	0.5	0.015	2.06
	0	167	94	57.3	12	1	0.015	11.75
	1.38	167	94	57.3	12	1	0.015	11.82
	4	167	94	57.3	12	1	0.015	5.95
	7	167	94	57.3	12	1	0.015	3.32
	14.2	167	94	57.3	12	1	0.015	1.46
	2.8	167	94	70.8	12	0	0.03	9.95
	4.35	167	94	70.8	12	0	0.03	6.08
	7.8	167	94	70.8	12	0	0.03	4.04
	2.89	167	94	70.2	12	0.25	0.03	9.61
	4.4	167	94	70.2	12	0.25	0.03	5.63
	7.9	167	94	70.2	12	0.25	0.03	3.63
	3.2	167	94	67	12	0.5	0.03	8.34
	5.7	167	94	67	12	0.5	0.03	4.31
	8.6	167	94	67	12	0.5	0.03	3.1
	3.5	167	94	64.8	12	1	0.03	7.77
	6.1	167	94	64.8	12	1	0.03	4.07
	12.5	167	94	64.8	12	1	0.03	2.5
	0	100	90	54.66	20	0	0	18.58
	0.93	100	90	54.66	20	0	0	19.04
	2.8	100	90	54.66	20	0	0	9.195
	4.35	100	90	54.66	20	0	0	5.59
	8.6	100	90	54.66	20	0	0	3.62
	0	100	90	54.11	20	0.25	0	18.55

Author	0.91	100	90	54.11	20	0.25	0	18.96
	2.9	100	90	54.11	20	0.25	0	9.02
	4.01	100	90	54.11	20	0.25	0	5.45
	8.835	100	90	54.11	20	0.25	0	3.05
	0	100	90	50.33	20	0.5	0	17.11
	1.07	100	90	50.33	20	0.5	0	17.59
	3.2	100	90	50.33	20	0.5	0	8.7
	5.7	100	90	50.33	20	0.5	0	5.11
	11.475	100	90	50.33	20	0.5	0	2.06
	0	100	90	47.1	20	1	0	15.63
	1.5	100	90	47.1	20	1	0	16.41
	3.76	100	90	47.1	20	1	0	5.12
	7.5	100	90	47.1	20	1	0	3.52
	14.475	100	90	47.1	20	1	0	1.15
	0	100	90	66	20	0	0.015	20.87
	0.79	100	90	66	20	0	0.015	21.19
	2.4	100	90	66	20	0	0.015	11.71
	3.7	100	90	66	20	0	0.015	7.53
	7.8	100	90	66	20	0	0.015	4.25
	0	100	90	65.2	20	0.25	0.015	20.56
	0.84	100	90	65.2	20	0.25	0.015	20.89
	2.4	100	90	65.2	20	0.25	0.015	11.41
	3.8	100	90	65.2	20	0.25	0.015	7.69
	7.3	100	90	65.2	20	0.25	0.015	3.89
	0	100	90	62.15	20	0.5	0.015	20.01
	1.05	100	90	62.15	20	0.5	0.015	20.09
	2.8	100	90	62.15	20	0.5	0.015	10.59
	4.8	100	90	62.15	20	0.5	0.015	6.41
	9.5	100	90	62.15	20	0.5	0.015	3.94
	0	100	90	57.3	20	1	0.015	19.14
	1.2	100	90	57.3	20	1	0.015	19.34
	3.2	100	90	57.3	20	1	0.015	9.5
	6.1	100	90	57.3	20	1	0.015	5.92
	11	100	90	57.3	20	1	0.015	3.66
	0	100	90	70.8	20	0	0.03	21.72
	0.77	100	90	70.8	20	0	0.03	21.73
	1.7	100	90	70.8	20	0	0.03	16.07
	3.1	100	90	70.8	20	0	0.03	10.06
	7.2	100	90	70.8	20	0	0.03	5.97
	0	100	90	70.2	20	0.25	0.03	21.53
	0.8	100	90	70.2	20	0.25	0.03	21.53
	1.8	100	90	70.2	20	0.25	0.03	15.75
	3.5	100	90	70.2	20	0.25	0.03	9.65
	7.9	100	90	70.2	20	0.25	0.03	5.59
	0	100	90	67	20	0.5	0.03	20.77
	0.95	100	90	67	20	0.5	0.03	20.88
	2.55	100	90	67	20	0.5	0.03	13.8
	4	100	90	67	20	0.5	0.03	8.37
	8.6	100	90	67	20	0.5	0.03	4.79
	0	100	90	64.8	20	1	0.03	20.45
	1.15	100	90	64.8	20	1	0.03	20.66
	2.8	100	90	64.8	20	1	0.03	12.55
	6	100	90	64.8	20	1	0.03	6.21
	9.5	100	90	64.8	20	1	0.03	3.96

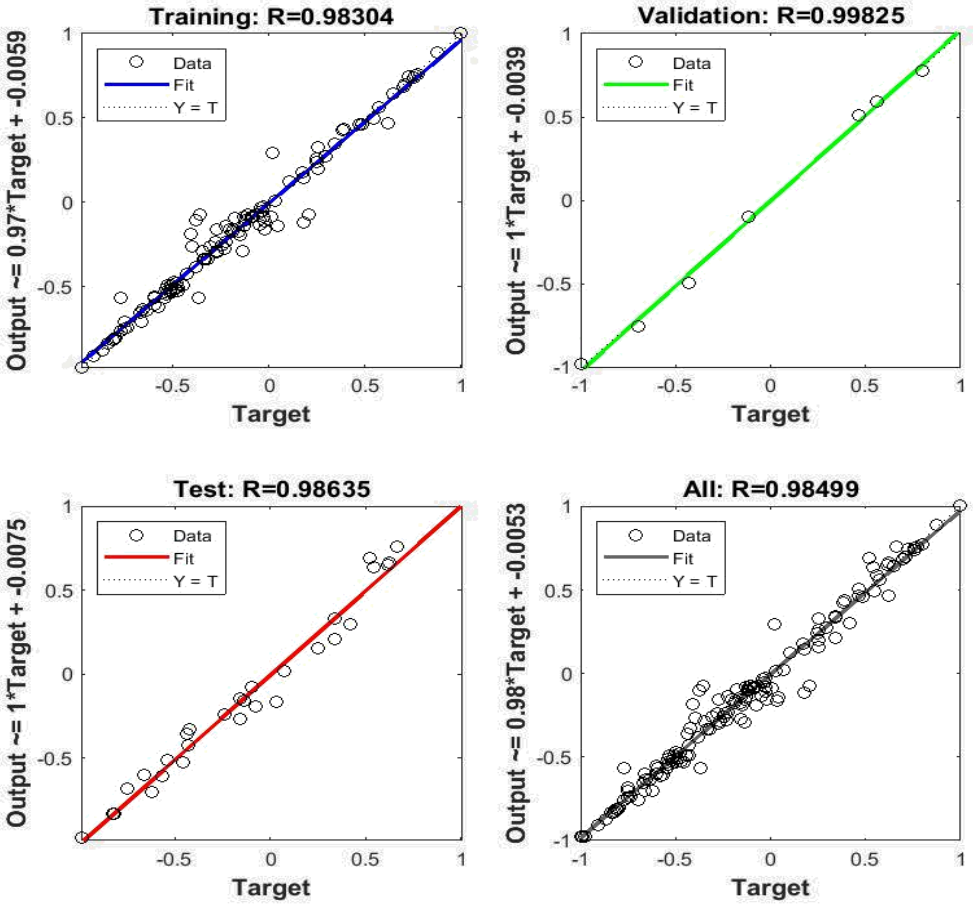

Figure B.1. Comparison between the "target" and "output" parameters for data used in ANN-4 model.

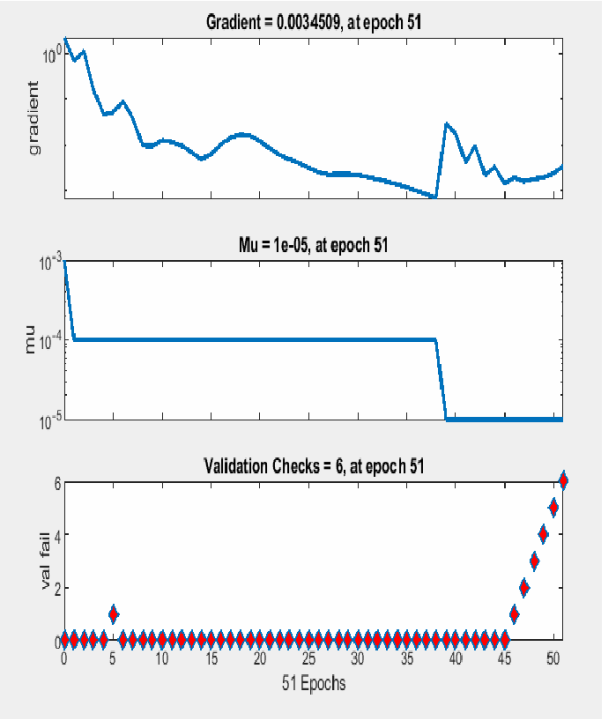

Figure B.2. The training state for ANN-4 model.

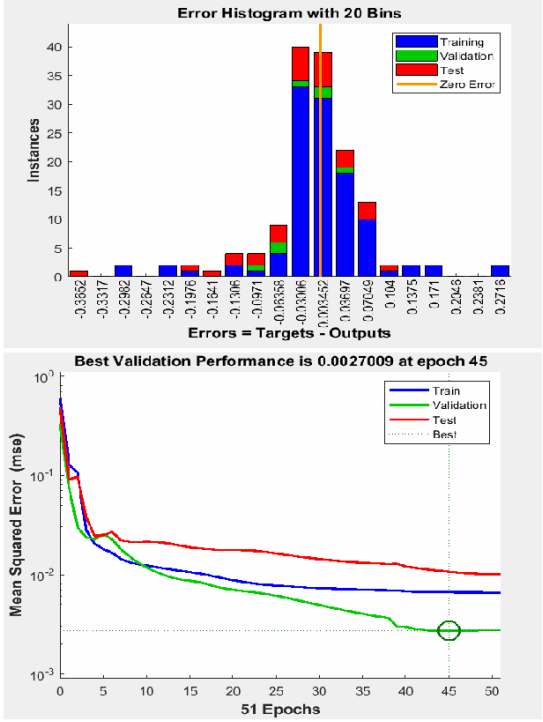

Figure B.3. Best validation performance in ANN-4 model.

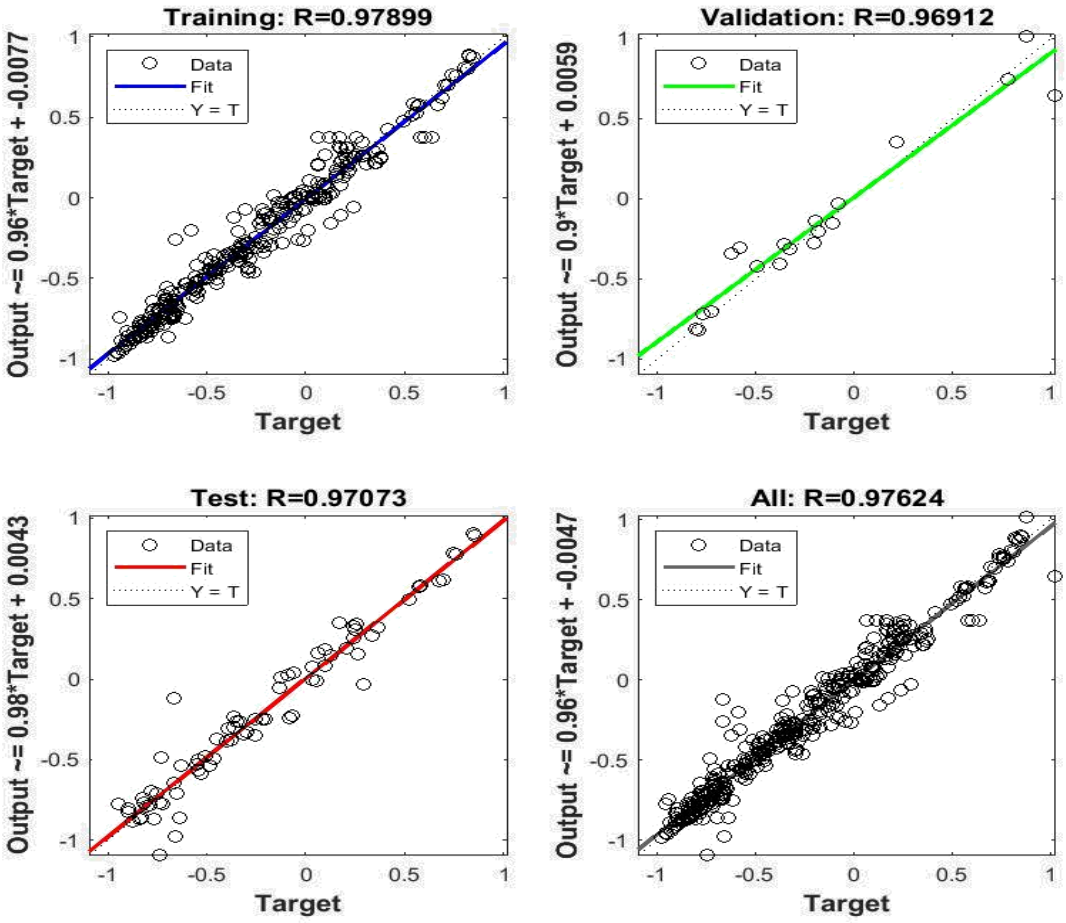

Figure B.4. Comparison between the "target" and "output" parameters for data used in ANN-5 model

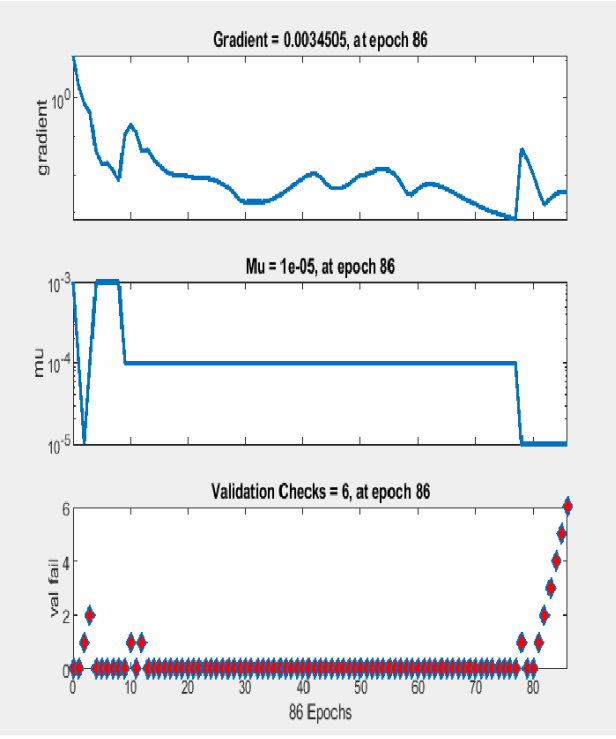

Figure B .5. The training state for ANN-5 model.

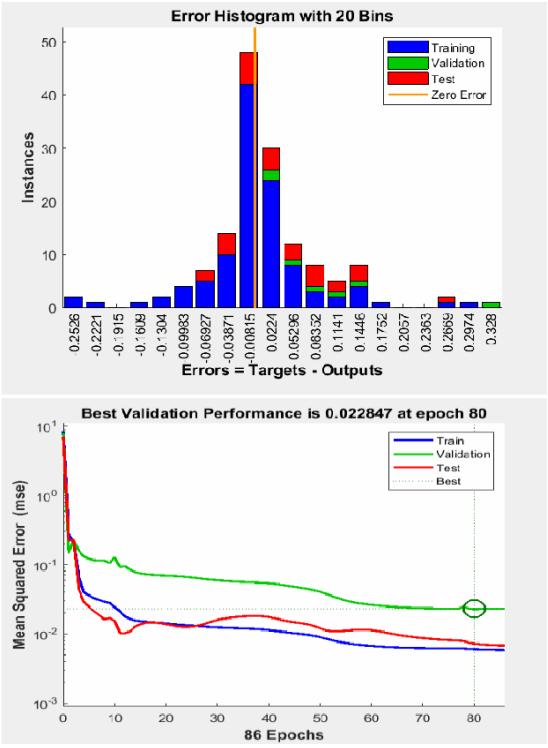

Figure B .6. Best validation performance in ANN-5 model.